Cooperative Control for Multi-vehicle Swarms

A THESIS SUBMITTED IN FULFILMENT OF THE REQUIREMENTS FOR THE DEGREE OF DOCTOR OF PHILOSOPHY

Omar Ilaya
BENG. (HONS)

SCHOOL OF AEROSPACE, MECHANICAL, MANUFACTURING ENGINEERING
COLLEGE OF SCIENCE, ENGINEERING AND HEALTH
RMIT UNIVERSITY

March 2009

Declaration

I certify, that except where due acknowledgement has been made, the work is that of myself alone; the work has not been submitted previously, in whole or in part, to qualify for any other academic award; the content of the thesis is the result of work which has been carried out since the official commencement date of the approved research program; any editorial work, paid or unpaid, carried out by a third party has been acknowledged; and ethics procedures and guidelines have been followed.

Omar Ilaya
March 2009

Acknowledgements

I would like to thank my senior supervisor, Associate Professor Cees Bil, for his guidance and support during my postgraduate career; and my second supervisor, Dr. Michael Evans, for his comments, and financial support of the research.

I would also like to acknowledge the kind support of the Australian Research Council, and the Australian Postgraduate Award Scheme for financial supporting the research.

Abstract

The cooperative control of large-scale multi-agent systems has gained a significant interest in recent years from the robotics and control communities for multi-vehicle control. One motivator for the growing interest is the application of spatially and temporally distributed multiple unmanned aerial vehicle (UAV) systems for distributed sensing and collaborative operations. In this research, the multi-vehicle control problem is addressed using a decentralised control system. The work aims to provide a decentralised control framework that synthesises the self-organised and coordinated behaviour of natural swarming systems into cooperative UAV systems. The control system design framework is generalised for application into various other multi-agent systems including cellular robotics, ad-hoc communication networks, and modular smart-structures. The approach involves identifying suitable relationships that describe the behaviour of the UAVs within the swarm and the interactions of these behaviours to produce purposeful high-level actions for system operators. A major focus concerning the research involves the development of suitable analytical tools that decomposes the general swarm behaviours to the local vehicle level. The control problem is approached using two-levels of abstraction; the supervisory level, and the local vehicle level. Geometric control techniques based on differential geometry are used at the supervisory level to reduce the control problem to a small set of permutation and size invariant abstract descriptors. The abstract descriptors provide an open-loop optimal state and control trajectory for the collective swarm and are used to describe the intentions of the vehicles. Decentralised optimal control is implemented at the local vehicle level to synthesise self-organised and cooperative behaviour. A deliberative control scheme is implemented at the local vehicle level that demonstrates autonomous, cooperative and optimal behaviour whilst the preserving precision and reliability at the local vehicle level.

Author Publication List

Ilaya, O. and Bil, C. (2006a). On Swarming UAVs in Military and Civilian Applications, Proceedings of UV Asia-Pacific Conference, Sydney, Australia, April.

Ilaya, O. and Bil, C. (2006b). Control System Design Applications to Innovative UAV Concepts and Operations: A Distributed Search Methodology Using Decentralised Model Predictive Control, Proceedings of 3rd International Symposium on Innovative Aerial-Space Flyer Systems, pp. Tokyo, Japan, November.

Ilaya, O., Bil, C. and Evans, M. (2006a). Multi-agent Control of UAV Swarming, Proceedings of 21st International UAV System Conference, pp. Bristol, UK, April,

Ilaya, O., Bil, C. and Evans, M. (2006b). Control Design of UAV Swarms, Proceedings of 5th International Advanced Engineering and Design Conference, Prague, Czech Republic, June. **[Best Paper Award]**

Ilaya, O., Bil, C. and Evans, M. (2006c). Multi-agent Formation Control of UAVs, Proceedings of 25th International Congress of the Aeronautical Sciences (ICAS 2006), pp. Hamburg, Germany, September,

Ilaya, O. (2007). Multi-objective Decentralized Model Predictive Control for Cooperative Multi-UAV Systems, Proceedings of AIAA Guidance, Navigation, and Control Conference, Hilton Head, USA, August. **[Finalist Best Paper Award]**

Ilaya, O. and Bil, C. (2007). Distributed and Cooperative Decision Making for Multi-UAV Systems with Applications to Electronic Warfare, Proceedings of 7th AIAA Aviation Technology, Integration and Operations Conference, Belfast, Northern Ireland, September.

Ilaya, O., Bil, C. and Evans, M. (2007a). A Particle Swarm Optimisation Approach to Graph Permutation Problems, Proceedings of IEEE Conference on Intelligence, Decision and Control, pp. Adelaide, Australia, February,

Ilaya, O., Bil, C. and Evans, M. (2007b). Neural-network Based Receding Horizon Control for Autonomous Guidance of a UAV Model, Proceedings of 12th AIAC Congress, March.

Ilaya, O., Bil, C. and Evans, M. (2008). Control Design for UAV Swarming. Proceedings of the I MECH E Part G: Journal of Aerospace Engineering, 222, 549 - 567. **[Invited Special Issue]**

Ilaya, O. and Bil, C. (2009). A Particle Swarm Optimisation Approach to Graph Permutations, In Particle Swarm Optimization (Ed, Lazinica, A.) In-Tech, Vienna, Austria, pp. 291 - 312. **[Invited Paper]**

Contents

Table of Figures

Chapter 1. Introduction and Related Works

The advancements of sensor technologies and small-scale robotics have helped generate a growing interest in the development of Unmanned Vehicles (UVs) for hazardous and repetitive missions [1]. In interplanetary exploratory missions, UVs can be used in lieu of manned vehicles to venture into unknown environments unsustainable for human activity. In military applications, UVs such as Unmanned Air Vehicles (UAVs) and Unmanned Ground Vehicles (UGVs) can be used in operations to reduce the risk of life and extend force capabilities into hostile environments. UVs can also be used in many civilian applications including crop dusting, search and rescue, and weather reconnaissance.

As a consequence to this growing interest, significant gains have been achieved at developing complex and more capable unmanned systems. Contrastingly, equivalent progress has not been made in the area of control. Current methods of control rely on *human-in-the-loop* to ensure successful operation of the vehicle. This is often achieved via *teleoperation*; where a human operator controls the vehicle through remote control. In highly complex and capable systems, such as the Global Hawk UAV, a team of 2-3 skilled operators is often required to control the vehicle and deconflict the information from the various onboard sensors.

In recent years, groups of UVs have been proposed for a variety of cooperative tasks, including distributed sensing, multimodal imaging, object manipulation, and cooperative attack. Observing the current trend in UV control systems, the number of operators required to control of a large group of vehicles would increase exponentially. One method to reverse this system-to-operator ratio is through *swarming*. Swarming involves the simultaneous operation of multiple vehicles using simple interaction rules to achieve a purposeful behaviour. This requires that the individual vehicles possess sufficient autonomy to sense and react to their environment and cooperate with neighbouring swarm members. By increasing the autonomy of the individual vehicles, the ability of the supervisory agent to observe and control each individual in the group reduces. However, predicting the response of the group

and guaranteeing completion of the task becomes difficult as individuals become less reliant on the supervisory controller.

In this thesis, the problem of controlling a group of vehicles in a leaderless and decentralised way is addressed. The research aims to develop a systematic approach to synthesising autonomous cooperative control in a group of vehicles tasked with a group objective. The problem is addressed from two levels of control. The first level looks at the individual vehicles and their interactions. The control architecture at the local vehicle level is treated as decentralised, and group behaviours emerge from the local interactions of the vehicles in the group. At the second level (the supervisory level) the group of vehicles is treated as a unified structure. Control at this level is hierarchical, and commands are issued from a high-level supervisory agent to the group of vehicles. A key enabler to this implementation strategy is the identification of group abstractions that reduce the control at the supervisory level to a lower-dimensional manifold preserving the essential features of the swarm. To ensure that the vehicles' emergent behaviour is coordinated towards the desired group objectives, this research aims to investigate the resolution of group objectives into local vehicle objectives using decentralised optimisation techniques. Based on this discussion, an extensive review of the literature on multi-agent systems is presented to motivate the developments presented in this thesis. In Section 1.6, an overview of the thesis is then provided which introduces the specific problems studied in this research.

1.1. BIOLOGICAL MOTIVATION

The collective behaviour observed in many social insects and animals provides the inspiration for the development of multi-agent and multi-vehicle systems [2, 3]. Cooperative behaviours arise in many biological networks; and range from the inter-molecular and inter-cellular interactions of bacterial swarms [4], to the coordinated motions of complex socially-aware animal groups [5]. Sociability in these biological species provides benefits to the group unattainable by individual endeavours. These include anti-predator vigilance, maximal-foraging, and collective migration. In schools of fish and flocks of birds, individuals coordinate their motions to travel in large cohesive groups to maximise food reward and defend against predation [6, 7]. Migratory birds, such as geese, swans, and pelicans, fly in regular V-shaped formations to maximise drag reduction and range [8-11]. Swarms of Japanese honeybees (*Apis cerana japonica*) [12, 13], communities of wild chimpanzees (*Pan troglodytes*) [14, 15], and packs of African wild dogs (*Lycaon pictus*) [16], all exhibit

cooperative and coordinated behaviours that include nest-consensus, group foraging, and cooperative hunting. These complex cooperative behaviours are achieved through the local interactions of the individuals and without direction of a group leader. The emergence of these complex macroscopic behaviours is the result of many simple microscopic behaviours interacting together towards a common goal [17].

Artificial models for biological swarms have consequently been recognised as a potential analogy for scientific and engineering applications. These include population-based optimisation techniques [18, 19], distributed computing, agent-based software, and multi-vehicle systems. Much work has been invested in the field of mathematical and theoretical biology to understand the relationship between the individual and the group behaviours of these biological swarms. The interactions of individuals in a school of fish, was first investigated by Breder in [20]. Breder promoted the view that individuals in a school of fish demonstrated a long-range attraction and a short-range repulsion that decayed over increasing distance. This attractive-repulsive potential model caused individuals to cluster and form cohesive groups. The swarm behaviour of the flock was the result of the dense interactions of the relatively simple attraction-repulsion forces of the individuals. Following from Breder's model, much work has been done by mathematical biologists to model the emergent behaviour of swarms using local rules of attraction and repulsion [5, 21-24].

In 1987, Reynolds [25] formalised the concepts of Breder into a set of distributed behavioural rules describing the observed flock motion of natural systems. Reynolds' behavioural model (also known as Reynolds' boids) is summarised by the following three heuristics:

1. flock centring: attempt to stay close to nearby flockmates;
2. obstacle: avoidance: avoid collisions with neighbouring flockmates; and
3. velocity matching: attempt to match the velocity of neighbouring flockmates.

These have been commonly referred to as *cohesion*, *separation*, and *alignment* respectively. A mathematical justification for flocking and swarming in social biological systems is presented in Grünbaum [26]. In [26], evidence is presented suggesting the influence of cohesion and alignment in flocks of aquatic species for improved foraging in asocial individuals. In foraging species, individuals randomly sample the environment to search for a favourable gradient. Based on this hypothesis, an individual would spend more time moving in the wrong directions than towards the region of a favourable gradient. Schooling and flocking encourages the migration of individuals towards a favourable gradient through the

cohesion and alignment of neighbours in the flock. Alignment and cohesion in social flocks and swarms serves to dampen the stochastic effects of individual sampling errors and directs the migration of individuals to a common direction [26]. This observed behaviour is the motivation for population-based optimisation techniques such as Particle Swarm Optimisation (PSO) [19, 27], Simulated Annealing (SA) [28], and Ant Colony Optimisation (ACO) [18, 29].

Parrish et al. [6] extended the behavioural model introduced in [25] to identify three parameter groups that quantitatively characterise the individual and group behaviours of the flock. These include 1) *behavioural matching*; 2) *positional preference*; and 3) *numerical preference*. Behavioural matching refers to the tendency of individuals to match their behaviour with neighbouring flockmates. In schools of fish, behavioural matching is demonstrated by the explicit alignment of individuals in the group [30, 31], whilst positional preference is used to describe the individuals' affinity to distribute themselves relative to each other [6]. The equilibrium of Breder's attractive-repulsive model is an example of the preferred position between neighbouring flockmates. Positional preference together with behavioural matching, quantitatively describe Reynolds' boids. The distributed and leaderless nature of the flock's cooperative task is further influenced by the numerical preference parameter. The numerical preference describes the subset of flockmates that an individual interacts with. The cardinality of this subset defines the number of interactions an individual has and is often referred to as the *rule size* [6].

The concept of a finite interaction range has received considerable attention in the literature [32]. In Couzin et al. [33], the limited spatial sensory capabilities of schools of fish and flocks of birds was simulated using bounded zones of attraction and repulsion. As the parameters of each zone was varied (including the radius of attraction and repulsion), transitions in the global behaviour were observed. Patterns included swarms, torus, and parallel group formations. The results obtained in [33] supported the behaviours demonstrated by schools of fish. The relationship between the interaction range of the individuals and the expressed global behaviours, further reinforced the notion of emergence in cooperative systems, and demonstrated the first evidence of 'collective memory' in animal groups. Furthermore, the relationship between the sensory and communication range of individuals in the group to the observed behaviour was established.

Recent studies using direct empirical observations by Ballerini et al. [34], suggest that the finite interactions of natural flocks and swarms is significantly less than the number of

observable neighbours as originally predicted by Couzin et al. [33]. Ballerini et al. concluded that the interactions of individuals in natural flocks and swarms are bounded by a topological distance influenced by the cortical elaboration of the visual input rather than a metric distance bounded by the sensory observation of an individual [34]. Grünbaum et al. [35] further elaborated on the anomalies observed in schools of fish to produce more accurate empirical models. Using motion analysis hardware, Grünbaum et al. investigated the aggregate behaviour of schools of fish (*Danio aequipinnatus*). Grünbaum et al. identified a behavioural switch responsible for the expressed collective behaviours in a school of fish. Grünbaum et al.'s findings further supported Couzin et al.'s flock model. Grünbaum et al.'s strategy assumes that individuals in the swarm perform a biased random walk in a periodic domain with dynamics influenced by the behaviours and positions of its neighbours. This behavioural matching and positional preference improves the ability of individuals to taxi adverse gradients in noisy environments, and further support the causal relationship between the local interactions of the neighbouring flockmates and the complex global behaviours of the group.

Understanding the mechanisms of self-organised motions in natural flocks and swarms provides innovative ideas for developing distributed cooperative control systems. In reality, the study of individual interactions in natural flocks and swarms is inherently difficult to approach experimentally. For example, in a plague of African migratory locusts (*Locusta migratoria migratorioides*), individuals demonstrate an ostensibly random and chaotic motion. The precise motion of these individuals is not completely understood. Studies have shown that these highly non-linear motions transpire through the multiple simultaneous interactions of the individuals [36]. Despite these seemingly chaotic motions, the collective group demonstrates a cohesive 'rolling' migratory pattern [37].

The large-scale and 'chaotic' behaviour of these individuals makes it difficult to create accurate models for biological swarms using purely local effects. Traditional approaches rely on Partial Differential Equations (PDE) to approximate the local density of individuals and preserve the group's collective behaviour. In [37], Edelstein-Keshet et al. model the migration of African locusts using a *travelling wave solution*. Many attempts have been made to model phenomena such as invasions using travelling wave solutions [38-40]; however, few have provided a realistic representation of biological groups with a finite population. The results of [37], suggests that cohesive and compact swarms such as locusts, cannot be modelled using traditional travelling wave solutions. More recently, Mogilner and Edelstein-Keshet [41], and Topaz and Bertozzi [42] consider non-local interactions on the swarm using

integro-differential advection-diffusion equations. The resulting continuum models produce coherent band-like structures. However, these models remain an approximation to the exact behaviour of individuals at best.

A recent body of work considers general particle-based models for self-propelled organisms as an alternative to understanding the construction and movement of coherent swarm structures using finite continuum models [43-45]. Viscek et al. [43] propose a simple swarm model based on particle dynamics that simulate Reynolds' boids. In Viscek et al.'s model, each particle is bounded by a unit circle representative of the interaction range. The particles are driven by discrete-time dynamics with absolute velocities. At each time step, each particle updates its direction based on the average direction of motion of its neighbouring particles. Viscek et al. showed that by using this nearest neighbour rule, the particle demonstrated Reynolds' rules and reached consensus on a common orientation. Jadbabaie et al. [46] extended the work of Viscek et al. to provide a formal treatment on the alignment problem of the particles. Similar to the work of Viscek et al., Gazi and Passino [47, 48] proposed a simple isotropic swarm model using the attraction-repulsion rules of Breder [20]. Stability analysis of these swarms was given in [49-51]. Using these attraction-repulsion rules, Gazi and Passino showed that the isotropic model demonstrated the basic features of aggregation, cohesion, and separation as identified by Reynolds. Similar studies were conducted using anisotropic swarms in [22, 52, 53] to demonstrate Reynolds' boids.

The literature on natural flocks and swarms provides the inspiration for the development of distributed artificial systems. The modelling issues and the behavioural synthesis for these systems, provides an insight into the developmental considerations for synthetic multi-agent systems. In the following section, a review of some of the design engineering motivations for multi-agent systems is discussed before a formal treatment on the technical aspects of the design considerations is given.

1.2. ENGINEERING MOTIVATION

Motivation for multi-agent cooperative control systems comes from a variety of applications; ranging from Distributed Artificial Intelligence (DAI) [54], to formation flying [55-59], and cooperative spacecraft operations [60-67]. Advancements in small-scale technologies such as compact and efficient processors, cameras, and wireless technologies, have also made it possible to develop smaller, inexpensive unmanned technologies for cooperative applications. The cooperative control of unmanned technologies, such as Unmanned Aerial Vehicles

(UAVs) [68, 69] is of great interest and utility to military [1, 70] and civilian applications [71]. These include cooperative target tracking [72-79], coordinated and synchronised attacks [80-87], distributed intelligence, surveillance, and reconnaissance [88-99], synchronous payload delivery and manipulation [100-104], urban tomography [105], and chemical cloud detection [106].

Advantages of using groups of autonomous vehicles to perform coordinated activities have been discussed extensively in the literature [107-109]. These include enhanced task performance, reduced cost, increased system reliability and robustness, inherent distribution of resources, and system re-configurability. Applications such as surveillance and reconnaissance benefit from the distribution of tasks. Using multiple coordinated sensory assets distributed over a large area drastically reduces the time to survey a region of interest. In applications such as the Separated Spacecraft Interferometry (SSI) program [110], imaging and astrometry is distributed over a network of space interferometers to enhance the resolution of the imaging task and permit the reconfiguration of the imaging topology. Multiple vehicle systems naturally admit the distribution of tasks and resources over multiple platforms, making the cooperative control strategy ideal for distributed or complex problems.

As a consequence to this growing interest, research on cooperative control has increased over the past decade. Major areas of research for multi-vehicle applications include pattern formation [55, 57, 59, 64, 111-124], flocking and self-assembly [32, 125-130], deployment and task allocation [131-135], and vehicle routing [136]. The planning and control of multi-vehicle systems consist of many sub-problems related to network control design. These include convergence and consensus protocols [137, 138], asynchronous distributed control algorithms [139-141], collective behaviour of flocks and swarms [142, 143], algebraic connectivity of complex networks [144, 145], dynamic graphs [146-148], and optimisation-based cooperative control [144, 145]. The design of multi-vehicle systems poses significant theoretical and practical challenges. In the remainder of this chapter, several of the sub-problems associated with multi-vehicle control systems are discussed.

1.3. INFORMATION FLOW

Vehicles in a shared environment depend on information to accomplish goals, avoid conflicts, and share resources [149]. Individuals in a group can collect information about their environment, and neighbouring vehicles either through direct sensory observations, or through *direct* and *indirect* communication strategies. The limited range and resolution of the

physical sensors bounds the information available to an individual through direct sensory observation [150]. In non-omnidirectional sensors, additional limitations arise from the directivity patterns of the physical sensor. These include the conic field of view of a camera, the radiation patterns of an antenna [151, 152], or the directivity of an optical range finger.

The bounded information flow induced by the sensory observations, restrict the information accessible by an individual. Thus, no vehicle will have the capacity to observe the entire group and have access to global information. By facilitating communication between individuals, vehicles can improve their perspective, and their ability to achieve tasks and resolve conflicts. Inter-vehicle communication is achieved through *explicit* and *implicit* communication strategies. *Explicit* communication strategies involve the deliberate act of transmitting and receiving information, either through dedicated peer-to-peer communication channels, or through broadcast-type signalling [153]. The decision to use peer-to-peer over broadcast-type strategies is dependent on several design and implementation factors. Peer-to-peer communication strategies are generally suited for applications where broadcast over large distances is limited by power constraints, such as in SSI; or in applications where the vulnerability of the broadcasted signal can compromise the integrity and security of the system. These include cooperative UAVs [154, 155], and internet agents. In intelligent highways and anti-collision systems [156, 157], the precision and directivity of peer-to-peer communication strategies ensures that information flow is consistent through the network with minimal degradation and corruption.

In applications where transmission and computational constraints are relaxed, or the communication network is dynamic and possibly ad-hoc (such as multi-vehicle systems and wireless internet connections), broadcast provides the most flexible approach to dynamic connectivity. Broadcast allows vehicles to wirelessly transmit information continuously or discretely to other vehicles over a wireless medium within a bounded proximity – irrespective of the number of vehicles in the transmission range. This makes broadcast-type strategies suitable for scalable decentralised control strategies. Drawbacks of this approach include the significant power required to transmit information over large distances with minimal degradation; the vulnerability of the signal to corruption, interference, and hijacking; and the complexity of the signal processor to filter and deconflict the possible simultaneous arrival of information from neighbouring communication networks.

Implicit communication, as opposed to explicit communication, involves the indirect transmission of information through the manipulation of the environment (*stigmergy*) or

through elaborations of direct sensory observations. Implicit communication strategies based on elaborations of direct sensory input, requires the maintenance of an internal model to extrapolate and predict the states of other vehicles in the environment. Examples include [158, 159] where communication-free cooperation is facilitated through vision-based sensing and inter-agent modelling. In [160], Otanez and Campbell developed a model by discretizing the continuous-states of a lead UAV into a set of identifiable behaviours using a hybrid automaton. The hybrid automaton provided a model to a secondary UAV to predict the behaviour of the lead vehicle from sensory observations on the continuous-state. By predicting the behaviour of the lead UAV, the secondary UAV could determine the feasibility and utility of engaging in a cooperative task (such as interferometric imaging) to improve the collective strategy of the group. Collective behaviours using this kind of interaction include flocking and pattern formation.

Approaches based on stigmergy have also been found in the literature for the cooperative control of UAVs [161, 162]. Parunak and Brueckner propose a model of pheromone-based coordination for decentralised multi-agent systems in [163]. In [164, 165], the authors extended the previous work to develop a simulation using multiple synthetic pheromones for navigation and spatial coordination of multiple swarming vehicles. In this strategy, vehicles deposit digital pheromones in the environment that signal to neighbouring vehicles the presence of threats or the direction of goals. This enabled the vehicles to indirectly communicate with each other through the environment. It should be noted however, in Parunak and Brueckner's model, the swarm agents do not physically deposit a chemical signal or engage in any direct inter-vehicle communication. Instead, the environment in which they reside and deposit digital pheromones, are maintained on a world map accessible through a set of place agents. Access to the world map is achieved through direct communication with the place agents. Therefore, the scheme is not a physical realisation of the stigmergic process and relies on conventional communication strategies. Despite the practical shortcomings of their approach, Parunak and Brueckner demonstrated the emergence of complex behaviour through implicit coordination [2]. In the following section, the various architectures that facilitate cooperative behaviour are discussed.

1.3.1. ARCHITECTURES

Physical and computational restrictions limit an individual's ability to use and transmit global information. The lack of global information means that individuals in a group lack the global

perspective to solve a centralised control problem using complete information. Ideally, some form of distribution (or decentralisation) should be observed; either through control delegation, or information flow. The flow of information through the group, and the control relations that define the interactions of the individuals, provides the notion of a *group architecture* [166] (or *group organisation* [107]). When the information is processed through a common central facility or decision maker, the group architecture is *centralised*. In this cooperative scheme, a centralised node manages the operation of the whole system. It is responsible for coordinating the information received by the individual vehicles, deconflicting individual tasks and resources, and distributing tasks and information to each vehicle in the group. Consequently, the centralised node must be sufficiently capable to manage the information and control policies of the entire interconnected group of vehicles.

Centralising the information and control through a common facility, maximises the perspective of a supervisory agent. This enables the definition of precise and optimal behaviours for each agent in the group. As a result, centralised architectures have been applied to many planning problems, such as formation control [57, 131, 167-170], cooperative conflict-free navigation [77, 170-173], air traffic control [174], task allocation [131, 175], and vehicle deployment problems [94]. Planning in a centralised architecture often involves the resolution of a performance function. Path planning problem for a group of vehicles was addressed by Capozzi and Vagners in [77, 170]. In [77, 170], Capozzi and Vagners developed an evolution-based planning system that uses the states of each vehicle in the group to coordinate and generate paths through an environment. The high-dimensionality of the centralised optimisation problem was handled by a metaheuristic search technique based on evolutionary programming. A similar approach was used by Doctor et al. in [94] where a metaheuristic PSO was used to coordinate a group of robots for cooperative search. In these approaches, the centralised agent used a priori information about the environment to generate collision-free reference trajectories for the vehicles to track. When the environment is dynamic or uncertain, feedback to the centralised agent is necessary to re-evaluate plans and accommodate changes. Environmental uncertainty was addressed by Bellingham et al. in [172] where the probability of losing a vehicle was considered at the planning stage.

Recently, the centralised path planning problem for a group of vehicles has been approached by exploiting the symmetric properties of the formation induced by the configuration of vehicles. In [176], Belta and Kumar propose a centralised trajectory computation scheme using techniques from differential geometry to ‘shape’ the kinetic

energy of the group. Using this approach, the problem was reduced to solving one geodesic on $SE(3)$ for the centroid of the group, and N orbits in $SO(3)$. By smoothly varying the kinetic energy metric, the method guaranteed smooth trajectories for the group of vehicles. It was also shown, that using this formulation, it is also possible to control the spatial adjacency of vehicles in the group. While this method ensures optimality with respect to the kinetic energy of the system, it fails to accommodate for collision avoidance with obstacles in the environment. Furthermore, the framework proposed in [176] is computationally involved, and does not scale well with the addition of vehicles in the group.

In an effort to reduce the control effort and improve scalability, Belta and Kumar [167] introduced a low-dimensional abstract manifold to capture the group's position, orientation, and shape with respect to a world frame. Belta and Kumar's group abstraction is independent from the number and ordering of vehicles in the group, and is suitable for describing large-scale swarms. Using this abstraction, controllers can be derived for each vehicle dependent on the feedback from the centralised agent. This has the practical advantage of reducing the communication and sensing of the individual vehicles, and reducing the control effort to trajectory tracking at the local vehicle level. Despite this, the centralised agent still required the states of each vehicle to evaluate the abstract state and solve the optimisation problem.

An alternative approach to concentrating the load on a single agent is to use intermediate sets of leaders between the centralised node and the group of vehicles [177, 178]. In this hybrid control strategy, the centralised problem is decomposed into varying levels of resolution. At each level, the group of agents control a subset of vehicles in the proceeding lower level. This approach has been applied to the control of large platoons of UAVs for cooperative military operations [177], and the search of targets in urban environments [178]. While these hybrid architectures reduce the load on a single agent, they still rely on some fusion at the intermediate level by a centralised control facility.

Ideally, the distributed nature of the vehicles and information network should be exploited to localise the information and control to the individual vehicles. In this decentralised scheme, fusion and control occur locally at each node on the basis of local observations and communicated information. Distributing the information and control in this way, yields the following characteristics for a decentralised architecture:

1. no single agent is capable or responsible for the coordination of the group as a whole;
2. there is no global control or common communication facility; and
3. agents do not have access to global information.

These constraints provide a number of important characteristics for decentralised systems. By eliminating the dependency on any centralised facility, computational/communication bottlenecks are removed, and the system as a whole is more tolerant to vehicle faults, network reconfiguration, and vehicle attrition and extension.

Various decentralised software architectures have been proposed in the literature for controlling multi-agent and multi-vehicle systems. In [179, 180] a distributed hierarchical system based on the cellular organisation of biological agents called the CEBOT architecture was proposed. In the CEBOT architecture, robots are represented by cells in an organisation, and are capable of dynamically reconfiguring their neighbourhood structure in response to changes in the environment. The reconfigurability of the CEBOT architecture makes it suitable for the formation control problem of multi-vehicle networks. A similar architecture based on cellular robotics is presented in [181]. In [181], the SWARM architecture was developed for the distributed control of a large number of autonomous robots. Interactions are strictly nearest-neighbour, and the group behaviour is an emergent property of the interconnected system. Consequently, the architecture is amenable to complex cooperative tasks such as assembly, communication, and computing [182]. Heterogeneity in distributed multi-vehicle systems was addressed using the ACTRESS [183] and ALLIANCE [184, 185] architectures. The ACTRESS system was used to facilitate cooperation between heterogenous groups for tasks such as box pushing [186]. In the ALLIANCE system, robots were able to sense the effects of their own actions and the actions of other robots through sensory perception and explicit broadcast communications. Unlike ACTRESS, each robot in the ALLIANCE architecture was designed using a behaviour-based controller that resulted in a fault tolerant, reliable, and adaptive mechanism for cooperative robot control. These strategies provided the necessary framework for implementing decentralised control laws for groups of vehicles, and have been successfully applied in many multi-robotic applications.

In practice, many multi-vehicle systems cannot conform to a strict decentralised dichotomy [166]. The emergence of behaviour is often poorly understood with context to physical implementations. It is often unclear on how (or whether it is even possible) to design decentralised control laws that achieve a desired group objective from simple local control laws [187]. Many of the proposed decentralised architectures in the literature feature, as part of their solution, the use of *virtual leaders* [55, 121, 143, 145, 188-194]. In this approach, a virtual entity is introduced to the group to provide a stable reference point for group convergence. This could include a reference trajectory for a formation to track [143, 189,

191-194], beacons to contain the volumetric space of a spatially distributed group of vehicles [188], or the shape and formation for a group of vehicles [195-197]. A representative body of work can be found in [117], where the problem of navigating a group of vehicles is addressed using virtual agents. In this strategy the path of a virtual leader is calculated and the relative offset of each vehicle is used to generate its corresponding reference trajectory. Similar to the approach taken in [117], Fang and Antsaklis [194] use a virtual leader to define the centroid for a group of vehicles to track. In this approach, the vehicles distribute themselves relative to the virtual leader using consensus protocols to align their centroid to the trajectory of the virtual agent. These approaches provide a suitable means to map the vehicle's configuration space to the group's configuration space, and ensure that the decentralised behaviour is directed towards a common goal. A recent body of work [66] considers the use of coordination variables (similar to Belta and Kumar) to unify the leader-follower approach with the purely decentralised strategy. In this unified framework, a coordination variable describes the desired group state from the observed states of the vehicles. Local control laws for each vehicle are then constructed using locally sensed information to achieve the desired coordination variable. The work presented in this thesis follows in similar spirit to the concepts introduced by this unified architecture. In the next section, the inter-vehicle relationships in a decentralised architecture are discussed.

1.3.2. INFORMATION FLOW IN DECENTRALISED SYSTEMS

An intuitive approach to capturing the local interactions of vehicles in a group, is to model this aspect of the information flow using graphs [46, 112, 120, 127, 128, 144, 147, 198-201]. In this approach, the group of vehicles is enumerated by a set of vertices, and interactions between adjacent vehicles denoted by the existence of an edge. Connectivity of the underlying graph topology is then specified by the *adjacency matrix*. In multi-vehicle systems, the connectivity of the underlying information graph is dependent on the states of the vehicles and evolves with the motion of the individuals. The spatiotemporal nature of the information graph is described by a *switching network*. Work on state-dependent graphs and switching networks is presented in [146, 148, 201, 202].

In [203], the discussion on state-dependent graphs provided in [202] is extended to demonstrate the relationship between the edges of a graph and the state of its mobile nodes. A weight is assigned to each edge of the graph that attenuates with the distance between adjacent nodes to provide the framework for the evolution of the network. A similar notion to

the attenuation of the finite interaction range of physical sensors and communication systems is considered in [200], where the notion of a *spatial adjacency matrix* is defined for both the omni-directional and non-omnidirectional case. Using the spatial adjacency matrix to model the local interactions of the vehicles, the underlying graph topology for the information flow is *directed*, and inter-vehicle relationships are non-commutative.

These methods capture the information flow in a straightforward manner. Recently, the algebraic properties of graphs have been investigated as a topic of interest for the analysis of interconnected systems. A parameter of significant interest to the study of information flow in decentralised systems is the graph Laplacian. It was shown in [204], that the topology of the interconnected graph for a group of vehicles determines the controllability of the group of agents. For a group of vehicles using nearest-neighbour rules, controllability is determined by the spectral properties of the graph Laplacian. In [144, 145], Fax and Murray developed a Nyquist-like criterion to investigate the effect of the information network on formation stability. Here, the spectral properties of the graph Laplacian played an important role in determining the desirable structural properties of the underlying graph topology. Following the work of Fax and Murray, various authors have also investigated the stability of a formation by using the spectral properties of the graph Laplacian (see [120, 205-207] for examples).

1.4. COOPERATION AND COORDINATION

The distributed nature of the cooperative control problem introduces the potential for disparities and inconsistencies in the vehicle's goals, plans, and knowledge [107]. To achieve coherent problem solving and cooperation in the vehicle's objectives, vehicles must share a consistent view and reach a consensus in the shared information; either through goals, knowledge, or a combination of both. Convergence to a common value is called the *consensus* or *agreement* problem in the literature. Information consensus guarantees that vehicles sharing information over a time-varying network have a consistent view of information appropriate for the coordination task.

1.4.1. CONSENSUS ALGORITHMS

A consensus algorithm provides a means by which distributed or decentralised systems can reach an agreement over shared information [208, 209]. Examples of the information state can include position, orientation, and shape of a formation [167, 210], the rendezvous time

for object manipulation and interception tasks [83, 211-213], the directivity of a swarm or multiple vehicles [46, 64, 214], or the cost of an aggregate function for cooperative decision-making [215-218]. As a result, consensus algorithms have applications in rendezvous [213, 219-224], formation control [121, 145, 198, 207, 225-227], flocking [56, 126-129, 228-230], attitude alignment [46, 64], decentralised task assignment [133], and sensor networks [90, 95, 99, 231, 232]. A growing body of work focuses on designing and analysing algorithms that make individual network agents agree upon the value of some function of their initial states. These include average-consensus [208, 233], and average max-min consensus [234]. In these works, the state variables associated to the individual agents do not necessarily correspond to physical variables, such as spatial coordinates or velocities. Rather, the information state could be partial solutions to a group objective. Based on the distributed nature of the information flow, consensus algorithms are designed with localised communication strategies [235].

The theoretical framework for posing and solving consensus problems for networked dynamic systems was introduced in [233, 236] by Olfati-Saber and Murray. For continuous information flow, the information state was modelled using a first-order differential equation [46, 145, 208, 233, 237, 238]. Based on the connectivity of the network, the state information of each vehicle was shown to converge to the information state of its neighbours. Work on discrete-time consensus protocols was also presented in [46, 238, 239] where the information state of each vehicle was updated by a first-order difference equation. It was shown in [238] that the information state of each vehicle in the discrete-time consensus protocol was updated as the weighted average of its current state and the current states of its neighbours.

Recently, the consensus problem has been applied to second-order differential equations [240, 241]. In [240], the consensus algorithm is extended to double integrator dynamics with information exchange topologies that switch randomly. Unlike the consensus algorithm for single integrator dynamics, more stringent conditions are required to guarantee consensus under switching directed topologies using consensus algorithms with double integrator dynamics.

1.4.2. CONVERGENCE AND STABILITY OF CONSENSUS ALGORITHMS

In [233], the convergence of a consensus algorithm was shown to be related to the graph Laplacian and its spectral properties. According to Geršgorin's disc theorem, all eigenvalues of the graph Laplacian have non-negative real parts, and the information state converges to

the kernel of the Laplacian. For a connected graph, the second smallest eigenvalue of the Graph Laplacian (i.e. the *Fiedler eigenvalue* [242]) provides a measure of the speed of convergence for a consensus algorithm [233]. Following the spectral properties of the graph Laplacian obtained using Geršgorin's disc theorem, it was shown in [211] that under a time-invariant information exchange topology, that the information state of each vehicle asymptotically reaches consensus if and only if the information exchange topology has a spanning tree. Furthermore, it was shown in [233] that for a strongly connected time-invariant information exchange topology, that consensus is achieved when the information state of each vehicle converges to the average value of the initial information state of each vehicle.

In practice, the information exchange topology for a group of vehicles is time-varying due to the motion of the vehicles. Consensus on time-varying networks has been studied in the literature where they are commonly referred to as *switching networks* [46, 128, 208, 230, 233, 235, 239]. Convergence analysis for a consensus protocol over a switching network is equivalent to stability analysis for a hybrid system [233]. In this formulation, the information exchange topology is piecewise constant over finite lengths of time, called the *dwell times* [46]. This induces a time-varying graph Laplacian that is piecewise constant over the dwell times. Proving consensus on a switching network is equivalent to proving convergence of an infinite product series describing the piecewise constant graph Laplacian. Jadbabaie et al. [46] uses this result to demonstrate the heading angles of a swarm of vehicles achieves consensus using nearest-neighbour rules based on Viscek et al.'s model in [43]. Nonlinear analysis has also been used to study consensus algorithms on switching networks [237, 239]. In these approaches, a set-valued Lyapunov approach is used to consider consensus problems with time-dependent communication links.

1.5. APPROACHES TO COOPERATIVE CONTROL

Various control strategies for cooperative multi-vehicle systems have been proposed in the literature using methods based on artificial potential fields, decentralised optimisation, and virtual structures. Many of these approaches impose certain information architectures, such as leader-follower [117, 143, 188-190, 192, 193, 243], or symmetric neighbour relations [216, 244, 245]. In the following sections, the various types of controllers used for cooperative control within the framework of decentralised architectures are discussed.

1.5.1. OPTIMISATION-BASED APPROACHES

Optimisation-based techniques for control are amenable to the multi-vehicle cooperative control problem. In this approach, a team objective is formulated using a cost objective function. When the problem is coupled, the control problem is cooperative and the task performance depends on the joint locations, roles, and inputs of the vehicles [246]. Solving the coupled objective function can be achieved through a centralised control architecture. Vehicle states, roles, and inputs are solved by a central computing facility and transmitted to the appropriate vehicles. For large-scale multi-vehicle systems, this can be computationally intractable or impossible based on communication constraints.

Ideally, the problem should be distributed to exploit the distributed nature of the vehicles. When the cost objective can be decoupled, the problem is distributed. Note, this form must preserve the original cost objective and some couplings will remain. The distributed control problem becomes a decomposition of the centralised cost objective to a set of sub-problems that are then distributed to each vehicle. If the goals are fixed and known at design-time, local control laws can be designed for each vehicle to solve the sub-problems [187]. In [247], the problem of generating optimal trajectories for a set of cooperative aircraft is addressed using a dual decomposition approach to decompose a large computationally intractable problem to a series of smaller tractable problems. Using this method, various numerical and analytical techniques can be used to solve the underlying optimisation problem. These include (but not limited to) mathematical programming techniques such as Mixed-Integer Linear Programming (MILP) and Nonlinear Mixed-Integer Linear Programming (NMILP) [68, 118, 131, 136, 248-250], intelligent-based metaheuristics such as genetic algorithms and neural networks [251-253], and geometric control techniques [114, 254, 255].

In some cases, it may be difficult to decompose a centralised global objective to a group of vehicles. One approach to formulating the problem is to use strictly local goals [187]. Local goals react to the vehicle's immediate environment, and solutions to the vehicle sub-problem are locally optimal. No cooperation is observed since there is no coupling or relationship between the individual goals. Strictly local control laws are an example of a decentralised optimisation problem where global functionality is an emergent property of the locally interacting vehicles. Using the notion of decomposition variables and overlapping constraints, [216], Inhalhan et al. developde the framework for a decentralised cooperative control of a group of vehicle. The centralised optimisation problem presented in [216] was described using the set of local performance function representing the goals of each vehicle. Optimality

(from a centralised perspective) for the decentralised system in [216] was shown to be Pareto optimal.

An intuitive approach to designing control laws for the decentralised strategy is through Model Predictive Control (MPC) (see [68, 136, 256-259] for applications to multi-aircraft systems). Distributed model predictive control has been proposed recently as a method for the coordination of multi-vehicle systems. Previous work on distributed model predictive control include Jia and Krogh [260], Motee, Jadbabaie, and Sayaar-Rodsaru [261, 262], Keviczky, Borelli and Balas [263-266], Dunbar and Murray [267-270], Kuwata, Richards, Schouwenaars and How [256, 271], and B. Johansson, Speranzon, M. Johansson, and K. Johansson [218]. In Camponogara, Jia and Krogh [272], the subsystems are coupled via states. Adjacent subsystems are coupled via dynamics and neighbouring subsystem states are treated as bounded contracting disturbances. An example of such a situation is a group of vehicles cooperatively converging to a desired formation. In contrast, Dunbar and Murray [267-270] considered the control of initially dynamically decoupled subsystems and introduced a coupling between adjacent systems using non-separable cost functions. In Dunbar and Murray approach, each vehicle communicates their most recent optimal control policy to neighbouring vehicles to cooperatively stabilize the formation to an equilibrium state. Stability of the interconnected system is guaranteed through the use of a compatibility constraint. The compatibility constraint restricts the deviation of transmitted plans from the executed plans. This introduces a significant degree of conservatism to the centralised problem and reduces the ability of MPC to recompute new optimal actions based on current conditions. Relaxing the compatibility constraint allows for greater deviations between successive plans at the risk of propagated instabilities. This restriction limits the application of distributed MPC to applications where the environmental conditions do not deviate significantly between successive sampling periods or where replanning does not interfere with previous plans.

A decentralised approach to MPC has been proposed in Camponogara, Jia and Krogh [256, 271] where the subsystem dynamics and cost functions are independent and only the states and inputs variables of neighbouring systems are coupled. The strategy was applied to a multi-vehicle scenario of linear dynamically decoupled subsystems with coupling constraints. In this application, vehicles update sequentially (in order), and are subject to linear collision avoidance constraints. The distributed MPC problem is solved using a mixed integer linear programming (MILP) approach and neighbours whose update has not occurred in the

sequence, are viewed as bounded, contracting disturbances (as in Jia and Krogh). Although this approach is effective for simple problems and aircraft models, this formulation is limited to linear constraints and objective functions. Recently, Keviczky et al. [263-266], have formulated a distributed model predictive control where each subsystem optimizes locally for itself and every neighbour at each update. The stability conditions for the interconnected system was established in [273] where it was shown that for sufficiency, the rate of information exchange needed to be increased as the system approached equilibrium. It was also shown that the performance deteriorates after a critical horizon length and system instabilities would be observed. While this approach has been shown to demonstrate appreciable convergence towards a global objective, each subsystem requires a model of neighbouring subsystems to solve the local optimisation problem at each sampling period. From a practical perspective, this approach may be limited by the available onboard computational resources, bandwidth, and knowledge of neighbouring subsystem plants. In addition, the solutions for neighbouring subsystems are often discarded and provide a prediction for the behaviour of neighbouring subsystems. It is still possible for neighbouring vehicles to deviate from this assumed behaviour without the addition of a compatibility constraint as suggested in [267-270].

1.5.2. BEHAVIOUR-BASED AND ARTIFICIAL POTENTIAL FIELD TECHNIQUES

In behaviour-based approaches [195], each vehicle has a set of basic motor schemas. Each schema represents a desired behavioural response to sensory input. Possible motor schemas include collision avoidance, obstacle avoidance, group migration, and formation seeking [274, 275]. Often these behaviour-based control techniques are combined with *artificial potential field* methods to create simplistic control laws [276, 277].

Potential field techniques for robotic applications were first described by Khatib [278] and have since been widely used in the mobile robotics community for tasks such as local navigation and obstacle avoidance [48, 275, 279-281]. In this method, a robot is modelled as a moving particle inside an artificial potential field generated by superimposing an attractive potential that pulls the robot to a goal configuration and a repulsive potential that pushes the robot away from obstacles [275]. Each vector potential represents a schema of the behaviour-based controller. The negative gradient of the generated global potential field is interpreted as an artificial force acting on the robot and dictating its motion.

The direct mapping between the sensory inputs and the actuator outputs provides a highly reflexive system for mobile path-planning and navigation. Selection of an appropriate artificial potential field can be difficult due to the emergent nature of the design process. One method for ensuring that an artificial potential field contains no local extrema is to formulate it as a *harmonic function* [282]. Various harmonic functions have been used in the field of mobile robotics for navigation, including stream functions (from potential flow theory) [282], Van der Waal forces, Morse functions [125] and Lennard-Jones type potentials [32, 283, 284].

Recently, artificial potential field methods have been extended to group behaviours such as swarming and flocking [32, 48, 51, 125, 193, 283-286], formation control [123, 287, 288], and distributed and decentralised sensory networks [95, 231, 289]. In Leonard and Fiorelli [188, 231], artificial potential fields were constructed in a virtual leader-follower architecture for formation control. Virtual leaders were used to describe a moving frame of reference that influenced the behaviour of the neighbouring vehicles (followers). Based on the leader-follower architecture, a control law using potential functions describing the inter-vehicle interactions of the followers, and the navigation of leaders was derived.

Each of the vehicles in the swarm move so as to minimise the total artificial potential energy in the system. By appropriate choice of potential function they are able to show asymptotic stability of various schooling and flocking behaviours. The framework presented in [188] allows for a homogenous group invariant to ordering, and size. Using this approach, Leonard and Fiorelli demonstrated the reactive nature of artificial potential field functions for flocking and schooling of multiple vehicles.

One of the limitations induced by Leonard and Fiorelli's control algorithm is the explicit nature of the communication network. Olfati-Saber [283] extended the work of Leonard and Fiorelli to include bump functions to truncate the artificial potential field induced by each agent and localise interactions to adjacent neighbourhoods. The distributed control law described by Olfati-Saber is used to synthesise flock behaviour. A similar approach using magnetic fields was proposed by Sigurd and How for collision avoidance in [281]. In [281], vehicles were modelled using a magnetic dipole to construct an artificial potential field from the magnetic density decay functions. This allowed the field generated by vehicles to be measured by neighbouring vehicles using single-axis magnetic sensors placed orthogonal to the generated field. Based on this measurement, a navigation function could be constructed from the gradient of the potential field to avoid collisions. [281] provided a novel and

practical demonstration of artificial potential field theory for the navigation of large groups of vehicles in a shared environment.

Behaviour-based and artificial potential field approaches are often limited in a fundamental theoretical understanding of how the complex global behaviour of the interconnected system emerges from the simple local interactions of the individuals. Often, these approaches rely on extensive empirical data and experience to design the appropriate control laws that yield the desired functionality of the system. Problems associated with the use of artificial potential field methods are attributed to the local minima that arise from the construction of complex potential environments from the simplistic behaviour-based vector fields. When the scaling parameters are improperly balanced, unpredictable and sub-optimal results can ensue. For example, if an attractive potential of a goal location is inadequately scaled with respect to the repulsive potential of an obstacle, the vehicle may fail to reach the desired destination [275]. The lack of an analytical design guideline limits the practical application of artificial potential based control systems [275].

1.5.3. VIRTUAL STRUCTURES AND RIGID BODY FORMULATIONS

Many of multi-vehicle applications have as part of their solution, the ability to collectively navigate through the environment and maintain geometric compliance to a desired structure. Using a centralised architecture, the simplest approach involves generating a set of reference trajectories and control laws for each vehicle in the group [290, 291] to manoeuvre each vehicle between configurations and avoid collisions [167]. In large-scale systems, the problem becomes computationally intractable as the size of the group increases. Communication and computational constraints limit the feedback to a centralised informant to process and deconflict the information at each sampling period. From a high-level supervisory perspective, the motion generation/control problem should be reduced to a lower-dimensional space that captures the behaviour of the group to minimise control effort at the supervisory level [167]. This is similar in notion to swarming; where the exact behaviours of the vehicle are of insignificant interest relative to the collective group behaviour.

One approach to reducing the control effort to a lower dimensional space is to model the group of vehicles as a *virtual structure* [292]. The concept of virtual structure was introduced in [292]. In the virtual structures approach, the motion of the group is treated using rigid body formulations, where each vehicle is represented by a particle in the system. Each particle in the structure maintains a fixed geometric relationship in the virtual structure [292]. The rigid

construction of virtual structures is amenable to the modelling of *formation graphs* [111, 293-295]. In [296, 297], the rigidity constraints of the virtual structure are relaxed to investigate the propagation of disturbances on a swarm. The resulting model is based on the concept of *tensegrity structures* where the inter-vehicle relationships are modelled using struts and cables. Using the rigid-body model, the motion-planning problem is reduced to a left-invariant control system on $SE(n)$, and the individual trajectories are $SE(n)$ orbits [167]. Motion-planning on $SE(n)$ involves the choice of a distance metric (see for example [291, 298]). The necessary conditions for rigid-body motion using distance metrics are derived in [291]. [113] and [299] extend the generation of optimal trajectories on $SE(n)$ to a formation of mobile robots using Lyapunov energy-type functions. Examples of such functions include positive definite convex *formation functions* [117, 294] and biologically inspired *artificial potential functions* [123]. The global minima of such functions exhibit $SE(n)$ symmetry, and expansion/contraction symmetries. These can be decoupled into group-level motion planning, and local-vehicle formation-keeping [123].

Virtual structures modelled on formation graphs and tensegrity structures unnecessarily constrain the problem. Formation graphs require identification and ordering of vehicles, which makes the overall architecture sensitive to failures, and re-organisation [210]. The rigidity constraint of the virtual structure approach is relaxed in [167] to control a scalable group of vehicles. In [167] an abstraction based on *Lie groups* (position and orientation of the vehicles) and *shape manifolds* for the group is presented that reduce the control variable to a lower dimensional manifold with a product structure. The resulting expression is a permutation and size invariant state description of the swarm. Decoupled controllers are then designed for each vehicle using feedback dependent on the current state of each vehicle and the state of the abstract manifold. [210] extends the work of [167] to address the problem of controlling a swarm of fully actuated point-like vehicles moving in three dimensions. A nine-dimensional abstraction for the swarm is used to capture the position and orientation of a spanning ellipsoid and is invariant to number of vehicles and permutations. The framework presented in [210] was again dependent on a supervisory agent. Vehicles represented in this scheme were characterised by simple feedback controllers and were socially incapable of self-organised or cooperative behaviour. The dependency of vehicles on a supervisory agent for group feedback limits the use of virtual structures to small-scale vehicle groups, such as spacecraft and satellite formations [57, 64, 66].

1.6. CONTRIBUTION AND OUTLINE

The goal of this dissertation is to develop a framework for controlling large groups of cooperative vehicles using decentralised control strategies. The research builds on the current body of knowledge to address the deficiency in mapping local interactions to purposeful group objectives. Traditionally, this problem has been approached either from the bottom-up or from the top-down. In the bottom-up approach, the local objectives of the vehicles have been designed using local interaction protocols. Examples of these include the phenomological models of socio-biological swarms. While these approaches accurately mimic the local interactions of natural flocks and swarms, there is little understanding of how or whether these strategies can be applied practically to solve a group objective. Approaching the control design using a top-down design strategy, involves decomposing a large-scale global group objective into a series of local subproblems. From a practical perspective, this approach can provide formal guarantees to the satisfaction of the group objective. Typical examples of this approach include the distributed and decentralised MPC scheme discussed in the literature. Despite the recent successes in developing these strategies, it is almost always implied that the group objective can be decomposed into a set of local objectives (for the distributed case) or that the local objectives somehow summate to produce the group objective (for the decentralised case). They also fail to account for the case when the group objective is intrinsically linked to the network topology. Often, these distributed and decentralised approaches assume a network topology that describes the interaction of the subsystems, and a cost function to describe the performance of the interacting subsystems. In some cases, such as in flocking, the network topology and the cost function are intrinsically linked together. Performance of the group is affected by their relative network topologies and the local interaction protocols. In this thesis, the problem of synthesising a group of agents to self-organise and direct their behaviour towards a common goal is addressed using both local network protocols and global objective functions. To frame this problem in a familiar and practical setting, the method is applied to a group of cooperative swarming UAVs. Local network protocols are represented by the flocking behaviour of neighbouring vehicles, whilst the group objectives are represented by the state of the collective group. The aim of this work is to answer the questions of whether and how the global group objectives can be achieved using purely localised rules of interactions.

This thesis presents the fundamental and theoretical works necessary to consider the development of a group of cooperative systems. The systematic presentation of these results

and the developed framework aims to provide practitioners a design approach for cooperative control systems. The remainder of this thesis is organised as follows. In Chapter 2, the information flow in a distributed system is investigated. Relevant ideas from the literature on algebraic graph theory are presented in preparation for the development of distributed control schemes in later chapters. Problems relating to the distribution of information are addressed, and a generalised model for the group of vehicles is presented. Consensus algorithms, consistent with the literature, are derived using properties from algebraic graph theory. The necessary and sufficient conditions for consensus in a distributed system under fixed and switching networks are described. A simple closed feedback consensus protocol is presented that achieves consensus on the coordination variable for a group of cooperative agents. The results of this chapter provide the theoretical framework for the developments in later chapters. Numerical simulations are also provided to illustrate the theory.

Chapter 3 presents a flocking protocol based on the generalised information consensus protocol presented in Chapter 2. The flocking protocol demonstrates consensus in the spatial distribution vehicles via numerical preference. Potential field functions are constructed to model the finite interactions of natural flocks and swarms. Using Lennard-Jones type potentials, stability is proven via Lyapunov arguments. Conditions for the asymptotic convergence for a group of vehicles to a stable flock configuration are also presented. Group level abstractions of the converged flock configuration are then discussed. These group level abstractions provide a low dimensional representation of the group at the supervisory control level, and permit a scalable approach to representing the shape spanned by the configuration of vehicles.

Chapter 4 approaches the problem of controlling the large group of vehicles as a unified structure and defining suitable optimisation problems for group navigation. It follows from the abstractions demonstrated by the group of vehicles applying the flock protocol and presents a rigid body construction for the flock configuration. Chapter 4 begins with a brief introduction of differential geometry. A review of the existence of useful metrics for the group navigation problem is then presented. The necessary conditions for generating optimal motions for the collective flock at the supervisory level are then presented. Following the works of Belta and Kumar in [254], a semi-rigid body model is introduced to consider the transition of the group of vehicles from an initial configuration to the rigid flock configuration. A modified metric for the semi-rigid body model of the evolving flock is then

presented. This provides a path planning method for a subset of vehicles to trace out a shape spanned by the group to conform to.

The problem of mapping the local interactions of the vehicles described in Chapter 3 to the group objectives presented in Chapter 4 is addressed in Chapter 5. A cooperative control scheme based on traditional model predictive control (MPC) is presented. The cooperative control scheme is implemented by decomposing the group task, to individual optimisation problems at the individual vehicle level. The decentralised MPC scheme allows the vehicles to deliberate the influence of their actions on the collective goal at each sampling period. Using the network exchange topology in Chapter 2, the vehicles exchange their plans at successive update periods, and negotiate a consensus on the cooperative solution. Sufficient conditions for convergence to a consensus are presented. The effect of coupling information is also discussed, and limitations of the implementation scheme are described.

Chapter 6 combines the developments of Chapter 3, Chapter 4, and Chapter 5 to present a unified framework for controlling a swarm of vehicles. The framework is demonstrated for a group of vehicles tasked with the cooperative objective of flock convergence in the local frame, and conformance to the prescribed shape and motions of a supervisory controller. The experiments validate the proposed framework and its applicability to the cooperative control problem. A detailed summary of the contributions of this thesis, and extensions for future research are presented in Chapter 7.

Chapter 2. Information Exchange and Consensus

In a multi-vehicle system, vehicles depend on information from neighbouring vehicles to cooperate and avoid conflicts. When the vehicles are coupled by a shared objective, the coupling naturally suggests what information should be available to each vehicle of the decentralised controller. Local information can be obtained through direct observation (*sensory perception*). Physical sensors, such as GPS and IMU, provide local state information regarding position, roll rate and bank angles, whilst long-range sensors such as cameras, laser range finders, and radar can provide non-local information, such as the position of neighbouring vehicles and obstacles. The accuracy and perspective of the information available to a vehicle by direct observation or state estimation, is limited by the sensors' range, resolution, and calibration error. In non-omnidirectional sensors, such as cameras, antennas, and radar, limitations also arise due to the directivity patterns of the sensor. Peer-to-peer communication (or *communication exchange*), can be used to resolve the limitations of the onboard sensors, and improve the resolution, accuracy and perspective of a vehicle. The use of communication networks to improve the quality of information is the basis of many distributed sensory systems and include applications such as Simultaneous Localisation and Map building (SLAM), and Decentralised Data Fusion (DDF) [300-303].

Central to any discussion on distributed multi-agent and multi-vehicle systems is the nature of *information flow* through the communication network. Properties such as the communication topology, and the propagation of information, impact the performance of the interconnected system. In a strongly connected and complete network, vehicles exchange information with every other vehicle in the group, and complete knowledge of the connected system is propagated to each node. This implies *maximal information flow* and centralises the control problem to each node. Whilst this strategy improves the redundancy of the system and can guarantee optimality, several factors limit the possibility to convey and use global information for multi-vehicle systems. Firstly, the communication topology of a group of vehicles is an intrinsic property of the vehicles' positions. The dynamic nature of the vehicles implies a dynamic communication topology that switches with accordance to the relative

position of the vehicles. In a group of vehicles navigating an obstacle field, the information flow is subject to link failure and creation as neighbouring vehicles negotiate obstacles. Limitations on hardware capabilities also act to reduce the area that information can be propagated and shared. These include available bandwidth, corruption of communication signals over large distances, interference, and transmitting power.

The distributed nature of the information flow naturally implies an inconsistent view of the entire system. For cooperative control strategies to be effective, neighbouring vehicles must share a consistent view of the environment. This shared information can take the form of a cooperative objective, state information, or internal model of the environment. A direct consequence of this assumption is that the group must reach a consensus on the shared information.

In this chapter, the consensus problem over spatiotemporal networks is investigated. The interplay between the communication topology and information consensus is investigated using methods from algebraic graph theory. For the purposes of generality, the physical realisation of the communication network is ignored and left for future development. The main application of these ideas will be the development and analysis of communication protocols for cooperative control strategies.

The aim of this chapter is to introduce the main concepts of information flow and provide a cohesive overview of the problems associated to network control design. Similar work can be found in Jadbabaie et al. [46], Olfati-Saber and Murray [233], Fax and Murray [145], Moreau [239], and Ren and Beard [208]. The main contribution of this chapter is to unify these concepts into a single mathematical framework, and highlight some of the important results from these key research areas that will be instrumental in cooperative control strategies. This chapter is organised as follows: in Section 2.1, a graph theoretic approach to modelling the communication network is presented. A consensus protocol based on the sum-of-squares properties of graphs is then presented in Section 2.2. This is followed by a stability and performance analysis of the system on a static network. Section 2.3 extends the works to include spatiotemporal networks (*switching networks*) before a summary of major results is presented in Section 2.4.

2.1. A GRAPH THEORETIC MODEL TO DISTRIBUTED SYSTEMS

In the following section, a brief review of graph theory is presented. Graphs are used to model the distributed nature of entities and their relations. In a group of vehicles, the communication network and spatial distribution can be modelled using a graph. The notions presented in this section provide the theoretical framework for the development and analysis of distributed systems and control laws used in later chapters. For a thorough analysis of graphs and their properties, see [304], [305] and [306].

2.1.1. BASIC DEFINITIONS

A graph G is a pair consisting of a set of vertices (or nodes) $V = \{v_1, v_2, \ldots, v_N\}$, and a set of edges $E \subseteq V \times V$. In a multi-vehicle system, each vehicle can be modelled as a vertex v_i in the graph G with spatial adjacency and connectivity described by the set of edges $e = (v_i, v_j) \in E$. The *order* $|V|$ and *size* $|E|$ of a graph G physically represents the number of vertices in the graph and the number of edge connections. Information flow from vehicle v_i to v_j is given by the path connecting v_i to v_j such that $(v_i, v_j) \in E$. An *undirected* (or bi-directional) graph satisfies the following edge relationship $\forall (v_i, v_j) \in E \Rightarrow (v_j, v_i) \in E$. Note, the equivalence relation is not preserved for *directed graphs*; i.e., the ordering of vertices is not commutative $\forall (v_i, v_j) \in E \Rightarrow (v_j, v_i) \notin E$ (Figure 2-1 (a)). The spatial distribution of vehicles in a formation is an example of an undirected graph since the inter-vehicle distances are commutative. Note, whilst the distribution of vehicles on a Euclidean space is an example of an undirected graph, the information flow is not necessarily represented by a directed graph. The directivity patterns of the communication links may restrict the flow of information in one direction and induce a directed communication graph. Let $\mathcal{N}_i$ denote the subset of vertices v_j that are neighbours of vertex v_i and define the *in-degree* of a vertex v_i as the total number of edges connecting v_j to v_i such that $(v_j, v_i) \in E$ and $v_j \in \mathcal{N}_i$. Similarly, define the *out-degree* of a vertex v_i as the total number of edges v_j to v_i such that $(v_i, v_j) \in E$ and $v_j \in \mathcal{N}_i$. Then, the *degree* $\deg(v_i)$ (or *valency*) of a vertex v_i is the number of edges incident to v_i and corresponds to the total number of its neighbours $|\mathcal{N}_i|$. For an

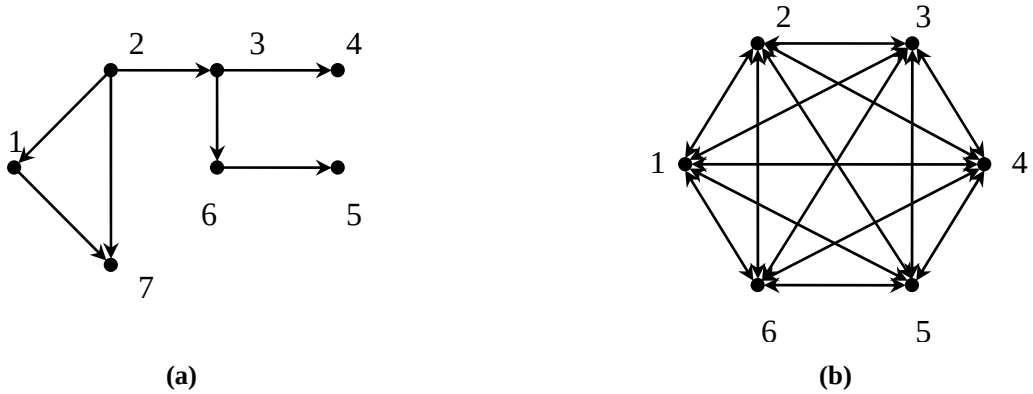

(a) **(b)**

Figure 2-1. (a) Sample directed graph G on $V = \{v_1, v_7\}$ with edge set $E = \{(v_1,v_7), (v_2,v_1), (v_2,v_7), (v_2,v_3),\ldots (v_3,v_4), (v_3,v_6), (v_6,v_5)\}$. (b) Sample undirected and complete graph G.

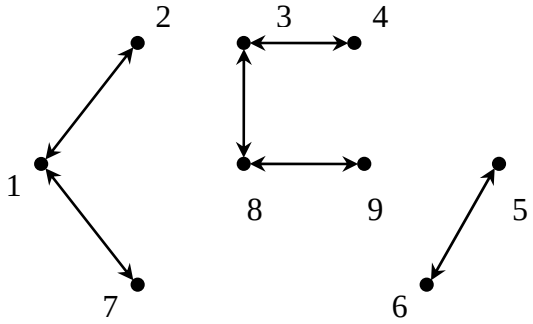

Figure 2-2. A graph with three components $\{(v_1, v_2, v_3), (v_3, v_4, v_8, v_9), (v_5, v_6)\}$.

undirected graph, the in-degree and out-degree of a vertex are equal. When every possible edge exists in a graph, the graph is said to be *complete* (Figure 2-1 (b)). A graph G is *connected* if there is a path in G between any given pair of vertices, and *disconnected* otherwise. Every disconnected graph can be split into a number of connected sub-graphs, called *components* F (Figure 2-2). The number of components of G is denoted as $c(G)$. A graph G is *strongly connected* if there exists a path in G from any given vertex to any other vertex in G.

2.1.2. ALGEBRAIC GRAPH THEORY

One area of graph theory that is useful for modelling and analysing interconnected systems is *algebraic graph theory*. Algebraic graph theory provides a matrix representation to the graph structures described using set notation in traditional graph theory. In the following section, the basic concepts of algebraic graph theory are reviewed for the modelling and analysis of networked systems. For a thorough treatment of algebraic graph theory, see [304-306].

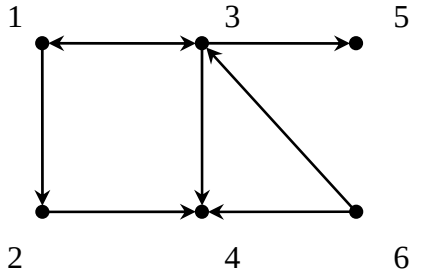

$$A = \begin{bmatrix} 0 & 1 & 1 & 0 & 0 & 0 \\ 0 & 0 & 0 & 1 & 0 & 0 \\ 1 & 0 & 0 & 1 & 1 & 0 \\ 0 & 0 & 0 & 0 & 0 & 0 \\ 0 & 0 & 0 & 0 & 0 & 0 \\ 0 & 0 & 1 & 1 & 0 & 0 \end{bmatrix}$$

Figure 2-3. Sample graph *G* and associated adjacency matrix *A*.

Let $G = (V, E)$ denote the graph with vertices v_i enumerated by $i = 1, \ldots, N$. The connectivity of the graph is described by the square matrix A (known as the *adjacency matrix*) with size $|V|$, and elements a_{ij} describing the connectivity of adjacent vertices v_i and v_j such that:

$$a_{ij} = \begin{cases} 1, & \text{if } (v_i, v_j) \in E \\ 0, & \text{otherwise} \end{cases} \tag{2.1}$$

An adjacency matrix defined in this way uniquely specifies an enumerated graph. Note that the adjacency matrix described in Equation (2.1) is discrete. In the proceeding analysis, a continuous approximation to Equation (2.1) is considered. An example of an adjacency matrix for a connected graph is given in Figure 2-3.

On a metric space, the adjacency of two vertices can be described using a *distance metric*. When the graph is used to describe the spatial distribution of a group of vehicles, the vehicles reside on a Euclidean space. The Euclidean norm provides a suitable metric to define the adjacency of neighbouring vehicles on a Euclidean space. Let $d_{ij} = \|x_i - x_j\|$ denote the Euclidean norm of two vertices, v_i and v_j, and let r denote a threshold on the interaction range of vertex v_i. Two vertices v_i and v_j are connected if and only if $d_{ij}/r \leq 1$. Let P denote the set of continuous locally Lipschitz functions with elements $\rho_{ij} : \mathbb{R} \to \mathbb{R}$ associated to the edge $e_{ij} = (v_i, v_j) \in E$ of graph G. Then a continuous approximation to the step function in Equation (2.1) is given by the following bump function:

$$a_{ij} \coloneqq \rho_{ij}(d_{ij} / r) \tag{2.2}$$

As an example, the following bump function is considered as a candidate function of the adjacency matrix:

$$\rho_{ij}(z) = \begin{cases} 1, & z \in [0, \varepsilon) \\ C^k(z), & z \in [\varepsilon, 1] \\ 0, & \text{otherwise} \end{cases} \tag{2.3}$$

where $\varepsilon \in (0,1)$, and $C^k(z)$ is a C^k continuous function. A formal definition of the bump function $\rho_{ij}(\cdot)$ in Equation (2.3) is given with respect to a vehicle's sensory and communication capabilities in Section 3.2.1.

Using Equation (2.1) or Equation (2.2), the neighbours of a vertex v_i can be defined using the following set notation:

$$\mathcal{N}_i = \{v_j \in V : a_{ij} \neq 0\} = \{v_j \in V : (v_i, v_j) \in E\} \tag{2.4}$$

Note $a_{ii} = 0$ for all v_i, and the graph has no loops, i.e., $(i,i) \notin E$.

Let Δ denote the $N \times N$ *degree matrix* defined as $\Delta = \Delta(G) = \{\Delta_{ij}\}$, where:

$$\Delta_{ij} = \begin{cases} \deg(v_i), & i = j \\ 0, & i \neq j \end{cases} \tag{2.5}$$

The degree provides a measure of the adjacency of vertices in a graph.

Associated with the adjacency and the degree matrices, is the *graph Laplacian* L. The Laplacian of a graph is defined as[1] [306, 307]:

$$L = \Delta - A \tag{2.6}$$

As an example, consider the graph given in Figure 2-3. The Laplacian associated to Figure 2-3 is given by:

$$L = \begin{bmatrix} 2 & -1 & -1 & 0 & 0 & 0 \\ 0 & 1 & 0 & -1 & 0 & 0 \\ -1 & 0 & 3 & -1 & -1 & 0 \\ 0 & 0 & 0 & 0 & 0 & 0 \\ 0 & 0 & 0 & 0 & 0 & 0 \\ 0 & 0 & -1 & -1 & 0 & 2 \end{bmatrix} \tag{2.7}$$

In multi-vehicle systems, this shared information can take the form of an n-dimensional ($n \geq 1$) vector. The following *n-dimensional graph Laplacian* is defined for the generalised case:

$$\hat{L} = L \otimes \mathbf{1}_n \tag{2.8}$$

where $\otimes$ denotes the Kronecker product, and $\hat{L}$ is a matrix of dimension $nN \times N$.

---

[1] In [150] the graph Laplacian was defined as $\Delta^{-1}(\Delta - A)$. In general, there is no contention for a proper definition of the graph Laplacian L. Regardless, the distinction between the various definitions is of little consequence to the theory.

By definition, every row sum of the Laplacian matrix is zero. Therefore, the Laplacian matrix always has a zero eigenvalue $\lambda_1 = 0$ corresponding to a right eigenvector:

$$w_r = \mathbf{1} = (1,1,\ldots,1)^T \tag{2.9}$$

and identical nonzero elements. This means that $\text{rank}(L) \leq N-1$. Associated with the graph Laplacian, is the *Laplacian potential* given by [236]:

$$\Psi_G = \frac{1}{2} x^T L x \tag{2.10}$$

Following the definition of the Laplacian potential, the following lemma summarises some of the basic properties of graph Laplacians.

Lemma 1. (Undirected Graphs)

Let $G = (V, E)$ with a non-negative adjacency matrix $A = A^T$ of order N. Then, the following properties hold:

1. *If L is a positive semi-definite matrix, then the Laplacian potential is also positive semi-definite and satisfies the following sum-of-squares (SOS) property:*

$$x^T L x = \sum_{i,j \in E} a_{ij} (x_i - x_j)^2 \tag{2.11}$$

   Note this positive definiteness of L does not necessarily hold for digraphs [233];

2. *The graph G has $c \geq 1$ connected components if and only if $\text{rank}(L) = N - c$. Particularly, G is connected if and only if $\text{rank}(L) = N - 1$;*

3. *If G is a connected graph, then:*

$$\lambda_2(L) = \min_{\substack{x \neq 0 \\ 1^T x = 0}} \frac{x^T L x}{\|x\|^2} \tag{2.12}$$

   and $\Psi_G(x) = 0$ if and only if $x_i = x_j$, $\forall i, j \in N$.

Proof.

All three results are well-known in the field of algebraic graph theory and their proofs can be found in [306] and [304].

Corollary.

If the graph is connected, then the values of all nodes must be equal.

The last remark provides an important result for the definition of a consensus protocol.

2.2. INFORMATION CONSENSUS IN INFORMATION NETWORKS

In distributed multi-agent systems, cooperating agents must agree on the information that is exchanged between connected vehicles. Shared information can include state information, group objectives, and world information. In this section, the agreement or *consensus* problem is addressed for an interconnected group of vehicles. For the purposes of generality, the problem is formalised using a simplified first-order differential model for the information flow (as in [46, 200, 224]):

$$\dot{x}_i = u_i \tag{2.13}$$

where $x_i \in \mathbb{R}$, and $u_i \in \mathbb{R}$ is the information state and control of vehicle v_i respectively, $\forall i \in N$, and $N > 1$. The information state can represent state information such as position, orientation, velocity, or some other coordination variable representative of the group task. In Chapter 3, this group coordination variable is described with reference to collective navigation of a flock of vehicles. For now, Equation (2.13) is used to represent the information dynamics for each vehicle v_i.

The interaction topology for the network of vehicles is given by the directed graph $G_x = (G, x)$ with concatenated set $x = (x_1, \ldots, x_N)^T$, $x \in \mathbb{R}^N$, and network topology G. Before proceeding with the definition of the consensus problem, some definitions introduced in [233] are re-iterated here:

Definition 1. (agreement)

Two vertices v_i and v_j connected by an edge $(v_i, v_j) \in E \vee (v_j, v_i) \in E$ are said to be in agreement if and only if $x_i = x_j$.

Definition 1 provides a formal description of agreement in cooperative agents. In distributed optimisation problems, the agents share information regarding solution quality to find an optimal solution to a centralised objective function. Two connected agents are then in agreement if and only if, the solutions that have been transmitted are identical. The notion of agreement can then be extended to include the collective graph in the following definition:

Definition 2. (consensus)

The vertices of a network have reached a consensus if and only if $x_i = x_j$, $\forall i, j \in N$, and $i \neq j$; i.e. all vertices are in agreement.

Following the definition of consensus for the group, Definition 3 describes the common value for the network.

Definition 3. (group decision variable)

When the vertices of a network have reached a consensus, the common value of all the vertices is the group decision variable.

The following definition for a subset of vertices in a graph will also provide useful for the formal definition of the consensus problem.

Definition 4. (cluster)

A cluster is any subset $J \subseteq V$ of the vertices of the graph. The proximity graph describing the neighbourhood $\mathcal{N}_i$ of vehicle v_i is an example of a cluster. The set of neighbours of a cluster $\mathcal{N}_j$ is given by:

$$\mathcal{N}_j := \bigcup_{v_i \in J} \mathcal{N}_i = \{v_j \in V : v_i \in J, (v_i, v_j) \in E\} \tag{2.14}$$

Finally, the consensus problem for a network of cooperative vehicles is now described using the concepts introduced earlier.

Definition 5. (consensus problem)

Let $\chi : \mathbb{R}^N \to \mathbb{R}$ be a function of N variables. Let $x_0 = x(0)$ denote the initial state of the system such that $x_0 = (x_1(0), \ldots, x_N(0))^T$. The χ-consensus problem for a group of N vehicles is to design a distributed feedback control law:

$$u_i = k_i(\tilde{x}_i) \tag{2.15}$$

dependent on the states of vertex x_i, and its neighbours' current state $\tilde{x}_i$, $\forall j \in \mathcal{N}_i$ such that all vertices asymptotically reach a stable equilibrium x^e satisfying $x^e = \chi(x_0)$ and corresponding to the group decision variable.

The following definition describes the conditions for asymptotic consensus:

Definition 6. (asymptotic consensus)

The set of vertices is said to have reached consensus asymptotically if $\|x_i(t) - x_j(t)\| \to 0$, as $t \to \infty$ for all $j \in \mathcal{N}_i$.

Table 2-1. Consensus protocols for distributed systems.

$\chi(x) = \text{Ave}(x) = \frac{1}{N}\sum_{i=1}^{N} x_i$	*average-consensus*	(2.16)
$\chi(x) = \max_i(x_i)$	*max-consensus*	(2.17)
$\chi(x) = \min_i(x)$	*min-consensus*	(2.18)

For distributed (and decentralised systems), distributed control laws are of significant utility. Central to the notion of distributed control laws, is the set of protocols that facilitate their implementation within the distributed framework. The following definition for a distributed protocol is provided:

Definition 7. (distributed protocol)

Denote $J_i = \{v_{j_1}, \ldots, v_{j_m}\}$ *the cluster of vertices with indices* $j_1, \ldots, j_m \in N$ *satisfying the property* $J_i \subseteq \{i\} \bigcup \mathcal{N}_i$. *Protocol (2.15) is said to be distributed if* $|J_i| < N$, $\forall i \in N$.

Following the definition of a distributed protocol, several examples of the χ-consensus problem for distributed problem are presented in Table 2-1.

The average-consensus problem (2.16) is an example of a distributed computational problem that yields the average group decision variable from a set of initial states x_0. In a group of vehicles or a school of fish, the attitude/velocity alignment problem is an application of the average-consensus problem [46, 127, 128]. The max-consensus (2.17) and min-consensus problem (2.18) can be used to describe distributed optimisation problems, where the group objective is to find the global minimum or maximum of a centralised objective function respectively [234]. Population based optimisation techniques such as PSO and ACO, are examples of distributed agents using the max-consensus or min-consensus protocols [18, 19]. Due its relevance and extensive application in the biological and engineering fields, the remainder of this chapter is dedicated to the analysis of the average-consensus protocol. While the following analysis and discussion focuses solely on the average-consensus problem, the concepts introduced in this chapter are sufficiently general to accommodate the definition of other consensus problems such as the max-consensus and min-consensus problems.

2.2.1. THE CONSENSUS PROTOCOL

In multi-vehicle systems, a consensus protocol is necessary to describe the mechanism by which neighbouring vehicles reach agreement and lead to group consensus. A simple consensus protocol based on the SOS properties of the interconnected graph G (Equation (2.11)) and Definition 6, can be defined as follows [233, 308]:

$$u_i = \sum_{j \in \mathcal{N}_i} a_{ij}(x_j - x_i) \tag{2.19}$$

Protocol (2.19) provides the closed loop dynamics of system (2.13) for time-invariant and dynamic information using the interconnection topology defined by the adjacency matrix of the graph G. Note, Protocol (2.19) describes a consensus protocol for a network with zero communication time-delays. In many real-world multi-vehicle networks, the physical implementation of communication hardware is plagued with communication lags and limited bandwidths. This can introduce communication delays and degraded performance. Work on communication networks with time-delays is currently an area of active research (see [233, 309] for example) and is beyond the scope of this investigation. For the remainder of this work, it is assumed that the communication is 'lag-free'. While this assumption limits the physical realisation of the communication network, the goal of this work is to provide a generalised theoretical framework for distributed (or decentralised) algorithms, and support the development of more complex communication systems. In the proceeding section, the convergence of the consensus protocol is investigated for time-invariant networks.

2.2.2. LYAPUNOV ANALYSIS OF THE CONSENSUS ALGORITHM FOR TIME-INVARIANT NETWORKS

The consensus protocol described in the previous section defines the mechanism in which a group of individuals reach a consensus. The convergence of the consensus protocol provides an insight into the stability of the system, and the nature of the group decision variable. In the following section, the convergence properties of the consensus protocol are analysed by treating the graph Laplacian in Equation (2.10) as a candidate Lyapunov function. The following theorem provides the necessary conditions for asymptotic convergence of the average-consensus protocol in Equation (2.19):

Theorem 1. (asymptotic convergence)

Let G be a connected graph. Suppose each vertex v_i applies protocol (2.19), then all vertices of the graph globally asymptotically reach an average-consensus, such that $x^e = \lim_{t\to+\infty} x(t)$, and $x_i^e = x_j^e = \mathrm{Ave}(x(0)), \forall i, j, i \neq j$.

Proof.

The closed-loop dynamics of system (2.13) applying protocol (2.19) evolve according to the gradient system of the Laplacian potential given by:

$$\dot{x} = -Lx = -\nabla\Psi_G(x), \quad x(0) \in \mathbb{R}^{Nn} \tag{2.20}$$

From Equation (2.20) the group decision variable for an interconnected graph can be obtained by explicit calculation of $\exp(-Lt)$. The equilibrium points of (2.20) correspond to stationary points of $\Psi_G(x)$ and the region outside of these points, the potential is strictly decreasing with time [237]; i.e., if x^e is an equilibrium of Equation (2.20), then $Lq^e = 0$. From Equation (2.10):

$$\Psi_G(x^e) = \frac{1}{2}(x^e)^T L x^e = 0 \tag{2.21}$$

Following the connectivity of G, $x_i^e = x_j^e = c$, $\forall i, j \in \mathcal{N}_i$, i.e. $x^e = (c,\ldots,c)^T$, $c \in \mathbb{R}$ and $\sum_{i=1}^{n} u_i = 0$. Since the Laplacian potential equals zero at equilibrium, then $\bar{x} = \mathrm{Ave}(x)$ is an invariant quantity, Given the invariance property of $\mathrm{Ave}(x)$, then $\mathrm{Ave}(x^e) = \mathrm{Ave}(x(0))$, and $\mathrm{Ave}(x^e) = c$. This implies $x_i^e = \mathrm{Ave}(x(0))$, $\forall i \in N$ [236]. In addition, the eigenvalues of $-L$ are negative in the complex plane, and any solution of the system asymptotically converges to a point x^e in the eigenspace associated with the average-consensus of the network of vehicles [236]. The proofs and results are well known in the field of algebraic graph theory and can be found in [304] and [236] and references therein.

From Theorem 1, the average-consensus protocol (2.19) converges to an equilibrium given by $x_i^e = \mathrm{Ave}(x(0))$. This implies that the group decision variable (the equilibrium point) corresponds to the average value of the network of agents under a connected time-invariant graph topology. This feature is later exploited in Chapter 5 to define a decentralised optimisation control law for cooperative agents.

2.2.3. PERFORMANCE OF NETWORK PROTOCOLS

Of significant interest to the design of distributed control laws, is the transient behaviour of the consensus protocols. In the previous section, formal guarantees on the convergence of the consensus protocol to a group decision variable were provided. In this section, the effect of the graph connectivity on the performance of the consensus protocols is investigated.

Define δ as the *group disagreement vector* for a group of agents:

$$x = c\mathbf{1} + \delta \tag{2.22}$$

where $c = \text{Ave}(x)$, and $\delta \in \mathbb{R}^N$ satisfying $\sum_{i=1}^{N} \delta_i = 0$. The disagreement vector represents the deviation of the group's state from the group decision variable. The group disagreement vector evolves according to the *group disagreement dynamics* given by:

$$\dot{\delta} = -L\delta \tag{2.23}$$

with solution given by:

$$\|\delta(t)\| \leq \|\delta(0)\| \exp(-\beta t) \tag{2.24}$$

Theorem 2. (performance of agreement)

The group disagreement vector δ, as a solution to (2.23), globally asymptotically vanishes with a speed equal to $\beta = \lambda_2(L + L^T/2)$, i.e., the Fiedler eigenvalue induced by the graph G with Laplacian L, i.e.

$$\|\delta(t)\| \leq \|\delta(0)\| \exp(-\beta t) \tag{2.25}$$

Proof.

Let $V(\delta) = \frac{1}{2}\|\delta\|^2$ be a valid Lyapunov function for the disagreement dynamics (2.23). Then from [310]:

$$\dot{V} = \frac{\partial V}{\partial \delta}\frac{\partial \delta}{\partial t} = -\frac{1}{2}\left[\delta^T (L + L^T)\delta\right] \tag{2.26}$$

and from (2.19), the following inequality holds:

$$\dot{V} \leq -\lambda_2\left(L + L^T/2\right)\|\delta\|^2 = -2\beta V(\delta) < 0 \tag{2.27}$$

Therefore, $\delta(t)$ vanishes globally exponentially fast with a speed of β as $t \to +\infty$.

It was shown in [304] that for dense graphs, the Fiedler eigenvalue λ_2 is relatively large, and for sparsely connected graphs, λ_2 is relatively small. For this reason, Fiedler [242] termed this eigenvalue the *algebraic connectivity* of a graph. From Theorem 2, it can be shown that a network with dense interconnections solves an agreement problem faster than a

sparsely connected network [233]. In the following example, the average-consensus protocol is demonstrated for a group of vehicles.

2.2.4. NUMERICAL EXAMPLE: THE AVERAGE-CONSENSUS PROTOCOL

In this section, the average-consensus protocol (2.19) is applied to a group of 100 agents. The performance of the protocol is tested on 3 time-invariant network topologies with varying interconnection topologies. For the purposes of generality and simplicity, it is assumed that the information resides on a unitary space and evolves according to the following decoupled linear dynamics:

$$\dot{x}_i(t) = A_i x_i(t) + B_i u_i(t),$$
$$\text{where } A_i = \begin{bmatrix} 0 & I_{n\times n} \\ 0 & 0 \end{bmatrix},\ B_i = \begin{bmatrix} 0 \\ I_{n\times n} \end{bmatrix} \tag{2.28}$$

The initial distribution is given by $x_i(0) = i$, for $i = 1,\ldots,20$. The graph topologies with their corresponding information state evolution are shown in Figure 2-4. From Figure 2-4, the topology given by the complete graph (in which each node is connected to every other node in the network) demonstrates the fastest convergence ($\beta = 1.0526$) of the three networks. In fact, the complete graph converges to the group decision variable 22 times faster than the $k = 1$ nearest neighbours. It should be noted that the complete graph topology has 9.5 connections more than the $k = 1$ nearest neighbour topology. In general, the complete interconnection structure is impractical for physical implementation; and is provided here for comparative purposes.

2.3. INFORMATION CONSENSUS ON DYNAMIC NETWORKS

The analysis so far has been limited to fixed communication topologies. The stability and performance of a fixed network topology was investigated in the previous section. It was shown that for a fixed network topology, the connectivity of the nodes influenced the rate of convergence of the information consensus. In the case of multi-vehicle systems, the information flow topologies are dynamic. This dynamic topology is time-varying due to the motions of vehicles in the group, and the subsequent communication link creation and failure.

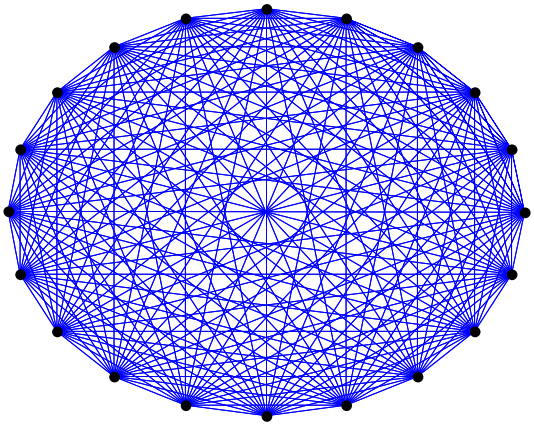

(a) k = 19

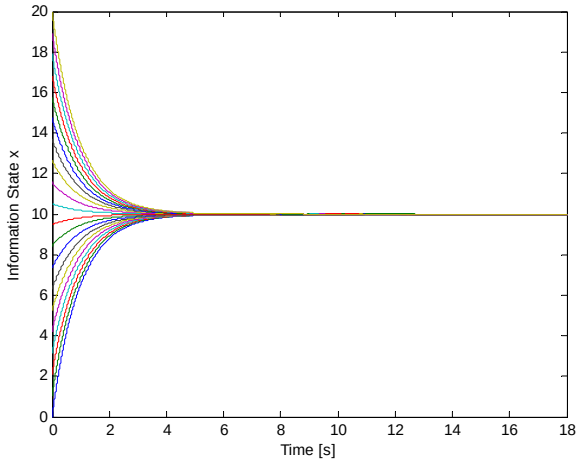

(b) β = 1.0526

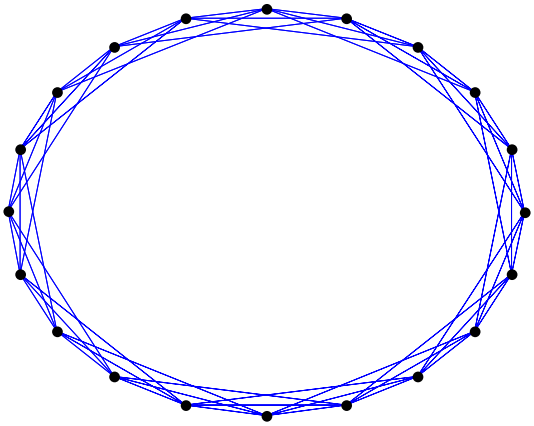

(c) k = 3

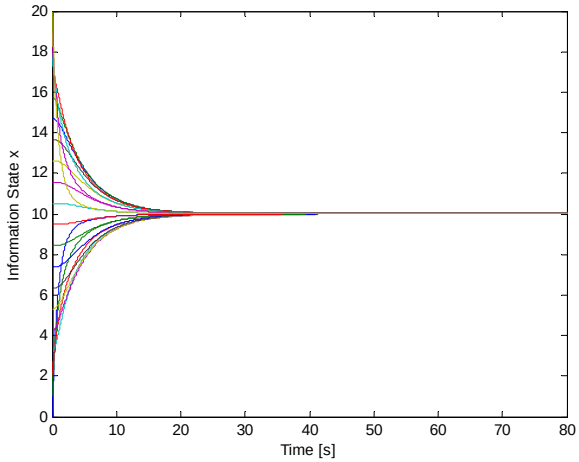

(d) β = 0.2174

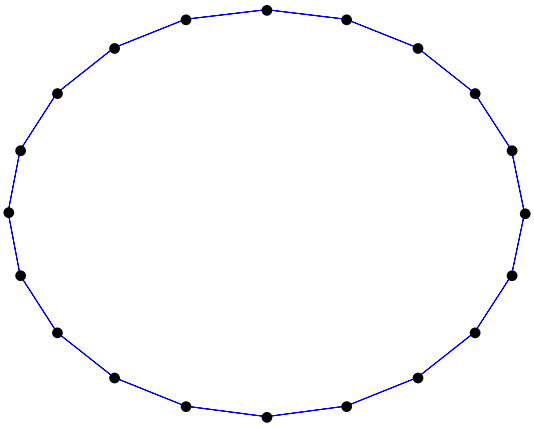

(e) k = 1

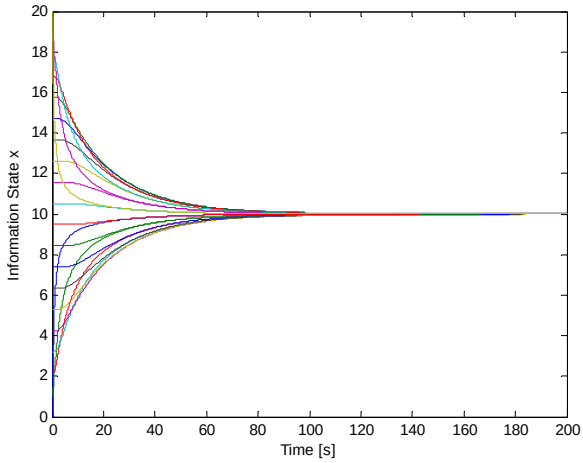

(f) β = 0.0489

Figure 2-4. Undirected interconnection graph for N = 100 with (a) complete connectivity (k = 100), (c) k = 6 connectivity, and (e) k = 2 connectivity. The corresponding state evolution and Fiedler eigenvalue for the interconnection graphs in (a), (c), and (e) are shown in (b), (d), and (f) respectively.

For example, information links across adjacent vehicles can be disrupted as neighbouring individuals bifurcate around obstacles and dissociate from the group. Similarly, communication links can be created or re-established as vehicles enter the interaction range of neighbouring vehicles. In terms of the network topology G, edges are added and removed from the graph over time. In this case, the communication graph is *state-dependent*. Network systems with a dynamic topology are commonly referred to as *switching networks* in the literature. In the proceeding section, the role of state-dependent graphs on the connectivity of switching networks is investigated.

2.3.1. DYNAMICS OF THE ADJACENCY MATRIX

To begin the following analysis, consider a group of N vehicles with dynamics given by the set of first-order differential equations:

$$\dot{x}_i = u_i \tag{2.29}$$

where $x_i = q_i^T \in Q_i = \mathbb{R}^n$ and $u_i \in U_i = \mathbb{R}^m$ is the configuration and control of vehicle v_i. For simplicity, it is also assumed that $n = m$ and the vehicles are fully actuated. The spatial distribution of vehicles in the group is described by the concatenated states $q \in \prod_{i=1}^{N} Q_i = R^{nN}$. Denote the spatial adjacency of a vehicle using Equation (2.2). A graph $G = (V, E, A)$ described in such a way defines a *spatial graph*, and the adjacency of neighbouring vehicles in the group. If r in Equation (2.2) is the communication range of a vehicle, then the spatial graph shares a one-to-one correspondence with the information network.

Suppose vehicle v_i applies the consensus protocol given in Equation (2.19):

$$u_i = \sum_{j \in \mathcal{N}_i} a_{ij}(x_j - x_i) \tag{2.30}$$

Then, the connectivity of the graph evolves according to Equation (2.29) and Equation (2.30). The average-consensus $\bar{q}$ obtained from Equation (2.30) physically represents a collision of the vehicles $j \in \mathcal{N}_i$.

Using the definition of the adjacency matrix A presented in Section 2.1.2, the dynamics of the adjacency matrix can be calculated [148]. Let $\nabla_x a_{ij}(x)$ denote the $nN \times 1$ gradient vector of $a_{ij}(x)$ obtained from Equation (2.2) with respect to x, and denote $\nabla_x A(x)$ as the $N \times nN^2$ matrix:

$$\nabla_x A(x) = \left(\nabla_x a_{ij}(x)^T\right) \tag{2.31}$$

Then:

$$\dot{A}(x) = (\dot{a}_{ij}(x)) = (\nabla_x a_{ij}(x)^T \dot{x}) = \nabla_x A(x)(I_N \otimes \dot{x}) \tag{2.32}$$

where I_N denotes the N-dimensional identity matrix and $\otimes$ denotes the Kronecker product.

By substituting the appropriate values from Equation (2.29) and Equation (2.30) into Equation (2.32) and using the SOS properties of the connected graph, the closed-loop dynamics of the spatial graph is obtained:

$$\dot{a}_{ij}(x) = (\nabla_x a_{ij}(x)^T \dot{x}) = \nabla_x a_{ij}(x)^T \cdot \left(-\frac{1}{2} \nabla \Psi_G(x) \right) = -\nabla_x a_{ij}(x)^T \cdot x^T L x \tag{2.33}$$

By explicit calculation, the evolution of the adjacency matrix can be determined given an initial distribution of nodes. Using the notations provided, a dynamic graph $G(t)$ can be described by the enumerated set of vertices V, and time-varying set of edges $E(t)$ given by the adjacency matrix dynamics in Equation (2.32); i.e. $G(t) = (V, E(t), A(t))$. Note Equation (2.33) defines an *autonomous system of differential equations*. In the proceeding section, the dynamic graph $G(t)$ is parameterised to define a switching network.

2.3.2. SWITCHING NETWORKS

In many multi-vehicle systems, the information network is characterised by a dynamic topology. The time-varying nature of the information network is attributed to the motion of the vehicles in the group, reconfiguration of the formation, or the attrition and extension of vehicles. The effect of the switching networks on the performance of distributed consensus protocols is of significant interest for the development of distributed and decentralised control laws. The remainder of this chapter is dedicated to the definition of switching networks, and the investigation of switching networks on consensus protocols.

Borrowing from the notation in [233], let $G_{s(t)}$ denote the dynamic graph $G(t)$ parameterised by a switching signal $s(t) : \mathbb{R} \to K$ with $K = \{1, \ldots, m\}$. The discrete-state $G_{s(t)}$ belongs to the finite collection of graphs given by:

$$\Gamma = \{G_{s(t)} = (V, E, A)\} \tag{2.34}$$

with continuous state $x \in \mathbb{R}^{nN}$. A system described in such a way is an example of a *hybrid system* [233]. Given protocol (2.19), the continuous-state of the system evolves according to the following hybrid system dynamics [233]:

$$\dot{x}(t) = -L(G_k)x(t), \quad k = s(t), \quad G_k \in \Gamma \tag{2.35}$$

By definition, the communication topology is piecewise constant over finite lengths of time, called the *dwell times* [46]; and nodes are constrained to change control laws only at discrete

intervals; i.e., $L(t)$ is piecewise constant with dwell times given by $T_k = t_{k+1} - t_k$, and $t_1, t_2, \ldots$ are the *switching instants* [311]. In the case of the cooperative rendezvous problem, the switching instants are induced when adjacent vehicles enter a new neighbourhood, and the graph topology is described by an *autonomous switching network*. One approach to analysing the stability of the switching network is to investigate the matrix properties of the graph topologies [311]. Let $\Phi(t,0)$ denote the state-transition matrix associated to $-L(t)$ and given as a function of the adjacency matrix dynamics in (2.32). Since the consensus protocol (2.19) is linear, its solution can be written as [311]:

$$x(t) = \Phi(t,0)x(0) \tag{2.36}$$

It was shown in [46] that a switching network with dwell times $T_k > 0$ converges to the average-consensus c of the connected graph, i.e.:

$$\lim_{t\to\infty} \Phi(t,0) \to c\mathbf{1} \tag{2.37}$$

and consensus is achieved if

$$\lim_{t\to\infty} \exp(-L(t_k)T_k) \cdot \exp(-L(t_{k-1})T_{k-1}) \cdot \ldots \cdot \exp(-L(t_0)T_0) = c\mathbf{1} \tag{2.38}$$

Furthermore the group disagreement vector δ (as described in Section (2.2.3)) vanishes exponentially fast with the least rate of:

$$\beta^* = \min_{G\in\Gamma} \lambda_2\left(\frac{L + L^2}{2}\right) \tag{2.39}$$

and the system converges to the average-consensus value c. The proof follows in similar spirit to the proof of Theorem 2 in Section 2.2.3 and can be found in [233]. The results of [46] and [233] provide an insight into the performance of a switching network under consensus protocol (2.19). In the proceeding section, the convergence properties of the consensus protocol (2.19) are demonstrated on a time-varying communication network for a group of cooperative vehicles.

2.3.3. NUMERICAL EXAMPLE: SWITCHING NETWORK

In the following example, consensus on a switching network is demonstrated for the N-vehicle cooperative rendezvous problem. The objective of the cooperative rendezvous problem is to reach a consensus on the goal location of the group of vehicles. Examples of a spatial goal location include the intercept point of a moving target, such as a missile or aircraft [83], the centroid of a formation [312], or the interface of two docking spacecraft [313].

For simplicity, consider $N = 10$ vehicles with first-order dynamics given by:

$$\dot{q}_i = u_i, \quad i = 1, \ldots, N \tag{2.40}$$

where $q_i = (x_i, y_i)^T \in Q_i = \mathbb{R}^2$ is the position of vehicle i on the plane $Q_i = \mathbb{R}^2$, $p_i = (\dot{x}_i, \dot{y}_i)^T \in TQ_i = \mathbb{R}^2$ is the corresponding velocity, and $u_i = (u_i^x, u_i^y)^T \in U_i = \mathbb{R}^2$ is its acceleration inputs. The initial states $q_i(0)$ are randomly initialised in the rectangle bounded by $[-10,10] \times [-10,10]$. A simple PD controller for the cooperative control problem is constructed using the average-consensus protocol in Equation (2.19):

$$u_i = \sum_{j \in \mathcal{N}_i} a_{ij}(q_j - q_i) \tag{2.41}$$

where a_{ij} is the vector of adjacency elements describing the connectivity of vehicle i to the subset of neighbours j in the group given by:

$$a_{ij} := \begin{cases} 1, & \text{if } \|q_j - q_i\| \le r \\ 0, & \text{otherwise} \end{cases} \tag{2.42}$$

The time-varying nature of the switching network is induced by the time-varying spatial distribution of the vehicles and evolves according to Equation (2.40) and Equation (2.41). Figure 2-8 shows the state trajectory of the group of vehicles in $\mathbb{R}^2$ and the corresponding rendezvous point. The convergence of the disagreement vector $\|\delta\|$ is shown in Figure 2-7, where the switching times of the network are indicated by the point markers. From Figure 2-7, consensus is reached asymptotically. Performance of the network is improved as a function of $\lambda_2\left(L(G_k) + L(G_k)^2/2\right)$, where $G_k \in \Gamma$. Snapshots of $G_k \in \Gamma$ are given in Figure 2-6. The time-varying nature of the interconnection graph in Equation (2.40) and Equation (2.41) describes an *autonomous hybrid differential-algebraic system.* Solving the precise time at which the interconnection topology of the group switches using analytical methods is difficult. In fact, solving hybrid differential-algebraic equations is currently an active area of research [314]; and is beyond the scope of this thesis. While impractical, current methods of determining switching times are performed through simulation or explicit calculations [315]. Through simulation, the set of graph topologies Γ for the switching network is determined and shown in Figure 2-6. The corresponding switch times are provided above the snapshot.

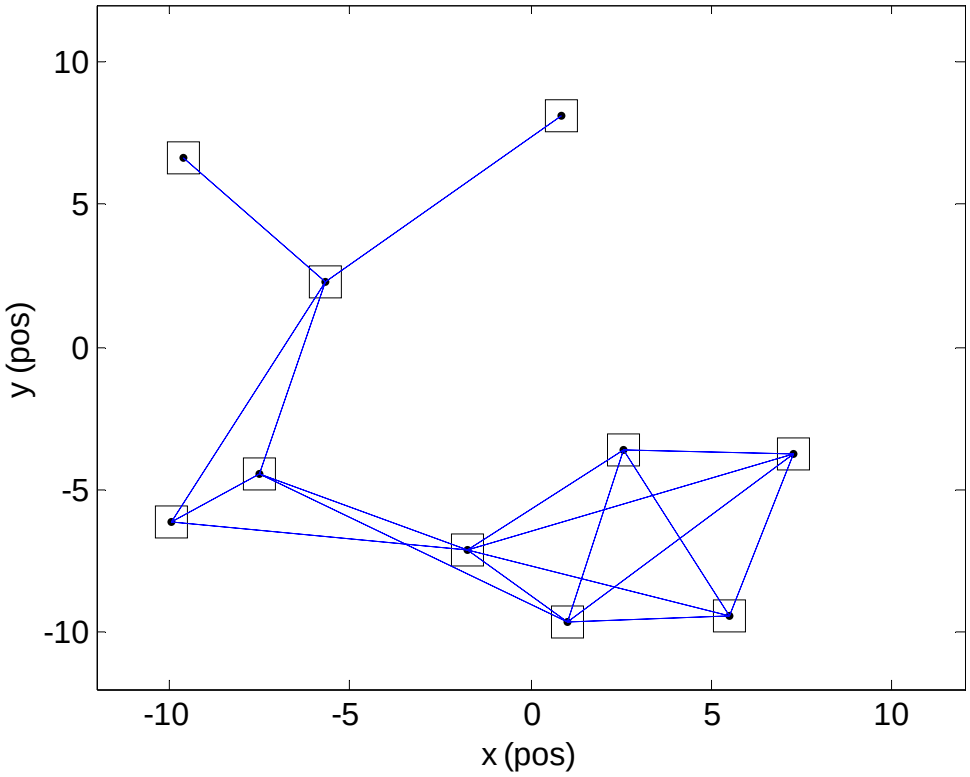

Figure 2-5. Initial distribution of vehicles in R^2 and spatially induced communication graph.

Figure 2-5 shows the initial distribution of the vehicles and the initial communication graph induced by $r = 10$. From Figure 2-5, the initial graph topology is *connected* (i.e., has only one connected component). Since the initial graph is connected, the degree of each node stabilises to $N-1$ corresponding to the complete graph k^N. This occurs at $T = 1.3955s$ in Figure 2-6 (f) and Figure 2-7. This can be demonstrated by considering the motion of two vehicles in the group. As two vehicles approach each other and reach a consensus on the rendezvous point, the neighbourhood of each vehicle collides. Consequently, the k-neighbourhood graph topology becomes a $k+n$ neighbourhood graph, and the valency of the vehicles in the group increases as the number of neighbours are increased.

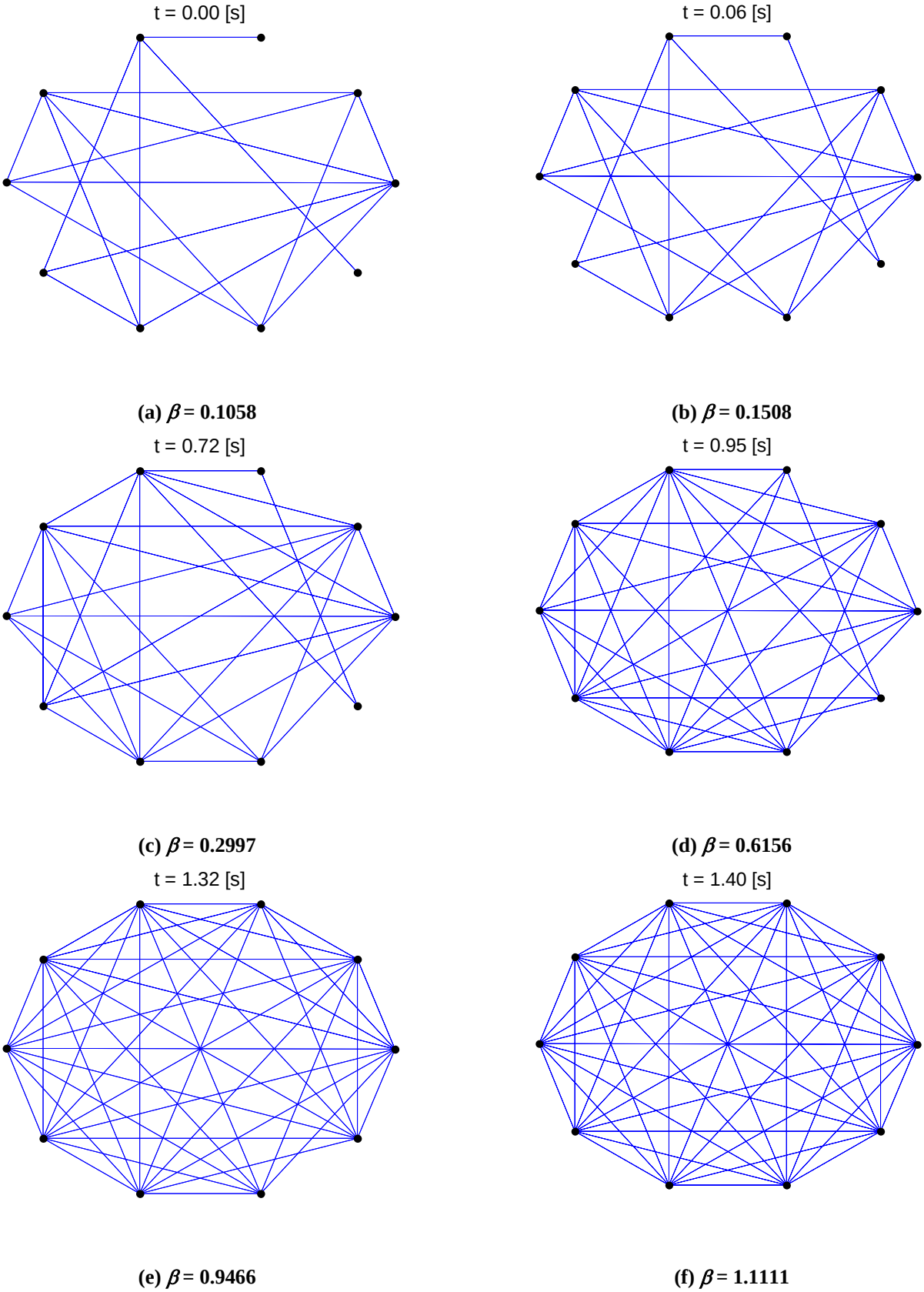

(a) β = 0.1058 **(b) β = 0.1508**

(c) β = 0.2997 **(d) β = 0.6156**

(e) β = 0.9466 **(f) β = 1.1111**

Figure 2-6. Discrete state-evolution of information network and switching times.

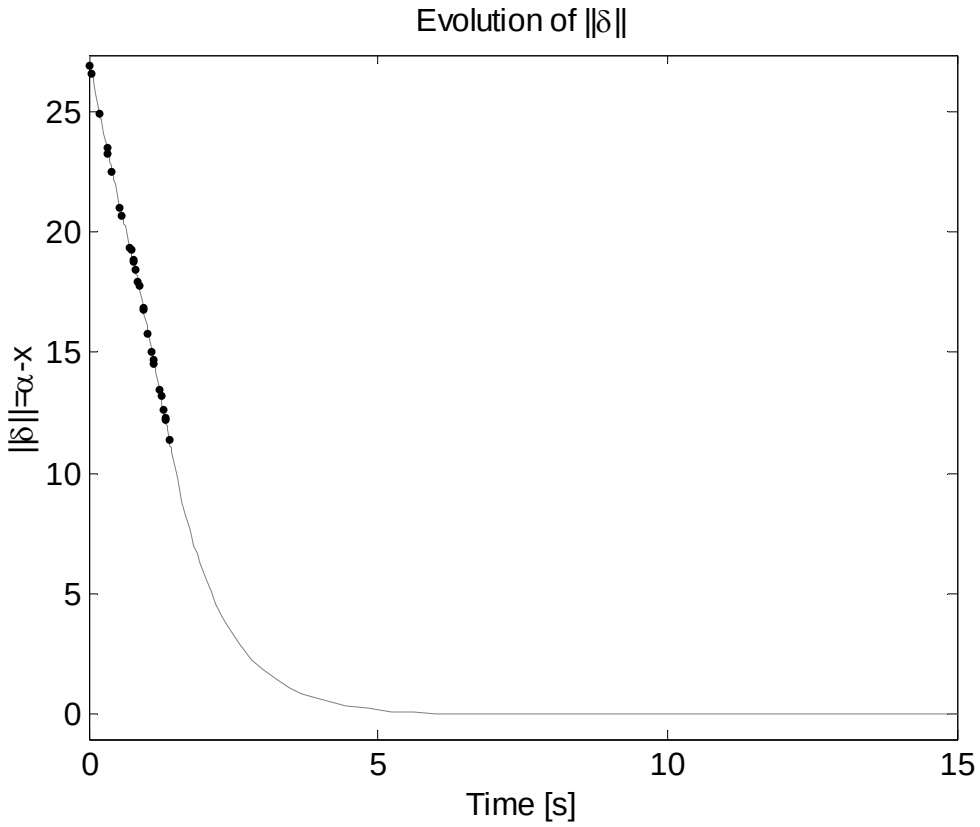

Figure 2-7. Convergence of the group disagreement vector.

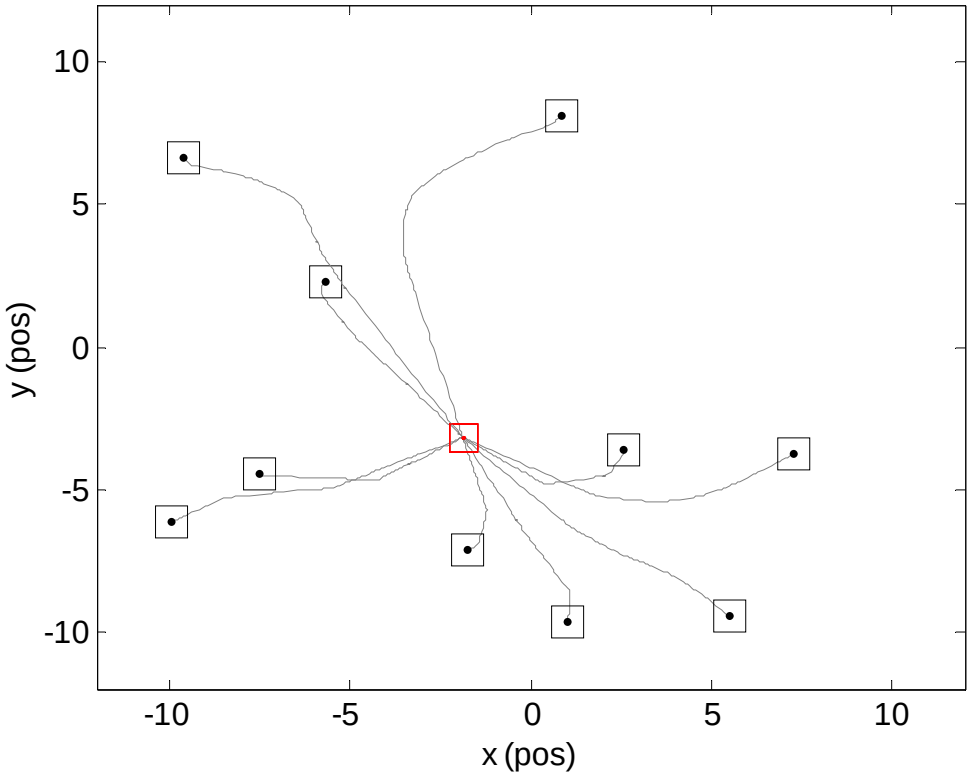

Figure 2-8. Rendezvous problem for *N* = 10 vehicles.

2.4. SUMMARY

In this chapter, the main areas of algebraic graph theory have been identified for the consensus problems. A consensus protocol was developed using the SOS properties of the graph. Using results from algebraic graph theory, the convergence of the consensus protocol was demonstrated. The results were extended to time-variant network topologies. It was demonstrated through simulation that for a time-varying information network, the vehicles will converge to the average-value of the average-valued consensus protocol. The chapter presented the various fields of graph theory and network design, to develop a unified dynamic information network for multi-vehicle systems. The information network developed in this chapter provides the basis for further developments in later chapters, particularly in Chapter 5 where a decentralised implementation scheme is developed. In the next chapter, the information network is used to develop a set of inter-vehicle behaviours for cooperative flocking.

Chapter 3. Dynamic Flocks and the Semi-Rigid Body Model

For purposeful applications of multi-vehicle systems, the cooperative control problem must be identifiable by a cooperative objective. To achieve the cooperative objective, the group of vehicles must reach consensus on a coordination variable. In multi-vehicle systems, this coordination variable is often specified with respect to the spatial distribution of vehicles in the group. It can include the precise location of the vehicles in the group, or a generalised group abstraction representative of the collective state of the vehicles. For example, the coordination variable for a flock of birds flying in V-formation can be represented using a state vector of position coordinates. The precise location of individuals in the flock is a suitable abstraction since the low-density of individuals in the flock, and the relatively coherent motion of the group make it possible to easily recognise the formation of a flock. In a plague of locusts however, the high-density of the group makes it difficult to identify the precise position of the individuals in the swarm at any given time. Consequently, abstractions based on the individual's states provide an unsuitable coordination variable for these types of groups. Instead, abstractions based on the collective states provide a more appropriate coordination variable for large-scale swarms. This could include the boundary or density of the swarm, or an abstract descriptor such as entropy and energy.

The distinction between the two levels of abstraction, extricates the notion of a swarm-based task from a formation-based task. Swarm-based tasks are often identifiable by only a small set of essential features representative of the group's collective behaviour (group abstractions); whilst, formation-based tasks, are described by the precise states of the individual agents. Using the precise states of the individuals as an abstraction provides a coherent relationship between the individuals, their interactions, and their influence on the cooperative objective. This makes it possible to optimise the behaviour of the individuals, and derive formal guarantees on the stability and performance of the system.

While strategies based on the precise states of the individuals can guarantee precision and optimality, they quickly become intractable as the number of individuals in the group is

scaled. In a group subject to attrition and extension, the dynamic nature of the population makes it difficult to define the precise states of the individuals without a centralised feedback control architecture. Information must continually be exchanged between the supervisory agent and the group of vehicles to evaluate the effectiveness of the current solution and re-evaluate plans according to available assets. Limitations on communication, sensory, and processing hardware makes it difficult to physically realise centralised control architectures. For example, in cooperative space interferometers, the position of the satellites are optimised to enhance the imaging

Swarming tasks on the other hand, naturally admit a distributed or decentralised architecture. The use of group abstractions trivialises the precise behaviour of the individuals. This makes swarming more robust to attrition and extension. The lack of a centralised processing facility however, presupposes the notion of autonomy and self-organisation. Swarms of self-organising vehicles have limited appeal and application in populated areas; unless the behaviour of the vehicles is guaranteed and observable. The challenge is now to design control strategies that preserve the scalability properties of swarming tasks and preserve the precision of formation tasks.

In this chapter, a theoretical framework for flock behaviour is presented. The flock model is used to model a cooperative objective and demonstrate swarm-based tasks in cooperative vehicle systems. The purpose of this model is to unify a group of vehicles as a flock, and develop group abstractions that identify the group as a singular entity. These group abstractions are then used in later chapters to develop control strategies at the supervisory level for precision and optimality. The flock algorithm presented in this chapter extends the work on consensus protocols introduced in the previous chapter to develop an artificial potential force model for the group of vehicles. The work is inspired by similar approaches in the field of mathematical biology to describe the behaviour of natural flocks and swarm, and the work on artificial flocks and swarms by Olfati-Saber in [32]. It aims to extend the current body of literature on artificial flock models by identifying controllable abstractions at a supervisory level that have appeared in similar models. The main contribution of this chapter is the identification of shape abstractions in Section 3.3 using scalable flock algorithms. It is shown in Section 3.3 that a stabilised flock exhibits the properties of a rigid-body system and provides the necessary group abstractions at the supervisory level to treat the group as a singular entity.

This chapter is organised as follows. Section 3.1 reviews the concepts of flocking as identified by Reynolds [25]. Section 3.2 builds on the heuristics of Section 3.1 to develop a mathematical model of flock behaviour. The transient properties of the flock are investigated in Section 3.2.3 and Section 3.2.4 to identify group abstractions for shape control. Finally, the rigidity properties of the flock are then investigated in Section 3.3 to construct a definition for the (semi)-rigid body model of the flock for motion control. Together with the results presented in Section 3.2, these are used to define the set of group abstractions suitable for control at the supervisory level in Chapter 4.

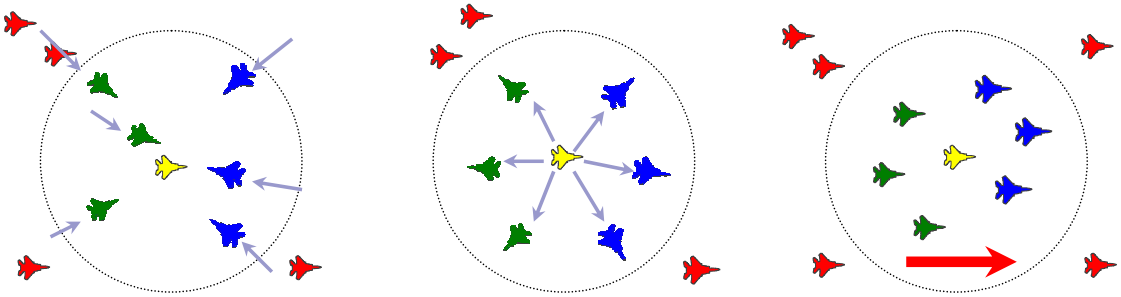

Figure 3-1. Reynolds' flock heuristic.

3.1. FLOCKING THEORY

One of the first heuristic models for a simulated flock was described by Reynolds in 1987 [25]. In [25], Reynolds identified three primitive behaviours necessary for a flock of agents to achieve flocking. Stated under *Reynolds' rules*, the behaviours that lead to simulated flocking are:

1. Collision Avoidance: avoid collisions with nearby flockmates;
2. Velocity Matching: attempt to match the velocity of nearby flockmates; and
3. Flock Centring: attempt to stay close to nearby flockmates.

These have also been stated under *Reynolds' boids* as *separation*, *alignment*, and *cohesion*. The first heuristic, collision avoidance, ensures that agents do not collide with static obstacles and neighbouring flockmates. Collision avoidance forces vehicles to steer away from neighbouring flockmates and obstacles to avoid collisions. When coupled with velocity matching, the relative separation distance of neighbouring flockmates remains invariant with respect to ongoing geometric flight [25]. This observation plays an important role in the development of a semi-rigid body model of the collective flock.

To prevent the vehicles from wandering, flock centring is introduced to force vehicles into the centre of the flock. In a distributed information network, the centre of the flock is the centre of neighbouring flockmates. The union of these neighbourhoods is the centre of the entire flock. If a vehicle is already close to the centre of the flock, the population density in its local neighbourhood is approximately homogenous in all directions; and the influence of flock centring on the vehicle is minimal. Alternatively, a vehicle located on the boundary of the flock, will have a greater displacement from the centre of the flock, and the influence of flock centring is large [25]. Together, these three behaviours ensure that agents aggregate to form a cohesive bond, and move with a common heading and velocity whilst avoiding collisions. In the proceeding section, a mathematical model for flocking is introduced.

3.2. A MATHEMATICAL MODEL

Consider N dynamically controlled vehicles with states q_i belonging to the manifold Q_i and control u_i belonging to the control spaces U_i. For fully actuated vehicles in free space, the states are position $x_i \in \mathbb{R}^d$ (where $d = 2$ for the planar case, and $d = 3$ in free space) and orientation $\theta_i \in \mathbb{R}$ vectors. The configuration of vehicle i can be written as $q_i = (x_i^T, \theta_i)^T \in Q_i = \mathbb{R}^n$, for all $i \in V$ with respect to some fixed inertial reference frame $\{F\}$, and controls $u_i \in U_i = \mathbb{R}^n$ as follows:

$$\begin{cases} \dot{q}_i = p_i \\ \dot{p}_i = u_i \end{cases} \tag{3.1}$$

For convenience, the vehicle states and controls are concatenated to form an nN-dimensional control system describing the collective flock:

$$\begin{cases} \dot{q} = p \\ \dot{p} = u \end{cases} \tag{3.2}$$

with $q \in \prod_{i=1}^{N} Q_i = R^{nN}$, $u \in \prod_{i=1}^{N} U_i = R^{nN}$. Given the vector $q = (q_1, \ldots, q_N)^T \in Q = \mathbb{R}^{nN}$, the distribution of vehicles in the group and their connectivity can be described using the graph pair (G, q). Here, the vector $q = (q_1, \ldots, q_N)^T \in Q = \mathbb{R}^{nN}$ and its induced pair (G, q) are referred to as the *configuration* and *structure* of the group respectively. In the proceeding section, the connectivity of the graph is constructed using the information flow and relative interaction range of the vehicles.

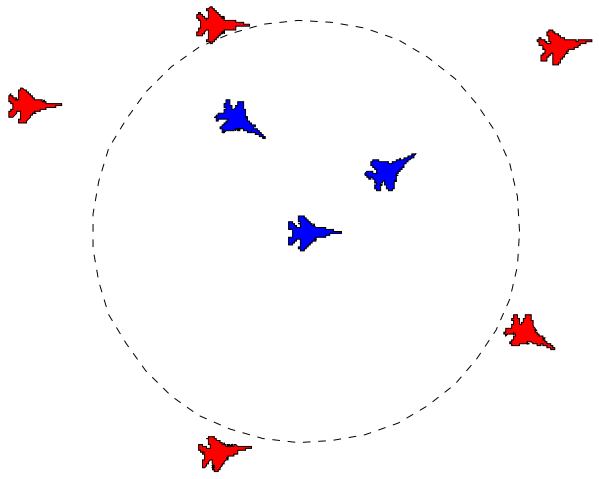

Figure 3-2. Closed-ball neighbourhood.

3.2.1. SENSING TOPOLOGY AND THE INTERACTION RANGE

In distributed and decentralised systems, the perspective of an individual is limited by the physical range of its sensors and communication devices. Let $r_i \geq 0$ denote the *interaction range* of vehicle v_i. r_i physically represents the interactivity of a vehicle and is used to explicitly define the sensor and communication radius of a vehicle's systems. A *spherical neighbourhood* is induced by the region enclosed by the closed ball defined by the radius r_i and centred at q_i:

$$B(q_i, r_i) := \{x \in \mathbb{R}^d : \|x - q_i\| \leq r_i\} \tag{3.3}$$

The set of *spatial neighbours* of vehicle v_i is the set of vehicles $v_j \in V$ bounded by the region enclosed by the ball $B(q_i, r_i)$ with radius r_i and centred at q_i. Any vehicle v_j within the closed ball $B(q_i, r_i)$ such that $\|q_j - q_i\| \leq r_i$ is connected to vehicle v_i. The set of spatial neighbours of vehicle v_i is given by:

$$\mathcal{N}_i = \{j \in V : \|q_j - q_i\| \leq r_i\} \tag{3.4}$$

Equation (3.4) describes a spherical neighbourhood. Spherical neighbourhoods can be used to model omni-directional sensors and communication devices, such as radars and antennas. Various sensory and communication models can be extrapolated from the generalised ball model to accommodate for the directivity of specific sensors and communication devices. For example, the conic field-of-view of a camera is considered in [283] using the conic neighbourhood specified in Equation (3.5):

(a) **(b)**

Figure 3-3. Examples of (a) spherical interaction range; and (b) conic interaction range.

$$C(x_i,\theta_i,r_i,\varphi_i) \coloneqq \{(x,\theta) \in \mathbb{R}^3 \times \mathbb{R} : \|x - x_i\| \le r_i, |\theta - \theta_i| \le \varphi_i\} \tag{3.5}$$

where $x_i \in \mathbb{R}^3$ and $\theta \in \mathbb{R}$ denote the position and orientation of vehicle v_i, and r_i and φ_i denote the range and viewing angles of the camera respectively. For the purposes of generality, it is assumed hereafter that all sensors and communication devices are omni-directional.

When information is communicated between adjacent vehicles and/or observed by physical sensors, the energy of the transmitted signal attenuates with distance from the signal source. The loss of signal quality over distance is modelled using a falloff function. Denote $\rho_i(\cdot)$ the sensor and communication falloff for vehicle $v_i \in V$ with finite interaction range r_i. Using the distributed adjacency matrix of Equation (2.3) in Section (2.12), a simple choice for a falloff function is derived by mollifying the step function in Equation (2.1) with a bump function:

$$\rho_{ij}(z) = \begin{cases} 1, & z \in [0,\delta) \\ \frac{1}{2}\left[1 + \sin\left(\pi \frac{(z-\delta)}{(r_i-\delta)} + \frac{\pi}{2}\right)\right], & z \in [\delta, r_i] \\ 0, & \text{otherwise} \end{cases} \tag{3.6}$$

where $z = \|q_j - q_i\|$, r_i is the interaction range of vehicle v_i and $\delta \in (0, r_i)$.

A spatially induced neighbourhood $\mathcal{N}_i$ with sensory and communication falloff given by Equation (3.6) defines a *spatial adjacency matrix* $A(q) = [a_{ij}(q)]$:

$$a_{ij}(q) \coloneqq \rho_{ij}(z) = \begin{cases} 1, & \text{if } 0 \le \|q_j - q_i\| < \delta, \quad j \ne i \\ \frac{1}{2}\left[1 + \sin\left(\pi \frac{(z-\delta)}{(r_i-\delta)} + \frac{\pi}{2}\right)\right], & \text{if } \delta \le \|q_j - q_i\| \le r_i, \quad j \ne i \\ 0, & \text{otherwise} \end{cases} \tag{3.7}$$

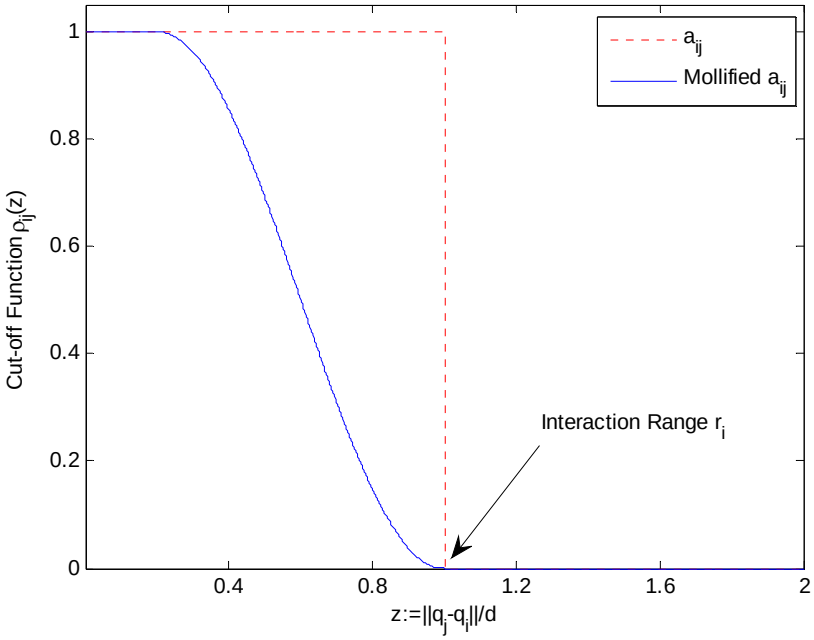

Figure 3-4. Sensory and communication falloff function.

The spatial adjacency matrix defines a *spatially induced graph* $G(q)$ [283]. If $r_i \neq r_j$, $\forall i, j \in V$, $i \neq j$, then a spatially induced graph $G(q)$ is a digraph. As an example, consider the case when $r_i > r_j$, then $j \in \mathcal{N}_i$ and $i \in \mathcal{N}_j$ since $\|q_j - q_i\| \leq r_i$ and $\|q_j - q_i\| \not\leq r_i$. In a homogenous flock, each vehicle has identical sensory and communication ranges; i.e., $r_i = r_j$, $\forall i, j \in V$, $i \neq j$. Consequently, a spatially induced graph $G(q)$ with homogenous vehicles induces an undirected graph.

3.2.2. THE FLOCK LATTICE

In the following section, the flock heuristics of Section 3.1 are investigated to describe the topology of a spatially induced graph for a flock of vehicles. Let $B_d(q_i, d_i)$ denote the exclusion zone for vehicle v_i with radius $0 < d_i \leq r_i$ and centred at q_i (see Figure 3-5). Then:

Definition 1. (collision)

Two vehicles v_i and v_j are said to have collided if vehicle v_j has entered the exclusion zone of vehicle v_i defined by the closed ball $B_d(q_i, d_i)$. The opposite is also true when vehicle v_i enters the exclusion zone of vehicle v_j.

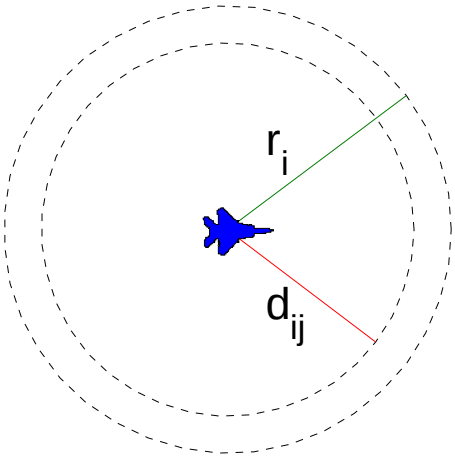

Figure 3-5. Interaction and exclusion zone of vehicle v_i.

From Reynolds' boids, cohesion naturally implies that a group of vehicles will collide to reach the centre of the flock $q_i = q_j = \bar{q}$, $\forall i, j \in V$, $i \neq j$; i.e.:

$$\left\| q_j - q_i \right\| \leq d_i , \quad \forall j \in \mathcal{N}_i , \quad i \neq j \tag{3.8}$$

On the other hand, separation ensures that potential collisions with neighbouring vehicles are avoided, i.e.:

$$\left\| q_j - q_i \right\| > d_i , \quad \forall j \in \mathcal{N}_i , \quad i \neq j \tag{3.9}$$

These two observations lead to the following inter-vehicle constraint for flocks of vehicles:

$$\left\| q_j - q_i \right\| = d_i , \quad \forall j \in \mathcal{N}_i , \quad i \neq j \tag{3.10}$$

The set of constraints in Equation (3.10) describe a spatially induced graph for flocking:

Definition 2. (flock lattice)

A flock lattice is a configuration of vehicles q *satisfying constraint (3.10) for all* $v_i \in V$.

In a homogenous flock, where $d_i = d_j = d_{ij}$, $\forall i, j \in V$, $i \neq j$, all edges of the spatial graph $G(q)$ induced by the flock lattice have equal lengths d_{ij} (equidistant flock). Consider the case when the spatial graph $G(q)$ induced by the flock lattice is disconnected; i.e., there exists $c(G(q))$ components. Let $F(q)$ denote a component of $G(q)$, such that $F(q)$ is a strongly connected flock lattice, then $G(q)$ contains $c(G(q))$ flocks.

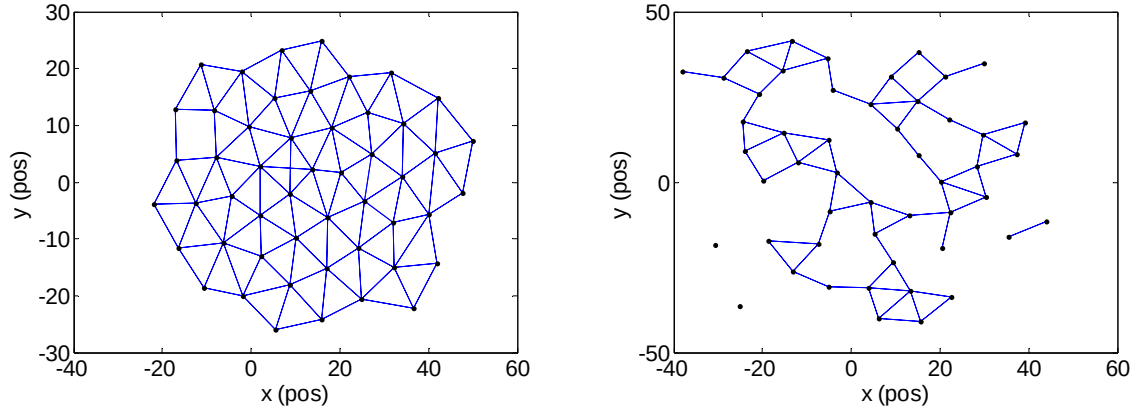

Figure 3-6. Examples of (a) a regular flock lattice, and (b) a quasi-flock lattice.

Definition 3. (cohesive flock [284])

A flock is cohesive $\forall t \in [t_0, t_f]$ *if there exists a closed polygon with centre* $\bar{q}(t) = \mathrm{Ave}(q(t))$ *that contains all vehicles* $\forall t \in [t_0, t_f]$. *For example, for a ball of radius* $R > 0$ *and centred at* $\bar{q}$, $\exists R > 0 : \|x(t)\| \le R$, $\forall t \in [t_0, t_f]$.

A closed polygon is used here to describe the permissible convex hull of a group of vehicles rather than a closed ball to generalise the possible topologies of a flock.

Definition 4. (quasi-flock lattice [284])

A quasi-flock lattice is any configuration $G(q)$ *such that the underlying graph structure is disconnected.*

Formally, let $|F(q)|$ denote the order of a component graph $F(q)$, then the density of the graph $G(q)$ is:

$$\mathrm{P}(G(q)) := \frac{\max_k |F_k(q)|}{\sum_{k=1}^{c(G(q))} |F_k(q)|} \tag{3.11}$$

A density of 1 denotes a strongly connected flock lattice $G(q)$ and $0 < \mathrm{P}(G(q)) < 1$ a *quasi-flock lattice*. A similar definition for net density and quasi-flock lattices was provided in [283]. Figure 3-6 (b) provides an example of a quasi-flock lattice.

3.2.3. STRUCTURAL ENERGY OF THE FLOCK LATTICE

The degree in which a configuration $G(q)$ conforms to a flock lattice is measured using the inter-vehicle constraints in Equation (3.10). A minimum for Equation (3.10) is found at $\|q_j - q_i\| = d_{ij}, \forall i, j \in V,\ i \neq j$. A natural choice for a deviation metric is given by:

$$\mathcal{E}(q) = \sum_{i=1}^{N} \sum_{j \in \mathcal{N}_i} \psi\left(\|q_j - q_i\| - d_{ij}\right) \tag{3.12}$$

where the locally Lipschitz continuous function $\psi(\cdot)$, satisfying $\psi : \mathbb{R}_{\geq 0} \to \mathbb{R}_{\geq 0}$ and $\psi(0) = 0$ has been introduced to define an *energy potential field* for the graph $G(q)$.

Corollary.

A configuration $G(q)$ is a global minimum of the potential function in Equation (3.12) if and only if $G(q)$ is a flock lattice satisfying the constraints in Equation (3.10).

To construct the energy potential field $\psi(\cdot)$ in Equation (3.12), a smooth continuous function is constructed to define the inter-vehicle constraints of the flock lattice. Consider the constraints introduced in Equation (3.10) and implemented in Equation (3.12). Using the norm $\|z\|$, the following gradient information is observed for flock convergence:

$$\nabla\|z\| := \begin{cases} 0 & \|z\| = d_{ij} \\ -1 & \|z\| < d_{ij} \\ +1 & \|z\| > d_{ij} \end{cases} \tag{3.13}$$

where $z = q_j - q_i$. From Equation (3.13), $\|z\|$ is not differentiable at singular configurations when $q_j - q_i = 0$, therefore, it is unsuitable for inter-vehicle interactions. Let $\phi(z) : \mathbb{R}^+ \to \mathbb{R}^+$ denote the attractive-repulsive pair-wise potential for inter-vehicle interactions with piecewise information given in Equation (3.13). A smooth energy potential recovering the piecewise information in Equation (3.13) is constructed using the following bounded sigmoid function:

$$\phi(z) := \frac{z}{\sqrt{1 + \|z\|^2}} \tag{3.14}$$

The integral of Equation (3.14) yields a smooth continuous function for inter-vehicle interactions:

$$\Phi(z) := \int_{s}^{z} \phi(z) ds = \sqrt{1 + \|z\|^2} - 1 \tag{3.15}$$

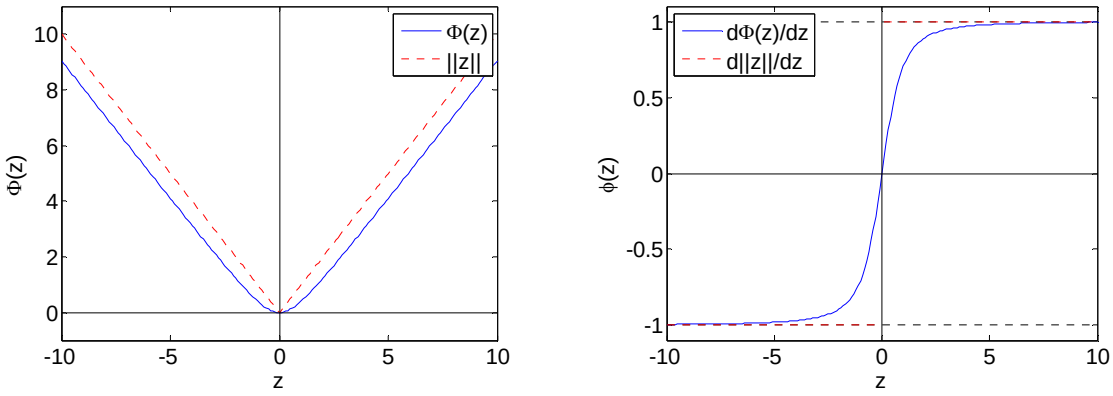

(a) **(b)**

Figure 3-7. (a) Norm functions ||z|| and Φ(z) and their derivatives (b).

Applying Equation (3.15) to the flock constraints in Equation (3.10) the following smooth inter-vehicle constraints is observed:

$$\Phi(q_j - q_i) = \Phi(d_{ij}) \tag{3.16}$$

By definition, the attractive-repulsive function in Equation (3.14) is effective $\forall z \in \mathbb{R}^n$. This corresponds to an infinite interaction range r for each vehicle $v_i \in V$. A simple approach to creating a pair-wise potential with finite cut-off, is to multiply the pair-wise potential with a bump function using a process known as *soft-cutting* [284]. Using the mollified adjacency matrix in Equation (3.7) as a finite sensory and communication model, the attractive-repulsive potential in Equation (3.14) is soft-cut to produce:

$$\phi_\rho(z) = \rho_{ij}(z/r) \cdot \frac{z - \Phi(d_{ij})}{\sqrt{1 - (z - \Phi(d_{ij}))^2}} \tag{3.17}$$

where $z = \Phi(q_j - q_i)$. Equation (3.17) provides a model for the finite attractive-repulsive interactions of neighbouring vehicles. Integration of the attractive-repulsive potential recovers the potential energy $\psi(z)$ of the collective system:

$$\psi(z) = \int_d^z \phi_\rho(s) ds \tag{3.18}$$

Using the energy potential described above, the conditions for flock convergence using energy dissipation techniques are presented in the following section. The results presented in the next section follow the results outlined in [294] and [316] and serve to provide a background to the main contribution of this Chapter – the development of a unified flock model at the supervisory level.

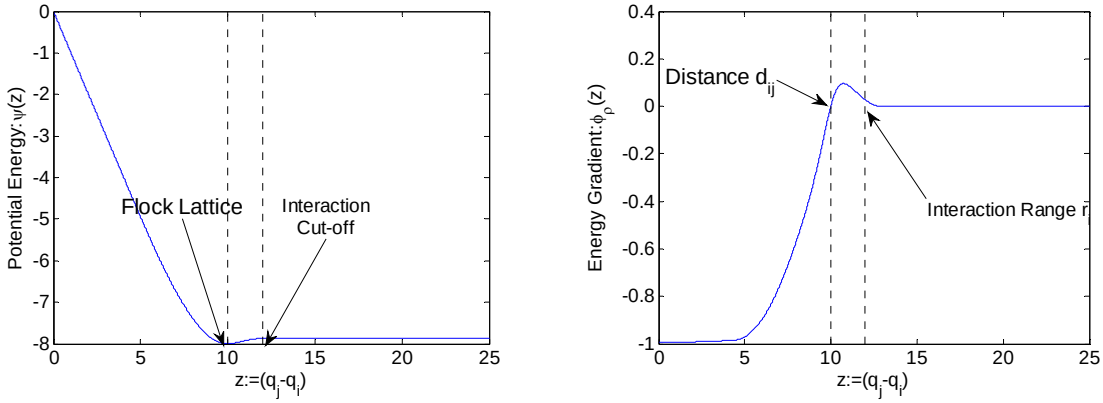

(a) **(b)**

Figure 3-8. (a) The structural potential energy of the flock lattice, and its (b) gradient.

3.2.4. FLOCKING AND THE DISSIPATION OF THE STRUCTURAL ENERGY

Let $\{M\}$ denote the body fixed frame of the flock centred at O'. Denote the relative position, velocity, and control of vehicle v_i in frame $\{M\}$ as:

$$\tilde{q}_i = q_i - \bar{q}\,, \quad \tilde{p}_i = p_i - \bar{p}\,, \quad \tilde{u}_i = u_i - \bar{u}\,, \quad \forall i \in N \tag{3.19}$$

where the notation $(\bar{\cdot})$ is used to denote the average consensus of the position, velocity and control. Note, the average consensus of the position $\bar{q}$ corresponds to the centroid O' of the flock.

Let $\mathbf{1} = (1,\ldots,1)^T \in \mathbb{R}^N$ denote the vector of ones and $\otimes$ the Kronecker product of two matrices. Then, the concatenated form of the relative position, velocity and control of the collective flock can be written as:

$$\begin{aligned} \tilde{q} &= q - \mathbf{1} \otimes \bar{q} \\ \tilde{p} &= p - \mathbf{1} \otimes \bar{p} \\ \tilde{u} &= u - \mathbf{1} \otimes \bar{u} \end{aligned} \tag{3.20}$$

From Equation (3.2), the *relative dynamics* of the flock is given by:

$$\begin{cases} \dot{\tilde{q}} = \tilde{p}, \\ \dot{\tilde{p}} = \tilde{u} \end{cases} \tag{3.21}$$

Denote M as the mass matrix of the flock of vehicles given by:

$$M = \begin{bmatrix} m_1 & 0 & 0 \\ 0 & \ddots & 0 \\ 0 & 0 & m_N \end{bmatrix} \tag{3.22}$$

Let $\mathcal{V}(q)$ denote the potential energy of the flock with pair-wise potential $\phi_\rho\big(\Phi(q_j - q_i)\big)$:

$$\mathcal{V}(q) \coloneqq \varphi(q) = \frac{1}{2}\sum_i \sum_{j \neq i} \psi\big(\Phi(q_j - q_i)\big) \tag{3.23}$$

and $\mathcal{K}(\tilde{p})$ the relative kinetic energy of the flock:

$$\mathcal{K}(\tilde{p}) = \frac{1}{2}\sum_{i=1}^{N}\left\|\tilde{p}_i\right\|^2 \tag{3.24}$$

The *Hamiltonian* for the system of vehicles in the flock is then given by the sum of the relative kinetic energy and the potential energy of the graph:

$$\mathcal{H}(q,\tilde{p}) = \mathcal{K}(\tilde{p}) + \mathcal{V}(q) \tag{3.25}$$

It was shown in [294] and [316] that reduction of $\mathcal{H}(q,\tilde{p})$ to zero produces a flock lattice satisfying the constraints in Equation (3.10). Indeed, the derivation of Equation (3.10) in Section 3.2.3 is based on this presumption. By controlling $\mathcal{H}(q,\tilde{p})$ it is possible to control the convergence of the vehicles to a flock lattice construction. This provides a meaningful flock abstraction to control the group at the supervisory level. In the following section, the theorems of [294] and [316] are summarised. These will be integral to understanding the transient behaviour of the flock and rationalise a group abstraction in later chapters.

Theorem 1. (zero structural energy [283])

1. *$\mathcal{V}(q) = 0$ if and only if the graph $G(q)$ satisfies the structural constraints in Equation* (3.16)*;*
2. *For $\mathcal{K}(\tilde{p}) = 0 \;\; \forall t \geq t_0$, the distance between any two vehicles remains constant for all $t \geq t_0$ and the graph topology $G(q)$ remains invariant for all $t \geq t_0$ Furthermore, no two vehicles collides;*
3. *The velocity of all vehicles in the flock are equal if $\mathcal{K}(\tilde{p}) = 0, \forall t \geq t_0$.*

Proof.

The Theorem and Proof are similar to Proposition 2 in [283].

1. *The zero potential energy follows directly from Equation* (3.16)*; i.e.:*

$$\phi_\rho(\Phi(q_j - q_i)) = 0 \Leftrightarrow \mathcal{V}(q) = \frac{1}{2}\sum_i\sum_{j\neq i}\psi\left(\Phi(q_j - q_i)\right) = 0, \quad \forall j \in \mathcal{N}_i, \quad \forall i \in N \tag{3.26}$$

Therefore, the configuration q satisfying Equation (3.16) *is a stable equilibrium of the energy potential.*

2. *From Equation* (3.24), *$\mathcal{K}(\tilde{p}) = 0 \Leftrightarrow \tilde{p}_i = 0, \;\; \forall i \in N$. This implies that the inter-vehicle distance $\left\|q_j - q_i\right\|$ between any two vehicles v_i and v_j is constant. The proof follows from the dynamics of the inter-vehicle distances; i.e.:*

$$\frac{d}{dt}\left\|q_j - q_i\right\|^2 = (p_j - p_i)^T(q_j - q_i) = (\tilde{p}_j - \tilde{p}_i)^T(q_j - q_i) \tag{3.27}$$

For $\tilde{p}_i = 0$ *and* $\tilde{p}_j = 0$, $\forall i, j \in N$, $(\tilde{p}_j - \tilde{p}_i)^T (q_j - q_i) = 0$, *hence concluding the proof of Part 2.*

3. *The proof follows from Part 2 and the fact that* $G(q(t))$ *remains invariant for all* $t \geq t_0$. *If there exists* $\tilde{p}_i \neq 0$, *then* $\mathcal{K}(\tilde{p}) \neq 0$ *and* $\|q_j - q_i\| \neq$ constant *for any* $j \in \mathcal{N}_i$. *Therefore,* $\tilde{p}_j = \tilde{p}_i$, $\forall j \neq i$. *Furthermore, by the connectivity induced by the invariant graph* $G(q(t))$ *in Theorem 1 in Section 2.2.2, the information state of neighbouring vehicles reaches the average consensus for all vehicles; i.e.* $\tilde{p}_i = \tilde{p}_j = \bar{\tilde{p}}$, $\forall i, j \in N$ *[283].*

The following provides a new definition of flocking for a group of vehicles using the Hamiltonian of the system.

Definition 5. (flocking)

Given a protocol $u = k(q, \tilde{p})$, *a dynamic graph* $(G(q), q, \tilde{p}, u)$ *is asymptotically stable if and only if both the following conditions hold [283]:*

1. *There exists a constant* $C > 0$ *such that* $\mathcal{H}(q(t), \tilde{p}(t)) \leq C$ *for all* $t \geq 0$;
2. $\lim_{t \to \infty} \mathcal{H}(q(t), \tilde{p}(t)) = 0$, *i.e. for all* $\varepsilon > 0$, *there exists* $T = T(\varepsilon) > 0$ *such that:*

$$\mathcal{H}(q(t), \tilde{p}(t)) \leq \varepsilon \tag{3.28}$$

for all $t > T$ *[283].*

Using the Hamiltonian for the flock of vehicles, the following centralised cost objective is defined:

$$\begin{aligned} &\min_{q, \tilde{p}} J(q, \tilde{p}) = \frac{1}{2} \sum_{i=1}^{N} \|\tilde{p}_i\|^2 + \frac{1}{2} \sum_i \sum_{j \neq i} \psi(\Phi(q_j - q_i)) \\ &\text{Subject to:} \quad \begin{cases} \dot{\tilde{q}}_i = \tilde{p}_i, \\ \dot{\tilde{p}}_i = \tilde{u}_i \end{cases} \end{aligned} \tag{3.29}$$

Solution to Equation (3.29) defines an implicit control law given by:

$$u_i^* := k(q_i, \tilde{p}_i) \tag{3.30}$$

and can be obtained from the gradient of the Hamiltonian. Denote $\nabla_{q_i} \mathcal{V}(q_i)$ the gradient of the potential energy of the system, with

$$\nabla_{q_i} \mathcal{V}(q_i) = \sum_{j \in \mathcal{N}_i} \phi_\rho(\Phi(q_j - q_i)) \cdot \mathbf{n}_{ij} := -u_i^f \tag{3.31}$$

and $\mathbf{n}_{ij}$ is the unit vector along the edge that connects vehicle v_i to vehicle v_j and given by:

$$\mathbf{n}_{ij} = \frac{(q_j - q_i)}{\Phi(q_j - q_i)} \tag{3.32}$$

Similarly, define the gradient of the kinetic energy of the flock as:

$$\nabla \mathcal{K}(\tilde{p}) = \tilde{p}^T \hat{L}(q)\tilde{p} = \sum_{j \in \mathcal{N}_i} a_{ij}(q)(\tilde{p}_j - \tilde{p}_i) := -u_i^p \tag{3.33}$$

with n-dimensional graph Laplacian $\hat{L}$ satisfying the SOS properties in Equation (2.11). A simple distributed PD controller can be defined for vehicle v_i with dynamics given in Equation (3.1) using Equation (3.31) and Equation (3.33):

$$u_i = w_1 \cdot u_i^f + w_2 \cdot u_i^p \tag{3.34}$$

where w_1, w_2 are relative weighting terms introduced to adjust the influence of each vehicle objective. Solving for stationary points in the control law given in Equation (3.34) can yield the optimal control law of Equation (3.30) and represents the solution space of the flocking vehicles. In Chapter 5, an optimisation routine based on Model Predictive Control (MPC) is derived for decentralised implementation into a flock of vehicles.

Remark.

The first term in Equation (3.34) represents the flock deviation metric in Equation (3.12) that yields the flock lattice. This corresponds to the cohesion and separation rules of Reynolds' rules. The second term of Equation (3.34) represents the velocity matching rule of Reynolds' rules. Combined, the control law in Equation (3.34) provides a unified flocking protocol for multi-vehicle systems. In the proceeding section, the transient behaviour of Equation (3.34) is investigated for stability. The analysis follows in similar spirit to the works of [284] using LaSalle's Invariance Principle (see Appendix A for a review of LaSalle's Invariance Principle).

3.3. RIGID FLOCK CONSTRUCTIONS

The structure $(G(q), q)$ induced by the spatial constraints of Reynolds' flocking rules characterises a rigid construction. Rigidity of the flock structure provides an important abstraction for group motion planning and control. Consider a group of vehicles with dynamics given in Equation (3.1). Denote the average position and velocity of the flock lattice as:

$$\bar{q} = \text{Ave}(q) \tag{3.35}$$

and

$$\bar{p} = \text{Ave}(p) \tag{3.36}$$

respectively, with average consensus protocol given by $\text{Ave}(x) \coloneqq \frac{1}{N}\sum_{i=1}^{N} x_i$. Let $\bar{u} = \text{Ave}(u)$ denote the average control state of the flock and define a 'virtual body frame' $\{M\}$ fixed to centroid O' with position and velocity given by $\bar{q}$ and $\bar{p}$ respectively. Then the translational dynamics of the collective flock is given by:

$$\begin{cases} \dot{\bar{q}} = \bar{p} \\ \dot{\bar{p}} = \bar{u} \end{cases} \tag{3.37}$$

where $\bar{q}, \bar{p}, \bar{u} \in \mathbb{R}^n$ ($n = 2$ for the planar case, and $n = 3$ for the three dimensional case). Let:

$$\tilde{q}_i = [x_i, y_i, z_i]^T = R^T(q_i - \bar{q}), \quad i = 1, \ldots, N \tag{3.38}$$

denote the relative position of vehicle v_i in frame $\{M\}$, and $(R, \bar{q}) \in SE(n)$ the group symmetry with rotation group $R \in SE(n)$. Then, from the structural constraints of the flock lattice in Equation (3.10) and Equation (3.38), the following property of the flock lattice is observed:

$$\left\|\tilde{q}_j - \tilde{q}_i\right\| = \left\|R(q_j - \bar{q}) - R(q_i - \bar{q})\right\| = \left\|R(q_j - q_i)\right\| = \left\|q_j - q_i\right\| \tag{3.39}$$

This proves that the structural constraints of the flock lattice are invariant under rotation and translation of the coordinates.

Finally, the following constraint is introduced to complete this definition on flock rigidity.

Definition 6. (infinitesimal motion [124])

An infinitesimal motion of a structure is given by the following inner-product:

$$\left\langle \tilde{p}_j - \tilde{p}_i, \tilde{q}_j - \tilde{q}_i \right\rangle = 0, \quad \forall e_{ij} \in E \tag{3.40}$$

The constraint in Equation (3.40) observes the length-preserving nature of rigid body systems. The following definition extends the concept of a rigid body system to flocking systems.

Definition 7. (rigid flock)

A flock is rigid if it preserves the condition of infinitesimal motion $\forall e_{ij} \in E$.

According to Definition 6 and Definition 7, a flock that has converged to a flock lattice is a rigid flock and the motions of the flock are length-preserving; i.e., the flock lattice preserves the constraints in Equation (3.40). Following the definition of 6 and 7, the behaviour of a group of vehicles applying Protocol (3.34) is analysed in Theorem 2.

Theorem 2. (stable flock convergence)

Consider a group of vehicles applying Protocol (3.34). Let $\Omega_c = \{(x, \tilde{p}) : \mathcal{H}(x, \tilde{p}) \leq c\}$ *be a level-set of the Hamiltonian* $\mathcal{H}(x, \tilde{p})$ *for the configuration of vehicles applying Protocol (3.34) such that for any solution starting in* Ω_c *forms a cohesive flock* $t \geq 0$. *Then, the configuration of vehicles converges to a flock lattice bounded by* $R = \sqrt{2\mathcal{H}(q(0), \tilde{p}(0))}$.

Proof.

Consider the Hamiltonian $\mathcal{H}(q, \tilde{p})$ *of the flock of vehicles in Equation (3.25) applying protocol (3.34). The time derivative of the Hamiltonian* $\dot{\mathcal{H}}(q, \tilde{p})$ *is given by:*

$$\dot{\mathcal{H}}(q, \tilde{p}) = -\tilde{p}^T \hat{L}(q) \tilde{p} \tag{3.41}$$

This implies that the energy of the system is monotonically decreasing for all $t \geq 0$. *Since the collective potential and velocity mismatch of the collective group are initially finite, it follows that the Hamiltonian is bounded by:*

$$\mathcal{H}(q(t), p(t)) \leq \mathcal{H}(q(0), \tilde{p}(0)) < \infty \tag{3.42}$$

The potential energy $\mathcal{V}(q)$ *and kinetic energy* $\mathcal{K}(\tilde{p})$ *are also bounded according to*

$$\mathcal{V}(q) \leq \mathcal{H}(q(0), \tilde{p}(0)) \tag{3.43}$$

and

$$\mathcal{K}(\tilde{p}) \leq \mathcal{H}(q(0), \tilde{p}(0)) \tag{3.44}$$

respectively. Let $\Omega_c = \{(q, \tilde{p}) : \mathcal{H}(q, \tilde{p}) \leq c\}$ *be a level set of the Hamiltonian* $\mathcal{H}(q, \tilde{p})$, *then from LaSalle's Invariance Principle (Equation A.1), the velocity mismatch is upper bounded by* c *[284] since:*

$$\frac{1}{2}\sum_i \left\|\tilde{p}_i\right\|^2 \leq \mathcal{H}(q(t), \tilde{p}(t)) \leq c, \quad \forall t \geq 0 \tag{3.45}$$

Suppose the flock is cohesive for all $t \geq 0$ *and bounded by a closed ball with radius* $R > 0$ *such that* $\left\|x(t)\right\| \leq R$, $\forall t \geq 0$. *By the boundedness of the velocity mismatch in Equation (3.45) and the boundedness of the relative position of vehicles in the flock, the following triangle inequality is observed [284]:*

$$\left\|q(t), \tilde{p}(t)\right\|^2 := \left\|q(t)\right\|^2 + \left\|\tilde{p}(t)\right\|^2 \leq R^2 + 2c =: \zeta \tag{3.46}$$

where $\zeta > 0$ *is a constant. From Equation (3.25), Equation (3.46) becomes:*

$$\left\|q(t), \tilde{p}(t)\right\|^2 := 2\mathcal{H}(q, \tilde{p}) \leq R^2 + 2c =: \zeta \tag{3.47}$$

Since the flock is upper bounded by $\mathcal{H}(q(0), \tilde{p}(0))$*, then the position of all vehicles remains inside the* n*-sphere with radius* $R = \sqrt{2\mathcal{H}(q(0), \tilde{p}(0))}$ *centred at* $\bar{q}$ *; i.e.:*

$$\mathbf{S}^n = \{q_i \in \mathbb{R}^n : \|q_i - \bar{q}\| \leq \|R\|\} \tag{3.48}$$

Equation (3.48), provides a physically meaningful shape abstraction for a group of vehicles with a configuration described by the flock lattice.

From LaSalle's Invariance Principle, all solutions starting in Ω_c *converge to the largest invariant set in* $S = \{q \in \Omega_c : (x) = 0\}$*. However, the connectedness of the flock* $t \geq 0$ *implies information flow in the local frame* $\{M\}$*. Based on Equation (3.41), and Section 2.2, this exchange of information state results in velocity consensus in the cohesive flock. From Theorem 1, the spatial graph* $G(q)$ *asymptotically converges to the flock lattice in Section 3.2.2 bounded by the ball centred at* $\bar{q}$ *with radius* $R = \sqrt{2\mathcal{H}(q(0), \tilde{p}(0))}$*. Therefore, the flock protocol in Equation (3.34) converges to a configuration* q *that is an extrema of* $\mathcal{V}(q)$ *such that* $\nabla\mathcal{V}(q) = 0$ *which yields the flock lattice satisfying Reynolds' rules [284].*

Remark.

From Theorem 2, a group of vehicles applying Protocol (3.34)will converge to the flock configuration described in Definition 6 and Definition 7. Moreover, the resulting space occupied by the flock configuration is bounded by Equation (3.48). Equation (3.48) provides a suitable shape abstraction that describes the group's state and is exploited in Chapter 5 to formulate a group objective for the cooperative control problem.

This concludes the analysis of the local-vehicle interactions using simple flock protocols. In the proceeding chapter, the shape abstractions induced by the flock rigidity constraints are explored to derive controllable group abstractions and plan the motions of the flock. This chapter concludes with a brief demonstration of the flocking protocols.

3.4. NUMERICAL EXAMPLE: FLOCKING FOR *N*-VEHICLES

In this section, the flocking protocol in Equation (3.34) is demonstrated for the N-vehicle problem on the plane. In the following simulations, each vehicle is assumed to be fully actuated with dynamics given by:

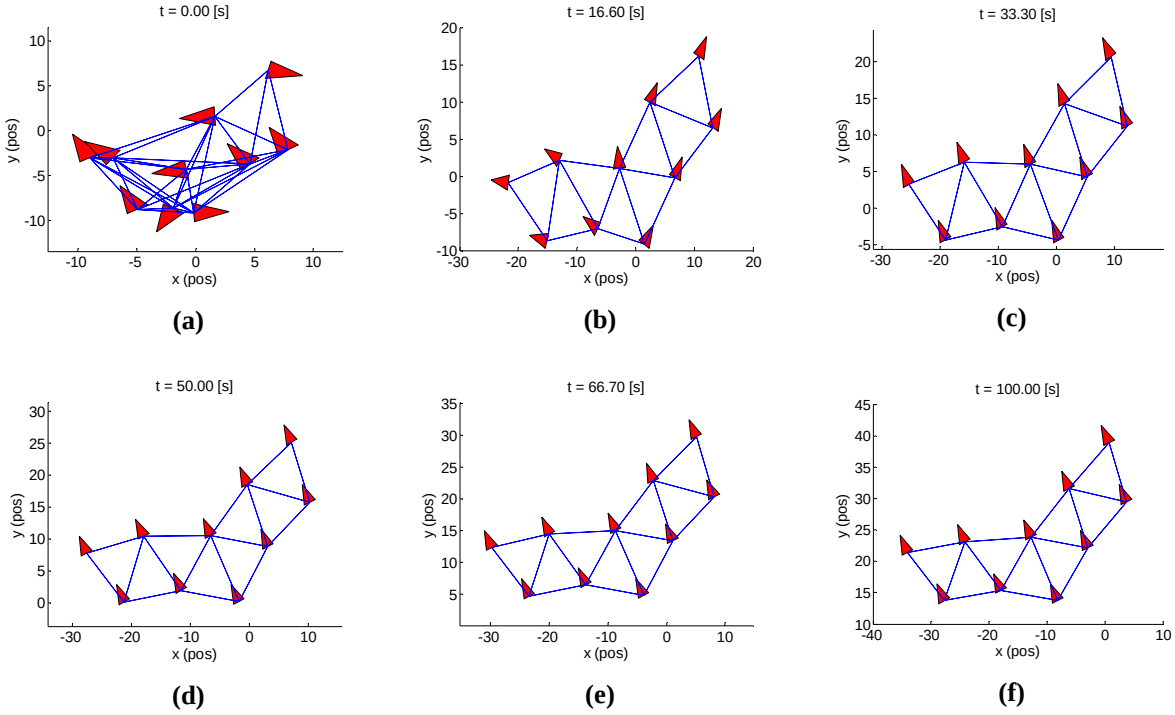

Figure 3-9. Flocking for *N* = 10 vehicles.

$$\begin{cases} \dot{q}_i = p_i \\ \dot{p}_i = u_i \end{cases} \tag{3.49}$$

and configuration $q_i = (x_i, y_i, \theta_i)^T \in Q_i = \mathbb{R}^3$. It is assumed that each vehicle interacts with neighbouring vehicles using a wireless communication device in the closed ball defined by Equation (3.3). For the following simulations, the flock parameters in Table 3-1 are arbitrarily selected.

Table 3-1. Simulation parameters for flocking in 2D.

d_{ij}	10
$r_i = r_j = r$	12
δ	$0.5r$

The position and velocity of each vehicle is initialised in the rectangles $q_i(0) \in [-20,20] \times [-20,20]$, and $p_i(0) \in [-1,1] \times [-1,1], \forall i \in N$ using a uniform random distribution. Consecutive snapshots of the flock evolution are shown in Figure 3-9; the corresponding interaction topologies are shown by the links in Figure 3-9. Figure 3-10 (a) and Figure 3-10 (b) show the corresponding potential and kinetic energy dissipation for the group of vehicles. From Figure 3-10 (a), the flock lattice induced by the flock protocol is a low-energy state for the optimisation problem given in Equation (3.29). Formulation of a centralised optimisation problem using the flock protocol is treated separately in Chapter 5.

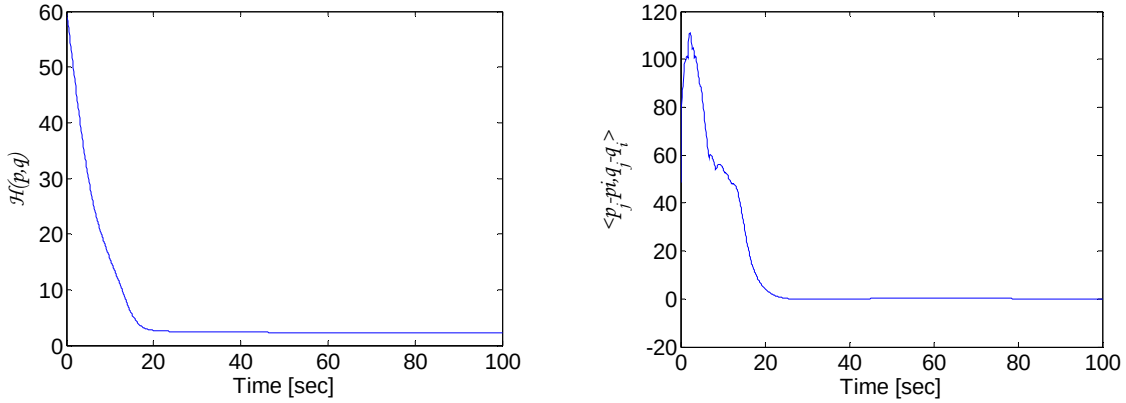

(a) **(b)**

Figure 3-10. (a) Hamiltonian of the system, and (b) stabilisation of the rigidity constraint.

Remark.

In the previous simulation, the vehicles were randomly initialised in a rectangle that preserved strong connectivity of the initial interaction graph. Protocol (3.34) ensured vehicles converged towards a flock lattice and maintained a strongly connected interaction graph for all $t > 0$. *In the following section, Protocol (3.34) is demonstrated on a group of vehicles with a disconnected initial graph topology. It will be shown how Protocol (3.34) fails to demonstrate a cohesive flock lattice i) for a group of initially disconnected vehicles, and ii) for a group of vehicles with large state variation. Through simulation, the influence of the interaction graph and the variation of state on the group's ability to converge and maintain a cohesive flock lattice are demonstrated.*

3.5. NUMERICAL EXAMPLE: DISSOCIATION OF THE FLOCK LATTICE

The ability of a group of vehicles to converge to a cohesive flock lattice is dependent on the initial distribution of the vehicles. The analysis of the flock protocol so far has concentrated on the case when the initial interaction graph is strongly connected for all $t > 0$. Consider the case when the initial swarm is sufficiently dispersed and the underlying graph topology is disconnected. Following Example 3.4, the initial position and velocity of the $N = 50$ vehicle problem is randomly selected from the rectangles $q_i(0) \in [-70,70] \times [-70,70]$, and $p_i(0) \in [-1,1] \times [-1,1]$, $\forall i \in N$ using a uniform random distribution. Vehicle dynamics and simulation parameters are given in Equation (3.49) and Table 3-1 respectively. Figure 3-11 (a) shows the initial distribution of vehicles in the plane with the links highlighting the corresponding interaction graph. From Figure 3-11 (a), 14 distinct components in the initial interaction graph are observed. Snapshots of the flock evolution are shown in Figure 3-11.

The initial distribution fails to converge to a cohesive flock lattice. Instead, the group dissociates to form a disconnected graph atypical of a flock lattice.

In the following example, the effect of velocity distribution on the convergence of Protocol (3.34) is demonstrated. The vehicles are randomly distributed in the rectangle $q_i(0) \in [-20,20] \times [-20,20]$ with velocities sampled in the range $p_i(0) \in [-10,10] \times [-10,10]$. In this case, the vehicles preserve strong connectivity in the initial interaction graph, whilst observing a large variance in the initial velocity distribution. Figure 3-12 shows consecutive snapshots of the flock's evolution. The corresponding interaction graphs are shown by the links in Figure 3-12. From Figure 3-12, the vehicles fail to converge to the desired flock lattice and the vehicles have dissociated.

The failure to converge towards a flock lattice is attributed to the variation of the initial velocities of the vehicles. For a strongly-connected interaction graph with Protocol (3.34), large-scale velocities instigate the propagation of *string instabilities* in the interconnected system. These string instabilities have the effect of disconnecting the interaction graph into smaller components. If the velocities are sufficiently large, then the flock lattice becomes dissociated and the group cannot sustain a cohesive flock. In fact, the ability of Protocol (3.34) to converge to and sustain a cohesive flock lattice is observed only for a limited set of initial conditions. These results are in concert with the findings of Olfati-Saber in [284]. In the following section, global goals are introduced to produce stable and purposeful flocking.

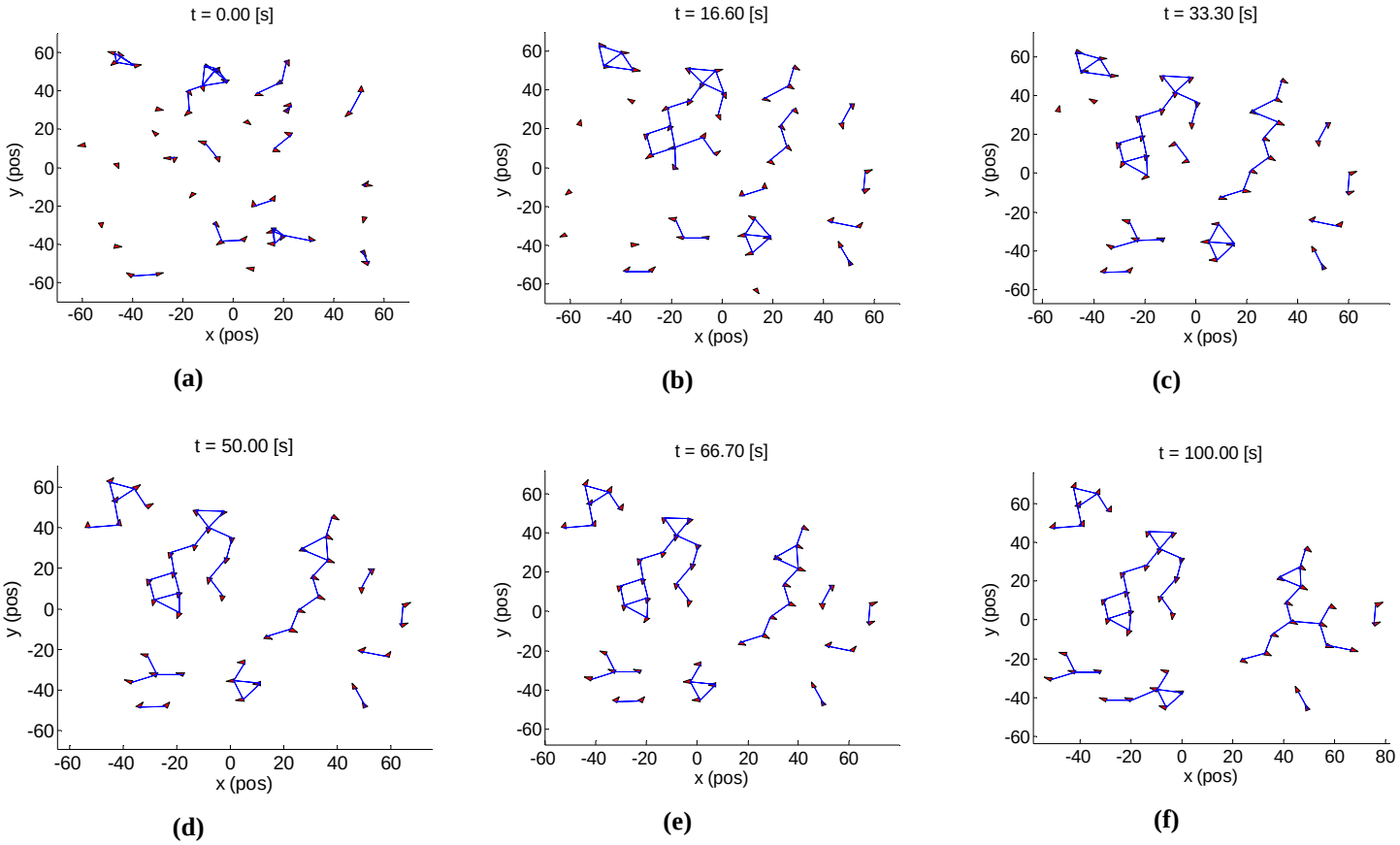

Figure 3-11. Dissociation of a flock lattice due to sparse connectivity.

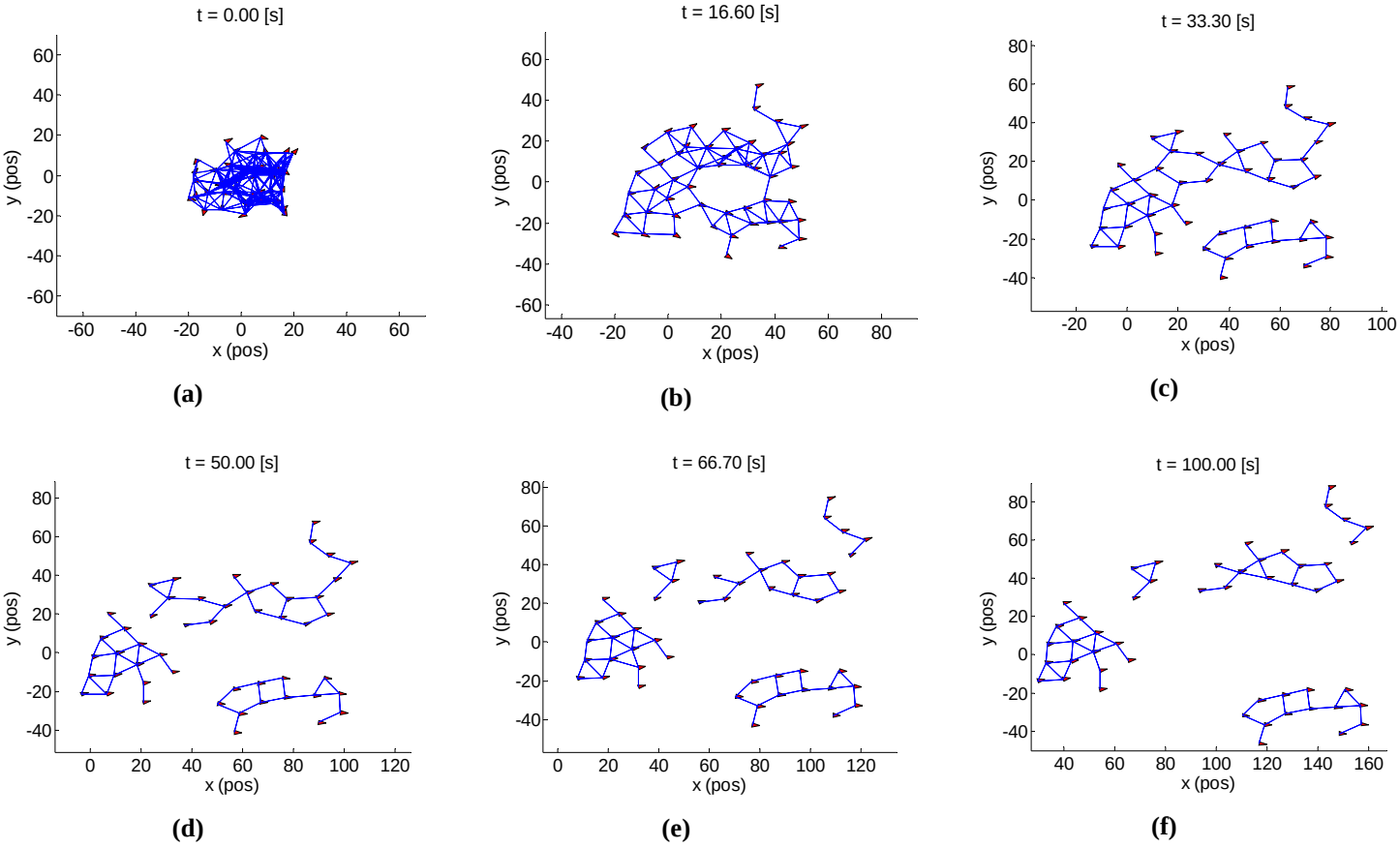

Figure 3-12. Dissociation of the flock lattice due to string instabilities.

3.6. INTRODUCTION OF THE NAVIGATION FUNCTION

To attenuate possible fragmentation and promote purposeful application of the flock, a navigation function is introduced to Protocol (3.34) that facilitates global convergence to a desired equilibrium:

$$u_i = w_1 \cdot u_i^f + w_2 \cdot u_i^p + w_3 \cdot u_i^g \tag{3.50}$$

where $u_i^g := f(q_i, p_i, q_d, p_d)$, and $q_d \in Q$, $p_d \in T_{q_d} Q$ is the desired equilibrium states of the centre of the flock. The pair (q_d, p_d) can be explicitly defined by a supervisory controller to provide a reference trajectory for the flock, or defined with respect to a group objective function. When the equilibrium states are defined by a supervisory agent, a simple navigational feedback controller can be developed for asymptotic convergence to the reference trajectory:

$$u_i^g = -k_1(q_d - \tilde{q}_i) - k_2(p_d - \tilde{p}_i) \tag{3.51}$$

where $k_1, k_2 > 0$. In the following example, the effect of the navigation function is demonstrated for a group of vehicles.

3.7. NUMERICAL EXAMPLE: NAVIGATION FEEDBACK

Consider the case when the group's objective is to stabilise to a flock lattice and cooperatively track a reference trajectory. The equilibrium pair (q_d, p_d) is given by the dynamics of the following *virtual agent*:

$$\begin{cases} \dot{q}_d = p_d \\ \dot{p}_d = -k(q_r - q_d) \end{cases} \tag{3.52}$$

where k is the gain matrix for the feedback controller in Equation (3.52) and q_r is the desired reference trajectory given by:

$$\begin{cases} (10t \quad 0), & t \in [0,40] \\ (400 \quad (400 - 10t) - 200), & t \in [40,60] \\ (1000 - 10t \quad -200), & t \in [60,100] \end{cases} \tag{3.53}$$

For the following example, the initial position and velocity of the $N = 15$ vehicle problem is randomly selected from the rectangles $q_i(0) \in [-70,70] \times [-70,70]$, and $p_i(0) \in [-1,1] \times [-1,1]$, $\forall i \in N$ using a uniform random distribution and the weighting parameters are chosen to be $c_1 = 1$, $c_2 = 1$, and $c_3 = 0.5$. Vehicle dynamics and simulation

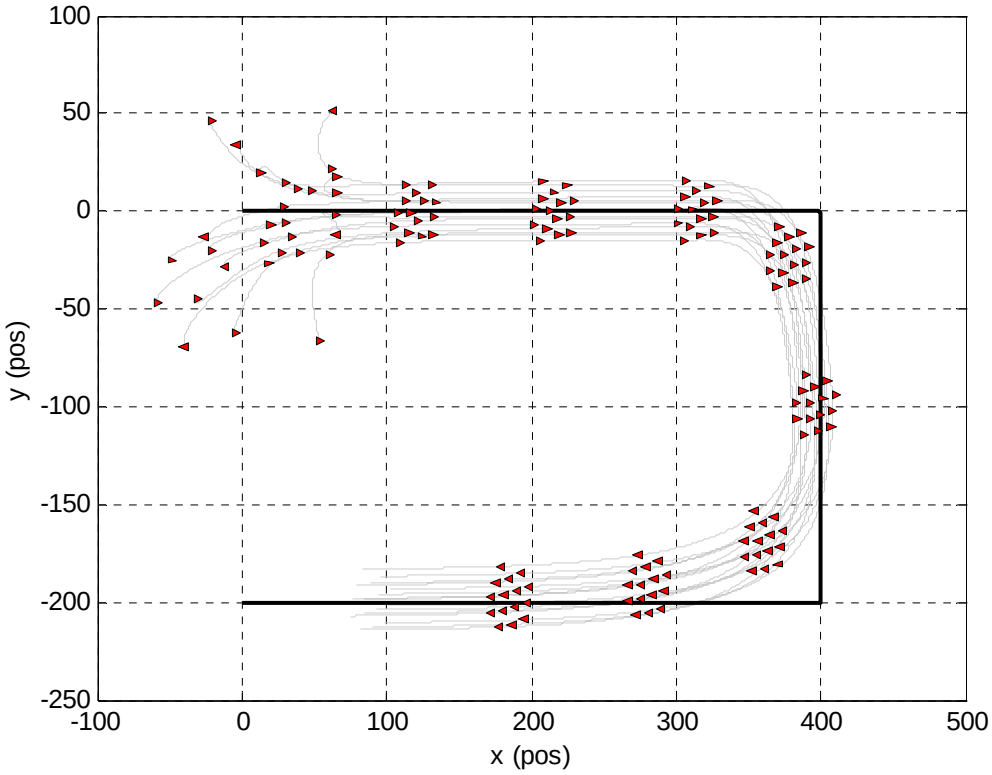

Figure 3-13. Flocking with navigational feedback for N = 15 vehicles.

parameters are given in Equation (3.49) and Table 3-1 respectively. These initial conditions are selected despite the flock dissociation witnessed in Example 3.5.

Applying Protocol (3.50), the motion of the flock is shown in Figure 3-13. Simulation verifies the convergence of the group to the flock lattice using the navigation function; despite the unfavourable initial conditions. This concludes the development of a flock protocol for group cohesion and cooperative behaviour. In the next chapter, the group's cooperative behaviour is considered at the supervisory level. It is here that the control of the group as a whole is considered using the protocols and abstractions introduced in this chapter.

3.8. SUMMARY

The flocking protocols for a group of vehicles were modelled using an artificial potential field approach. It was shown that the artificial potential field approached produced a decentralised control law that could be implemented at the local vehicles. When aggregated, the collective behaviour demonstrated by the vehicles applying the artificial potential field based control law demonstrated flock behaviour. An energy functional was used to describe the collective flock and provide a group abstraction identifiable by a supervisory agent. It was

shown that the minimisation of this energy functional (from a centralised perspective) would also result in the desired flock behaviour. Furthermore, it was shown that the flock would converge to a lattice construction bounded by the n-sphere of radius $R = \sqrt{2\mathcal{H}(q(0), \tilde{p}(0))}$. This provides a useful shape abstraction for a supervisory agent to control the motion and the shape of the flock independently. In the proceeding chapter, the motion of the vehicles adhering to a flock lattice is examined before a suitable cooperative control scheme is developed. The proceeding chapter serves to introduce the concept of group motion planning for the group of vehicles with configuration described in this chapter.

Chapter 4. Group Motion Planning and Shape Control

Moving large groups of vehicles from an initial configuration to a final configuration with minimal supervision and control is fundamental to developing autonomous and cooperative multi-vehicle systems. The large-scale nature of flocks and swarms makes it difficult to develop control strategies at both the local vehicle level, and the group level. Traditional approaches based on centralised architectures constrain the number of vehicles that can be controlled and monitored by a supervisory agent. For example, in the common approach to path-planning for a formation of vehicles, the supervisory agent must calculate and assign reference trajectories to each vehicle in the group. The tracking problem is then handled by the individual vehicles. At each sampling period, the supervisory agent measures (via sensors or communication), the states of each vehicle to minimise the divergence of the group from the desired trajectory. Many of the path-planning problems represented in this way, are amenable to optimisation problems involving the minimisation (or maximisation) of a performance function. However, the dimensionality of large-scale multi-vehicle groups, such as flocks and swarms, prevent the resolution of the path-planning problem at the supervisory level using conventional optimal control techniques. Many optimal control techniques cannot handle systems of very high dimensionality; and so these approaches are generally limited to small-scale groups. Approaches based on distributed artificial intelligence have shown some promise in reducing the control efforts of a supervisory controller. These approaches work on the premise of behaviour-based control; where the individual vehicle controllers are designed using vehicle-level behaviours rather than group-level behaviours. The group-level behaviours emerge as a consequence of the local interactions of the vehicles. This makes it difficult to develop analytical relationships between the vehicle-level behaviours to the group-level behaviours that are amenable to scaling. The lack of a formal understanding between these two levels of behaviour, prevent the practical application of these strategies. In addition, decentralised path-planning strategies make it difficult to provide a meaningful level of control to a supervisory agent.

Based on the practical limitations of a fully autonomous distributed path-planning strategy, this chapter will focus on the development of a path-planning strategy for a centralised architecture to control a large group of vehicles. This chapter deviates from the traditional research by addressing the dimensionality of the problem. By reducing the motion generation and control problem to a lower dimensional manifold, the information that is communicated and processed by the supervisory agent is amenable to optimisation. Furthermore, by using tools from differential geometry, optimal control problems for group navigation can be formulated that are certified open-loop optimal for a given configuration. This eliminates the need for continual communication between the vehicles and the supervisory agent during operation. The work in this chapter is inspired by the abstractions of large-scale flocks and swarms, such as plagues of locusts and schools of fish. The developments of this chapter rely on the reduction of the flock model introduced in the previous chapter to a subset of essential features characteristic of the overall group that preserves the properties of scalability. This chapter effectively extends the work in the previous chapter, to develop a low-dimensional abstraction of the collective flock at the supervisory level using the high-dimensional interactions of the vehicles.

This chapter is organised as follows: Section 4.1 begins by introducing the notion of manifolds and tensor fields to lay the groundwork for further analysis. Section 4.2 continues by providing a background on matrix Lie groups that will be necessary to understanding the scalability and invariance of the vehicle control task. A background on Riemannian metrics and affine connections are then presented in Section 4.3 and Section 4.4 respectively. These will be necessary to develop the notion of a metric on a manifold for optimal control of a group of vehicles in Section 4.5 and Section 4.6. Optimality conditions to these metrics are then provided in Section 4.7. Using the matrix lie groups presented in Section 4.2, and the model introduced in Chapter 3 for the inter-vehicle relationships of a flock, Section 4.8 presents the main contribution of this chapter to building a rigid body model of a flock. The rigid body model is then extended in Section 4.10 to a semi-rigid body model more typical of a dynamic flock.

4.1. INTRODUCTION TO MANIFOLDS AND TENSOR FIELDS

The set of all configurations of a system is called the *configuration space* and has the structure of a *differentiable manifold* [317]. Denote Q an n-dimensional smooth manifold

with a set of smooth real valued functions $C^\infty(Q)$. The *tangent space* T_qQ to the manifold Q at the point q is the set of all derivations on $C^\infty(Q)$ with elements given by the set of all linear functions on T_qQ. If $\{q^1,\ldots,q^i,\ldots\}$ denotes the set of all local coordinates on Q, then the set of associated derivations $\{\frac{\partial}{\partial q^i}\}$ forms a basis for T_qQ given by:

$$X_q = X_1 \frac{\partial}{\partial q^1} + \ldots + X_2 \frac{\partial}{\partial q^2} \tag{4.1}$$

The *vector field* X on Q is a smooth map $X : Q \to TQ$ that associates a tangent vector $X_q \in T_qQ$ to each point $q \in Q$. Similarly the set $\{dq^i\}$ forms the dual basis for a *one-form* field on α on Q that associates a co-tangent vector α_q to each point $q \in Q$. Let $\langle \cdot,\cdot \rangle$ denote the natural pairing between tangent and cotangent spaces, then $\left\langle dq^i, \frac{\partial}{\partial q^i} \right\rangle$ describes the action of a cotangent vector $\alpha_q \in T_q^*Q$ on a tangent vector $X_q \in T_qQ$ and:

$$\left\langle dq^i, \frac{\partial}{\partial q^i} \right\rangle = \delta_{ij}, \quad i, j = 1,\ldots,n \tag{4.2}$$

If Q is a manifold with dimension n, then the *tangent bundle* TQ and *co-tangent bundle* T^*Q of the manifold is given by a manifold of dimension $2n$ with the union described over all $q \in Q$ of the tangent space and cotangent space respectively, i.e.:

$$TQ = \{(q,v) \mid q \in Q, v \in T_qQ\} \tag{4.3}$$

and

$$T^*Q = \{(q,v) \mid q \in Q, v \in T_qQ\} \tag{4.4}$$

respectively. A manifold that will be useful in the analysis and control of multi-vehicle systems is the *Riemannian manifold*. The Riemannian manifold is constructed by assigning a metric to each tangent space T_qQ that varies smoothly as q varies over Q [317]. Before proceeding with the formal treatment on Riemannian manifolds, a brief introduction into tensors over vector spaces is presented.

4.1.1. TENSOR FIELDS

Tensors define geometrical objects with properties independent of coordinates and reference frames. They can be used to define physical laws with physical meanings and can be combined to generate higher dimensional tensors [317]. Examples of tensors are scalars, vectors and co-vectors. The components of a tensor are coordinate-dependent and change according to a change of basis. Tensors that transform like vectors are called *contravariant*

tensors, and those that transform like a co-vector are called *covariant tensors*. A *tensor field* is a smooth assignment of a tensor over each point q in a manifold Q such that at each point q the vectors and co-vectors belong to the tangent space and its dual space respectively. A (covariant) *metric tensor* g is a symmetric bilinear positive form over a vector space that is used to measure distance in a space. At a given point q in a manifold Q, the metric tensor takes two vectors and returns a real number in a bilinear form. In standard tensor notation, a vector is denoted by v^i and a co-vector by u_i. Metric tensors are denoted by g_{ij} and preserve Einstein's summation convention [317]. The smooth assignment of a metric tensor g to each point q yields a *metric tensor field* denoted in local coordinates by $\mathsf{g}_{ij}(q)dq^i dq^j$ [317]. Physically, a manifold assigned a metric field recovers the geometric properties of the manifold, such as distance, angle, parallel lines, and straight lines along a curve [318].

4.1.2. DISTRIBUTIONS AND CO-DISTRIBUTIONS

A *distribution* Δ assigns a subspace of the tangent space TQ to each point on $q \in Q$. The rank of Δ at point $q \in Q$ is the dimension of the subspace $\Delta_q \subseteq Q$. Given a (local) family of vector fields $X = \{X_1, \ldots, X_k\}$, a distribution is given by the linear subspace of the tangent space TQ [319]:

$$\Delta_q = \text{span}\{X_1, \ldots, X_k\} \tag{4.5}$$

Equation (4.5) provides an equivalent characterisation of the constraints on the configuration manifold and captures the possible directions of motion in a drift free control system [320]. This class of control systems is general enough to include under-actuated, holonomic or nonholonomic systems.

Similar to the notion of a distribution on a tangent space, is the *co-distribution*. The co-distribution is a map that assigns to each $q \in Q$ a linear subspace of $T_q^* Q$. Given a distribution Δ, there exists a unique annihilating co-distribution $\Delta^\perp$ given by the following:

$$\Delta^\perp = \left\{ \alpha \in T_q^* Q \middle| \langle \alpha, X \rangle = 0 \right\}, \quad \forall X \in \Delta \tag{4.6}$$

Provided Δ is non-singular in some open set $U \subset Q$, $\Delta^\perp$ is also non-singular.

A non-singular k-dimensional distribution Δ is *integrable* if there exists k functions $\phi_1, \ldots, \phi_k$ that map U to Q such that $\Delta^\perp = \text{span}\{d\phi_1, \ldots, d\phi_k\}$. Integrability of the co-distribution is equivalent to the integrability of its annihilator.

4.2. MATRIX LIE GROUPS

It was shown in Chapter 3 a flock of vehicles preserves the concepts of *symmetry*. The symmetry of an object (such as the flock of vehicles), can be quantified using the concepts of a *Lie group*. A *Lie group* G is a smooth manifold for which the group operations of multiplication and inversion are smooth functions. Let $g, h \in G$ denote the elements of a group G and $e = \mathrm{Id}$ the group identity. A mapping $L_g : G \to G$ given by $L_g(h) = gh$ is called *left translation* and the vector field X is said to be *left invariant* if:

$$X(gh) = T_h L_g X(h), \quad \forall h \in G \tag{4.7}$$

where $T_h L_g$ is the tangent map to L_g at h. Let $\xi_{1,2,\ldots} \in T_e G$ denote vectors in the tangent space at identity $T_e G$. A left invariant vector field is given by [321]:

$$X(g) = T_e L_g \xi \hat{=} g \cdot \xi \tag{4.8}$$

From Equation (4.8), the value of $X(g)$ is uniquely determined by its values at $g = e$. Therefore, the tangent space $T_e G$ is identified by the set of left invariant vector fields $\mathbf{g}$ describing the finite dimensional *Lie algebra* of G. The Lie bracket of two left invariant vector fields remains left invariant [321]. Define a *Lie bracket* on $\mathbf{g}$ by:

$$g \cdot [\xi_1, \xi_2] \hat{=} [g \cdot \xi_1, g \cdot \xi_2], \quad \xi_1, \xi_2 \in T_e G \tag{4.9}$$

Let $\mathrm{ad}_{\xi_1} \xi_2 = [\xi_1, \xi_2]$ and $\mathbf{g}^*$ be the dual space of $\mathbf{g}$ that describes the set of co-vectors of α such that $\langle \alpha, \xi_1 \rangle$ is a linear function of $\xi_1 \in \mathbf{g}$. The dual operator of ad_{ξ_1} is a mapping described by $\mathrm{ad}^*_{\xi_1} : \mathbf{g}^* \to \mathbf{g}^*$ and defined by $\langle \mathrm{ad}^*_{\xi_1} \alpha, \xi_2 \rangle = \langle \alpha, [\xi_1, \xi_2] \rangle$, $\forall \alpha \in \mathbf{g}^*$.

For a *matrix Lie group*, the group operation is given by matrix multiplication and the corresponding Lie algebra $\mathbf{g}$ is also a matrix Lie algebra with Lie brackets demonstrating the following multiplication properties:

1. $[\xi, \xi] = 0$ for every $\xi \in \mathbf{g}$;
2. $[\xi_1 + \xi_2, \xi_3] = [\xi_1, \xi_3] + [\xi_2, \xi_3]$, $\forall \xi_1, \xi_2, \xi_3 \in \mathbf{g}$;
3. $[\xi_1, [\xi_2, \xi_3]] + [\xi_2, [\xi_3, \xi_1]] + [\xi_3, [\xi_1, \xi_2]] = 0$, $\forall \xi_1, \xi_2, \xi_3 \in \mathbf{g}$; and
4. $[\xi_1, \xi_2] = \xi_1 \xi_2 - \xi_2 \xi_1$.

Condition 2 is typically referred to as *Jacobi's identity*, and implies $[\xi_1, \xi_2] = -[\xi_1, \xi_2]$ (*anti-symmetry*).

Consider the configuration space which represents a dynamic system, and therefore a differentiable manifold. The notion of symmetry of a dynamical system is captured

mathematically using the *actions of a Lie group* on a smooth manifold and its induced action on the tangent bundle of that manifold [317]. The following definition of a symmetry ensues:

Definition 1. (symmetry)

A symmetry of a differential equation is a transformation that preserves the family of solutions.

The Euler vector field in the plane $\mathbb{R}^2$ with coordinates (x_1, x_2) and $x_1 \frac{\partial}{\partial x_1} + x_2 \frac{\partial}{\partial x_2}$ and rotated about the origin is an example of a symmetry on a vector field. The set of all symmetries of a given field form a group [317]. In the case of the Euler field, the generalised form of the Lie group is $GL(2, \mathbb{R})$.

4.2.1. KINEMATIC LIE GROUPS

Of particular utility and importance to the analysis of multi-vehicle systems, is the Special Orthogonal group $SO(3)$ given by:

$$SO(3) = \left\{ R \in \mathbb{R}^{3\times 3} \middle| RR^T = I_3, \det R = +1 \right\} \tag{4.10}$$

corresponding to the set of rotations for a rigid body in three dimensions. A similar form also exists for the planar case. Associated to the Special Orthogonal group $SO(3)$, is the matrix Lie algebra $\mathbf{so}(3)$ given by the 3×3 skew-symmetric matrices:

$$\mathbf{so}(3) = \left\{ \hat{\omega} \in \mathbb{R}^{3\times 3} \middle| \hat{\omega}^T = -\hat{\omega} \right\} \tag{4.11}$$

with bracket structure:

$$\left[\hat{\omega}_1, \hat{\omega}_2\right] = \hat{\omega}_1\hat{\omega}_2 - \hat{\omega}_2\hat{\omega}_1, \quad \hat{\omega}_1, \hat{\omega}_2 \in \mathbf{so}(3) \tag{4.12}$$

where the notation $(\hat{\cdot})$ is used to denote the skew-symmetric form of a vector[2]. Let $\times$ denote the cross product on $\mathbb{R}^3$ and define the operator $\cdot^\wedge : \mathbb{R}^3 \to \mathbf{so}(3)$ as $x^\wedge y \triangleq x \times y$, $\forall x, y \in \mathbb{R}^3$. Then:

$$\left[\hat{\omega}_1, \hat{\omega}_2\right] = \left(\omega_1 \times \omega_2\right)^\wedge, \quad \hat{\omega}_1, \hat{\omega}_2 \in \mathbf{so}(3) \tag{4.13}$$

and $\omega \mapsto \hat{\omega}$ is a Lie algebra isomorphism between the Lie algebra $\mathbf{so}(3)$ (with matrix commutator) and $\mathbb{R}^3$ (with cross product).

---

[2] For a vector $x = (x_1, x_2, x_3) \in \mathbb{R}^3$, the skew-symmetric form is given by the following matrix $\hat{x} \in \mathbb{R}^{3\times 3}$:

$$\hat{x} = \begin{bmatrix} 0 & -x_3 & x_2 \\ x_3 & 0 & -x_1 \\ -x_2 & x_1 & 0 \end{bmatrix}$$

For a rigid body system, the group of rigid transformations on $\mathbb{R}^3$ is defined as the set of rotations $R \in SO(3)$, and translations $d \in \mathbb{R}^3$ belonging to the Special Euclidean group $SE(3)$ with group element described by the pair $g = (R, d) \in SO(3) \times \mathbb{R}^3$, i.e.:

$$SE(3) = \left\{ g \middle| g = \begin{bmatrix} R & d \\ 0_{1\times 3} & 1 \end{bmatrix}, R \in \mathbb{R}^{3\times 3}, RR^T = I_3, \det R = +1, d \in \mathbb{R}^3 \right\} \tag{4.14}$$

Associated with the Special Euclidean group $SE(3)$ is the matrix Lie algebra $\mathbf{se}(3)$ given by:

$$\mathbf{se}(3) = \left\{ \xi = \begin{bmatrix} \hat{\omega} & v \\ 0_{1\times 3} & 0 \end{bmatrix} \middle| \xi = (\hat{\omega}, v), \hat{\omega} \in \mathbb{R}^{3\times 3}, \hat{\omega}^T = -\hat{\omega}, v \in \mathbb{R}^3 \right\} \tag{4.15}$$

where ξ is the algebra element given by $\xi = (\omega, v) \in \mathbf{so}(3) \times \mathbb{R}^3$. Note the vector space $\mathbf{se}(3)$ is isomorphic to $\mathbb{R}^6$ via the mapping $\hat{\xi} \mapsto \xi = (\omega, v) \in \mathbb{R}^6$ [319].

4.2.2. MOTION PARAMETERISATION

Let $\{M\}$ denote a body-fixed frame centred at O' of a rigid body, and $\{F\}$ a fixed inertial reference frame. Denote a curve on $SE(3)$ as $g(t) : [-a, a] \to SE(3)$. An element $\xi(t)$ of the Lie algebra $\mathbf{se}(3)$ can be associated to the tangent vector $\dot{g}(t)$ of the curve at any arbitrary point t by:

$$\xi(t) = g^{-1}(t)\dot{g}(t) = \begin{bmatrix} R^T\dot{R} & R^T\dot{d} \\ 0 & 0 \end{bmatrix} \tag{4.16}$$

A curve on $SE(3)$ described by $g(t) = (R(t), d(t)) \in SE(3)$ and velocity given by the tangent vector physically represents the motion of the rigid body with vector pair $\xi(t) = (\omega, v) \in \mathbb{R}^6$ describing the angular and linear velocities respectively. In kinematics, elements of this form are called *twists* [319] and the Lie algebra $\mathbf{se}(3)$ corresponds to the space of twists [291]. It can be easily verified that the motion $\xi(t)$ computed from Equation (4.16) is a left invariant representation of the tangent vector $\dot{g}(t)$ and is independent of the choice of frame $\{F\}$. Alternatively, the tangent vector $\dot{g}(t)$ can be identified with a *right invariant* twist (invariant with respect to the choice of the body-fixed frame $\{M\}$) [291].

Any element of the vector space $\mathbf{se}(3)$ can be expressed as a 6×1 vector of components corresponding to a chosen basis [291]. The standard basis for $\mathbf{se}(3)$ is:

$$L_1 = \begin{bmatrix} 0 & 0 & 0 & 0 \\ 0 & 0 & -1 & 0 \\ 0 & 1 & 0 & 0 \\ 0 & 0 & 0 & 0 \end{bmatrix} \qquad L_2 = \begin{bmatrix} 0 & 0 & 1 & 0 \\ 0 & 0 & 0 & 0 \\ -1 & 0 & 0 & 0 \\ 0 & 0 & 0 & 0 \end{bmatrix}$$

$$L_3 = \begin{bmatrix} 0 & -1 & 0 & 0 \\ 1 & 0 & 0 & 0 \\ 0 & 0 & 0 & 0 \\ 0 & 0 & 0 & 0 \end{bmatrix} \qquad L_4 = \begin{bmatrix} 0 & 0 & 0 & 1 \\ 0 & 0 & 0 & 0 \\ 0 & 0 & 0 & 0 \\ 0 & 0 & 0 & 0 \end{bmatrix} \tag{4.17}$$

$$L_5 = \begin{bmatrix} 0 & 0 & 0 & 0 \\ 0 & 0 & 0 & 1 \\ 0 & 0 & 0 & 0 \\ 0 & 0 & 0 & 0 \end{bmatrix} \qquad L_6 = \begin{bmatrix} 0 & 0 & 0 & 0 \\ 0 & 0 & 0 & 0 \\ 0 & 0 & 0 & 1 \\ 0 & 0 & 0 & 0 \end{bmatrix}$$

The twists L_1, L_2, and L_3 represent the instantaneous rotations about the x, y, and z axes; L_4, L_5, and L_6 represent the instantaneous translations along the x, y, and z axes, respectively [291]. The components of a twist $\xi \in \mathbf{se}(3)$ in this basis are given precisely by the velocity vector pair $\{\omega, v\}$. If $\{\omega_1, v_1\}$ and $\{\omega_2, v_2\}$ are vector pairs corresponding to the twists ξ_1 and ξ_2, the vector pair corresponding to their Lie bracket $[\xi_1, \xi_2]$ is given by [291]:

$$\{\omega, v\} = \{\omega_1 \times \omega_2, \omega_1 \times \omega_2 + v_1 \times v_2\} \tag{4.18}$$

The Lie bracket of two elements of a Lie algebra is an element of the Lie algebra and can be expressed as a linear combination of the basis vectors; i.e.:

$$[L_i, L_j] = \sum_k c_{ij}^k L_k \tag{4.19}$$

where l_{ij}^k are *structure constants* of the Lie algebra (with respect to the chosen basis) and determine the bracket operation on the Lie algebra [322].

4.2.3. ADJOINT ACTION OF *SE*(3) ON *se*(3) AND FRAME TRANSFORMATION RULES

In the following section, the actions of a Lie group for rigid body motion are defined. The following definitions are well established and can be found in [319].

Definition 2. (left action)

Let Q be a smooth manifold and G a Lie group. A left action of G on Q is a smooth map $\Phi_g : Q \to Q$, $g \in G$ such that:

- $\Phi_e(q) = q$, *for any* $q \in Q$;

- *For every,* $g,h \in G$ *and* $q \in Q$, $\Phi_g(\Phi_h(q)) = \Phi_{gh}(q)$.

Definition 3. (conjugation map)

Let G *be a Lie group. The map* $I_g : G \to G$, $g \in G$ *given by* $I_g(h) = ghg^{-1}$ *is called the conjugate map.*

Consequently, the map I_g defines a left action of G onto itself.

Definition 4. (adjoint action)

The tangent map of I_g *at identity* e, $\mathrm{Ad}_g = T_e I_g$ *is called the adjoint action of* G *on* $\mathbf{g}$, *its Lie algebra.*

For the subgroup $SO(3)$ of $SE(3)$:

$$\mathrm{Ad}_g \xi = g\xi g^{-1} \tag{4.20}$$

and $\xi \in \mathbf{g}$ is written in matrix form [319]. Therefore, the adjoint action of the group $g = \begin{bmatrix} R & d \\ 0 & 1 \end{bmatrix} \in SE(3)$ on the Lie algebra $\xi \in \mathbf{se}(3)$ is given by:

$$\xi = \begin{bmatrix} \hat{\omega} & v \\ 0 & 0 \end{bmatrix} \in \mathbf{se}(3), \quad \mathrm{Ad}_g \xi = g\xi g^{-1} = \begin{bmatrix} \overline{R\omega} & Rv - \overline{R\omega} d \\ 0 & 0 \end{bmatrix} \in \mathbf{se}(3) \tag{4.21}$$

where the notation $\overline{(\cdot)}$ is used to represent the skew-symmetric operator of multiplied matrices. Similarly, the adjoint action Ad_g of the twist written in vector form is represented by the 6×6 matrix $[\mathrm{Ad}_g]$:

$$\zeta = \begin{bmatrix} \omega \\ v \end{bmatrix} \in \mathbf{se}(3), \quad \mathrm{Ad}_g \zeta = [\mathrm{Ad}_g]\zeta \in \mathbf{se}(3), \quad [\mathrm{Ad}_g] = \begin{bmatrix} R & 0 \\ \hat{d}R & R \end{bmatrix} \tag{4.22}$$

The adjoint action of $SE(3)$ on $\mathbf{se}(3)$ can be used to write transformation rules for trajectories and twists when the inertial or the body frame is displaced.

For a rigid body moving in free space, let $\{F\}$ be a fixed inertial reference frame and $\{M\}$ be a body-fixed frame at O'. The motion of the body in the inertial frame is uniquely described by the curve $g(t) = g_{FM}(t) \in SE(3)$; where the rotation of $\{M\}$ and the position of O' are defined with respect to $\{F\}$.

Proposition 1 gives the transformation rules for displacements of body-fixed frames.

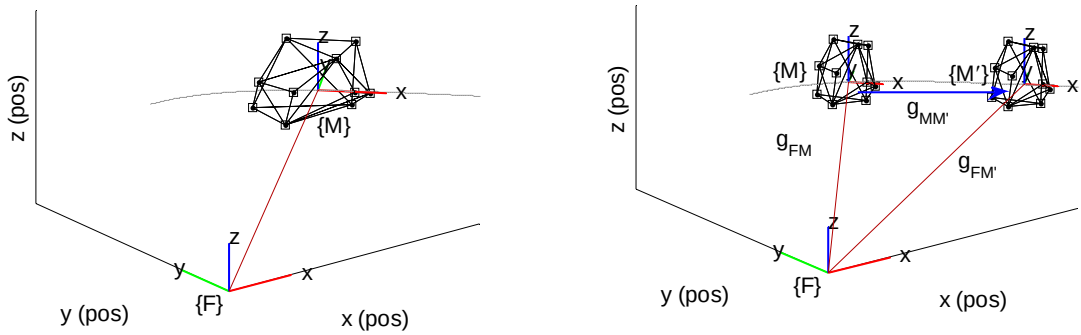

(a) **(b)**

Figure 4-1. Coordinate frames for specifying rigid body motions.

Proposition 1. (body frame displacements)

Assume the body frame is displaced by (a constant) $g_{MM'}$ *to* $\{M\}$ *(see Figure 4-1 (b)). Let* $g'(t) = g_{FM'}(t) \in SE(3)$ *describe the motion of* $\{M'\}$ *in* $\{F\}$ *and* $\xi'(t)$ *be the corresponding twist. Then, the following are true:*

- $g'(t) = g(t)g_{MM'}$; and
- $\xi'(t) = \mathrm{Ad}_{g_{MM'}}\xi(t)$.

Proof.

The first part follows immediately from the composition rule for elements in $SE(3)$. *For the second part, the result follows from the composition rule* $g_{FM'} = g_{FM}g_{MM'}$, *the definition of the adjoint map and the definition of twists, i.e.:*

$$\begin{aligned}\xi'(t) &= g'^{-1}(t)\dot{g}'(t) = g_{FM'}^{-1}\dot{g}_{FM'} = g_{MM'}^{-1}g_{FM}^{-1}\dot{g}_{FM}g_{MM'} \\ &= \mathrm{Ad}_{g_{MM'}^{-1}}\xi(t) = \mathrm{Ad}_{g_{MM}}\xi(t)\end{aligned} \tag{4.23}$$

or, if the twists are written in vector form,

$$\zeta'(t) = [Ad_{g_{MM}}]\zeta(t) \tag{4.24}$$

where the 6×6 *matrix form of the adjoint action is given by (4.22).*

The following proposition describes the transformation rules for changes in the inertial frame.

Proposition 2. (inertial frame transformations)

Suppose inertial frame $\{F\}$ *is displaced by a constant* $g_{FF'}$ *to a new* $\{F'\}$ *and the body fixed frame* $\{M\}$ *is left unchanged. Let* $g'(t) = g_{F'M} \in SE(3)$ *denote the motion of* $\{M\}$ *as seen from* $\{F'\}$*. The following describes the relation between curves and twists when the inertial frame is displaced:*

- $g'(t) = g_{F'F} g(t)$;
- $\xi'(t) = \xi(t)$.

Proof.

For the first part, $g'(t) = g_{F'M}(t) = g_{FF'}^{-1} g_{FM}(t) = g_{F'F} g(t)$*. For the second part:*

$$\xi'(t) = g'^{-1}(t)\dot{g}(t) = g_{F'M}^{-1}\dot{g}_{F'M} = g_{FM}^{-1} g_{F'F}^{-1} g_{FF'}\dot{g}_{FM} = g_{FM}^{-1}\dot{g}_{FM} = \xi(t) \tag{4.25}$$

Corollary.

The twist $\xi(t) = g^{-1}(t)\dot{g}(t)$ *is invariant to changes in the pose of the inertial frame. The adjoint of the transformation of the body-fixed frame relates the twists when the body frame is displaced.*

4.2.4. INVARIANT PROPERTIES OF THE LIE GROUP CONSTRUCTION

A *differentiable vector field* is a smooth assignment of a tangent vector to each element of the manifold [323]. In the case of $SE(3)$, a differentiable vector field X is obtained by left translation of an element $\xi \in \mathbf{se}(3)$. Let $\bar{\xi}$ denote a vector field obtained via left translation of the Lie algebra element ξ, then the value of a vector field X at an arbitrary point $g \in SE(3)$ is given by:

$$X(g) = \bar{\xi}(g) = g \cdot \xi \tag{4.26}$$

and X is a *left invariant vector field* [324]. Physically, left-invariance corresponds to independence of the choice of inertial reference frame [291]

Let $L_1, L_2, \ldots, L_6$ denote the basis of the Lie algebra $\mathbf{se}(3)$, and denote $\bar{L}_1(g), \bar{L}_2(g), \ldots$ $\bar{L}_6(g)$ the basis of the tangent space at any point $g \in SE(3)$. Then, a vector field X can be expressed as [323]:

$$X = \sum_{i=1}^{6} X^i \bar{L}_i \tag{4.27}$$

where X^i is a real-valued function that varies over the manifold Q [323]. If the coefficients X^i are constant, then X is left invariant. For a rigid body, let $g(t)$ denote the motion of the of the centroid O' with respect to a fixed inertial reference frame $\{F\}$, and $V = \frac{dg}{dt}$ the vector field tangent to $g(t)$. Denote $\{\omega, v\}$ the vector pair of functions associated to any arbitrary vector field X, with components

$$\omega = \left[X^1, X^2, X^3\right]^T, \quad v = \left[X^4, X^5, X^6\right]^T \tag{4.28}$$

then, the vector pair $\{\omega, v\}$ associated to V corresponds to the instantaneous twist for the motion [319]. Motions for which the twist $\{\omega, v\}$ is constant are known in kinematics as *screw motions* [319]. Screw motions physically correspond to rotation of the rigid body around the centreline with a constant angular velocity ω and concurrent translation of the body along the line with constant translational velocity v.

4.3. RIEMANNIAN METRICS ON THE LIE GROUP

Physically, the Riemannian metric provides the notion of length of a vector (or distance between two points on a manifold) [324]. By understanding the properties of the Riemannian metric on a Riemannian manifold, the definition of a metric on $SE(3)$ for motion planning will become intuitive. In the following sections, the properties of the Riemannian metric are introduced as a preliminary understanding into the development of metrics on $SE(3)$.

Definition 5. (Riemannian metric)

A smoothly varying, positive definite, bilinear, symmetric form $\langle \cdot, \cdot \rangle$ assigned to the tangent space T_qQ at each point q on the manifold Q is a Riemannian metric.

Definition 6. (Riemannian manifold)

A manifold endowed with a Riemannian metric defines a Riemannian manifold.

On an n-dimensional manifold, the metric is locally characterised by an $n \times n$ matrix of C^∞ functions $\mathsf{g}_{ij} = \langle X_i, X_j \rangle$ where X_i and X_j are basis vector fields. The Riemannian metric provides the notion of the length of curves on a manifold [291]. In mechanical problems, the kinetic energy of a system defines a Riemannian metric that induces a Riemannian manifold. Curves that minimise the energy metric between two points are called *geodesics*. Geodesics are a generalisation of straight lines in Euclidean space $\mathbb{R}^n$ to

Riemannian manifolds. A formal treatment of geodesics on Riemannian and semi-Riemannian manifolds is presented in Section 4.4.2. The following proposition formalises the relationship between Riemannian metrics and Lie groups and provides a physical interpretation of the Riemannian metric of a Lie group.

Proposition 3. (Riemannian metrics on Lie groups)

On any Lie group, and thus $SE(3)$*, an inner product on the Lie algebra* $\mathbf{se}(3)$ *can be extended to a Riemannian metric over the manifold using left (or right) translation [321].*

Proof.

Consider the inner product of two arbitrary elements $\xi_1, \xi_2 \in \mathbf{se}(3)$ *on the Lie group* $SE(3)$ *given by:*

$$\langle \xi_1, \xi_2 \rangle_I = \zeta_1^T W \zeta_2 \tag{4.29}$$

where ζ_1 *and* ζ_2 *are the* 6×1 *vectors of components* ξ_1 *and* ξ_2 *with respect to some basis and* W *is a positive definite matrix. Let* V_1 *and* V_2 *denote two arbitrary tangent vectors at the group element* $g \in SE(3)$*. The inner product* $\langle V_1, V_2 \rangle_g$ *on the tangent space* $T_g SE(3)$ *is given by:*

$$\langle V_1, V_2 \rangle_g = \langle g^{-1} V_1, g^{-1} V_2 \rangle_I \tag{4.30}$$

A metric obtained in this way describes a left invariant metric [291].

Proposition 4. (left invariance of the Riemannian metric)

Physically, a left invariant metric is independent of the choice of the inertial frame.

Proof.

Let $g_1(t)$ *and* $g_2(t)$ *represent two motions of a rigid body passing through a point* g *at* $t = t_0$*. Denote* $V_1 = (dg_1(t)/dt)$ *and* $V_2 = (dg_2(t)/dt)$ *the corresponding velocity vector fields such that* $V_1, V_2 \in T_g SE(3)$*. Let* C *describe a displacement of the inertial reference frame. In the new reference frame, the motions become* $\tilde{g}_1(t) = Cg_1(t)$ *and* $\tilde{g}_2(t) = Cg_2(t)$*, and the velocity vector fields* $\tilde{V}_1 = CV_1$ *and* $\tilde{V}_2 = CV_2$*. Then from Equation (4.30):*

$$\langle \tilde{V}_1, \tilde{V}_2 \rangle_{Cg} = \langle \tilde{g}_1^{-1} \tilde{V}_2, \tilde{g}_1^{-1} \tilde{V}_2 \rangle = \langle g^{-1} C^{-1} \tilde{V}_1, g^{-1} C^{-1} \tilde{V}_2 \rangle_I = \langle V_1, V_2 \rangle_g \tag{4.31}$$

Hence, the metric $\langle \cdot, \cdot \rangle$ is invariant to change in inertial reference frame. A right invariant metric is similarly defined.

A detailed description of invariant metrics on $SE(3)$ is presented in Section 4.5. In the proceeding section, the Riemannian connection is used to define a measure of length for a curve on a manifold.

4.4. THE AFFINE CONNECTION AND ITS KINEMATIC CONNECTION TO RIGID BODY MOTION

In the previous section, the motion of a rigid body was established using the smooth curve $g(t) \in SE(3)$. The velocity of each point along $g(t) \in SE(3)$ was shown to correspond to a value in the vector field V belonging to the tangent space $T_g SE(3)$. In the following section, higher-order tangent spaces are analysed to develop kinematic control laws for the group of vehicles. Specifically, the acceleration and jerk of the rigid body are investigated. Differentiation of vector fields along a curve involves the subtraction of vectors at different points. In the tangent space, these points are not related. In this section, the problem of differentiating a vector field along a curve is addressed using the theory of affine connections. Affine connections are used to provide a means of transporting vectors along a curve from one tangent space to another. Before proceeding with the definition of affine connections, it is first useful to describe the notion of a *covariant derivative* of a vector field.

4.4.1. THE AFFINE CONNECTION

Definition 6. (covariant derivative)

Let $X \in T_g SE(3)$ be an arbitrary vector field defined along the curve $g(t) \in SE(3)$. The covariant derivative of X along $g(t)$ is:

$$\left.\frac{DX}{dt}\right|_{t_0} = \lim_{t \to t_0} \frac{X^{t_0}(t) - X(t_0)}{t} \tag{4.32}$$

i.e., for the covariant derivative of X to be defined at a point g, only the value of X at g and the rate of change of X along $g(t)$ is required.

Proposition 6. (covariant derivative of a vector field)

The covariant derivative of a vector field is another vector field.

Proof.

Taking the covariant derivative of a vector field Y along its integral curve, yields a covariant derivative of X with respect to the vector field Y, i.e.:

$$\nabla_Y X\big|_{g_0} = \frac{DX}{dt}\bigg|_{t_0} \tag{4.33}$$

where DX/dt is taken along the integral curve of Y passing through g_0 at $t = t_0$ [291].

Definition 7. (affine connection)

Let X, Y denote smooth vector fields. An affine connection on $SE(3)$ is a smooth map $\nabla : X(SE(3)) \times X(SE(3)) \to X(SE(3))$ denoted by $\nabla : X, Y \mapsto \nabla_X Y$ that assigns to each pair X, Y a smooth vector field $\nabla_X Y$ such that for all smooth functions f, g on $SE(3)$ and for all vector field X, Y, Z the following properties are observed:

1. $\nabla_{fX+gY} Z = f\nabla_X Z + g\nabla_Y Z$;
2. $\nabla_X (Y + Z) = \nabla_X Y + \nabla_Y Z$; *and*
3. $\nabla_X (fY) = f\nabla_X Y + X(f)Y$.

where $\nabla_X Y$ is the covariant derivative of Y with respect to X and represents the differentiation of vectors (and tensors).

Note, the affine connection and covariant derivative are often used interchangeably in the literature.

Definition 8. (Christoffel symbols)

Given the local coordinates $(q^1, \ldots, q^i, \ldots, q^n)$ of an arbitrary manifold Q and a metric g, denote g_{jk} and g^{jk} as coordinate representations of the metric g and its inverse g^{-1}. The Christoffel symbols Γ_{ij}^k on Q are given by:

$$\Gamma_{ij}^k = \tfrac{1}{2}\mathsf{g}^{mk}\left(\frac{\partial \mathsf{g}_{mj}}{\partial q^i} + \frac{\partial \mathsf{g}_{mi}}{\partial q^j} - \frac{\partial \mathsf{g}_{ij}}{\partial q^m}\right) \tag{4.34}$$

Following Proposition 6 and Definitions 6-8, the affine connection, or covariant derivative, can be expressed as a linear combination of vector fields. Given the local coordinates $(q^1, \ldots, q^i, \ldots, q^n)$ of an arbitrary manifold Q and metric g, the affine connection can be

applied to a pair of coordinate vector fields $\frac{\partial}{\partial q^i}$ via association with the Christoffel symbols Γ_{ij}^k:

$$\nabla_{\frac{\partial}{\partial q^i}}\left(\frac{\partial}{\partial q^j}\right) = \Gamma_{ij}^k \frac{\partial}{\partial q^k} \tag{4.35}$$

where the summation convention is used to denote the summation of repeated indices.

On $SE(3)$, the Christoffel symbols Γ_{ij}^k of the connection at a point $g \in SE(3)$ are given by:

$$\nabla_{\bar{L}_i} \bar{L}_j = \Gamma_{ij}^k \bar{L}_k \tag{4.36}$$

where $\bar{L}_1, \ldots, \bar{L}_6$ is the basis in $T_g SE(3)$.

Associated to the affine connection ∇ on an arbitrary manifold Q is the *torsion tensor* T and *curvature tensor* R given by Equation (4.37) and Equation (4.38) respectively:

$$\mathsf{T}(X,Y) = \nabla_X Y - \nabla_Y X - [X,Y] \tag{4.37}$$

$$\mathsf{R}(X,Y)Z = \nabla_X \nabla_Y Z - \nabla_Y \nabla_X Z - \nabla_{[X,Y]} Z \tag{4.38}$$

On a Riemannian manifold, there exists a unique affine connection ∇ which is torsion-free and compatible with the metric [325]:

$$X\langle Y,Z\rangle = \langle \nabla_X Y, Z\rangle + \langle Y, \nabla_X Z\rangle \tag{4.39}$$

and symmetric, i.e.:

$$\nabla_X Y - \nabla_Y X = [X,Y] \tag{4.40}$$

This connection is known as the *Riemannian* or *Levi-Civita connection* and induces a compatible Riemannian metric on the manifold Q. In Section 4.6.2, the Riemannian connections corresponding to left invariant metrics on the $SE(3)$ manifold are investigated. In the proceeding section, the notion of length on a manifold is investigated with respect to the Riemannian metric induced by the Riemannian connection. Together, these concepts will be used to construct length-minimal curves for motion planning of a rigid body system.

4.4.2. GEODESICS AND THEIR RELATIONSHIP TO LENGTH

Given a Riemannian metric $\langle \cdot,\cdot \rangle$ on $SE(3)$, the length $L(g)$ of a smooth curve $g:[a,b] \to SE(3)$ is given by [325]:

$$L(g) = \int_a^b \langle V,V\rangle^{\frac{1}{2}} dt \tag{4.41}$$

A curve that minimises the functional $L(g)$ also minimises the *energy functional* $E(g)$ [325]:

$$E(g) = \int_a^b \langle V,V\rangle dt \tag{4.42}$$

If a curve minimises a functional, it must also be a critical point. Critical points of the energy functional $E(g)$ satisfy the following equation [325]:

$$\nabla_{\frac{dg}{dt}} \frac{dg}{dt} = 0 \tag{4.43}$$

and are known as *geodesics*.

For a rigid body with motion $g(t) \in SE(3)$, velocity $V(t) = dg(t)/dt$ and Riemannian connection ∇, the acceleration $\mathcal{A}(t)$ (and higher derivatives) of the rigid body, is given by the covariant derivative of the velocity $V(t)$ (and acceleration $\mathcal{A}(t)$ etc); i.e.:

$$\mathcal{A}(t) = \frac{D}{dt}\left(\frac{dg}{dt}\right) = \nabla_V V \tag{4.44}$$

From Equation (4.43) and Equation (4.44), the acceleration of a rigid body moving along a geodesic is zero.

The minimum acceleration curves for the terminal conditions $g : [a,b] \to SE(3)$ and $V : [v_0, v_1] \to SE(3)$ can be obtained by minimising the square of the L^2 norm of the acceleration:

$$L_a = \int_a^b \langle \nabla_V V, \nabla_V V \rangle dt \tag{4.45}$$

Here ∇ is the Riemannian connection and $\langle \cdot, \cdot \rangle$ is the Riemannian metric over the manifold.

Suppose $q(t) \in Q$ is the configuration of the system and $\dot{q}(t) \in T_q Q$ its velocity, then a geodesic in the local coordinates is given by the solution of the following second-order differential equation:

$$\ddot{q}^i + \Gamma^i_{jk} \dot{q}^j \dot{q}^k = 0 \tag{4.46}$$

where Γ^i_{jk} are the Christoffel symbols. This vector field is known as the *geodesic spray* or *geodesic flow* and is a local representation of a vector field on $T_q Q$ [326]. In Section 4.7, solutions to Equation (4.46) are used to define optimal motion control plans for a group of vehicles.

4.4.3. THE EXPONENTIAL MAP

Let Q denote a manifold with a connection ∇, and let $\phi_\xi : \Re \to G$ denote the left invariant vector field X_ξ passing through e at $t = 0$, such that $\phi_\xi(0) = e$ and $\frac{d}{dt}\phi_\xi(t) = X_\xi(\phi_\xi(t))$. Then $\phi_\xi(t)$ is the unique one-parameter subgroup of G whose tangent vector at the identity e is equal to ξ. The function $\exp : T_e G \to G$ defined by $\exp(\xi) = \phi_\xi(1)$ is called the

exponential map of the Lie algebra $\mathbf{g}$ into G. Furthermore, $\exp : \mathbf{g} \to G$ is a local diffeomorphism from a neighbourhood of zero in $\mathbf{g}$ onto a neighbourhood of e in G. This gives a local chart for Q called the *normal coordinates* and are instrumental in the parameterisation of a Lie group. For a matrix Lie group, the exponential map $\exp : \mathbf{g} \to G$ is given by the ordinary series expansion:

$$\exp \xi = \sum_{k=0}^{\infty} \frac{\xi^n}{n!} \tag{4.47}$$

Given a twist $\xi \in \mathbf{se}(3)$ with vector pair $\{\omega, v\}$ that induces a screw motion $g(t)$ about the screw axis $\{\omega, v\}$, the exponential map $\exp : \mathbf{se}(3) \to \mathbf{se}(3)$ is defined as:

$$\exp(t\xi) = g(t) \tag{4.48}$$

Using Equation (4.16), it can be shown that the exponential map given in Equation (4.48) agrees with the exponentiation of matrices in Equation (4.47). The exponential map for the special orthogonal group $SO(3)$ can be computed explicitly, and is given by Rodrigue's formula:

$$\exp(\hat{\omega}) = I_3 + \frac{\hat{\omega}}{\|\omega\|} \sin(\|\omega\|) + (1 - \cos(\|\omega\|)) \frac{\hat{\omega}^2}{\|\omega\|^2} \tag{4.49}$$

where $\|\cdot\|$ is the Euclidean norm of a vector.

Similarly, the exponential map for the special Euclidean group $SE(3)$ with Lie algebra described by the following 4×4 matrix:

$$\xi = \begin{bmatrix} \hat{\omega} & v \\ 0 & 0 \end{bmatrix}, \quad \omega, v \in \mathbb{R}^3 \tag{4.50}$$

and $[\xi_1, \xi_2] = \xi_1 \xi_2 - \xi_2 \xi_1$, can be described by:

$$\exp \xi = \begin{bmatrix} I & v \\ 0 & I \end{bmatrix}, \quad \omega = 0 \quad \text{and} \quad \exp \xi = \begin{bmatrix} \exp(\hat{\omega}) & Av \\ 0 & I \end{bmatrix}, \quad \omega \neq 0 \tag{4.51}$$

where:

$$A = I_3 + \frac{\hat{\omega}}{\|\omega\|^2} (1 - \cos(\|\omega\|)) + \frac{\hat{\omega}^2}{\|\omega\|^3} (\|\omega\| - \sin(\|\omega\|)) \tag{4.52}$$

Now, consider the motion of a rigid body given by:

$$\frac{dg(t)}{dt} = g(t)\xi(t) \tag{4.53}$$

Since $\xi(t)$ belongs to the Lie algebra $\mathbf{se}(3)$, $\forall t$, then it can be expressed as a linear combination of the basis vectors in Equation (4.17) [324]. The solution of this differential equation can be written as the product of exponentials:

$$g(t) = \prod_{i=1}^{6} \exp(S^i(t) L_i) \tag{4.54}$$

where $S^i(t)$ are analytic functions dependent on g and are taken as the set of *local coordinates*.

4.5. THE METRIC PROPERTIES OF *SE*(3)

In Section 4.3, the invariant properties of the Riemannian metric on $SE(3)$ were briefly described as a measure of length of a curve on a manifold. The length of a curve is one example of a metric for optimal trajectory generation. In this section, the metric properties on $SE(3)$ are investigated to develop other invariant metrics for optimal trajectory generation for groups of vehicles. The results in this section can be found in a similar form in [319].

Consider the motion of a group of vehicles. Let q_M be a vector in the body-fixed frame $\{M\}$ corresponding to the position of a vehicle in the flock, and let q_F denote the same vector in the fixed inertial frame $\{F\}$. These vectors can be related by the lifted action of $SE(3)$ on $\mathbb{R}^3$:

$$q_F = R_{FM} q_M \tag{4.55}$$

where $g_{FM} = (R_{FM}, d_{FM}) \in SE(3)$ is the position and orientation of the frame $\{M\}$ relative to frame $\{F\}$ [319]. Let $W \in \mathbb{R}^{n \times n}$ denote the symmetric matrix representation of the left invariant quadratic form $\langle \cdot, \cdot \rangle$. By Proposition 4, a metric is invariant under change of coordinate frames if:

$$WR = RW, \quad R \in SO(3) \tag{4.56}$$

A final property for the development of motion plans for a group of vehicles, is the definition of a bi-invariant metric on $SE(3)$. The following theorem presents the conditions for which a metric on $SE(3)$ is bi-invariant and follows from [319].

Lemma 1. (bi-invariance of the quadratic form $\langle \cdot, \cdot \rangle$)

Let $\langle \cdot, \cdot \rangle$ be a quadratic form (bilinear and symmetric) defined at the identity of $SE(3)$ and extended by left invariance throughout the manifold. Then, $\langle \cdot, \cdot \rangle$ is bi-invariant if and only if:

$$\langle \xi_1, \xi_2 \rangle_I = \langle \mathrm{Ad}_g \xi_1, \mathrm{Ad}_g \xi_2 \rangle_I, \quad \forall g \in SE(3), \quad \forall \xi_1, \xi_2 \in \mathbf{se}(3) \tag{4.57}$$

Proof.

By Proposition 4, $\langle \cdot,\cdot \rangle$ *is both left and right invariant for any* $\xi_1, \xi_2 \in \mathbf{se}(3)$ *and any* $g \in SE(3)$. *From Equation (4.20) and Equation (4.57):*

$$\langle \xi_1, \xi_2 \rangle_I = \langle g\xi_1, g\xi_2 \rangle_g = \langle g\xi_1 g^{-1}, g\xi_2 g^{-1} \rangle_{gg^{-1}} = \langle g\xi_1 g^{-1}, g\xi_2 g^{-1} \rangle_I \tag{4.58}$$

Left invariance of the quadratic form $\langle \cdot,\cdot \rangle$ *was given in Proposition 3 and Proposition 4. To prove bi-invariance of* $\langle \cdot,\cdot \rangle$, *it is sufficient to prove right invariance of the quadratic form. Let* $V_1(h)$ *and* $V_2(h)$ *be two vectors from* $T_h SE(3)$ *and* h *an arbitrary element of* $SE(3)$. *For any* $g \in SE(3)$, *the following is observed:*

$$\begin{aligned} \langle V_1(h)g, V_2(h)g \rangle_{hg} &= \langle (hg)^{-1}V_1(h)g, (hg)^{-1}V_2(h)g \rangle_{(hg)^{-1}hg} \\ &= \langle g^{-1}h^{-1}V_1(h)g, g^{-1}h^{-1}V_2(h)g \rangle_I \\ &= \langle gg^{-1}h^{-1}V_1(h)gg^{-1}, gg^{-1}h^{-1}V_2(h)gg^{-1} \rangle_I \\ &= \langle h^{-1}V_1(h), h^{-1}V_2(h) \rangle_I \\ &= \langle V_1(h), V_2(h) \rangle_h \end{aligned} \tag{4.59}$$

hence, $\langle \cdot,\cdot \rangle$ *is both left and right invariant (bi-invariant).*

Lemma 2. (commutation of invariant metrics)

Let $W \in \mathbb{R}^{n \times n}$ *denote the symmetric matrix representation of the quadratic form* $\langle \cdot,\cdot \rangle$ *on* $SE(3)$ *that satisfies Equation (4.56). Then,*

$$W = \gamma I \tag{4.60}$$

for some $\gamma \in \mathbb{R}$.

Proof.

Let v *be an eigenvector of* W *corresponding to an eigenvalue* λ. *Then, from Equation (4.56):*

$$WRv = RWv = \lambda Rv \tag{4.61}$$

Therefore, Rv *is an eigenvector of* W *for any* $R \in SO(3)$ *and* $Ww = \lambda w$ *for any unit vector* $w \in \mathbb{R}^3$. *By taking* w *as the standard Euclidean basis in* $\mathbb{R}^3$, *it follows that* $W = \gamma I$.

Theorem 1. (bi-invariance of the metric on *SE*(3))

The quadratic form $\langle \cdot,\cdot \rangle$ *on* $SE(3)$ *with matrix representation* W *is bi-invariant if and only if* W *has the form:*

$$W = \begin{bmatrix} \alpha I & \beta I \\ \beta I & 0 \end{bmatrix} \tag{4.62}$$

Proof.

By Lemma 1, $\langle \cdot,\cdot \rangle$ *is bi-invariant if and only if for all* $\xi_1, \xi_2 \in \mathbf{se}(3)$ *and* $g \in SE(3)$ *Equation (4.57) is valid. Let:*

$$W = \begin{bmatrix} M & N \\ N^T & P \end{bmatrix} \tag{4.63}$$

denote the generalised form of W *with* $M, N, P \in \mathbb{R}^{3\times 3}$, *and* M, P *are symmetric. Expanding the quadratic form* $\langle \cdot,\cdot \rangle$ *in Equation (4.57), and using the matrix representation in Equation (4.63):*

$$\begin{bmatrix} M & N \\ N^T & P \end{bmatrix} = [\mathrm{Ad}_g^T] \begin{bmatrix} M & N \\ N^T & P \end{bmatrix} [\mathrm{Ad}_g], \quad \forall g \in SE(3) \tag{4.64}$$

Using the definition of the adjoint mapping on $\mathbb{R}^6$ *in Equation (4.22), the conditions for bi-invariance becomes:*

$$\begin{bmatrix} M & N \\ N^T & P \end{bmatrix} = \begin{bmatrix} R^T & -R^T\hat{d} \\ 0 & R^T \end{bmatrix} \begin{bmatrix} M & N \\ N^T & P \end{bmatrix} \begin{bmatrix} R & 0 \\ \hat{d}R & R \end{bmatrix} \tag{4.65}$$

which is equivalent to:

$$M = R^T M R - R^T \hat{d} N^T R + R^T N \hat{d} R - R^T \hat{d} P \hat{d} R \tag{4.66}$$

$$N = R^T N R - R^T \hat{d} P R \tag{4.67}$$

$$P = R^T P R \tag{4.68}$$

By Lemma 2, P *in Equation (4.68) must be of the form:*

$$P = \gamma I \tag{4.69}$$

Letting $d = 0$ *in Equation (4.66) and Equation (4.67), then:*

$$N = \beta I, \quad M = \alpha I \tag{4.70}$$

Using $P = \gamma I$, $N = \beta I$, *and* $M = \alpha I$ *in Equation (4.66), it follows that* $\gamma(\hat{d})^2 = 0$, $\forall d \in \mathbb{R}^3$, *and* $\gamma = 0$, *hence proving the theorem.*

The following proposition is used to prove the lack of bi-invariant metrics on $SE(3)$

Proposition 5. (lack of bi-invariant metrics on *SE*(3))

There does not exist a bi-invariant (positive-definite) metric on $SE(3)$.

Proof.

Following Theorem 1, the matrix W *in Equation (4.62) has two distinct eigenvalues [323]:*

$$\lambda_1 = \tfrac{1}{2}(\alpha + \sqrt{\alpha^2 + 4\beta^2}), \quad \lambda_2 = \tfrac{1}{2}(\alpha - \sqrt{\alpha^2 + 4\beta^2}) \tag{4.71}$$

both of multiplicity 3 and product $\lambda_1\lambda_2 = -\beta^2$. *If* $\beta = 0$, *then* $\lambda_2 = 0$. *On the other hand, if* $\beta \neq 0$, *then* $\lambda_2 < 0$. *Therefore, the matrix cannot be positive definite.*

4.6. CHOICE OF METRICS ON *SE*(3)

The definition of minimal-distance curves on the manifold $SE(3)$ is integral to the problem of motion planning. In Section 4.4.2, the notion of length on a manifold was defined using a Riemannian metric. The non-existence of a bi-invariant metric on $SE(3)$ was proven in Section 4.5. However, non-existence of a bi-invariant metric on $SE(3)$ does not necessarily translate to the non-existence of the notion of length on $SE(3)$. Rather, it implies that the definition of a metric is not intrinsic. The notion of length on $SE(3)$ is restricted to a *choice* of metrics defined at an identity that is extended to the group by translation [319]. In this section, several metrics suitable for motion planning between a given set of initial and final conditions for a group of vehicles are presented that minimise a given cost function.

The family of left invariant metrics on **se**(3) parameterised by 3 scalars α, β, and γ, can be expressed in matrix form as [114]:

$$W = \begin{bmatrix} \alpha I & \beta I \\ \beta I & \gamma I \end{bmatrix} \tag{4.72}$$

Different values of α, β, and γ yield unique left invariant metrics. For example, when $\beta = \gamma = 0$, the metric known as the *Killing form* is obtained and is used to provide a measure of the angular velocities ($\alpha\omega^T\omega$) within the space of twists [114]. The metric known as the *Klein form* is obtained when $\alpha = \gamma = 0$ and provides a measure of ($2\omega^T\gamma$). A popular metric, known as the Park metric [298], is obtained when $\beta = 0$ and is used to derive a weighted quadratic sum of the linear and angular velocities $\alpha(\omega^T\omega) + \gamma(v^Tv)$.

4.6.1. THE KINETIC ENERGY METRIC

A metric of particular interest to trajectory planning is the kinetic energy of the system. The kinetic energy of the rigid body shares the familiar structure and characterisations of the Park metric. By construction, the kinetic energy (and generalised Park metric) is a scalar metric independent of the choice of inertial reference frame. Therefore, it is a left invariant metric. When restricted to the group of rotations $SO(3)$, the metric is bi-invariant [298].

In the following, the kinetic energy metric is derived when the body fixed frame and the fixed inertial reference frame are initially aligned. Let $\{M\}$ denote the body fixed frame centred at centroid O' of the rigid body, and let $\{F\}$ denote a fixed inertial reference frame. Moreover, let the body fixed frame $\{M\}$ be aligned with the principal axis of the rigid body. Then, W assumes the diagonal structure of Equation (4.73):

$$W = \begin{bmatrix} H & 0 \\ 0 & mI \end{bmatrix} \tag{4.73}$$

where m is the mass of vehicle v_i, $\forall i \in N$, and H is the diagonal inertia matrix of the body about the body frame $\{M\}$ given by:

$$H = \begin{bmatrix} H_{xx} & 0 & 0 \\ 0 & H_{yy} & 0 \\ 0 & 0 & H_{zz} \end{bmatrix} \tag{4.74}$$

where H_{xx}, H_{yy}, H_{zz} denote the moments of inertia about the x, y and z axes, respectively.

Let $\{\omega, v\} \in \mathbf{se}(3)$ represent the instantaneous twist of the motion and associated with the vector V. Then, the norm of the vector V assumes the familiar expression for the kinetic energy:

$$\langle V, V \rangle = \omega^T H \omega + m v^T v \tag{4.75}$$

Assume that the body fixed frame is displaced from frame $\{M\}$ to $\{M'\}$ by:

$$g_{MM'} = \begin{bmatrix} R & d \\ 0 & 1 \end{bmatrix} \tag{4.76}$$

The kinetic energy does not change if the body fixed frame is changed. This implies that the matrix W_g defining the energy metric of the new description of the motion is dependent on the body fixed frame $\{M\}$. The following proposition describes this dependence.

Proposition 6. (frame dependence of the energy metric)

Assume the rigid body is displaced from frame $\{M\}$ to $\{M'\}$ according to Equation (4.76). Then the matrix of the kinetic energy metric is given by:

$$W_g = \begin{bmatrix} R^T H R - mR^T(\hat{d})^2 R & -mR^T \hat{d} R \\ mR^T \hat{d} R & mI \end{bmatrix} \tag{4.77}$$

Proof.

From Proposition 1, the twist induced by the change of body frame $\{M\}$ to $\{M'\}$ is given by:

$$\xi_1' = \mathrm{Ad}_{g_{MM'}} \xi_1, \quad \xi_2' = \mathrm{Ad}_{g_{MM'}} \xi_2, \quad [Ad_{g_{MM'}}] = \begin{bmatrix} R & 0 \\ \hat{d}R & R \end{bmatrix} \tag{4.78}$$

and the metrics at identity are given by:

$$\langle \xi_1', \xi_2' \rangle_I = \langle \mathrm{Ad}_{g_{MM'}} \xi_1, \mathrm{Ad}_{g_{MM'}} \xi_2 \rangle_I = \zeta_1^T [\mathrm{Ad}_{g_{MM'}}]^T W [\mathrm{Ad}_{g_{MM'}}] \zeta_2 \tag{4.79}$$

The matrix of the metric becomes:

$$W_g = [\mathrm{Ad}_{g_{MM'}}]^T W [\mathrm{Ad}_{g_{MM'}}] = \begin{bmatrix} R^T & -R^T \hat{d} \\ 0 & R^T \end{bmatrix} \begin{bmatrix} H & 0 \\ 0 & mI \end{bmatrix} \begin{bmatrix} R & 0 \\ \hat{d}R & R \end{bmatrix} \tag{4.80}$$

and is the same as the form in Equation (4.77).

4.6.2. THE RIEMANNIAN CONNECTION ON *SE*(3)

In this section, the Riemannian connections corresponding to the left invariant metrics in Equation (4.72) and Equation (4.73) are investigated.

Let ∇ denote the Riemannian connection compatible with the left invariant metric $W = [w_{ij}]$ in Equation (4.73). Then, for any three vector fields X, Y, and Z the following is observed [325]:

$$\begin{aligned} \langle Z, \nabla_X Y \rangle = \tfrac{1}{2} \{ & Y\langle X, Z \rangle + X\langle Z, Y \rangle - Z\langle X, Y \rangle + \cdots \\ & + \langle [Z, Y], X \rangle + \langle [Z, X], Y \rangle + \langle [X, Y], Z \rangle \} \end{aligned} \tag{4.81}$$

with Christoffel symbols given by (with respect to the chosen basis $\overline{L}_i$):

$$\Gamma_{ji}^k = \tfrac{1}{2} \sum_m w_{km}^{-1} (c_{ij}^s w_{sm} + c_{mj}^s w_{si} + c_{mi}^s w_{sj}) \tag{4.82}$$

where c_{ij}^k are the structure constants defined in Equation (4.19) and w_{km}^{-1} is the element at km of W^{-1}. If ∇ is the Riemannian connection associated to the Riemannian metric in Equation (4.73) with vector fields given by $X = X^i \hat{L}_i$ and $Y = Y^i \hat{L}_i$, then the covariant derivative is given by [324]:

$$\nabla_X Y = \left\{ \frac{d\omega_y}{dt} + \frac{1}{2}\omega_x \times \omega_y, \frac{dv_y}{dt} + \omega_x \times v_y \right\} \tag{4.83}$$

where d/dt is the derivative along the integral curve of X. Following Equation (4.38) and the covariant derivative in Equation (4.83), the Riemannian curvature $\mathsf{R}(X,Y)Z$ for any three vector fields X, Y, and Z is:

$$\mathsf{R}(X,Y)Z = \{\tfrac{1}{4}(\omega_x \times \omega_y) \times \omega_z, 0\} \tag{4.84}$$

Having defined the necessary tools from differential geometry, the optimal motion generation problems for a rigid body can now be developed.

4.7. NECESSARY CONDITIONS FOR OPTIMAL MOTIONS

In this section, the conditions for which a trajectory minimises an integral cost function are presented. Example cost functions include the kinetic energy, velocity, acceleration, and jerk of the group of vehicles. The results presented follow the works of [324] and the concepts of *calculus of variations*. For brevity, only the main results of [324] are presented without proof. For a detailed discussion on optimal motion generation using the calculus of variations, and the relevant proofs, see Appendix B in [324].

Let $g : [a,b] \to SE(3)$ denote a curve between the points a and b. Then an optimal motion planning problem is given by the following integral cost function:

$$J = \int_a^b \left\langle h\left(\frac{dg}{dt}\right), h\left(\frac{dg}{dt}\right) \right\rangle dt \tag{4.85}$$

In the following, specific examples of cost functions for optimal motion planning for a group of vehicles are presented. Furthermore, it is assumed that the group of vehicles obeys the constraints induced by the flock lattice in Equation (3.40) and behaves like a rigid body system.

4.7.1. MINIMUM-DISTANCE CURVES – GEODESICS

Given a Riemannian metric, the length of a curve $g(t)$ defined between the points $g(a)$ and $g(b)$ following Equation (4.85) is given by [291]:

$$J = L(g) = \int_a^b \left\langle \frac{dg}{t}, \frac{dg}{t} \right\rangle^{\frac{1}{2}} dt \tag{4.86}$$

Moreover, a curve that minimises the functional in Equation (4.86) also minimises the *energy functional* given by [291]:

$$E(g) = \int_a^b \langle V, V \rangle dt \tag{4.87}$$

where $V = (dg(t)/dt)$, and the critical points are given by *geodesics* [291].

A geodesic $g(t)$ on $SE(3)$ equipped with the metric in Equation (4.73) is given by [324]:

$$\begin{gathered} \frac{d\omega}{dt} = -H^{-1}(\omega \times (H\omega)) \\ \ddot{d} = 0 \end{gathered} \tag{4.88}$$

In the case when $H = \alpha I$, an analytical expression for the geodesic passing through:

$$g(0) = \begin{bmatrix} R(0) & d(0) \\ 0 & 1 \end{bmatrix}, \quad g(1) = \begin{bmatrix} R(1) & d(1) \\ 0 & 1 \end{bmatrix} \tag{4.89}$$

is given by [324]:

$$g(t) = \begin{bmatrix} R(t) & d(t) \\ 0 & 1 \end{bmatrix} \in SE(3) \tag{4.90}$$

where:

$$\begin{gathered} R(t) = R(0)\exp(\hat{\omega}_0 t) \\ d(t) = (d(1) - d(0))t + d(0) \\ \hat{\omega}_0 = \log(R(0)^T R(1)) \end{gathered} \tag{4.91}$$

In the case when $H \neq \alpha I$, no closed form solution exists and numerical methods must be employed [254].

4.7.2. MINIMUM-ACCELERATION AND MINIMUM-JERK CURVES

Following the definition of the cost function for the minimum distance curves, expressions for higher-derivative curves can similarly be obtained. The first and second time derivatives of the velocity yield the acceleration and jerk of the group of vehicles. The corresponding minimum-acceleration functional and minimum-jerk functional is given by Equation (4.92) and Equation (4.93) respectively:

$$J_{\mathcal{A}} = \int_a^b \langle \nabla_V V, \nabla_V V \rangle dt \tag{4.92}$$

$$J_{jerk} = \int_a^b \langle \nabla_V \nabla_V V, \nabla_V \nabla_V V \rangle dt \tag{4.93}$$

where $V = (dg(t)/dt)$ and $g(t) : [a,b] \to SE(3)$. In [324], the necessary conditions for optimality for the minimum-acceleration functional and minimum-jerk functional is given in Equation (4.94) and Equation (4.95) respectively:

$$\begin{gathered} \omega^{(3)} + \omega \times \ddot{\omega} = 0 \\ d^{(4)} = 0 \end{gathered} \tag{4.94}$$

$$\begin{aligned} &\omega^{(5)} + 2\omega \times \omega^{(4)} + \tfrac{5}{4}\omega \times (\omega \times \omega^{(3)}) + \tfrac{5}{2}\dot{\omega} \times \omega^{(3)} \cdots \\ &\cdots + \tfrac{1}{4}\omega \times (\omega \times (\omega \times \ddot{\omega})) + \tfrac{3}{2}\omega \times (\dot{\omega} \times \ddot{\omega}) - (\omega \times \ddot{\omega}) \times \dot{\omega} \\ &\cdots - \tfrac{1}{4}(\omega \times \dot{\omega}) \times \ddot{\omega} - \tfrac{3}{8}\omega \times ((\omega \times \dot{\omega}) \times \dot{\omega}) - \tfrac{1}{8}(\omega \times (\omega \times \dot{\omega})) \times \omega = 0 \end{aligned} \tag{4.95}$$

$$d^{(6)} = 0$$

where $(\cdot)^{(n)}$ denotes the nth derivative of $(\cdot)$.

In general, analytical solutions to the minimum acceleration and minimum jerk curves do not exist for arbitrary boundary conditions. It was shown in [324], for the special case when the initial velocities and accelerations are collinear with the initial velocity of the geodesic between the two endpoints, and the final velocities and accelerations are collinear with the final velocity of the geodesic, the minimum acceleration curves are re-parameterised geodesics; and analytical solutions to the minimum-acceleration functional and minimum-jerk functional can be obtained. This is only true for $SE(3)$ with the metric in Equation (4.73) and $H = \alpha I$ [322]. For $H \neq \alpha I$ in Equation (4.73), the differential equations to be satisfied can become difficult to derive and solve. In this case, numerical methods such as shooting, relaxation, or projection methods should be employed [327, 328].

4.8. THE RIGID-BODY CONSTRUCTION

In the previous sections, the necessary conditions for optimal motion generation for a group of vehicles were discussed. In this section, the group of vehicles is considered by using a rigid body model and applying the optimal motions to the navigation of the group. Applying the flock protocol in Equation (3.34), a flock of vehicles will converge to the rigid body construction induced by the flock lattice with edge constraints:

$$\left(\Phi(q_j - q_i)\right)^T \left(\Phi(q_j - q_i)\right) = \Phi(d), \quad \forall e_{ij} \in E \tag{4.96}$$

i.e. from Equation (3.40):

$$\left\langle \tilde{p}_j - \tilde{p}_i, \tilde{q}_j - \tilde{q}_i \right\rangle = 0, \quad \forall e_{ij} \in E \tag{4.97}$$

In the configuration manifold Q, the coordinates of the corresponding differential one-form ω can be written as:

$$\omega_{ij} := [\cdots \quad \Phi(q_j - q_i) \quad \cdots] \tag{4.98}$$

where the non-zero elements in the above matrix appearing in the ith and jth positions respectively correspond to the edge e_{ij}. The rigidity constraint in Equation (4.98) is not unique and depends on the ordering given to the edges of the structural graph.

The set of constraints define a co-distribution capturing the feasible velocities along the geodesic [329] given by:

$$\omega = \text{span}\{\omega_{ij}\}, \quad i, j = 1, \ldots, N \tag{4.99}$$

and annihilating distribution Δ_{rigid} [254]:

$$\Delta_{rigid} = \text{Range}(D(q)) \tag{4.100}$$

where

$$D(q) = \begin{bmatrix} -\hat{q}_1 & I_n \\ \vdots & \vdots \\ -\hat{q}_N & I_n \end{bmatrix} \tag{4.101}$$

and $(\hat{\cdot})$ is the skew-symmetric matrix. Using the annihilating distribution, the rigidity constraint induced by the flock lattice on the configuration manifold Q can then be expressed as [254]:

$$\dot{q} \in \Delta_{rigid}(q) \tag{4.102}$$

It was shown in [254], that the rigidity constraint in Equation (4.102) is satisfied for all $t \geq 0$ if and only if:

$$q_i(t) = d(t) + R(t)q_i(0), \quad i = 1,\ldots,N \tag{4.103}$$

where $(R(t), d(t))$ is a trajectory for the left invariant control system in Equation (4.16); i.e.:

$$\dot{g}(t) = g(t)\xi(t) \tag{4.104}$$

with initial conditions $R(0) = I_n$, $d(0) = 0$. Here, the Lie algebra $\xi(t)$ corresponds to the left invariant twist of the rigid structure induced by the flock lattice constraints. Furthermore, motion planning for the N vehicle rigid body motion problem can be reduced to a left invariant control system on $SE(n)$ by [254]:

$$\dot{q}_i = R\begin{bmatrix} -q_i(0) & I \end{bmatrix} \cdot \xi(t) \tag{4.105}$$

The annihilating distribution $\Delta_{rigid}(q)$ locally describes the set of all rigid body motion directions that conforms to a flock lattice. Following the rigid body model of the flock lattice, optimal motion generation for the group of N -vehicles is reduced to generating one geodesic on the $SE(3)$ of the group structure, and N -geodesics on the $SO(3)$ of each vehicle. While this formulation accounts for the converged state of the flock lattice in the local frame, it fails to consider the flexing during the transitional phase of the flock. In Section 4.10, the rigid body model is extended to include the transitional phase of the flock lattice by introducing the notion of a *semi-rigid body* model of the group of vehicles using the Hamiltonian of the system. For now, optimal motion generation for a group of vehicles using the current rigid body model is demonstrated for the converged flock of vehicles.

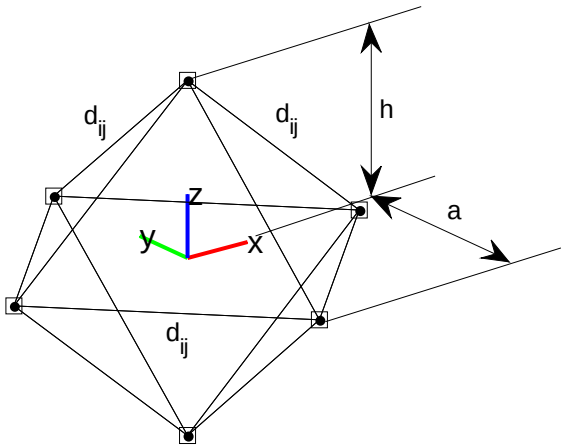

Figure 4-2. Configuration of the rigid flock structure in local frame for 6 vehicles in *SE*(3).

4.9. NUMERICAL EXAMPLE: MOTION OF THE RIGID FLOCK LATTICE

Consider a group of vehicles with dynamics given in Equation (3.49). Suppose the vehicles have converged to a coherent flock lattice with motions satisfying $\langle q-q, p-p \rangle = 0$. Then, the flock of vehicles can be treated as a rigid body system with inter-vehicle distribution given by d_{ij}. In the local frame $\{M\}$, the distribution of vehicles is given by the following flock lattice (Figure 4-2):

$$q_1 = \begin{bmatrix} \frac{\sqrt{2}d_{ij}}{2} \\ 0 \\ 0 \end{bmatrix}, \quad q_2 = \begin{bmatrix} 0 \\ \frac{\sqrt{2}d_{ij}}{2} \\ 0 \end{bmatrix}, \quad q_3 = \begin{bmatrix} -\frac{\sqrt{2}d_{ij}}{2} \\ 0 \\ 0 \end{bmatrix}$$
$$q_4 = \begin{bmatrix} 0 \\ -\frac{\sqrt{2}d_{ij}}{2} \\ 0 \end{bmatrix}, \quad q_5 = \begin{bmatrix} 0 \\ 0 \\ \frac{\sqrt{2}d_{ij}}{2} \end{bmatrix}, \quad q_6 = \begin{bmatrix} 0 \\ 0 \\ -\frac{\sqrt{2}d_{ij}}{2} \end{bmatrix} \tag{4.106}$$

and the inertial frame $\{F\}$ is assumed to be coincident with the local frame $\{M\}$ at $t = 0$.

Assuming compliance to a rigid body model, the objective is to navigate the group of vehicles with configuration given in Equation (4.106) from one configuration $g(0) = (R(0), d(0))$ to some desired final configuration $g(1) = (R(1), d(1))$. For the remainder of this section, the following conditions are considered:

$$R(0)=\begin{bmatrix}1&0&0\\0&1&0\\0&0&1\end{bmatrix},\quad d(0)=\begin{bmatrix}0\\0\\0\end{bmatrix}$$
$$R(1)=\begin{bmatrix}0&0&1\\0&1&0\\-1&0&0\end{bmatrix},\quad d(1)=\begin{bmatrix}200\\0\\200\end{bmatrix} \tag{4.107}$$

These correspond to a translation of the centre of the virtual structure induced by the flock lattice from the coordinates $q=(0,0,0)$ to $q=(200,0,200)$, and a rotation of $\mathrm{Rot}(y,-\frac{\pi}{2})$ about the local frame. It is assumed that the group of vehicles is homogenous with vehicle mass given by $m_i=m,\ i=1,\ldots,6$. Optimal motion with respect to energy and acceleration are now considered.

4.9.1. MINIMUM ENERGY CURVES

For a group of vehicles with configuration (4.106) and masses $m_i=m,\ i=1,\ldots,6$, the mass moment of inertia H is given by:

$$H=\frac{m}{2}\begin{bmatrix}2a^2&0&0\\0&a^2+\frac{4}{3}h^2&0\\0&0&a^2+\frac{4}{5}h^2\end{bmatrix} \tag{4.108}$$

From Equation (4.73), the kinetic energy metric is given by:

$$W=\begin{bmatrix}H&0\\0&\frac{3m}{2}I_3\end{bmatrix} \tag{4.109}$$

and assumes the diagonal form of the Park metric.

Metric (4.109) induces the following cost function associated with the kinetic energy:

$$J=\int_a^b\langle V,V\rangle dt \tag{4.110}$$

It was shown in Section 4.7.1 that the minimum of Equation (4.110) is given by the geodesics on $SE(3)$, and can be found by solving the following differential equations:

$$\begin{aligned}\frac{d\omega}{dt}&=-H^{-1}(\omega\times(H\omega))\\ \ddot{d}&=0\end{aligned} \tag{4.111}$$

Solutions are given in Equation (4.91), and correspond to uniform rectilinear translation of the centroid of the virtual structure, and uniform rotation between 0 and $-\frac{\pi}{2}$ about y. The interpolating motions for the rigid body in Figure 4-2 is shown in Figure 4-3 (a).

4.9.2. MINIMUM ACCELERATION CURVES

As discussed in Section 4.7.2, analytical solutions to minimum acceleration curves generally do not exist for arbitrary boundary conditions. However, it is still possible to obtain trajectories satisfying the necessary conditions for minimum-acceleration in Equation (4.92) (and Equation (4.93) for minimum-jerk) by solving the associated boundary-value problem numerically. For the following example, the interpolating motion satisfying the differential equations in Equation (4.92) were solved using a finite-difference method with 100 grid points [330] in MATLAB. Figure 4-3 (b) shows the corresponding interpolating motions for the minimum-acceleration curves for the configuration in Figure 4-2.

4.10. THE SEMI-RIGID BODY CONSTRUCTION

In Section 4.8, a rigid body model was constructed for a group of vehicles with fixed inter-vehicle distances. This assumption, while sufficiently general to accommodate time-invariant vehicle distributions, fails to capture the transient behaviour of the group of vehicles moving from one configuration to the next. Consider the case for a group of vehicles with random initial distribution applying the flock protocol in Equation (3.34). A group of vehicles applying the flock protocol will converge to a flock lattice (as described in Chapter 3) and maintain a fixed connectivity satisfying the rigidity constraints in Equation (3.40) and behave as a rigid body. The transition from the initial configuration to the flock lattice however, will induce a flexing of the graph topology that violates the rigidity constraints in Equation (3.40). In this phase, the flock is characterised by a *semi-rigid body* model with vehicle motions violating the paths defined by the geodesics in Section 4.7. To effectively plan the motions for a group of vehicles, the effect of these geodesically-conflicting motions must be considered.

From Equation (4.5), the rigid body constraints induce the following co-distribution on the tangent space T^*Q [331]:

$$\omega_{rigid} = \text{span}\{\omega_{ij}, i, j, \ldots, N\} \tag{4.112}$$

The annihilating distribution of ω_{rigid} (i.e., $\omega_{rigid}(\Delta_{rigid}) = 0$) provides the set of rigidity constraints Δ_{rigid} of the virtual structure on T^*Q. For $q_i \in Q_i$, and $q \in \prod_i^N Q_i$, $i = 1, \ldots, N$, the annihilating distribution of ω_{rigid} is given by [254]:

$$\Delta_{rigd} = \text{Range}(C(q)) \tag{4.113}$$

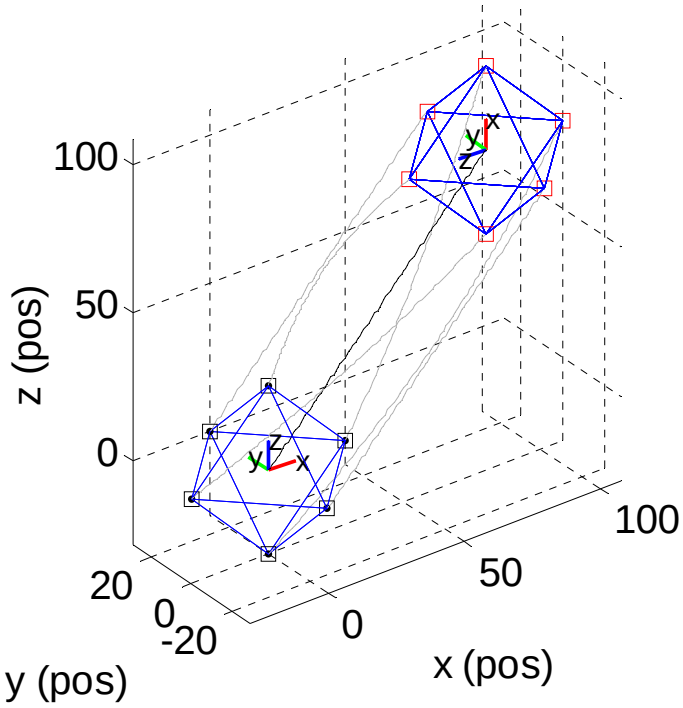

(a)

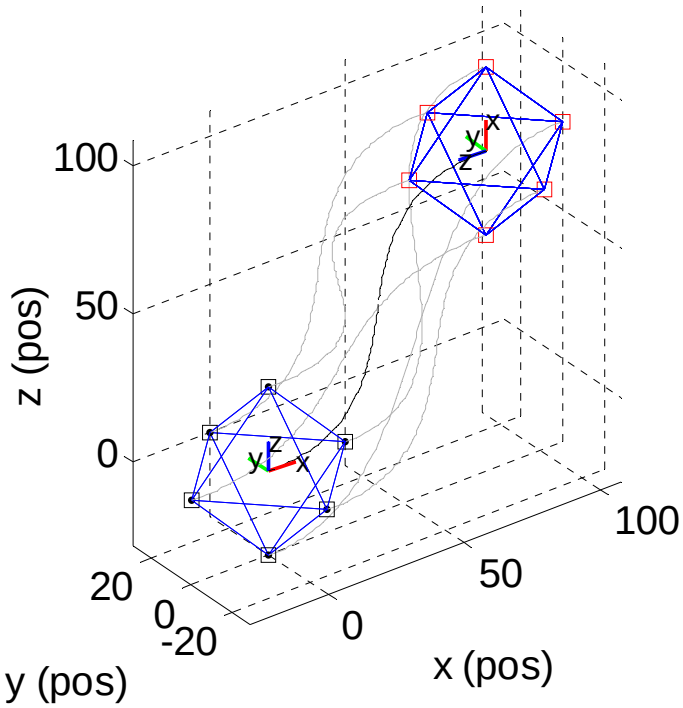

(b)

Figure 4-3. Optimal trajectories for a rigid flock lattice with respect to (a) minimum energy, and (b) minimum acceleration.

where $\text{Range}(C(q))$ is the column space of matrix $C(q)$, and $C(q)$ is the matrix whose columns are the basis for Δ_{rigid} given by:

$$C(q) = \begin{bmatrix} -\hat{q}_1 & I_3 \\ \vdots & \vdots \\ -\hat{q}_1 & I_3 \end{bmatrix} \tag{4.114}$$

On the tangent manifold, the rigidity constraints are then given by:

$$\dot{q} \in \Delta_{rigid} \tag{4.115}$$

The set of motions violating the rigid body constraints, are then given by the orthogonal complement to the rigid distribution $\Delta_{rigid}(q)$. Given a Riemannian metric W with product structure in Equation (4.29), the orthogonal complement of $\Delta_{rigid}(q)$ yields the non-rigid distribution [254]:

$$\Delta_{non-rigid}(q) = \text{Null}(D(q)^T W) \tag{4.116}$$

where $D(q)$ is the matrix whose columns are the basis of $\Delta_{non-rigid}$. Denote $V_q = \dot{q} \in T_q Q$ an arbitrary tangent vector to the point $q \in Q$, and $\text{proj}_{\Delta_{rigid}} V_q$, $\text{proj}_{\Delta_{non-rigid}} V_q$ the projection of V_q onto the distribution Δ_{rigid} and $\Delta_{non-rigid}$ respectively[3]. Then, for a semi-rigid body induced by the flocking protocol in Equation (3.34), the tangent vector V_q can be recovered using the sum of the projection onto the rigid and non-rigid distributions, i.e. [333]:

$$V_q = \text{proj}_{\Delta_{rigid}} V_q + \text{proj}_{\Delta_{non-rigid}} V_q \tag{4.117}$$

This provides the velocity at a point q as a function of the rigid and non-rigid contributions. In the following section, the semi-rigid body model constructed in this section, is used to construct a shape abstraction based on the energy metric of the system of equations.

4.11. SHAPE ABSTRACTIONS OF THE SEMI-RIGID CONSTRUCTION

In Chapter 2, it was shown for a group of vehicles, that the flock lattice configuration is a minimum of the structural potential in Equation (3.12). By controlling the dissipation of the energy functional in Equation (3.12), the convergence of the group of vehicles from an arbitrary configuration to a desired flock lattice configuration can be controlled at a supervisory level. For a configuration of vehicles $q \in Q = \mathbb{R}^n$ in the local frame $\{M\}$ and

[3] In [176, 332], the notation Ver_q and Hor_q is used to denote the tangent space and orthogonal complement to the point q respectively.

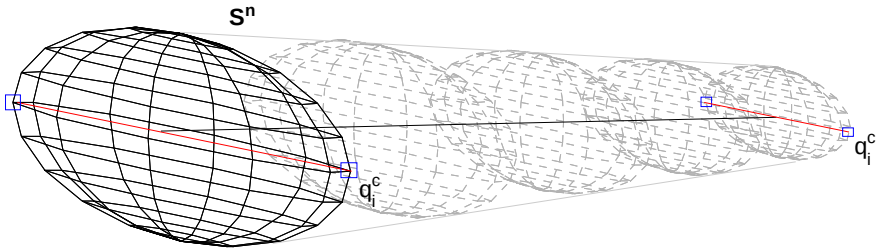

Figure 4-4. The *n* – sphere shape abstraction for a group of vehicles with controllable antipodal points.

centred at $\bar{q}$, the position of a vehicle in the local frame applying Protocol (3.34) is located in the closed n-sphere centred at $\bar{q}$ with radius $R = \sqrt{2\mathcal{H}(q(0), \tilde{p}(0))}$.

Based on these observations, the energy of the system becomes a parameter of significant interest for identifying and controlling the group of vehicles at a supervisory level. In fact, the energy of the system provides a one-dimensional abstraction for the region occupied by the configuration of vehicles. Minimising the energy of the system, effectively controls the evolution of the sphere (or circle in the planar case) bounding the region occupied by the vehicles in the group.

Following the notation introduced in Section 4.10 for the semi-rigid body model of the flock, the quadratic form of the energy metric in Equation (4.73) can be re-written in terms of the rigid and non-rigid contributions [254]:

$$\left\langle V_q^1, V_q^2 \right\rangle = V_q^{1^T} W V_q^2 = \left\langle \text{proj}_{\Delta_{rigid}} V_q^1, \text{proj}_{\Delta_{rigid}} V_q^2 \right\rangle + \left\langle \text{proj}_{\Delta_{non-rigid}} V_q^1, \text{proj}_{\Delta_{non-rigid}} V_q^2 \right\rangle \qquad (4.118)$$

The problem of interest is to control the convergence of the group of vehicles at the supervisory level to the desired flock lattice; irrespective of the number of vehicles in the group. To adjust the expansion and contraction of the shape bounding the group of vehicles along the rigid and non-rigid projection, the following form of Equation (4.118):

$$\left\langle V_q^1, V_q^2 \right\rangle = \sigma_r \left\langle \text{proj}_{\Delta_{rigid}} V_q^1, \text{proj}_{\Delta_{rigid}} V_q^2 \right\rangle + (1-\sigma_r) \left\langle \text{proj}_{\Delta_{non-rigid}} V_q^1, \text{proj}_{\Delta_{non-rigid}} V_q^2 \right\rangle \qquad (4.119)$$

where the term $\sigma_r \in (0,1)$ has been introduced as a *shape control parameter* (see also [254, 332, 333] for a similar treatment). For $\sigma_r = 1$, the virtual structure is described by the rigid body model in Section 4.8. The vehicles move along geodesics corresponding to the optimal rigid body motions for the collective group. In this case, the behaviour of the vehicles is strictly defined by the performance of the collective group. In the extreme case, when $\sigma_r = 0$, the rigidity constraints of the virtual structure are relaxed, and motions are strictly non-rigid. This corresponds to motions orthogonal to the optimal rigid body motions of the

group. Setting $\sigma_r = .5$, the Christoffel symbols in Equation (4.46) become zero, and the motion of the group of vehicles becomes the optimal uncoordinated interpolating motions of the individual vehicles; straight lines uniformly parameterised in time [254].

Using the metric in Equation (4.119) and the geodesic flow in Equation (4.46), the motion of a vehicle can be obtained by solving a two-point boundary value problem. For example, if the state of each vehicle is known at initialisation and at some future time, then solving the boundary value problem can be achieved using any number of numerical techniques. While this is possible when state information for each vehicle is available to a supervisory agent, it is highly impractical from a computational and hardware point-of-view. Ideally, the motion generation and control for the group of vehicles at the supervisory level should be reduced to lower-dimensional manifold. Since the position of a vehicle in the flock is always located in the n-sphere given by:

$$\mathbf{S}^n = \{q_i \in \mathbb{R}^n : \|q_i - \bar{q}\| \leq \|R\|\} \tag{4.120}$$

then controlling the group of vehicles can be reduced to controlling the expansion and contraction of two antipodal points $q_1^c, q_2^c \in Q = \mathbb{R}^n$ along the surface of the n-sphere (see Figure 4-4). The points (q_1^c, q_2^c) can be considered as *virtual agents* with dynamics given by:

$$\begin{cases} \dot{q}_i^c = p_i^c \\ \dot{p}_i^c = u_i^c \end{cases}, \quad i = 1,2 \tag{4.121}$$

The virtual agents define a *virtual structure* bounded by:

$$\mathbf{S}^n = \left\{q \in \mathbb{R}^n : \langle q - \bar{q}, q - \bar{q} \rangle \leq \tfrac{1}{2} \langle q_2^c - q_1^c, q_2^c - q_1^c \rangle \right\} \tag{4.122}$$

The virtual structure is used constraint the N to the closed n-sphere in Equation (4.122). In the proceeding chapter, a cooperative control scheme using distributed optimisation techniques is presented to provide the final relationship between the individual vehicle positions and the shape abstraction described by the virtual agents (q_1^c, q_2^c). The result is a cooperative control scheme based on the virtual structure approach. Before proceeding with the development of the individual vehicle control laws, the optimal shape control problem for the supervisory level is demonstrated using the semi-rigid body model of the flock. The motion defined by this strategy, provides a constraint on the group objective that couples the vehicles and promotes group cooperation.

4.12. NUMERICAL EXAMPLE: SEMI-RIGID FLOCK CONTROL

In this section, the shape abstraction described in the previous section is demonstrated for a group of $N = 5$ vehicles with dynamics given in Equation (3.49) initial distribution, and velocity given by:

$$q_1(0) = \begin{bmatrix} 0 \\ 0 \end{bmatrix}, \quad q_2(0) = \begin{bmatrix} 5 \\ 5 \end{bmatrix}, \quad q_3(0) = \begin{bmatrix} 5 \\ -5 \end{bmatrix}, \quad q_4(0) = \begin{bmatrix} -5 \\ -5 \end{bmatrix}, \quad q_5(0) = \begin{bmatrix} -5 \\ 5 \end{bmatrix}$$
$$\dot{q}_1(0) = \dot{q}_2(0) = \dot{q}_3(0) = \dot{q}_4(0) = \dot{q}_5(0) = \begin{bmatrix} 0 & 0 \end{bmatrix}^T \tag{4.123}$$

where $\dot{q}(0)$ is the concatenated set of velocities for the group of vehicles. Suppose that the vehicles apply the flock protocol in Equation (3.34), then, from Theorem 2 in Chapter 3 the group of vehicles will converge to a flock lattice spanning the disk:

$$\mathbf{S}^2 = \{q_i \in \mathbb{R}^n : \|q_i - \overline{q}\| \leq \sqrt{2\mathcal{H}(q(0), \dot{q}(0))}\} \tag{4.124}$$

The objective is to navigate the group of vehicles from the initial disk configuration spanned by the distribution in Equation (4.123), to the desired final disk configuration in Equation (4.124) along a predefined trajectory. Controlling the shape spanned by the flock is achieved by generating the motions of the N_c antipodal points along the surface of the disk between the initial shape and the final shape. The motion of the antipodal points is governed by the dynamics in Equation (3.49), and is obtained by smoothly varying the kinetic energy metric in Equation (4.73). The metric in Equation (4.73), assumes that any two points in the local frame observes the rigidity constraints in Equation (3.40). However, since the flock evolves according to the flock protocol in Equation (3.34) and is described by the semi-rigid body model in Section 4.10, then the metric is no longer constant.

Following the definition of a semi-rigid body model, and Equation (4.119), the metric induced by the semi-rigid body construction W_{σ_r}, can be obtained by considering the projections of the motion along the rigidity preserving and rigidity violating directions. Expanding Equation (4.119) for the rigid body model:

$$\begin{aligned} \left\langle V_q^1, V_q^2 \right\rangle &= \sigma_r \left\langle \text{proj}_{\Delta_{rigid}} V_q^1, \text{proj}_{\Delta_{rigid}} V_q^2 \right\rangle + (1-\sigma_r) \left\langle \text{proj}_{\Delta_{non-rigid}} V_q^1, \text{proj}_{\Delta_{non-rigid}} V_q^2 \right\rangle \\ &= \sigma_r v^{1^T} C(q)^T W C(q) v^2 + (1-\sigma_r) w^{1^T} D(q)^T W D(q) w^2 \end{aligned} \tag{4.125}$$

where v, and w are the components of the projections on the basis:

$$\begin{aligned} \text{proj}_{\Delta_{rigid}} V_q &= C(q)v \\ \text{proj}_{\Delta_{non-rigid}} V_q &= D(q)w \end{aligned} \tag{4.126}$$

and from Equation (4.125) the following is observed:

$$v = (C(q)^T WC(q))^{-1} C(q)^T WV_q$$
$$w = (D(q)^T WD(q))^{-1} D(q)^T WV_q \tag{4.127}$$

Following Equation (4.125), the new semi-rigid body metric with shape control parameter σ_r is defined as:

$$\begin{aligned} &\left\langle V_q, V_q \right\rangle_{\sigma_r} := V_q{}^T W_{\sigma_r} V_q \\ &= \sigma_r v^{1T} C(q)^T WC(q) v^2 + (1-\sigma_r) w^{1T} D(q)^T WD(q) w^2 \\ &= \sigma_r \left[\left((C(q)^T WC(q))^{-1} C(q)^T WV_q \right)^T C(q)^T WC(q) (C(q)^T WC(q))^{-1} C(q)^T WV_q \right] + \\ &+ (1-\sigma_r) \left[\left((D(q)^T WD(q))^{-1} D(q)^T WV_q \right)^T D(q)^T WD(q) (D(q)^T WD(q))^{-1} D(q)^T WV_q \right] \end{aligned} \tag{4.128}$$

Solving Equation (4.128) for W_{σ_r}, yields the new matrix of the energy metric for the semi-rigid body model [254]:

$$\begin{aligned} W_{\sigma_r}(q) = \sigma_r WC(q) \left(C(q)^T WC(q) \right)^{-T} C(q)^T W + \cdots \\ \cdots + (1-\sigma_r) WD(q) \left(D(q)^T WD(q) \right)^{-T} D(q)^T W \end{aligned} \tag{4.129}$$

Using the semi-rigid body energy metric in Equation (4.129), the optimal trajectories for the antipodal points can now be determined.

From Equation (4.114) and Equation (4.116), the column spaces $C(q)$ and $D(q)$ for two points in a plane is given by the following:

$$C(q^c) = \begin{bmatrix} -\mathrm{y}_1^c & 1 & 0 \\ \mathrm{x}_1^c & 0 & 1 \\ -\mathrm{y}_2^c & 1 & 0 \\ \mathrm{x}_2^c & 0 & 1 \end{bmatrix}, \quad D(q^c) = \begin{bmatrix} \frac{\left(\mathrm{x}_2^c - \mathrm{x}_1^c\right)}{\left(\mathrm{y}_1^c - \mathrm{y}_2^c\right)} \\ -1 \\ \frac{\left(\mathrm{x}_1^c - \mathrm{x}_2^c\right)}{\left(\mathrm{y}_1^c - \mathrm{y}_2^c\right)} \\ 1 \end{bmatrix} \tag{4.130}$$

Using the column spaces in Equation (4.130), the semi-rigid energy metric in Equation (4.129), and Equation (4.34), the 64 Christoffel Symbols for the geodesic flow equations in (4.46) can be obtained. For the general case of $n = 2$, $N_c = 2$, the Christoffel symbols are provided in Appendix B.

For the following example, assume $m_1 = m_2 = m = 1$, and the boundary conditions for the two antipodal points is given by:

$$q^c(0) = \begin{bmatrix} \max\{\|\bar{q}_0 - q_i(0)\|\} \\ 0 \\ -\max\{\|\bar{q}_0 - q_i(0)\|\} \\ 0 \end{bmatrix}, \quad q^c(1) = \begin{bmatrix} R(\frac{-\pi}{6}) & d(1) \\ 0 & 1 \end{bmatrix} \cdot q^c(0) \tag{4.131}$$

where $\max\{\|\bar{q}_0 - q_i(0)\|\} = \sqrt{10^2}$, $d(1) = [100 \quad -50]^T$, and $R(-\frac{\pi}{6})$ is the rotational subgroup $SO(2)$ parameterised by θ and corresponding to a rotation about the body fixed frame $\{M\}$ by $\theta = -\frac{\pi}{6}$.

Figure 4-5 shows the corresponding trajectories of the antipodal points solved using the semi-rigid body energy metric in Equation (4.129) for $\sigma_r = 0.1$, $\sigma_r = 0.5$, and $\sigma_r = 0.75$. From Figure 4-5, as the shape control parameter $\sigma_r \to 0$, the antipodal points are only permitted to move along the antipodal line connecting them. This causes the disk spanned by the flock to expand and contract. As $\sigma_r \to 0.5$, the Christoffel symbols become zero and the trajectories are the optimal motions described in Section 4.7.1; i.e. straight lines. On the other hand, as $\sigma_r \to 1.0$, the non-rigid motions are penalised, and the corresponding geodesics are optimal rigid motions. This corresponds to the case when the antipodal points remain a fixed during the group's motion. In this example, the rigid body case $\sigma_r = 1$ is not available since the initial and final configurations specified are not consistent with the rigid body model.

4.13. SUMMARY

In this chapter, the concepts of differential geometry were introduced and applied to the motion generation problem for a group of vehicles. By treating the converged flock configuration as a rigid body, optimal control techniques familiar to rigid body motion were applied. This provided a useful abstraction for the group of vehicles. The rigid body model was then extended to include the motions induced by the flock protocols that would violate the rigid body paths. The resulting model was a semi-rigid body construction. To map the individual vehicles to this rigid body model, and preserve scaling, virtual agents were used to represent the shape spanned by the group. Using the convergence results in Chapter 3, the shape abstraction was defined using the n-sphere. The group motion and shape abstraction both provide a method for controlling the group at the supervisory level. Convergence of the individuals to the desired shape and pose as prescribed by the supervisory controller represents the cooperative control problem for the individual vehicles. In the next chapter, the relationship between this desired group level behaviour, and the local vehicle level is considered by designing a cooperative control scheme based on traditional model predictive control. This provides the last piece of the decentralised cooperative control framework to realise the cooperative objective.

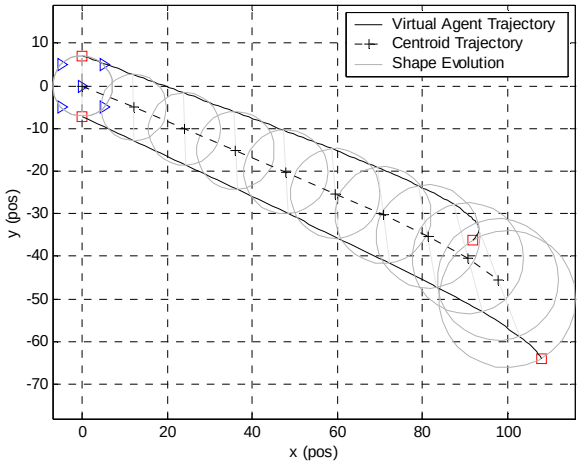

(a) σ_r = 0.1

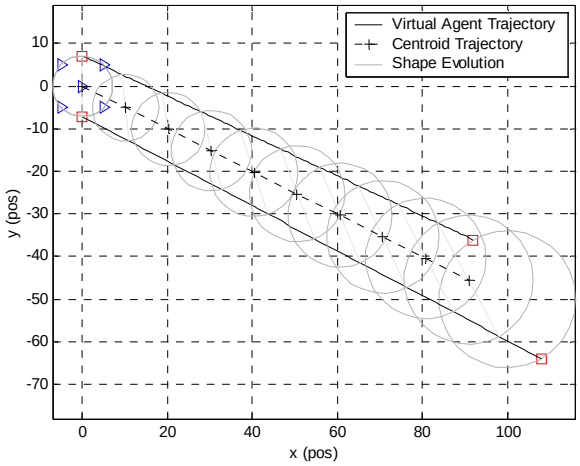

(b) σ_r = 0.5

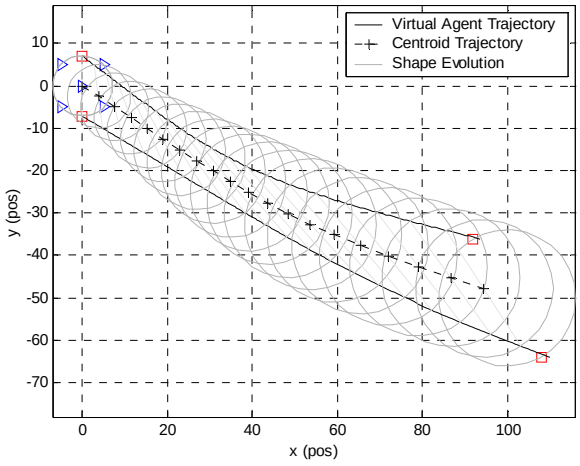

(c) σ_r = 0.75

Figure 4-5. Motions induced by the semi-rigid body metric for various shape control parameters σ_r.

Chapter 5. Cooperation Through Decentralised Model Predictive Control

In this chapter, the problem of cooperative control for a group of vehicles is addressed. A decentralised cooperative control scheme based on traditional Model Predictive Control (MPC) is proposed. The cooperative control scheme uses shared information to reach a consensus on the coordination variable representative of the group task. The shared information refers to optimal plans generated by each vehicle at the sampling periods. The plans correspond to solutions to a finite-time optimisation problem. The finite-time optimisation problem represents arbitration between the local goals of the vehicles and the global goals of the group. Solutions to the finite-time optimal control problem correspond to the open-loop state trajectory that takes the vehicle's current state to a final optimal state in the desired abstract manifold. This provides the necessary (and final) relationship between the local interactions of the vehicles and the group-level behaviours. Coordination follows from the exchange of these plans with neighbouring vehicles to negotiate a consensus on the final group state matching the commanded group states of the supervisory agent.

The main objective of this chapter is to develop a decentralised coordination scheme for the cooperative vehicles using a traditional MPC scheme to develop plans and exchange information at each sampling period. The chapter is organised as follows. In Section 5.1, the original centralised MPC scheme is introduced and a numerical demonstration is presented in Section 5.2 for the flock of vehicles described in Chapter 3. In Section 5.3, the main contribution of this chapter, the decentralised cooperative control scheme, is presented. The closed-loop stability of the system is then presented in Section 5.4 followed by a discussion in Section 5.5 on the limitations of the distributed implementation. The proposed cooperative control scheme will then be demonstrated for a group of vehicles in Chapter 6 for search and rescue.

5.1. PROBLEM FORMULATION

Consider N dynamically decoupled vehicles with time-invariant state equations given by:

$$\dot{q}_i(t) = f_i\big(q_i(t), u_i(t)\big) \tag{5.1}$$

with state vector $q_i(t) \in \mathbb{R}^{n_i}$ belonging to the set of feasible states $Q_i \subseteq \mathbb{R}^{n_i}$, and input vector $u_i(t) \in \mathbb{R}^{m_i}$ belonging to the set of feasible inputs $U_i \subseteq \mathbb{R}^{m_i}$ for vehicle v_i. The state of each vehicle is updated according to the continuous function $f_i : \mathbb{R}^{n_i} \times \mathbb{R}^{m_i} \to \mathbb{R}^{n_i}$ and is assumed stabilisable at the equilibrium pair (q_i^e, u_i^e) of vehicle v_i. For fully actuated vehicles in free space, the states are described by position and orientation vectors; i.e. $q_i = (x_i, \theta_i)^T$.

Let $q(t) \in \prod_{i=1}^{N} Q_i = \mathbb{R}^{Nn_i}$, and $u(t) \in \prod_{i=1}^{N} U_i = \mathbb{R}^{Nn_i}$ denote the concatenated form of the state and input vectors of the collective flock, and let (q^e, u^e) denote the corresponding equilibrium pair of the collective system. Then,

$$\dot{q}(t) = f(q(t), u(t)) \tag{5.2}$$

is the nN-dimensional control system for the collective flock with concatenated state vector $q(t) = [q_1(t), \ldots, q_N(t)]$, and input vector $u(t) = [u_1(t), \ldots, u_N(t)]$ stabilisable by the state update functions $f(q(t), u(t)) = [f_1(q_1(t), u_1(t)), \ldots, f_N(q_N(t), u_N(t))]$ to the equilibrium pair (q_i^e, u_i^e).

5.1.1. COUPLING CONSTRAINTS

The above discussion implies that the vehicles in Equation (5.2) are completely decoupled in the collective system. If the vehicles are truly autonomous and act independently from any centralised control, then the system is decentralised and the behaviour is an emergent property of the (possibly competing) interactions of the vehicles. For purposeful group behaviour, the vehicles must cooperate to achieve a global group goal. This could include objectives such as formation stabilisation, multi-point rendezvous, and synchronised interception. The group objective induces a coupling constraint on the vehicle's behaviour, and describes a *distributed information architecture*. Whilst this contrasts the decoupled nature of the decentralised control architecture, it turns out that the distributed control architecture is only used to describe the information flow in the system, and not the control of the vehicles. Decentralisation is achieved by using the group abstractions in Chapter 3, and endowing the vehicles with sufficient autonomy, to plan and coordinate their actions with neighbouring vehicles and avoid collisions. In this section, the coupling constraints of vehicles are modelled using the graph structures introduced in Chapter 3.

To remain consistent with the finite interactions of the vehicles in the flock, and the physical limitations of the sensors and communication devices, the interaction graphs depicted in Section 3.2.1 are used to model the coupling constraints in the flock. Associate the ith vehicle to node v_i of the interaction graph $G = (V, E)$, and an edge $e = (v_i, v_j) \in E$ connecting vehicle v_i to v_j, $i \neq j$. If there exists an edge $e = (v_i, v_j) \in E$ between vehicle v_i and v_j, then vehicle v_i and v_j are coupled either through the cost function or constraints. In Section 3.2.1, the sensory and communication radius r_i for vehicle v_i induced a spatial interconnection graph $G = (V, E)$, with adjacency matrix:

$$a_{ij}(x) := \rho_{ij}(z) = \begin{cases} 1, & \text{if } 0 \leq \|x_j - x_i\| < \delta, \quad j \neq i \\ \frac{1}{2}\left[1 + \cos\left(\frac{(z-\varepsilon)}{(1-\varepsilon)}\right)\right], & \text{if } \delta \leq \|x_j - x_i\| \leq r_i, \quad j \neq i \\ 0, & \text{otherwise} \end{cases} \tag{5.3}$$

and spatial neighbourhood of vehicle v_i defined by:

$$\mathcal{N}_i = \{ j \in V : \|x_j - x_i\| \leq r_i \} \tag{5.4}$$

For the purposes of generality, it is assumed that the flock is homogenous, and the vehicles share identical sensory and communication capabilities; i.e., $r = r_i = r_j$ and $\rho = \rho_i = \rho_i$, $\forall i, j \in N$, $i \neq j$.

Remark.

In Section 2.3, for a group of mobile vehicles with finite interaction range r, the induced spatial information network is time-varying. In the proceeding sections, a time-invariant information network is assumed. Stability becomes more difficult to prove when the interaction graph is a switching network. It was shown in Section 2.3, that the switching network of the information exchange topology is an example of an autonomous hybrid differential-algebraic system. Analytical methods to analyse the stability of these types of systems is currently an area of active research in the mathematics and control fields. Therefore, the proof of stability for the time-varying case can only be shown using a numerical example. This is provided in Section 5.5.

5.1.2. THE CENTRALISED OPTIMISATION PROBLEM

In the following, a centralised optimisation problem is formulated for a group of vehicles with some shared objective. Let $\tilde{x}_i$ denote the states of all neighbouring vehicles v_j of vehicle

v_i such that $\tilde{x}_i = \{x_j \in \mathbb{R}^{n_j} \mid (j,i) \in E\}$, $\tilde{x}_i \in \mathbb{R}^{\tilde{n}_i}$ with $\tilde{n}_i = \sum_{j|(j,i)\in E} n_j$, and let $\tilde{u}_i \in \mathbb{R}^{\tilde{m}_i}$ denote the set of corresponding inputs $\forall j \in \mathcal{N}_i$. Denote the corresponding equilibrium pair for the group of neighbours with $(\tilde{x}_i^e, \tilde{u}_i^e) \subseteq (x^e, u^e)$ and define $l_i : \mathbb{R}^{n_i} \times \mathbb{R}^{m_i} \times \mathbb{R}^{\tilde{n}_i} \times \mathbb{R}^{\tilde{m}_i} \to \mathbb{R}$ as the distributed integrated cost function associated to vehicle v_i, $\forall i \in N$ satisfying $l_i(x_i, u_i, \tilde{x}_i, \tilde{u}_i) \geq c(|x_i, u_i, \tilde{x}_i, \tilde{u}_i|)^2$ and $l_i(x_i^e, u_i^e, \tilde{x}_i^e, \tilde{u}_i^e) = 0$. The centralised cost function for the interconnected system is then given by:

$$l(x,u) = \sum_{i=1}^{N} l_i(x_i, u_i, \tilde{x}_i, \tilde{u}_i) \tag{5.5}$$

where the sum of $l_i(x_i, u_i, \tilde{x}_i, \tilde{u}_i)$ recovers the cost of $l(x,u)$. The information network induces the following coupling constraints:

$$g_{i,j}(x_i, x_j) \leq 0 \tag{5.6}$$

between neighbouring vehicles v_i and v_j, where $g_{i,j} : \mathbb{R}^{n_i} \times \mathbb{R}^{n_j} \to \mathbb{R}^{n_{i,j}^c}$ is a continuous (possibly non-convex) function. Using $\tilde{x}_i$, Equation (5.6) can be rewritten as:

$$g_i(x_i, \tilde{x}_i) \leq 0 \tag{5.7}$$

Note the undirected nature of the information flow induces redundant constraints on the cost function.

Having defined the cumulative cost of the interconnected system, and the constraints induced by the information flow, consider the following infinite time optimal control problem:

$$\begin{aligned} J_\infty^*(x(t)) := & \min_{\{u_0, u_1, \ldots\}} \int_0^\infty l(x,u)dt \\ \text{Subject to:} \quad & \dot{x}_i(t) = f_i(x_i(t), u_i(t)) \\ & i = 1, \ldots, N, \quad t \geq 0 \\ & x_i(t) \in X_i, \quad u_i(t) \in U_i \\ & g_{i,j}(x_i(t), \tilde{x}_i(t)) \leq 0, \quad \forall j \in \mathcal{N}_i \\ & x_0 = x(0) \end{aligned} \tag{5.8}$$

Given Problem (5.8), the control objective is to stabilise the collective system to the equilibrium pair (x^e, u^e). When the variable x_i is the dynamic states of vehicle v_i, the optimisation problem in Equation (5.8) the equilibrium pair (x^e, u^e) corresponds to a distribution of vehicles. For a given initial state of the collective system $x(0) \in \mathbb{R}^{Nn_i}$,

Problem (5.8) is feasible if the set of optimal inputs $\{u^*(0), u^*(1), \ldots\}$ drives the N systems to their equilibrium points x_i^e while satisfying state, input and coupling constraints.

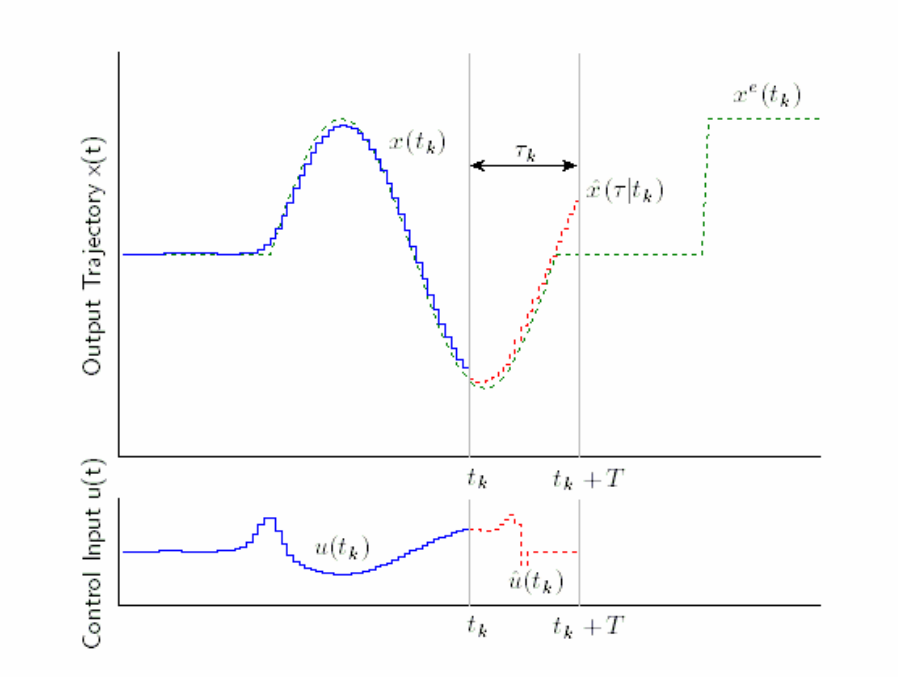

Figure 5-1. Traditional MPC scheme.

5.1.3. FINITE HORIZON CONTROL

In many cases, solving an infinite horizon control problem is computationally intractable. An infinite horizon controller can be designed by repeatedly solving a finite time optimal control problem over a receding horizon. At each sampling period, an open-loop optimal control problem is solved over a finite horizon, and the optimal input is applied in the proceeding sampling period. A new finite time optimal control problem is then solved at the next sampling period over the shifted horizon using the new state measurements obtained by applying the optimal control input from the previous horizon. The resultant controller is referred to as a Receding Horizon Controller (RHC) or Model Predictive Controller (MPC) [334].

To decompose the optimisation problem in Equation (5.8) into a set of finite time sub-problems, let $\tau_k \in [t_k, t_k + T]$ denote the prediction horizon interval with update time t_k, $k \in \mathbb{N} = \{1,2,\ldots\}$, and prediction length T. For any prediction horizon τ_k, the predicted states $\hat{x}_i(t_k) = \{x_i(t_{k+1} \mid t_k), \ldots, x_i(t_{k+\Delta k} \mid t_k), \ldots, x_i(t_{k+T} \mid t_k)\}$ are obtained by applying the predicted set of control inputs $\hat{u}_i(t_k) = \{u_i(t_k \mid t_k), \ldots, u_i(t_{k+\Delta k} \mid t_k), \ldots, u_i(t_{k+T-1} \mid t_k)\}$ to system (5.1) using the current set of state measurements $x_i(t_k)$ at time t_k. The concatenated set of predicted states

and predicted control inputs for the collective flock at time t_k is similarly denoted by $\hat{x}(t_k) \in \mathbb{R}^{N\tilde{n}}$ and $\hat{u}(t_k) \in \mathbb{R}^{N\tilde{m}}$, respectively. Let $X_f \subseteq \mathbb{R}^{Nn_i}$ denote the terminal region associated to the prediction horizon (i.e., $x(t_{k+T} \mid t_k) \in X_f$). Then, the terminal cost function $l^T(x(t_{k+T} \mid t_k))$ takes the state $x(t_k)$ from time t_k to the terminal state $x(t_{k+T})$ at time t_{k+T}. Using the finite time horizon $\tau_k \in [t_k, t_k + T]$, and the predicted states $\hat{x}(t_k) \in \mathbb{R}^{N\tilde{n}}$, and control trajectories $\hat{u}(t_k) \in \mathbb{R}^{N\tilde{m}}$, Problem (5.8) can be expressed as the following constrained finite time optimal control problem:

$$J_T^*(x(t_k)) := \min_{\{\hat{u}(t_k)\}} \int_{t_k}^{t_{k+T}} l\big(x(\tau_k \mid t_k), u(\tau_k \mid t_k)\big) d\tau_k + l^T\big(x(t_{k+T} \mid t_k)\big)$$

Subject to:

$$\begin{gathered}
\dot{x}_i(\tau_k \mid t_k) = f_i(x_i(\tau_k \mid t_k), u_i(\tau_k \mid t_k)) \\
i = 1, \ldots, N, \quad \tau_k \in [t_k, t_k + T] \\
x_i(\tau_k \mid t_k) \in X_i, \quad u_i(\tau_k \mid t_k) \in U_i \\
\tau_k \in [t_k, t_k + T] \\
g_{i,j}(x_i(\tau_k \mid t_k), x_j(\tau_k \mid t_k)) \le 0, \quad \forall j \in \mathcal{N}_i \\
x(t_k \mid t_k) = x(t_k) \\
x(t_{k+T} \mid t_k) \in X_f
\end{gathered} \tag{5.9}$$

Denote the optimal solution to Equation (5.9) at time t_k with $\hat{u}^*(t_k) := \{u^*(t_k \mid t_k), \ldots, u^*(t_{k+T-1} \mid t_k)\}$. At the next sampling period, each vehicle applies the first sample of $\hat{u}^*(t_k)$, such that:

$$u(t_{k+1}) = u^*(t_k \mid t_k) \tag{5.10}$$

and the remainder of the predicted input is discarded. The optimisation problem (5.9) is repeated at the next sampling period t_{k+1} over the next shifted horizon $\tau_{k+1} \in [t_{k+1}, t_{k+T+1}]$ (see Figure 5-1). This process of re-sampling and recomputing over each horizon closes the open-loop solution of Equation (5.9).

5.2. NUMERICAL EXAMPLE: RECEDING HORIZON CONTROL FOR FLOCKING

In the following example, the concepts of model predictive control are applied to a group of vehicles using a centralised architecture. Consider a group of 6 vehicles with position initialised along the line:

$$q_1(0)=\begin{bmatrix}0\\0\end{bmatrix},\quad q_2(0)=\begin{bmatrix}2\\0\end{bmatrix},\quad q_3(0)=\begin{bmatrix}4\\0\end{bmatrix},\quad q_4(0)=\begin{bmatrix}6\\0\end{bmatrix}$$
$$q_5(0)=\begin{bmatrix}8\\0\end{bmatrix},\quad q_6(0)=\begin{bmatrix}10\\0\end{bmatrix} \tag{5.11}$$

and velocity randomly selected in the range $p_i(0)\in[-1,1]\times[-1,1]$, $\forall i\in N$. Each vehicle is assumed to have dynamics decoupled from the other vehicles, and described by $x_i(t)=(q_i(t),\dot{q}_i(t))\in X_i=\mathbb{R}^{2n}$, $u_i(t)\in U_i=\mathbb{R}^n$:

$$\dot{x}_i(t)=A_i x_i(t)+B_i u_i(t),\quad t\geq 0 \tag{5.12}$$

where:

$$A_i=\begin{bmatrix}0 & I_n\\ 0 & 0\end{bmatrix},\quad B_i=\begin{bmatrix}0\\ I_n\end{bmatrix} \tag{5.13}$$

and I_n is the n-dimensional identity matrix. Concatenating the vehicle dynamics to produce the group dynamics:

$$\dot{x}(t)=Ax(t)+Bu(t),\quad t\geq 0 \tag{5.14}$$

with $x\in\prod_{i=1}^{N}X_i=\mathbb{R}^{2nN}$, $u\in\prod_{i=1}^{N}U_i=\mathbb{R}^{nN}$, $A=\text{diag}(A_1,\ldots,A_N)$, $B=\text{diag}(B_1,\ldots,B_N)$.

The control objective is to asymptotically stabilise the group of vehicles to the equilibrium $x^e=(x_1^e,\ldots,x_N^e)$ of a common objective. In this example, the objective is to stabilise the group of vehicles to the flock lattice in Chapter 3. Using the Hamiltonian of the system from Section 3.2.4:

$$\mathcal{H}(x)=\frac{1}{2}\sum_{i=1}^{N}\left\|\tilde{p}_i\right\|^2+\frac{1}{2}\sum_{i}\sum_{j\neq i,\,j\in\mathcal{N}_i}\psi\left(\Phi(q_j-q_i)\right) \tag{5.15}$$

the centralised integrated cost function for flocking is given by:

$$l(x,u)=\frac{1}{2}\sum_{i=1}^{N}\left\|\dot{q}_i\right\|^2+\frac{1}{2}\sum_{i}\sum_{j\neq i,\,j\in\mathcal{N}_i}\psi(\Phi(q_j-q_i))+\left\|u\right\|^2 \tag{5.16}$$

where the minimum of Equation (5.16) yields the position values $q^e=(q_1^e,\ldots,q_N^e)$ at x^e corresponding to the flock lattice of Chapter 3. Note the term $\left\|u\right\|^2$ has been introduced to penalise the control input. While the $\mathcal{L}_2$-norm used to penalise the control input here is non-linear, the scale of the optimisation problem is assumed to be solvable. A more conservative approach to formulating the optimisation problem in Equation (5.16) would be to linearise the penalty on the control input through the introduction of an appropriate penalty function such as the $\mathcal{L}_\infty$-norm or to soften the constraints. Assuming that the optimisation problem in Equation (5.16) is solvable with the penalty function and the constraint definitions, solutions

to the centralised objective function in Equation (5.16) at each sampling period t_k, can be obtained by repeatedly solving Equation (5.9) over successive horizons $\tau_k \in [t_k, t_k + T]$.

For the following simulation, the horizon length is varied between $T = 2.4s$, $T = 3.6s$, $T = 4.8s$ and the control input for each vehicle v_i is bounded by Equation (5.17):

$$U_i := \{u_i = (u_{ix}, u_{iy}) \in \mathbb{R}^2 \mid -1 \leq u_{ix}, u_{iy} \leq 1\} \tag{5.17}$$

The MPC scheme is implemented in a centralised architecture with full state-feedback to a supervisory agent. Information from each vehicle is transmitted to the supervisory agent at each sampling period $t_k = 0.6$ seconds and is used to solve the corresponding finite-time optimal control problem in Equation (5.9) over the horizon $\tau_{k+1} \in [t_{k+1}, t_{k+T+1}]$. Optimal control trajectories for proceeding horizons are then transmitted to each vehicle. It is assumed that an inner-loop controller for each vehicle is then used to track the control trajectories provided by the supervisory agent with zero error at each sampling period. For the following simulation, it is also assumed that the computational time of the supervisory agent, and the information exchanged times between the supervisory agent and the vehicles are negligible. In practice, the computational and information exchange times are non-negligible since delays will affect the stability and performance of the system.

To solve the finite-time horizon control problem at each sampling period, a global optimisation search procedure based on the dual-primal gradient-based recurrent neural network is used [335-340]. The dual-primal gradient-based recurrent neural network presented in [337] is based on the reduction of the duality gap induced by the Dual-Quadratic Programming (DQP) representation of Problem (5.9) and Equation (5.16). The dual-primal gradient-based recurrent neural network has the advantage of guaranteeing convergence to the global minimum without the explicit expression of the gradient information of the objective. This means that the dual-primal gradient-based recurrent neural network is sufficiently robust to be applied naïvely to many DQP problems. A detailed description of the dual-primal gradient-based recurrent neural network and its functioning is given in [337, 339, 340] with applications presented in [335, 336, 338].

The dissipation of the structural potential for the flock lattice for $T = 2.4s$, $T = 3.6s$, and $T = 4.8s$ is shown in Figure 5-2. Increasing the horizon length, in general, improves the response of the system and leads to a faster convergence. The state trajectories of the group of vehicles converging to the flock lattice for $T = 2.4s$ $T = 3.6s$, and $T = 4.8s$ are shown in Figure 5-3, Figure 5-4, and Figure 5-5. Triangles are used to represent the direction

of the corresponding velocity vector. The corresponding model predictive control law for each vehicle is shown in Figure 5-6 and Figure 5-7.

From Figure 5-6 and Figure 5-7, the effect of the hard constraint has minimal effect on the solution quality for specified scenario. In each of the cases, vehicles most further from the centre of the flock ride the control limit at the initial stage of the simulation. This suggests that based on the distance of the vehicles and the connectivity of the network, the vehicles will be initially forced to move towards the centre of the group. This is in concert with the flock protocol introduced in Section 3.2.4. Despite this initial saturation, however, the penalty function successfully minimises the control input over successive periods. This is shown by the gradual decay of the control input for each vehicle in Figure 5-6 and Figure 5-7 that follows the sharp initial control input. This highlights an area of further study involving the investigation of the relationship between the hard constraints of the vehicle's actuators and the communication radius of the network's connectivity.

As in many linear quadratic optimisation problems, the hard constraints and the $\mathcal{L}_2$-norm penalty functions can be made complementary by simply representing the hard constraints as linear inequalities and softening the constraints. This would have the added benefit of linearising the problem space and reducing the complexity of the optimisation problem. Another approach to specifying the penalty function of the control input and controlling the degradation on the response of Equation (5.16) is to minimise the deviation between successive control inputs. This would have the effect of smoothing out any overshoot or oscillatory behaviour in the control response.

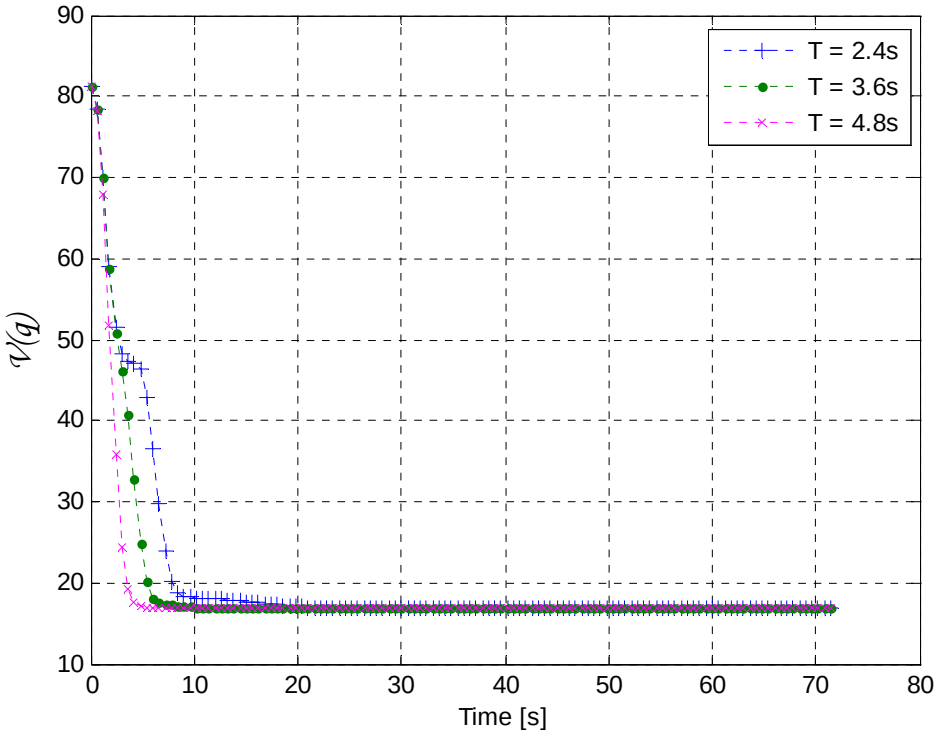

Figure 5-2. Dissipation of the structural potential for T = 2.4s, T = 3.6s, and T = 4.8s.

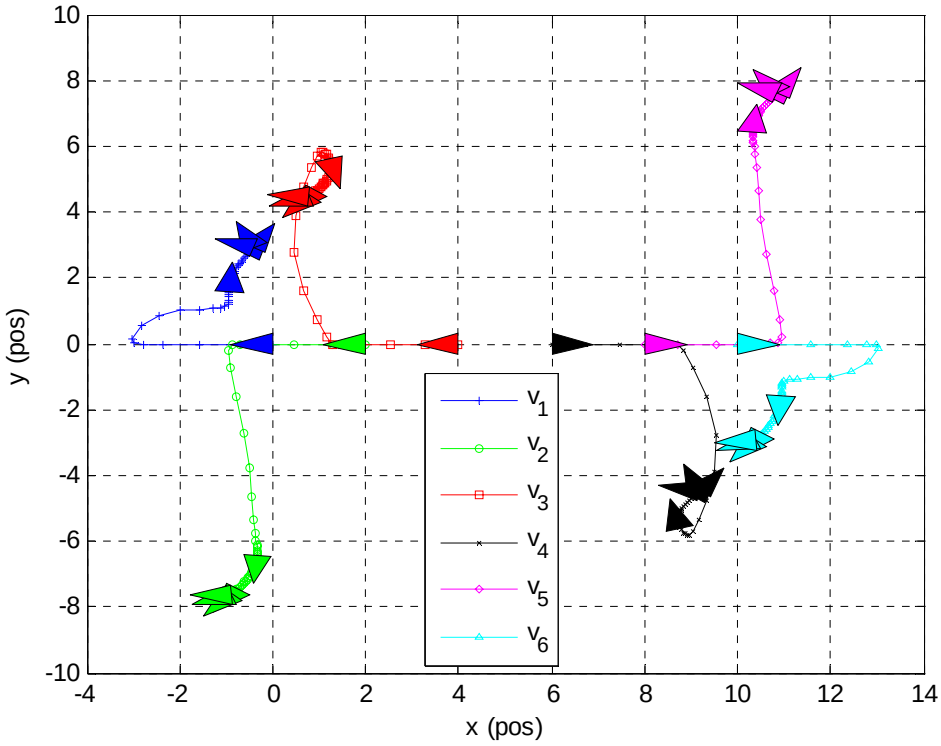

Figure 5-3. Convergence of the flock lattice for T = 2.4s using the centralised model predictive control law.

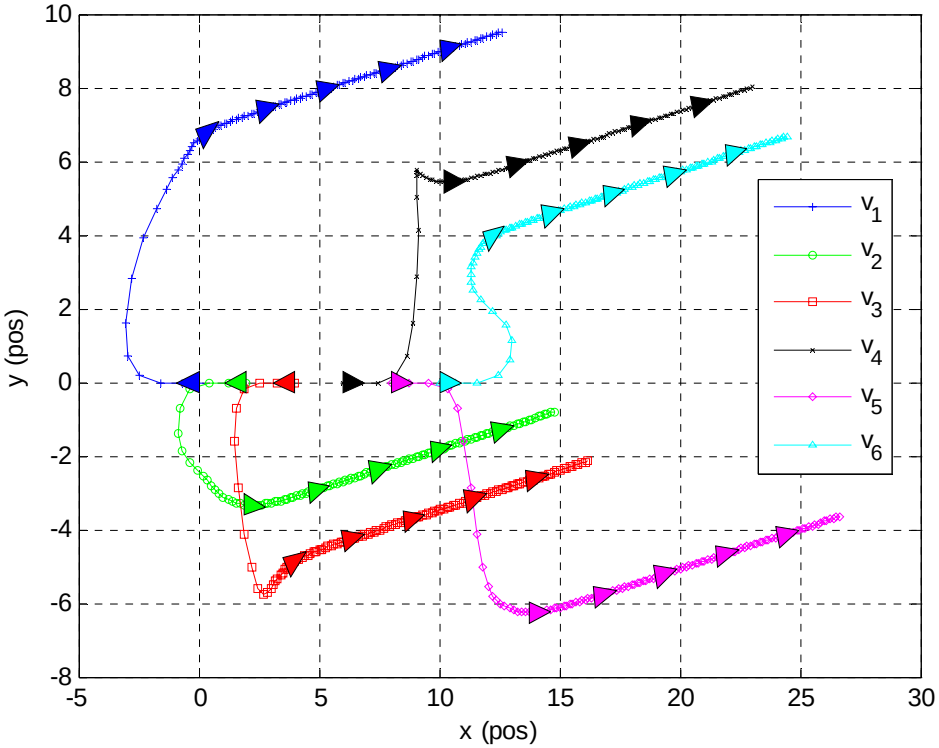

Figure 5-4. Convergence of the flock lattice for T = 3.6s using the centralised model predictive control law.

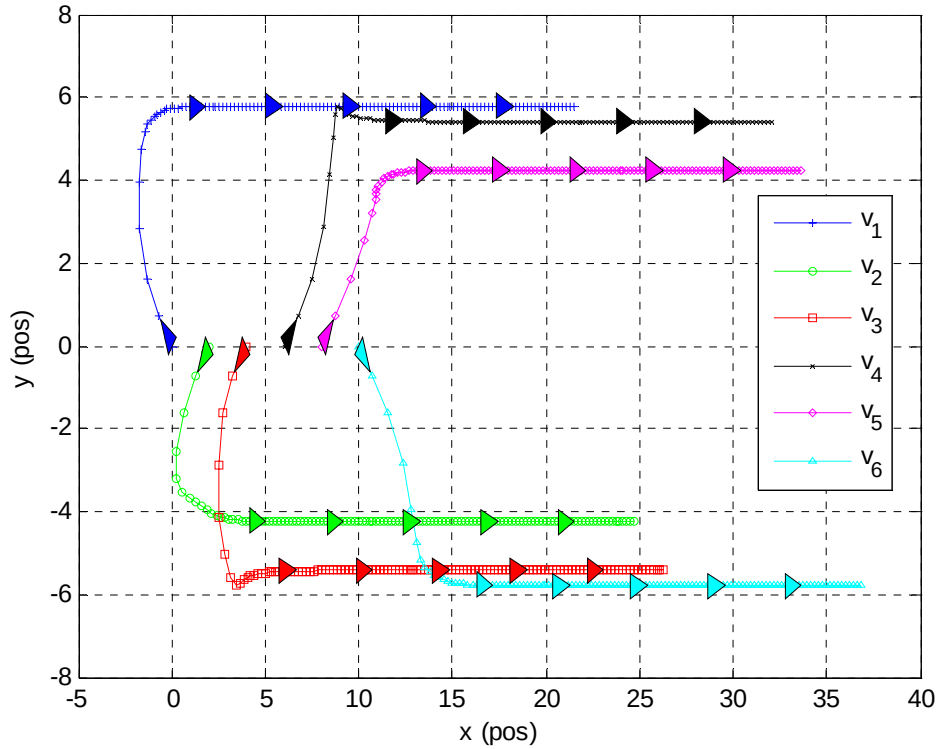

Figure 5-5. Convergence of the flock lattice for T = 4.8s using the centralised model predictive control law.

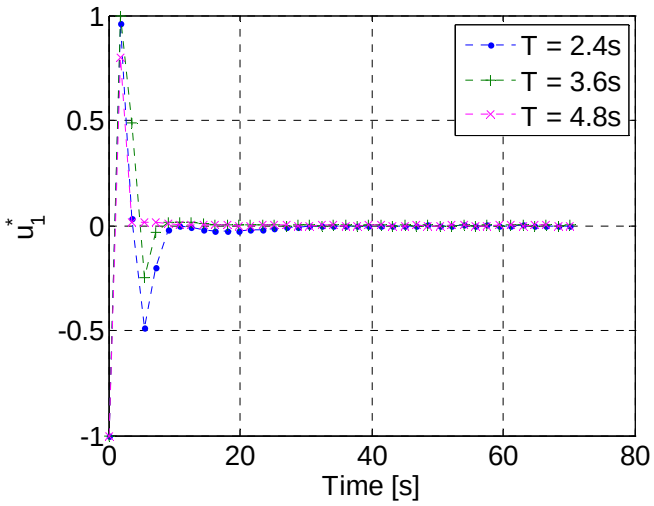

(a) v_1

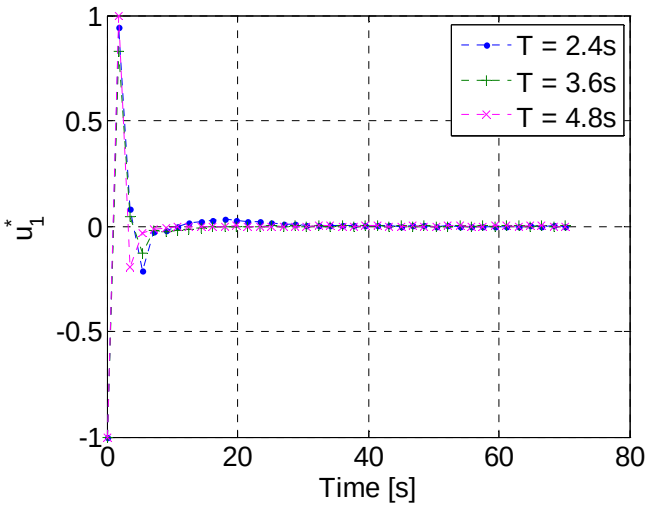

(b) v_2

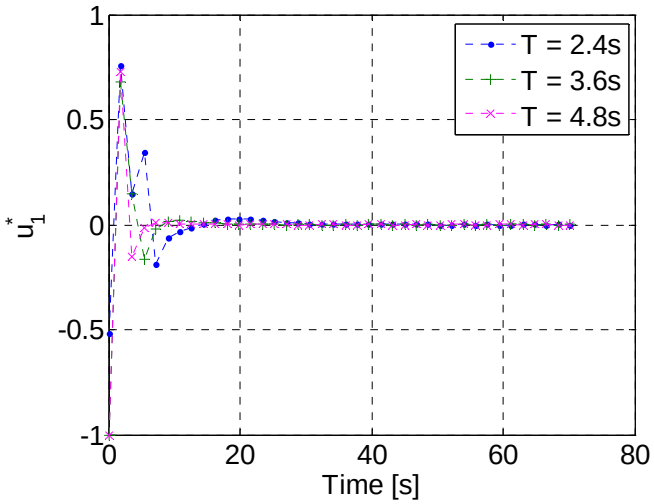

(c) v_3

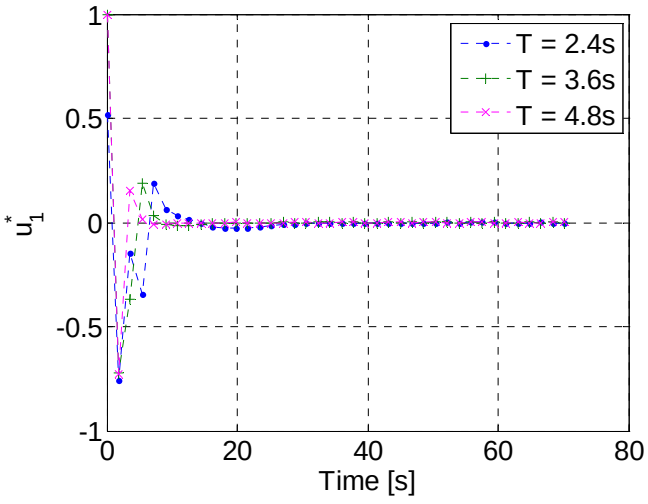

(d) v_4

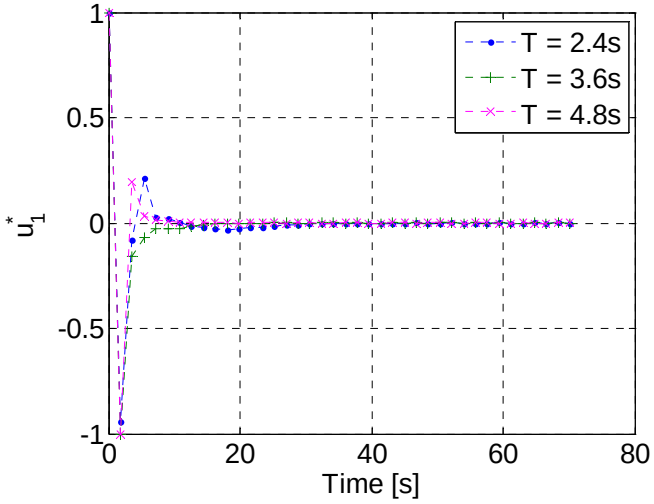

(e) v_5

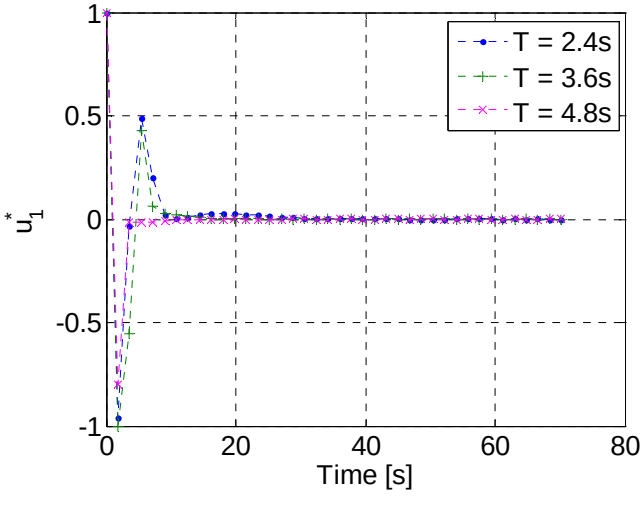

(f) v_6

Figure 5-6. Centralised model predictive control law $u_1(t)$ for T = 2.4s, T = 3.6s, and T = 4.8s.

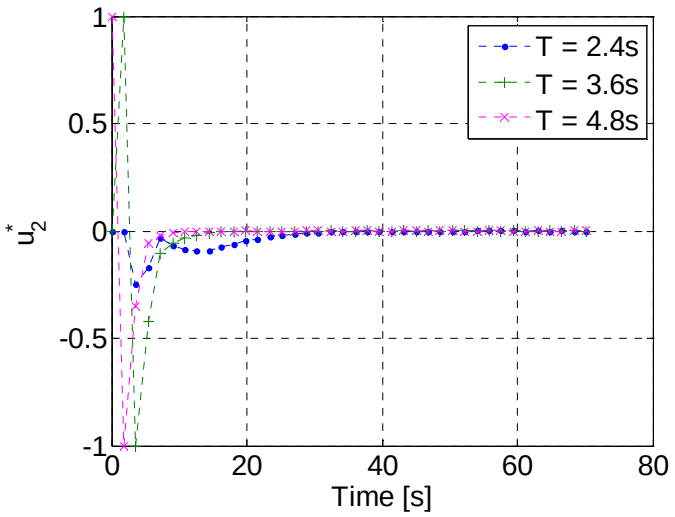

(a) v_1

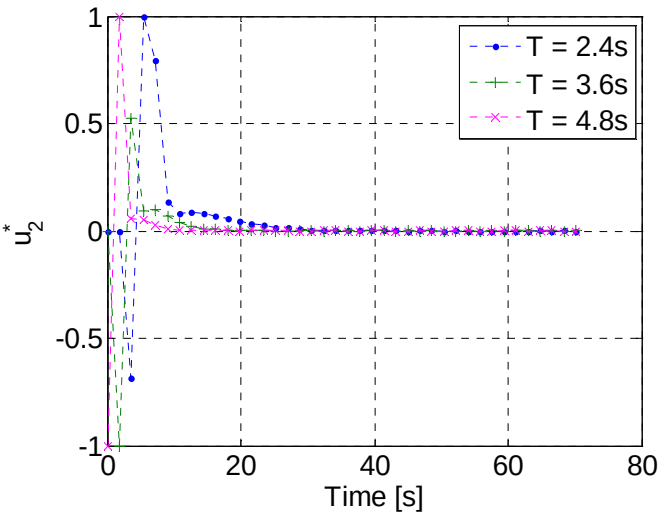

(b) v_2

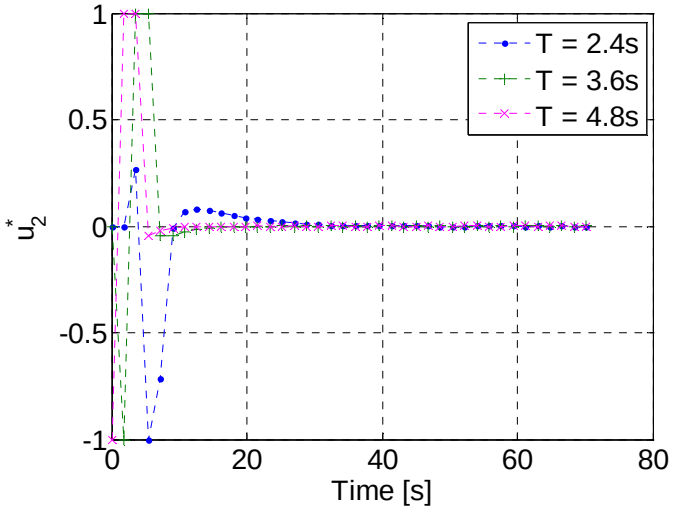

(c) v_3

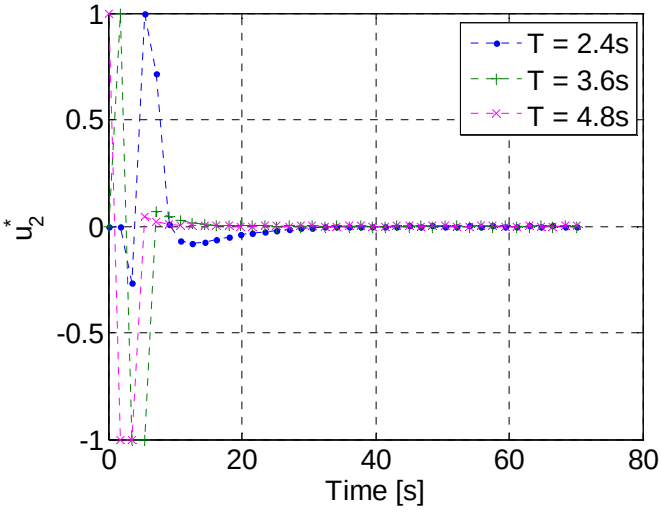

(d) v_4

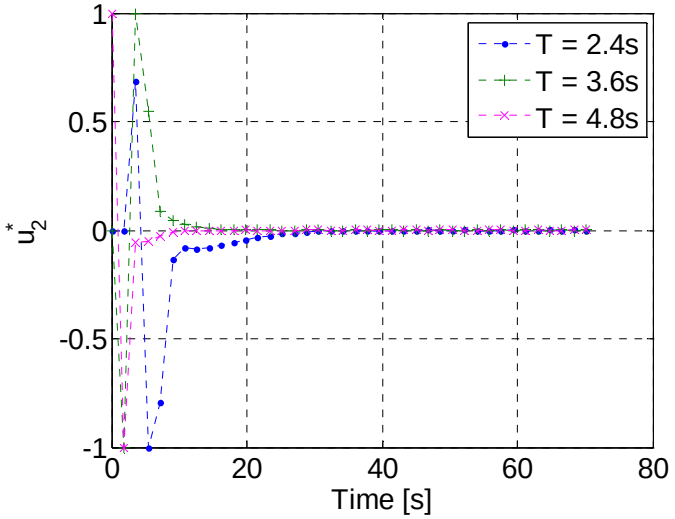

(e) v_5

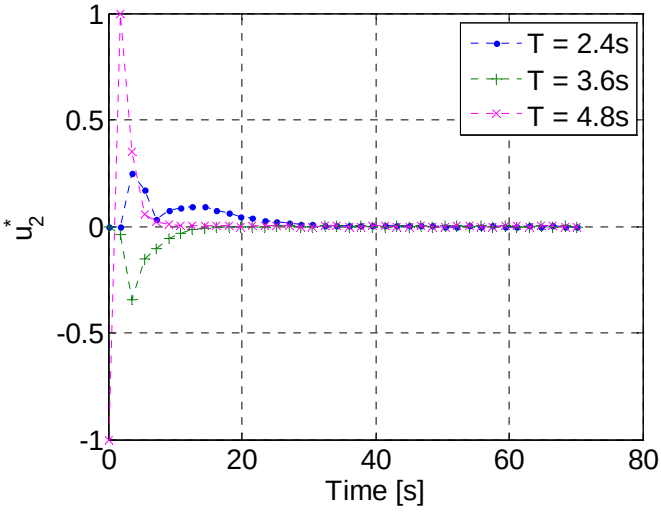

(f) v_6

Figure 5-7. Centralised model predictive control law $u_2(t)$ for T = 2.4s, T = 3.6s, and T = 4.8s.

5.3. COOPERATIVE DECENTRALISED MODEL PREDICTIVE CONTROL STRATEGY

In this section, the centralised optimal control problem is decoupled into N finite time optimal control problems for implementation into N vehicles. The coupling induced by the information flow is used to reach a consensus and solve the optimal control problem of Equation (5.9). Two types of information are available to each vehicle in the flock; i) the states and controls of the interconnected vehicles, and ii) the partial solutions of the optimisation problem. Partial solutions are defined as those intrinsically coupled to the perspective of the individual vehicles. Due to the bounded sensory and communication limits of each vehicle, the information available to each vehicle is localised to a finite range.

Each vehicle has information about its current states and its neighbours' current states through sensory and communication means. Based on the information provided, each vehicle computes its own open-loop optimal trajectories. At each sampling period, vehicles exchange the set of predicted state trajectories for the next shifted horizon with neighbouring vehicles and receive their predicted plans over the next shifted horizon. The received plans for the proceeding shifted horizon act to constrain the optimal control problem in Equation (5.9) and are used by the vehicles to estimate the effect of the neighbours' plans on their own plans for the proceeding prediction horizon. A more formal description is presented in Definition 1. In the case of flocking, the predicted trajectories of neighbouring vehicles are used to define a time-invariant network over the prediction horizon. For $t_k \in [0,\infty)$, the dynamic flock topology is approximated by a *switching network* with a fixed topology over predicted dwell times. In later sections, the decentralised model predictive controller is implemented with respect to other multi-vehicle objectives.

Definition 1. (notation)

Over the prediction horizon $\tau_k \in [t_k, t_{k+T}]$, *in the optimal control problem for each system* $i = 1,\ldots,N$, *and associated with the initial state* $x_i(t_k)$, *the following notation is defined for the decentralised model predictive control strategy:*

Table 5-1. Notation for decentralised model predictive control.

current state	$x_i(t_k) \in \mathbb{R}^{n_i}$	*the current state of vehicle* v_i *at time* t_k
neighbours' current state	$\tilde{x}_i(t_k) \in \mathbb{R}^{\tilde{n}_i}$	*the current state of neighbours* j *of* i *(i.e.* $j \in \mathcal{N}_i$*) at time* t_k
planned control trajectory	$\hat{u}_i(t_k) \in \mathbb{R}^{Tm_i}$	*the control being optimised and applied to the system over the interval* $[t_k, t_{k+T}]$ *using state* $x_i(t_k)$ *at time* t_k
planned state trajectory	$\hat{x}_i(t_k) \in \mathbb{R}^{Tn_i}$	*the state trajectories obtained over the interval* $[t_k, t_{k+T}]$ *by applying the set* $\hat{u}_i(t_k)$ *to system (5.1)*
assumed state trajectory	$\hat{\tilde{x}}_i(t_k) \in \mathbb{R}^{T\tilde{n}_i}$	*the set of neighbours' plans transmitted at time* t *to vehicle* v_i *and derived using states* $x_j(t_{k-1})$, $\forall j \in \mathcal{N}_i$

where the state $x_i(t_k) \in X_i$ *and input* $u_i(t_k) \in U_i$ *constraint for each vehicle contain the origin in their interior.*

By definition, the assumed state trajectories of the neighbours for the i*th vehicle at time* t_k *over the interval* $\tau_k \in [t_k, t_{k+T}]$, $\forall j \in \mathcal{N}_i$ *is the concatenated set of planned state trajectories for neighbours* $\forall j \in \mathcal{N}_i$ *over the interval obtained using state* $x_j(t_{k-1})$ *at time* t_{k-1} *by neighbour* $\forall j \in \mathcal{N}_i$ *(i.e.* $\{\hat{x}_j(t_{k-1}), \ldots, \hat{x}_{|N_i|}(t_{k-1})\}$, $\forall j \in \mathcal{N}_i$*). Vehicle* v_i *assumes that vehicle* v_j *does not deviate from its transmitted plans. An important point is that the initial condition of every assumed state trajectory is equal to the actual initial state value of the corresponding system, i.e.:*

$$\tilde{x}_i(t_k) = \hat{\tilde{x}}_i(t_k \mid t_{-1}) \tag{5.18}$$

for every $i = 1, \ldots, N$*. To be consistent with the notation* $\hat{\tilde{x}}_i$*, let* $\hat{\tilde{x}}_{i\_j}$ *be the vector of assumed state trajectories of neighbour* v_j *for vehicle* v_i*, i.e.:*

$$\hat{\tilde{x}}_{i\_j}(t_k \mid t_{-1}) = x_j(t_k) \tag{5.19}$$

Using the definitions provided, the finite time optimal control problem for vehicle v_i at time t_k is given by:

$$J^*_{i,T}(x_i(t_k),\hat{x}_i(t_k)) := \min_{\{\hat{u}_i(t_k)\}} \int_{t_k}^{t_{k+T}} l_i\big(\hat{x}_i(\tau_k \mid t_k),\hat{u}_i(\tau_k \mid t_k),\hat{x}_i(\tau_k \mid t_k)\big)d\tau_k$$
$$+ l_i^T\big(x_i(t_{k+T} \mid t_k),\hat{x}_i(t_{k+T} \mid t_k)\big)$$

Subject to:

$$\begin{gathered}
\dot{x}_i(\tau_k \mid t_k) = f_i(x_i(\tau_k \mid t_k),u_i(\tau_k \mid t_k)) \\
i = 1,\ldots,N, \quad \tau_k \in [t_k, t_k + T] \\
x_i(\tau_k \mid t_k) \in X_i, \quad u_i(\tau_k \mid t_k) \in U_i \\
\tau_k \in [t_k, t_k + T] \\
(i,j) \in \mathcal{N}_i \\
g_{i,j}(x_i(\tau_k \mid t_k), x_j(\tau_k \mid t_k)) \le 0, \quad \forall j \in \mathcal{N}_i \\
x(t_k \mid t_k) = x(t_k) \\
x(t_{k+T} \mid t_k) \in X_f(\alpha_i)
\end{gathered} \tag{5.20}$$

where

$$X_f(\alpha_i) := \left\{x \in \mathbb{R}^n : \left\|x - x_i^e\right\|_P^2 \le \alpha_i, \alpha_i \ge 0\right\} \tag{5.21}$$

and $\alpha_i \in [0,\infty)$ is a constant, and $P = P^T > 0$ is a *terminal weighting matrix*. The control objective is to cooperatively and asymptotically stabilise all the vehicles to the equilibrium pair (x^e,u^e) of the collective flock. Cooperation is achieved by the minimisation of the cost function in Equation (5.20). The optimal solution to the optimal control problem in Equation (5.20) is then given by:

$$\hat{u}_i^*(t_k) = (\hat{u}_i^*(t_k \mid t_k),\ldots,\hat{u}_i^*(t_{k+T} \mid t_k)) \tag{5.22}$$

Consider a linearization of system (5.1) about the origin $(x_i,u_i) = (x_i^e,0)$ as:

$$\dot{x}_i(t_k) = A_i x_i(t_k) + B_i u_i(t_k) \tag{5.23}$$

with $A_i = \partial f_i/\partial x_i\,(x_i^e,0)$ and $B_i = \partial f_i/\partial u_i\,(x_i^e,0)$. If Equation (5.23) is stabilisable, then a linear feedback control law:

$$u_i(t) := K_i(x_i^K(t) - x_i^e) \tag{5.24}$$

is defined such that $A_i + B_i K_i$ has eigenvalues in the open left-half complex plane and is asymptotically stable [341]. Application of the first component of the ith sub-problem defines an implicit control law in Equation (5.24) that stabilises vehicle v_i in $X_i^f(\varepsilon_i)$ to the equilibrium (x_i^e,u_i^e) with closed-loop dynamics:

$$\dot{x}_i^K(t) = f_i(x_i^K(t), K_i(x_i^K(t) - x_i^e)) \tag{5.25}$$

for all $t \geq 0$, and the collective equilibrium is a function of the assumed state trajectories $\hat{x}_i(t_k)$. The generalised form of Equation (5.25) is then given by:

$$\dot{x}_i^K(t) = f_i(x_i^K(t), K_i(x_i^K(t), \hat{x}_i(t))) \tag{5.26}$$

Lemma 1. (region of attraction)

There exists a constant $\alpha_i \in [0,\infty)$ specifying a neighbourhood $X_f(\alpha_i)$ of the origin in the form of [341]:

$$X_f(\alpha_i) := \left\{ x \in \mathbb{R}^n : \left\| x - x_i^e \right\|_P^2 \leq \alpha_i, \alpha_i \geq 0 \right\} \tag{5.27}$$

Proof.

The proof follows from the works of [342]. Define the function $V : \mathbb{R}^n \to \mathbb{R}$ for some positive definite, symmetric matrix P by:

$$V_i(x_i^K) := \int_{t_{k+1}}^{t_{k+T}} \left\| x_i(\tau_k \mid t_k) \right\|_Q^2 + \left\| u_i(\tau_k \mid t_k) \right\|_R^2 d\tau_k =: \left\| x_i \right\|_P^2 \tag{5.28}$$

Computing the time derivative of Equation (5.28) along a solution of Equation (5.26) yields:

$$\begin{aligned} \tfrac{d}{dt} V_i(x_i^K(t_k)) &:= \tfrac{d}{dt} \left\| x_i(t_k) \right\|_P^2 \\ &= x_i^T(t_k)((A_i + B_i K_i)^T P_i + P_i(A_i + B_i K_i)) x_i(t_k) + 2 x_i^T(t_k) P \phi(x_i(t_k)) \end{aligned} \tag{5.29}$$

where $\phi(x_i(t_k)) := f(x_i(t_k), K_i x_i(t_k)) - (A_i + B_i K_i) x_i(t_k)$. The last term in Equation (5.29) is bounded by the inequality theorem in [341]:

$$\begin{aligned} x_i^T(t_k) P \phi(x_i(t_k)) &\leq \left\| x_i^T(t_k) P \right\| \cdot \left\| \phi(x_i(t_k)) \right\| \leq \left\| P \right\| \cdot L_\phi \cdot \left\| x_i(t_k) \right\|^2 \\ &\leq \frac{\left\| P \right\| \cdot L_\phi}{\lambda_{\min}(P)} \cdot \left\| x_i(t_k) \right\|_P^2 \end{aligned} \tag{5.30}$$

where $L_\phi := \sup \left\{ \left\| \phi(x_i(t_k)) \right\| / \left\| x_i(t_k) \right\| \middle| x_i(t_k) \in X_f(\alpha_i), x_i(t_k) \neq 0 \right\}$. For $\alpha_i \in [0,\infty)$:

$$L_\phi \leq \frac{\kappa \cdot \lambda_{\min}(P)}{\left\| P \right\|} \tag{5.31}$$

in the region of $X_f(\alpha_i)$ and $\kappa \in [0,\infty)$, and Inequality (5.30) becomes:

$$x_i^T(t_k) P \phi(x_i(t_k)) \leq \kappa \cdot x_i^T(t_k) P(x_i(t_k)) \tag{5.32}$$

Substituting Equation (5.32) into Inequality (5.29) yields:

$$\tfrac{d}{dt} \left\| x_i(t_k) \right\|_P^2 \leq x_i^T(t_k)((A_i + B_i K_i + \kappa I)^T P + P(A_i + B_i K_i + \kappa I)) x_i(t_k) \tag{5.33}$$

Introducing the following Lyapunov candidate function as in [341]:

$$(A_i + B_i K_i + \kappa I)^T P + P(A_i + B_i K_i + \kappa I) = -Q + K_i^T R K_i \in \mathbb{R}^{n\times n} \tag{5.34}$$

and substituting Equation (5.34) into Inequality (5.34):

$$\frac{d}{dt}\left\|x_i(t_k)\right\|_P^2 \leq x_i^T(t_k)(-Q + K_i^T R K_i)x_i(t_k) \tag{5.35}$$

It follows that for sufficiently large constants $\alpha_i > 0$*, Inequality (5.35) is satisfied such that* $\frac{d}{dt}\left\|x_i^K(t_k)\right\|_P^2 \leq -\left\|x_i^K(t_k) - x_i^e\right\|_{Q+K_i^T R K_i}$*, and the region defined by:*

$$X_f(\alpha_i) := \left\{x \in \mathbb{R}^n : \left\|x - x_i^e\right\|_P^2 \leq \alpha_i, \alpha_i \geq 0\right\} \tag{5.36}$$

is an invariant region of attraction for the system (5.1) controlled by (5.24) [342]. Any trajectory of system (5.26) beginning in $X_f(\alpha_i)$ *stays in* $X_f(\alpha_i)$ *and converges to the origin [341].*

Various methods can be used to define the equilibrium pair for a collective multi-agent system. In the virtual leader architecture [188, 231, 295] equilibrium of the collective flock is described by the relative inter-vehicle distance of neighbouring vehicle to the leader agent. In many decentralised and cooperative systems, the equilibrium is not known a priori. Instead, equilibrium emerges from the locally interacting and cooperating agents. Examples include flocking [25, 46, 127, 128, 236] and the network consensus problem [218, 233]. Central to the stability analysis of the decentralised model predictive control strategy for cooperative vehicles, is the definition of an equilibrium pair. The equilibrium for a group of vehicles provides a *coordination variable* for group consensus. In a cooperative decentralised multi-vehicle system, consensus on the coordination variable (or equilibrium pair) yields the cooperative behaviour of the group. In Section 2.2.1, it was shown that for a group of vehicles exchanging information using the consensus protocol in Equation (2.19) will converge to the average-value of the information state; i.e.:

$$\chi(x) = \text{Ave}(x) = \frac{1}{N}\sum_{i=1}^{N} x_i \tag{5.37}$$

where the information state of vehicle v_i is denoted by x_i. When the communicated information is the positional states of the vehicles, the average-consensus is given by the centroid of the formation of vehicles. In Chapter 3, an inter-vehicle distance offset d was introduced to induce spatial flocking in a group of vehicles. The consensus protocol was then used to prove the convergence of a group of connected vehicles to the flock lattice with distribution centred on the average position $\bar{q}$ of the initial distribution q_0, and velocity equalling the average velocity $\bar{p}$ of the connected group. Following these observations, the

following definition for the decentralised optimisation problem in Equation (5.20) with information exchange prescribed by Equation (2.19) is made:

Definition 2. (group equilibrium state)

The equilibrium state for a group of interconnected vehicles $x^e \in \mathbb{R}^n$ *is given by the average valued consensus of the communication network; i.e.:*

$$x^e := \text{Ave}(x) \tag{5.38}$$

and by the invariance property, is a constant such that $x^e = c$, $\forall i \in N$.

Following Problem (5.20) and Definition 2, the terminal region induced by the consensus protocol with is given by:

$$X_i^f := R = \sqrt{2\mathcal{H}(x(0), \dot{x}(0))} \tag{5.39}$$

where $\mathcal{H}(x(0), \dot{x}(0))$ is equivalently defined as $\mathcal{H}(q(0), \tilde{p}(0))$ Section 3.2.4. Based on the neighbouring plans $\hat{x}_i(t_k)$ of vehicle v_i, it is possible to define an error state using the consensus protocol in Equation (2.19). From Definition 1, at time t_k, $x_i(t_k) \in X_i$, and $\hat{x}_i^*(t_k) = \{\hat{x}_i^*(t_k \mid t_k), \ldots, \hat{x}_i^*(t_{k+T} \mid t_k)\}$ (where $\hat{x}_i^*(t_k \mid t_k) = x_i(t_k)$) for the ith vehicle, and $\hat{x}_i(t_k) = \{\hat{x}_j^*(t_{k-1} \mid t_{k-1}), \ldots, \hat{x}_j^*(t_{k-1+T} \mid t_{k-1}), \ldots, \hat{x}_{|\mathcal{N}_i|}^*(t_{k-1} \mid t_{k-1}), \ldots, \hat{x}_{|\mathcal{N}_i|}^*(t_{k-1+T} \mid t_{k-1})\}$, $\forall j \in \mathcal{N}_i$ over the prediction interval $\tau_{k-1} \in [t_{k-1}, t_{k-1+T}]$. The trajectories $\hat{x}_i^*(t_k)$ and $\hat{x}_i(t_k)$ overlap for $j \in \mathcal{N}_i$, except for the first sampling interval of the jth vehicle and the last sampling interval of the ith vehicle. The first sampling interval of the jth vehicle is the previous state of the vehicle; i.e. $x_j(t_{k-1})$ and can be excluded from the error state. For purposeful consensus, only the prediction interval of the jth vehicle over $\tau_{k,j}^{\wedge} \in [t_{k+1}, t_{k+T}]$ is considered. The predicted state of the jth vehicle is truncated for the ith vehicle over the interval $\tau_{k,j}^{\wedge} \in [t_{k+1}, t_{k+T}]$, such that the predicted states of the jth vehicle at time t_{k-1} transmitted to the ith vehicle produces the set of assumed states $\hat{x}_{i\_j} := \hat{x}_{i\_j}(t_k) = \{x_{i\_j}(t_k \mid t_{k-1}), \ldots$ $\ldots, x_{i\_j}(t_{k-1+T} \mid t_{k-1})\}$ at time t_k for the ith vehicle.

The objective is to minimise the deviation of the assumed state trajectories of neighbouring vehicles with the predicted states for the ith vehicle for $i = 1, \ldots, N$ to achieve consensus. For a homogenous group of vehicles, the prediction horizon length of each vehicle is equal. The mismatch in the last sampling interval of the ith vehicle with the jth vehicle corresponds to

a prediction made by the j th neighbour at time t_{k-1} and a prediction made by the i th vehicle at time t_k. For compatibility purposes, the final sampling period of the i th vehicle's prediction is truncated such that $\tau_{k,i}^{\wedge} \in [t_k, t_{k-1+T}]$. This assumption is valid since the assumed state of the j th vehicle has not been made yet. This yields the following optimisation horizon $\tau_k^* \in [t_k, t_{k-1+T}]$ for the overlapping regions of the sampling periods of the j th vehicle, and consensus is defined over the optimisation horizon.

A well known property of the model predictive control law given in Equation (5.24) is not guaranteed stabilisable due to the receding horizon [343]. In Section 5.4, an appropriate terminal cost constraint is introduced to stabilise the system and achieve consensus. For now, it is immediate to show that the error state $x_i^{\varepsilon}(\tau_k^* \mid t_k)$ between the predicted state of the i th vehicle at time t_k and the assumed state from the j th vehicle using state $x_j(t_{k-1})$ is given by the following:

$$\hat{x}_i^{\varepsilon}(\tau_k^* \mid t_k) = \sum_{j \in \mathcal{N}_i} \left\| \hat{x}_j(\tau_k^* \mid t_{k-1}) - \hat{x}_i(\tau_k^* \mid t_{k-1}) \right\| \tag{5.40}$$

where $\tau_k^* \in [t_k, t_{k-1+T}]$. Using the error state $x_i^{\varepsilon}(\tau_k^* \mid t_k)$ and the dynamic model in Equation (5.1), the consensus problem is converted into a regulation problem. Thus, the decentralised finite time optimal control problem associated with the i th vehicle at time t_k can be re-written as:

$$J_{i,T}^*(x_i(t_k), \hat{x}_i(t_k)) := \min_{\{\hat{u}_i(t_k)\}} \int_{t_k}^{t_{k+T}} l_i(\hat{x}_i^{\varepsilon}(\tau_k^* \mid t_k), \hat{u}_i(\tau_k^* \mid t_k)) d\tau_k^* + l_i{}^T(\hat{x}_i^{\varepsilon}(t_{k+T} \mid t_k))$$

Subject to:

$$\begin{gathered}
\dot{x}_i^{\varepsilon}(\tau_k^* \mid t_k) = f_i(x_i^{\varepsilon}(\tau_k^* \mid t_k), u_i(\tau_k^* \mid t_k)) \\
i = 1, \ldots, N, \quad \tau_k^* \in [t_k, t_{k-1+T}] \\
x_i(\tau_k^* \mid t_k) \in X_i, \quad u_i(\tau_k \mid t_k) \in U_i \\
(i, j) \in \mathcal{N}_i \\
g_{i,j}(x_i(\tau_k \mid t_k), x_j(\tau_k \mid t_k)) \le 0, \quad \forall j \in \mathcal{N}_i \\
x(t_k \mid t_k) = x(t_k) \\
x(t_{k+T} \mid t_k) \in X_f(\alpha_i)
\end{gathered} \tag{5.41}$$

Let $\|\cdot\|_P^2 = x^T P x$ denote the generalised weighted norm of a vector or matrix. Then, the individual cost function l_i associated with the i th vehicle can be rewritten as the following bounded cost function over the optimisation horizon $\tau_k^* \in [t_k, t_{k-1+T}]$:

$$l_i(\hat{x}_i^{\varepsilon}, \hat{u}_i) = \left\| \hat{x}_i^{\varepsilon} \right\|_Q^2 + \left\| \hat{u}_i \right\|_R^2 \tag{5.42}$$

and

$$l_i^T(\hat{x}_i^{\varepsilon}(t_{k+T}\mid t_k)) = \left\|(\hat{x}_i^{\varepsilon}(t_{k+T}\mid t_k)\right\|_P^2 \tag{5.43}$$

over the terminal period, where $Q \in \mathbb{R}^{n\times n}$, $R \in \mathbb{R}^{m\times m}$, and $P \in \mathbb{R}^{n\times n}$ are weighting matrices associated to the 2-norm. Problem (5.41) can then be rewritten as:

$$J_{i,T}^*(x_i(t_k), \hat{x}_i(t_k)) := \min_{\{\hat{u}_i(t_k)\}} \int_{t_k}^{t_{k+T}} \left\|\hat{x}_i^{\varepsilon}(\tau_k^*\mid t_k)\right\|_Q^2 + \left\|\hat{u}_i(\tau_k^*\mid t_k)\right\|_R^2 d\tau_k^* + \left\|(\hat{x}_i^{\varepsilon}(t_{k+T}\mid t_k)\right\|_P^2$$

Subject to:

$$\begin{gathered}
\dot{x}_i^{\varepsilon}(\tau_k^*\mid t_k) = f_i(x_i^{\varepsilon}(\tau_k^*\mid t_k), u_i(\tau_k^*\mid t_k)) \\
i = 1,\ldots,N, \quad \tau_k^* \in [t_k, t_{k-1+T}] \\
x_i(\tau_k^*\mid t_k) \in X_i, \quad u_i(\tau_k\mid t_k) \in U_i \\
(i,j) \in \mathcal{N}_i \\
g_{i,j}(x_i(\tau_k\mid t_k), x_j(\tau_k\mid t_k)) \le 0, \quad \forall j \in \mathcal{N}_i \\
x(t_k\mid t_k) = x(t_k) \\
x(t_{k+T}\mid t_k) \in X_f(\alpha_i)
\end{gathered} \tag{5.44}$$

Definition 3. (compatibility constraint)

Problem (5.44) involves only the state and input variables of the ith vehicle at time t_k and its neighbours' assumed states from time t_{-1}. To ensure compatibility with the predicted plans $\hat{x}_j(t_k)$ of the jth neighbour at successive intervals and the transmitted plans of proceeding sampling times (i.e. assumed states of the ith agent $\hat{x}_{i\_j}(\tau_k\mid t_k)$), the following compatibility constraint is introduced to Problem (5.44):

$$g_{i,j}(x_i(\tau_k\mid t_k), x_j(\tau_k\mid t_k)) \le 0 \Rightarrow g_{i,j}(\cdot) := \left\|\hat{x}_{i\_j}(\tau_k\mid t_{-1}) - \hat{x}_i(\tau_k\mid t_k)\right\| \le \kappa \tag{5.45}$$

where $\|\cdot\|$ is the standard Euclidean norm. Constraint (5.45) enforces a degree of consistency between what a vehicle is actually doing and what neighbours believe that agent is doing between successive horizons. A similar compatibility constraint was defined in [267].

Having defined the distributed optimal control problem for each vehicle in the flock, the main implementation algorithm is now introduced.

Definition 4. (implementation algorithm)

0. ***Initialisation**: At time t_{-1}, each vehicle solves Problem (5.20) with initial state $x(t_{-1})$ independently from neighbouring assumptions. Hence, $\mathcal{N}_i(t_{-1}) = \emptyset$, $\forall i = 1,\ldots,N$. The assumed states are given by the empty set $\hat{x}(t_{-1}) = \emptyset$ over the current horizon*

(i.e. $[t_{-1}, t_{-1} + H_p]$*),* $\forall i = 1,\ldots,N$*. By definition, the flock topology is described by a disconnected graph at initialisation, and the compatibility constraints are relaxed. The optimal control* $u_i^*(t_0 \mid t_{-1})$ *is then applied* $\forall i = 1,\ldots,N$ *over the proceeding horizon* $\tau_0 \in [t_0, t_{0+T}]$*;*

Following the initialisation stage, over every prediction horizon $\tau_k \in [t_k, t_{k+T}]$*, each vehicle* $i = 1,\ldots,N$*:*

1. *Solves Problem (5.44) using measurements of its current state* $x_i(t_k)$ *and the assumed states of its neighbours* $\widehat{x}_i(\tau_k \mid t_{k-1})$*,* $\forall j \in \mathcal{N}_i$ *to obtain the set of optimal trajectories* $\hat{x}_i^*(\tau_k, t_k)$ *and control inputs* $\hat{u}_i^*(\tau_k \mid t_k)$*;*

2. *Implements the first sample of* $\hat{u}_i^*(\tau_k \mid t_k)$*,* $\tau_k \in [t_k, t_{k+T}]$*, i.e.:*

$$u_i^*(t_k) = \hat{u}_i^*(t_k \mid t_k) \tag{5.46}$$

3. *Transmits the associated state trajectories* $\hat{x}_i^*(\tau_k \mid t_k)$*,* $\tau_k \in [t_k, t_{k+T}]$ *to neighbouring vehicles* $j \in \mathcal{N}_i$ *and receives the plans* $\widehat{x}_i(\tau_k \mid t_k)$*,* $\tau_k \in [t_k, t_{k+T}]$ *of neighbouring vehicles* $j \in \mathcal{N}_i$*;*

4. *Repeats steps 1 to 3 at time* t_{k+1}*, based on the new state information* $x_i(t_{k+1})$*, and trajectory plans of neighbours* $\widehat{x}_i(\tau_k \mid t_k)$*.*

By Definition 4, it is possible that at initialisation, the local objectives of a subset of vehicles in the flock $v_l \in V_l \subseteq V$ will be met over the prediction horizon $\tau_{-1} \in [t_{-1}, t_{-1+T}]$ and $x_l(\tau_{-1} \mid t_{-1}) = x_l^e$. Let $v_l \in V_l$ denote the subset of vehicles such that $v_l \notin \mathcal{N}_i$, $\forall i \in N$, $l \neq i$, then by application of $\hat{u}_l^*(t_{-1} \mid t_{-1})$, vehicles $v_l \in V_l$ will reach and remain at equilibrium for all future time. For a flock of vehicles, the distribution of vehicles in the group is bounded by an ellipsoid with radius R. By the dissipation of the structural energy (see Section 3.2.4), the distribution of vehicles converges to the flock lattice construction, and the structural graph topology is described by a connected graph. Therefore, the vehicles $v_l \in V_l$ will become a neighbour of vehicle $i \in N$ at some future time such that $v_l \in \mathcal{N}_i$. By the adjacency of vehicles and the connectivity of the information network, vehicles v_l and v_i exchange predicted plans. If v_i has not yet reached equilibrium $x_i(\tau_{-1} \mid t_{-1}) \neq x_i^e$, then the predicted

plans of v_i serve to act as an input to the optimisation problem of v_l. In proceeding optimisations, v_l accommodates for v_i's predicted plans; it cannot be guaranteed that the decentralised optimal value function $J^*_{l,T}(x_i(t_k), \tilde{x}_i(t_k))$ decreases with each prediction horizon update. The mutual exchange of information via the communication network of the flock of vehicles naturally suggests that a consensus must be reached to achieve a stable equilibrium. In the following section, the stability of the decentralised model predictive scheme is investigated using the consensus protocols in more detail.

5.4. STABILITY ANALYSIS

In this section, the conditions that lead to stability of the individual vehicles are presented using Lyapunov arguments. The objective is to show that through the application of the decentralised model predictive control law in Equation (5.46), the closed-loop state $x(t)$ converges to the neighbourhood of objective states x^e. Without loss of generality, the value function $J^*_{i,T}(\cdot)$ is treated as a candidate Lyapunov function. Before proceeding with the analysis, the following assumptions are made:

Assumption 1.

1. *$\forall i \in N$, the function $f_i : \mathbb{R}^n \times \mathbb{R}^m \to \mathbb{R}^n$ in Equation (5.1) is twice continuously differentiable with $f_i(x_i^e, 0) = 0$ and f_i is stabilisable;*
2. *X_i^f is control invariant, $X_i^f \subseteq X_f$;*
3. *There exists a constant $\rho_{\max} \in (0, \infty)$ such that $\left\| x^*(\tau_k \mid t_k) - x^e \right\| \leq \rho_{\max}$ and $\left\| \hat{x}(\tau_k \mid t_k) - x^e \right\| \leq \rho_{\max}$, for all $\tau_k \in [t_k, t_{k+T}]$;*

Following the standard arguments in [342], it is assumed that initial feasibility of the implementation in Equation (5.44) implies subsequent feasibility. Therefore, it is sufficient to prove that only $J^*_T(x(t_k))$ decreases. The following lemma provides a bound on the decrease of $J^*_T(x(t_{k+1}))$:

Lemma 2. (bounded candidate function)

$J^*_{i,T}(x_i(t_{k+1}), \hat{x}_i(t_{k+1}))$ is a valid Lyapunov function and the state of the closed-loop system converges to the origin; i.e. $\lim_{t_k \to \infty} x(t_k) = 0$.

Proof.

The proof follows from Lyapunov arguments, close in spirit to the arguments of [270, 341, 344].

For any t_k, the collective decentralised value function for the flock of vehicles is given by:

$$J^*_T(x(t_k), \hat{x}(t_k)) := \int_{t_k}^{t_{k+T}} \sum_{i=1}^{N} \left\| \hat{x}^{\varepsilon}_i(\tau^*_k \mid t_k) \right\|^2_Q + \left\| \hat{u}_i(\tau^*_k \mid t_k) \right\|^2_R d\tau^*_k + \left\| (\hat{x}^{\varepsilon}_i(t_{k+T} \mid t_k) \right\|^2_P \tag{5.47}$$

Applying the optimal control in Equation (5.46) to Equation (5.47), takes the system to time t_{k+1} with states $x^{\varepsilon}(t_{k+1})$. An upper bound is constructed by considering a feasible and suboptimal solution to Problem (5.47) for vehicle v_i, over the proceeding prediction interval $\tau_{k+1} \in [t_{k+1}, t_{k+1+T}]$, $\forall i \in N$. For vehicle v_i, the state update is bounded by:

$$\begin{aligned} J^*_{i,T}(x_i(t_{k+1}), \hat{x}_i(t_{k+1})) &:= \int_{t_{k+1}}^{t_{k+1+T}} \left\| \hat{x}^{*,\varepsilon}_i(\tau^*_{k+1} \mid t_{k+1}) \right\|^2_Q + \left\| \hat{u}^*_i(\tau^*_{k+1} \mid t_{k+1}) \right\|^2_R d\tau^*_{k+1} \cdots \\ &\quad \cdots + \left\| (\hat{x}^{*,\varepsilon}_i(t_{k+1+T} \mid t_{k+1}) \right\|^2_P \\ &\leq \int_{t_{k+1}}^{t_{k+1+T}} \left\| \hat{x}^{\varepsilon}_i(\tau^*_{k+1} \mid t_{k+1}) \right\|^2_Q + \left\| \hat{u}_i(\tau^*_{k+1} \mid t_{k+1}) \right\|^2_R d\tau^*_{k+1} \cdots \\ &\quad \cdots + \left\| (\hat{x}^{\varepsilon}_i(t_{k+1+T} \mid t_{k+1}) \right\|^2_P \end{aligned} \tag{5.48}$$

For all $i \in N$, the upper bound for the collective optimal value function $J^*_T(x(t_{k+1}), \hat{x}(t_{k+1}))$ is then given by:

$$\begin{aligned} J^*_T(x(t_{k+1}), \hat{x}(t_{k+1})) &\leq \int_{t_{k+1}}^{t_{k+1+T}} \sum_{i=1}^{N} \left\| \hat{x}^{\varepsilon}_i(\tau^*_{k+1} \mid t_{k+1}) \right\|^2_Q + \left\| \hat{u}_i(\tau^*_{k+1} \mid t_{k+1}) \right\|^2_R d\tau^*_{k+1} \cdots \\ &\quad \cdots + \left\| (\hat{x}^{\varepsilon}_i(t_{k+1+T} \mid t_{k+1}) \right\|^2_P \\ J^*_T(x(t_{k+1})) - J^*_T(x(t_k)) &\leq \cdots \\ &\quad \cdots \int_{t_{k+1}}^{t_{k+1+T}} \sum_{i=1}^{N} \left\| \hat{x}^{\varepsilon}_i(\tau^*_{k+1} \mid t_{k+1}) \right\|^2_Q + \left\| \hat{u}_i(\tau^*_{k+1} \mid t_{k+1}) \right\|^2_R d\tau^*_{k+1} \cdots \end{aligned} \tag{5.49}$$

$$\cdots - \int_{t_k}^{t_{k+T}} \sum_{i=1}^{N} \left\| \hat{x}_i^{*,\varepsilon}(\tau_k^* \mid t_k) \right\|_Q^2 + \left\| \hat{u}_i^*(\tau_k^* \mid t_k) \right\|_R^2 d\tau_k^* \cdots$$

$$\cdots + \sum_{i=1}^{N} \left\| (\hat{x}_i^{\varepsilon}(t_{k+1+T} \mid t_{k+1}) \right\|_P^2 - \sum_{i=1}^{N} \left\| (\hat{x}_i^{*,\varepsilon}(t_{k+T} \mid t_k) \right\|_P^2$$

It follows that if inequality (5.49) holds, then $J_T^*(x(t_{k+1})) \le J_T^*(x(t_k))$, *and* $J_{i,T}^*(x_i(t_{k+1}), \hat{x}_i(t_{k+1}))$ *is a positive non-decreasing function along the closed-loop trajectories. Furthermore, since* $J_T^*(\cdot)$ *is lower bounded by zero and the trajectories initialised at* $x_i(0) \in X_i$ *remain in* X_i *for all* $t_k \ge 0$, *Equation (5.49) is sufficient to ensure that the state of the closed loop system converges to zero as* $t_k \to \infty$ *[265].*

Before proceeding with the main results of this introduction, the following assumptions and definitions are made.

Assumption 2. (terminal state)

The assumed state $\hat{x}_{i\_j}(t_{k-1+T} \mid t_{k-1})$ *of the* j *th neighbour of vehicle* v_i *remains invariant over the terminal period* T *for all* $j \in \mathcal{N}_i$ *at time* t_k.

Following Assumption 2, the terminal constraint of Problem (5.44) is given by:

Definition 5. (terminal cost)

The terminal constraint for Problem (5.44) using the average-valued consensus is given by:

$$l_i^T = \left\| \hat{x}_i(t_{k+T} \mid t_k) - x_i^e(t_k) \right\|_P^2 \tag{5.50}$$

where

$$x_i^e(t_k) = \frac{1}{|\mathcal{N}_i|} \sum_{j=1}^{|\mathcal{N}_i|} \hat{x}_{i\_j}(t_{k-1+T} \mid t_{k-1}) \tag{5.51}$$

Theorem 1. (convergence to the average consensus)

$J_T^*(\cdot)$ *decreases over successive sampling periods toward a closed neighbourhood of the objective state by the bound:*

$$\begin{gathered} \int_{t_{k+1}}^{t_{k+T}} \sum_{i=1}^{N} \sum_{j \in \mathcal{N}_i} \left\| x_i^*(\tau_k^* \mid t_k) - x_j^*(\tau_k^* \mid t_k) + d_{ij} \right\|_Q^2 - \left\| x_i^*(\tau_k^* \mid t_k) - \hat{x}_j(\tau_k^* \mid t_k) + d_{ij} \right\|_Q^2 d\tau_k^* \le \cdots \\ \cdots \le \frac{1}{2} \kappa \left[4\rho_{\max} + \kappa \right] \end{gathered} \tag{5.52}$$

Proof.

By Definition 4, the prediction intervals of successive optimal state and control trajectories overlap at successive sampling periods. Therefore, the predicted state and control trajectories at any sampling period t_{k+1} *can be given as* $\hat{x}_i(\tau_k^* \mid t_{k+1}) = x_i^*(\tau_k^* \mid t_k)$ *and* $\hat{u}_i(\tau_k^* \mid t_{k+1}) = u_i^*(\tau_k^* \mid t_k)$ *respectively over the interval* $\tau_k^* \in [t_{k+1}, t_{k+T}]$. *Consequently, the inequality in Equation (5.49) can be simplified and written as:*

$$\begin{aligned} & J_T^*(x(t_{k+1}) - J_T^*(x(t_k)) \leq \cdots \\ & \cdots \int_{t_{k+1}}^{t_{k+T}} \sum_{i=1}^{N} \sum_{j \in \mathcal{N}_i} \left\| x_i^*(\tau_k^* \mid t) - x_j^*(\tau_k^* \mid t_k) + d_{ij} \right\|_Q^2 - \left\| x_i^*(\tau_k^* \mid t_k) - \hat{x}_j(\tau_k^* \mid t_k) + d_{ij} \right\|_Q^2 d\tau_k^* + \cdots \\ & \cdots + \left\| \hat{x}(t_{k+1+T} \mid t_{k+1}) - x^e \right\|_P^2 - \left\| x^*(t_{k+T} \mid t_k) - x^e \right\|_P^2 + \cdots \\ & \cdots + \int_{t_{k+T}}^{t_{k+1+T}} \left\| \hat{x}(\tau_k^+ \mid t_{k+1}) - x^e \right\|_{Q+K^T RK}^2 d\tau_k^+ \end{aligned} \tag{5.53}$$

where $\tau_k^+ \in [t_{k+T}, t_{k+1+T}]$, *and* $d_{ij} = x_j^e - x_i^e$. *From Definition 2, and the connectivity of the information network* $G(x)$, $x_j^e = x_i^e = \text{Ave}(x)$ *and* $d_{ij} = 0$ *for* $\forall j \in \mathcal{N}_i \quad i \neq j$. *Hence, the average-valued consensus complies with the invariance properties of the consensus protocol and the inequality in Equation (5.53). By the properties of Lemma 1, the sum of the last three terms in the inequality above is non-positive, and the inequality holds after removal of these terms. Hence:*

$$\begin{aligned} & J_T^*(x(t_{k+1}) - J_T^*(x(t_k)) \leq \cdots \\ & \cdots \int_{t_{k+1}}^{t_{k+T}} \sum_{i=1}^{N} \sum_{j \in \mathcal{N}_i} \left\| x_i^*(\tau_k^* \mid t_k) - x_j^*(\tau_k^* \mid t_k) + d_{ij} \right\|_Q^2 - \left\| x_i^*(\tau_k^* \mid t_k) - \hat{x}_j(\tau_k^* \mid t_k) + d_{ij} \right\|_Q^2 d\tau_k^* \end{aligned} \tag{5.54}$$

Using the triangle inequality:

$$\|\alpha\|_p^2 - \|\beta\|_p^2 \leq \|\alpha + \beta\|_p^2 \tag{5.55}$$

Equation (5.54) becomes:

$$\begin{aligned} & \left\| x_i^*(\tau_k^* \mid t_k) - x_j^*(\tau_k^* \mid t_k) + d_{ij} \right\|_Q^2 - \left\| x_i^*(\tau_k^* \mid t_k) - \hat{x}_j(\tau_k^* \mid t_k) + d_{ij} \right\|_Q^2 \leq \cdots \\ & \qquad \cdots \left\| x_i^*(\tau_k^* \mid t_k) - \hat{x}_j(\tau_k^* \mid t_k) + d_{ij} \right\|^2 + \cdots \\ & \qquad \cdots + 2 \left\| x_i^*(\tau_k^* \mid t_k) - \hat{x}_j(\tau_k^* \mid t_k) + d_{ij} \right\| \cdot \left\| x_j^*(\tau_k^* \mid t_k) - \hat{x}_j(\tau_k^* \mid t_k) \right\| + \cdots \\ & \qquad \cdots + \left\| x_j^*(\tau_k^* \mid t_k) - \hat{x}_j(\tau_k^* \mid t_k) \right\|^2 \end{aligned} \tag{5.56}$$

where the inequality has been replaced by a summand of three norms. The first norm corresponds to the initial point and is trivial for analysis.

From the compatibility constraint in Equation (5.45) and the bounded constraint in Assumption 1, the following bounds are introduced $\left\|\bar{x}_{i\_j}(\tau_k^* \mid t_{k-1}) - \hat{x}_j(\tau_k^* \mid t_k)\right\| \le \kappa$, $\left\|x_i^*(\tau_k^* \mid t_k) - x_i^e\right\| \le \rho_{\max}$, *and* $\left\|\hat{x}_j(\tau_k^* \mid t_k) - x_j^e\right\| \le \rho_{\max}$ *to Equation (5.56):*

$$\begin{aligned}
&\left\|x_i^*(\tau_k^* \mid t_k) - x_j^*(\tau_k^* \mid t_k) + d_{ij}\right\|_Q^2 - \left\|x_i^*(\tau_k^* \mid t_k) - \hat{x}_j(\tau_k^* \mid t_k) + d_{ij}\right\|_Q^2 \le \cdots \\
&\quad \cdots 2\left\|x_i^*(\tau_k^* \mid t_k) - \hat{x}_j(\tau_k^* \mid t_k) + d_{ij}\right\| \cdot \left\|x_j^*(\tau_k^* \mid t_k) - \hat{x}_j(\tau_k^* \mid t_k)\right\| + \left\|x_j^*(\tau_k^* \mid t_k) - \hat{x}_j(\tau_k^* \mid t_k)\right\|^2 \\
&\quad \cdots \le 2\left[\left\|x_i^*(\tau_k^* \mid t_k) - x_i^e\right\| + \left\|\hat{x}_j(\tau_k^* \mid t_k) - x_j^e\right\|\right]\kappa + \kappa^2 \\
&\quad \cdots \le \kappa\left[4\rho_{\max} + \kappa\right]
\end{aligned} \tag{5.57}$$

Using the bound in Equation (5.57), the integrated expression in Equation (5.54) becomes:

$$\begin{aligned}
&\int_{t_{k+1}}^{t_{k+T}} \sum_{i=1}^{N} \sum_{j \in \mathcal{N}_i} \left\|x_i^*(\tau_k^* \mid t_k) - x_j^*(\tau_k^* \mid t_k) + d_{ij}\right\|_Q^2 - \left\|x_i^*(\tau_k^* \mid t_k) - \hat{x}_j(\tau_k^* \mid t_k) + d_{ij}\right\|_Q^2 d\tau_k^* \le \cdots \\
&\qquad \cdots \le \frac{1}{2}\kappa\left[4\rho_{\max} + \kappa\right]
\end{aligned} \tag{5.58}$$

where κ *is the compatibility constraint given by Equation (5.45).*

Equation (5.58) provides a bounding result on the decrease in $J_T^*(\cdot)$ from one update to the next. The value $\rho_{\max}$ and κ are new optimisation variables. In the proceeding section, the transient response of the cooperative control scheme is discussed.

5.5. TRANSIENT RESPONSE OF THE COOPERATIVE CONTROL SCHEME

By considering the centralised cost function in Equation (5.5) as a cooperative control objective, and the solutions to Problem (5.9) as the coordination variables of the cooperative task, the decentralised model predictive control strategy presented in Section 5.3, provides the cooperative control framework to coordinate the actions of a group of vehicles and resolve the cooperative task. Coordination is achieved by exchanging information between vehicles in the group, and reaching a consensus on the coordination variable. In this case, the information is the plans of the vehicles over successive prediction horizons, and represents partial solutions to the cooperative objective.

Information consensus for a time-invariant and a time-varying network was investigated in Chapter 1. It was shown for a time-invariant network, that a connected group of vehicles will asymptotically reach a consensus on the information state at a rate equal to the Fiedler eigenvalue of the graph Laplacian. A similar discussion was also presented for the time-varying network topology described by a hybrid autonomous equation. In both cases, the

information flow was modelled using a first-order differential equation, and assumed continuous information exchange. Since the information exchange of the decentralised model predictive control strategy is also assumed continuous, then it would be expected that the convergence of the coordination variable would reflect the behaviour of the time-invariant or time-varying network model. For the decentralised model predictive control strategy however, the information state represents a partial solution to the cooperative objective, and evolves according to the solution space of the optimisation problem in Equation (5.41). Nonetheless, assuming a Lyapunov value function for the cost objective, the information state will demonstrate asymptotic convergence. This presumption is based on the Lyapunov arguments in Section 5.4. The rate at which the coordination variable reaches consensus, is then dependent on the convergence of the information state. This is directly related to the quality of the solution found over each horizon.

In the unconstrained case of the receding horizon problem, the information state (plans over the proceeding horizon) of each vehicle is permitted to converge to the optimum value at each sampling period. Since the information is localised to each vehicle, then the plans generated by each vehicle are optimal only for that vehicle. Conflicts occur when the plans optimised for one vehicle, do not complement the plans optimised for a neighbouring vehicle. By considering the plans of neighbouring vehicles at each sampling period, the vehicles can coordinate their actions to reach a consensus. If the optimal plans generated by neighbouring vehicles at successive sampling periods are not constrained, and are permitted to deviate excessively from the previous sampling period, then it would be expected that the decentralised model predictive controller would demonstrate poor convergence as the vehicles attempt to compensate for the mismatch between the previous plans and the new plans of their neighbours. For this reason, the compatibility constraint κ was introduced to Problem (5.41) to mitigate the information mismatch between previously transmitted plans and newly developed plans at each horizon.

Whilst the compatibility constraint can be used to minimise oscillations about the equilibrium and improve the convergence of the coordination variable, it can also reduce the transient response of decentralised model predictive control strategy. Consider the case when κ is small. Then, the permitted deviation of successive plans will also be small at consecutive updates. This results in a sluggish transient response. Despite this, the system will eventually reach a consensus based on the stability properties of the Lyapunov function. On the other hand, by relaxing the compatibility constraint and permitting large deviations

between successive updates, the convergence of the system would be characterised by oscillations about the consensus point as vehicles attempt to reach a consensus on irrelevant and obsolete information. The effect of the compatibility constraint is now stated formally:

Theorem 2. (bound on optimal state)

The S th iteration deviates at most from the original plan by $S\kappa$.

Proof.

The proof can be found by applying the compatibility constraint recursively over successive updates. From Equation (5.45), the compatibility constraint is given by:

$$\left\| \hat{x}_{j\_i}(\hat{\tau}_{k,j} \mid t_{k-1}) - \hat{x}_i(\hat{\tau}_{k,i} \mid t_k) \right\| \leq \kappa \tag{5.59}$$

where $\hat{\tau}_{k,i} \in [t_k, t_{k-1+T} + T]$, and $\hat{\tau}_{k,j} \in [t_{k+1}, t_{k+T} + T]$. In addition, the following assumption holds:

$$\hat{x}_{j\_i}(\hat{\tau}_{k,j} \mid t_{k-1}) = \hat{x}_i(\hat{\tau}_{k-1,i} \mid t_{k-2}) \tag{5.60}$$

That is, the assumed state trajectories of vehicle v_i by the j th neighbour at time k, is the predicted state of vehicle v_i at time $k-1$. Consider the interval $\tau_k^* \in [t_k, t_{k-1+T}]$ for which the optimisation problem is defined in Equation (5.41). Then for $k=1$, the following compatibility constraint is observed for the terminal value t_{k-1+T}:

$$\left\| \hat{x}_{j\_i}(t_T \mid t_0) - \hat{x}_i(t_T \mid t_1) \right\| \leq \kappa \tag{5.61}$$

Applying recursively for S consecutive updates, such that $k = 1,2,\ldots,S$:

$$\begin{aligned}
k &= 1 \qquad \left\| \hat{x}_{j_i}(t_T \mid t_0) - \hat{x}_i(t_T \mid t_1) \right\| \leq \kappa \\
k &= 2 \qquad \left\| \hat{x}_{j_i}(t_{T+1} \mid t_1) - \hat{x}_i(t_{T+1} \mid t_2) \right\| \leq \kappa \\
k &= 3 \qquad \left\| \hat{x}_{j_i}(t_{T+2} \mid t_2) - \hat{x}_i(t_{T+2} \mid t_3) \right\| \leq \kappa \\
&\vdots \qquad\qquad \vdots \\
k &= S \qquad \left\| \hat{x}_{j_i}(t_{S-1+T} \mid t_{S-1}) - \hat{x}_i(t_{S-1+T} \mid t_S) \right\| \leq \kappa
\end{aligned} \tag{5.62}$$

Summing both sides of the inequalities yields:

$$\sum_{k=1}^{S} \left\| \hat{x}_{j\_i}(t_{k-1+T} \mid t_{k-1}) - \hat{x}_i(t_{k-1+T} \mid t_k) \right\| \leq S\kappa \tag{5.63}$$

and from the triangle inequality:

$$\left\| \hat{x}_{j\_i}(t_{S-1+T} \mid t_0) - \hat{x}_i(t_{S-1+T} \mid t_S) \right\| \leq S\kappa \tag{5.64}$$

Hence, after the S th update, the current state deviates from the original optimal state by at most $S\kappa$.

From Theorem 2, the quality of the solution at $k>1$, is proportionally constrained to the quality of the original solution obtained at $k=1$ and is proportional to the sampling rate of the information exchange between neighbouring vehicles. The effect of this constraint is similar to a step-size discretisation in a digital controller. By increasing the sampling rate of the information exchange, the transient response of the system would be expected to demonstrate poor convergence. In contrast, decreasing the sampling rate would lead to 'sluggish' transient behaviour. This is demonstrated by the numerical example in Section 5.6.

The introduction of the compatibility constraint effectively diminishes the model predictive control scheme's ability to handle uncertainty and changes to the operating conditions. Nonetheless, the compatibility constraint is necessary to promote coherence in the shared information and coordinate the actions of the individuals. By carefully selecting parameter κ at design-time, the compatibility constraint can be tolerated to provide a good balance between the transient response of the system, and the convergence of the solution. In the following section, the transient response of the cooperative control scheme is demonstrated for the consensus problem.

5.6. NUMERICAL EXAMPLE: TRANSIENT RESPONSE OF THE COOPERATIVE CONTROL SCHEME

Consider the consensus problem for $N=4$ agents with information state $x_i \in \mathbb{R}$, control input $u_i \in \mathbb{R}$, and dynamics given by:

$$\dot{x}_i(t) = A_i x_i(t) + B_i u_i(t),$$
$$\text{where } A_i = \begin{bmatrix} 0 & I_{n\times n} \\ 0 & 0 \end{bmatrix},\ B_i = \begin{bmatrix} 0 \\ I_{n\times n} \end{bmatrix} \tag{5.65}$$

Given the initial distribution of information for the group of agents:

$$\begin{aligned} x(0) &= [0 \quad 3.3 \quad 6.6 \quad 10]^T \\ \dot{x}(0) &= [0 \quad 0 \quad 0 \quad 0]^T \end{aligned} \tag{5.66}$$

where $x=[x_1, x_2, x_3, x_4]^T$, $\dot{x}=[\dot{x}_1, \dot{x}_2, \dot{x}_3, \dot{x}_4]^T$, the objective is to achieve consensus on the information state x. The consensus protocol given in Equation (2.19) produces the following cost function for the cooperative control problem from Equation (5.41):

$$\hat{x}_i^{\varepsilon}(\tau_k^* \mid t_k) = \sum_{j\in\mathcal{N}_i} \left\| \hat{x}_j(\tau_k^* \mid t_{k-1}) - \hat{x}_i(\tau_k^* \mid t_{k-1}) \right\| \tag{5.67}$$

Problem (5.41) is solved by applying the decentralised control scheme in Definition 4. For the following simulation, $T = 3.6s$, and $\kappa = \{0.001 \quad 0.01 \quad 10.0 \quad 100.0\}$. Figure 5-8 shows the transient response for the cooperative decentralised model predictive scheme for each value of κ. For comparison, the consensus protocol with dynamics given in Equation (2.20) is included in Figure 5-8. This is shown by the broken lines in Figure 5-8 for the corresponding vehicle. The convergence of the disagreement vector $\|\delta\|$ for the cooperative decentralised model predictive control scheme is shown in Figure 5-9 and is compared to the solution obtained from the dynamics of Equation (2.20). From Figure 5-8, the compatibility constraint influences the transient response and the convergence of the system to the average value. For $\kappa >> 0$, the information state rapidly converges towards the average value, but fails to settle on the equilibrium. On the other hand, for $\kappa << 0$, the compatibility constraint limits the divergence of S successive plans by $S\kappa$, and acts to dampen the oscillations induced by achieving a consensus with neighbouring agents (shown in Figure 5-10). The compromise for this asymptotic behaviour is a sluggish transient response.

5.7. SUMMARY

In this chapter, the problem of cooperative control for a group of agents was addressed by formulating the cooperative control problem as an optimisation problem. Cooperation was represented by the coupling of objectives and constraints in the centralised objective function. A cooperative control scheme was then created by decentralising a traditional model predictive control strategy. This was done to exploit the predictive nature of MPC to develop plans that could be exchanged. This allowed the vehicles to negotiate on new plans and arrive at a consensus on the coordination variable. In the proceeding chapter, the concepts of information consensus, flocking, group tracking, and decentralised model predictive control are unified into a singular and robust design methodology for cooperative control for a group of vehicles.

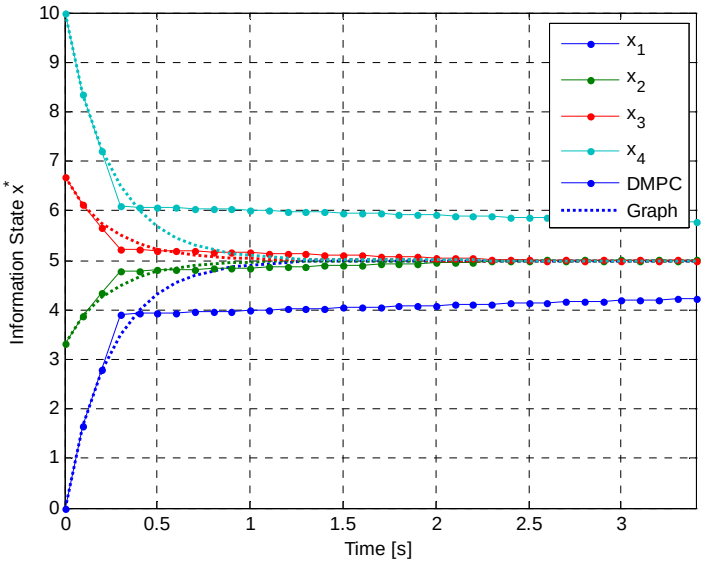

(a) κ = 0.001

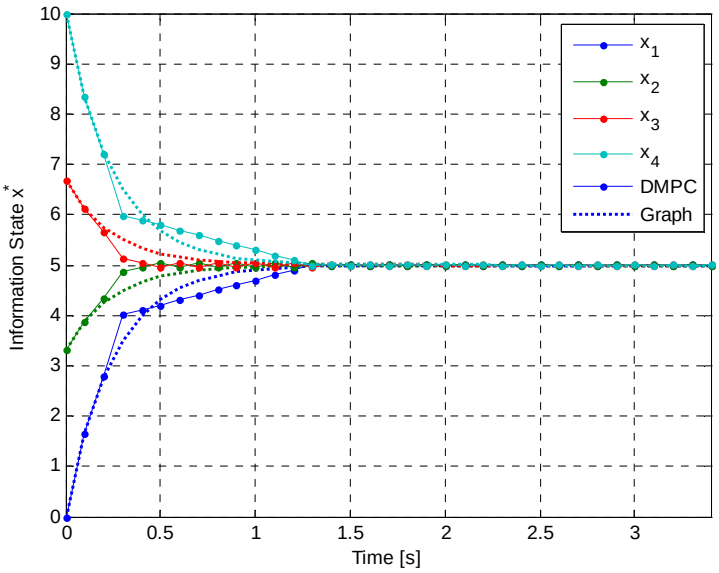

(b) κ = 0.01

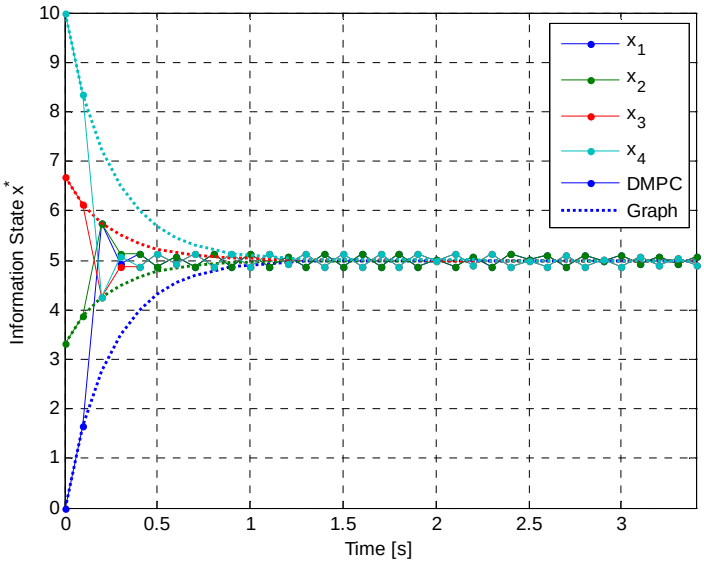

(c) κ = 10

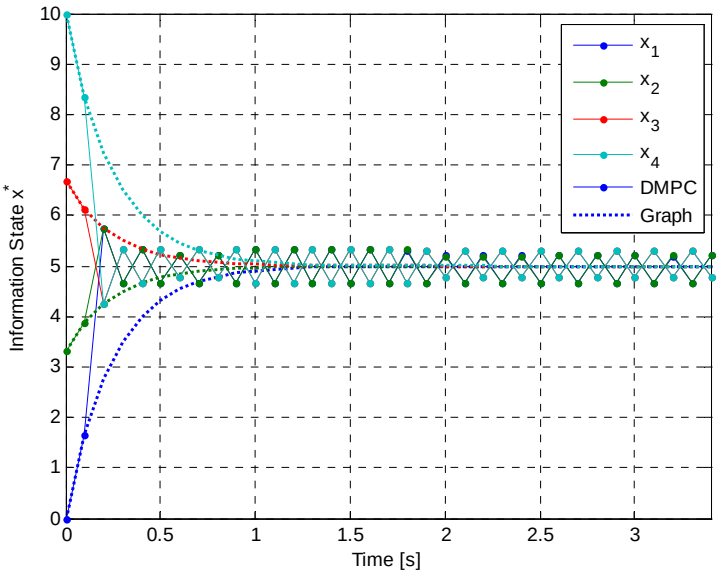

(d) κ = 100

Figure 5-8. The effect of the compatibility constraint on the transient response of the cooperative decentralised model predictive control scheme.

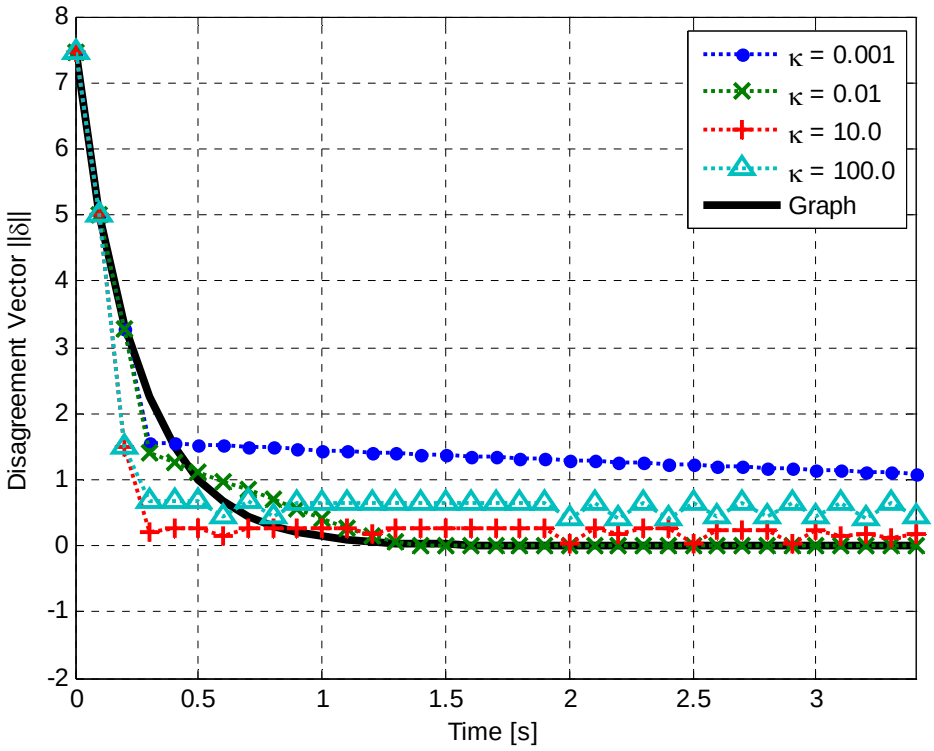

Figure 5-9. Effect of the compatibility constraint on the convergence of the disagreement vector for the consensus problem.

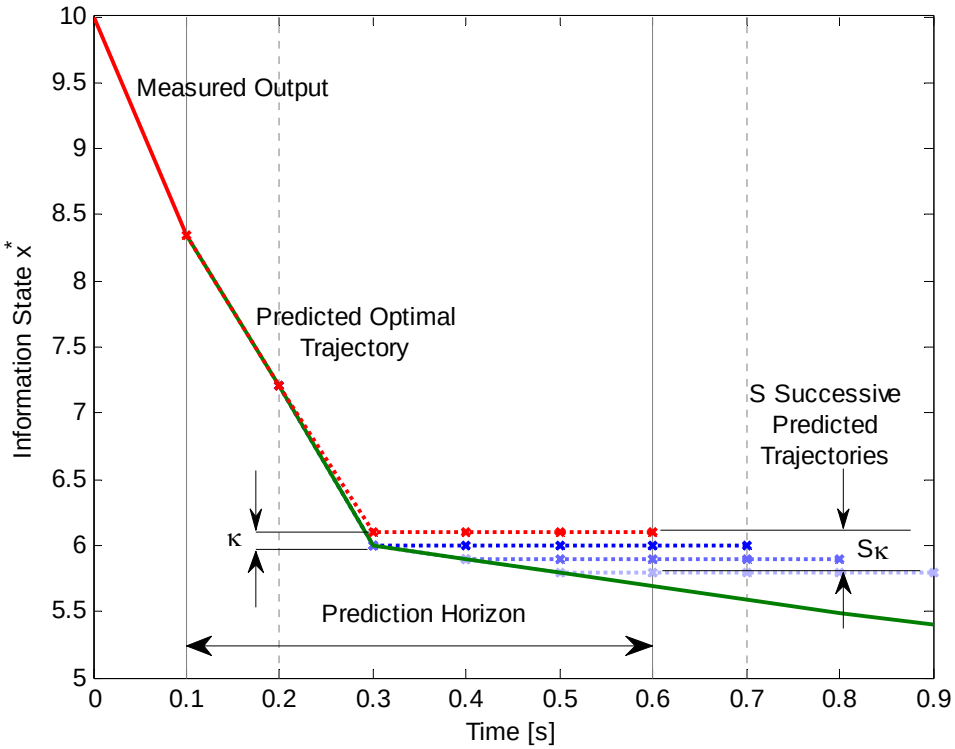

Figure 5-10. Divergence of predicted trajectories over successive prediction horizons.

Chapter 6. Application

In this chapter, the cooperative decentralised model predictive control scheme presented in the previous chapter is applied to a group of autonomous vehicles. The scheme is implemented locally on each vehicle and is used to coordinate the actions of the vehicles towards the group objective. A switching network using the finite interaction range in Chapter 2 is used to describe the underlying communication graph topology for the coordination scheme. The group cooperative objective is defined using the shape and group abstractions described in Chapter 4. Controlling the group of vehicles involves two levels of control. At the supervisory level, the optimal motions of the group, and the desired shape spanned by the vehicles is evaluated using the strategies described in Chapter 4. These are then transmitted to the individual vehicles to define a group objective. The cooperative control problem is then solved dynamically online at the local vehicle level using the cooperative decentralised model predictive control scheme. Using only local information, each vehicle develops a set of plans over a prediction horizon and evaluates the effect of these plans on the cooperative objective. Plans are exchanged between neighbouring vehicles at successive sampling periods to coordinate the behaviour of the vehicles and achieve a consensus on the group's actions. Cohesion of the group at the local vehicle level is addressed using the flock protocols described in Chapter 3. These represent the local vehicle objectives and are combined with the group's cooperative objective to formulate a distributed optimisation problem for each vehicle. Here, the role of the decentralised model predictive control strategy is to arbitrate between the local vehicle levels and the group cooperative objectives, and provide the mapping from the precision of the local flock protocol, to the generalised group abstractions.

This chapter serves to demonstrate a practical implementation of the strategies developed thus far and is organised as follows. A description of the system and the centralised cooperative objective is described in Section 6.1. The desired motion and shape of the group, as prescribed by the supervisory controller, is described in Section 6.2. Decomposition of the tasks of the individual vehicles is then presented in Section 6.3 before the decomposition of

the centralised cooperative objective for each vehicle is presented in Section 6.4. Numerical experiments are then presented in Section 6.5 to demonstrate the effectiveness of the proposed cooperative control scheme before Section 6.6 concludes with final remarks.

6.1. SYSTEM IMPLEMENTATION

The advancement of sensor technologies and small-scale robotics has seen a growing interest in the development of unmanned aerial vehicles for surveillance, reconnaissance, and intelligence operations. Unmanned sensory platforms can be used in lieu of dedicated manned vehicles for dangerous or repetitive operations. Recent developments in small-scale and inexpensive UAVs present an opportunity to develop teams of UAVs for cooperative sensing and imaging tasks and modalities. Groups of UAVs can be used to produce dynamic and spatiotemporal sensor networks. Search and rescue operations using spatially distributed sensory networks can be used to greatly improve the coverage time over a region of interest. Motivated by the recent interest in mobile sensory platforms, the strategies discussed in the previous chapters are applied to a group of UAVs for cooperative sensor coverage.

Consider N vehicles deployed in a search region χ of known dimension. The objective is to cooperatively stabilise the group into a cohesive flock that maximises the sensory footprint of the collective system. As the flock moves around the search region, sensory information about the environment is collected; reducing the uncertainty of the environment. Each vehicle v_i, $i = 1,\ldots,N$ is assumed to have decoupled dynamics given by:

$$\begin{aligned} &\dot{x}_i(t) = A_i x_i(t) + B_i u_i(t), \quad t \geq 0, \\ &\text{and } A_i = \begin{bmatrix} 0 & I_n \\ 0 & 0 \end{bmatrix}, \quad B_i = \begin{bmatrix} 0 \\ I_n \end{bmatrix} \end{aligned} \tag{6.1}$$

where $x_i(t) = (q_i(t), \dot{q}_i(t)) \in X_i = \mathbb{R}^{2n}$, and $u_i(t)$ are the state and control inputs of vehicle v_i, $q_i(t) \in Q_i = \mathbb{R}^n$, $\dot{q}_i(t) \in T_q Q_i = \mathbb{R}^n$, $u_i(t) \in \mathbb{R}^n$ are the configuration and control manifolds, and I_n is the n-dimensional identity matrix. Each vehicle is also subject to the following input constraints:

$$u_i \in U_i \tag{6.2}$$

Concatenating vehicles states, the following $2nN$-dimensional control system is obtained for the collective group:

$$\begin{aligned} &\dot{x}(t) = Ax(t) + Bu(t), \quad t \geq 0, \\ &\text{and } A = \text{diag}(A_1,\ldots,A_N), \; B = \text{diag}(B_1,\ldots,B_N) \end{aligned} \tag{6.3}$$

with $q \in Q = \prod_{i=1}^{N} Q_i = \mathbb{R}^{nN}$, $\dot{q} \in T_q Q = \prod_{i=1}^{N} T_q Q_i = \mathbb{R}^{nN}$, $u \in U = \prod_{i=1}^{N} U_i = \mathbb{R}^{nN}$.

The group of vehicles with dynamics given in Equation (6.3) can be controlled at the supervisory level by commanding the position and orientation of the centroid O' of the flock of vehicles, and the shape spanned by the configuration of vehicles in the frame $\{M\}$ fixed to the centroid O'. This leads to the following definitions derived from the concepts introduced in Chapter 4:

Definition 1. (Pose Abstraction)

If G is a Lie group, then $g \in G$ defines the gross position and orientation of the flock of vehicles in the world frame $\{F\}$, and is referred to as the group variable.

Definition 2. (Shape Abstraction)

The shape spanned by the group of vehicles in the flock is identified by the shape variable $s \in S$.

Definition 3. (Group Abstraction)

The pose abstraction and the shape abstraction together define the group's abstract variable $\alpha = (g, s) \in \mathrm{A}$ on the group manifold A.

The group abstraction α provides a mapping from the configuration space Q to the lower dimensional manifold A that captures the group's behaviours. The group abstraction α is invariant to the number and ordering of vehicles in the flock. For a group of vehicles with configuration $q \in Q$ in the local frame $\{M\}$, the motion of the group parameterised by time t in an arbitrary n-dimensional Special Euclidean space $SE(n)$, is described by the pair $g(t) = (R(t), d(t)) \in SE(n)$, where:

$$SE(n) = \left\{ g \middle| g = \begin{bmatrix} R & d \\ 0 & 1 \end{bmatrix}, R \in \mathbb{R}^{n \times n}, RR^T = I_n, \det \mathbb{R} = I, d \in \mathbb{R}^n \right\} \tag{6.4}$$

where d is given by the centroid of the flock as described in Section 4.2.1, and given by:

$$d \coloneqq \bar{q} = \frac{1}{N} \sum_{i}^{N} q_i \in \mathbb{R}^n \tag{6.5}$$

and R is the rotational component of the flock. To consider the rotation and shape of the flock, the concept of the virtual agent from Section 4.11 is re-introduced.

Definition 4. (virtual agent)

The virtual agents v_i^c, $i = 1,2$, *is the pair* (v_1^c, v_2^c) *of controllable antipodal points located on the surface of an* n*-sphere.*

Denoting $x_i^c(t) = (q_i^c(t), \dot{q}_i^c(t)) \in X_i^c = \mathbb{R}^{2n}$ the states of the ith virtual agent, $i = 1,2$, then the n-sphere bounded by the pair (v_1^c, v_2^c) is given by:

$$\mathbf{S}^n = \left\{ q \in \mathbb{R}^n : \langle q - d, q - d \rangle \leq \tfrac{1}{2} \left\langle q_2^c - q_1^c, q_2^c - q_1^c \right\rangle \right\} \tag{6.6}$$

where Equation (6.6) is a bounding on the shape spanned by the group of vehicles $i = 1, \ldots, N$ in the local frame $\{M\}$. Therefore, the positions of the virtual agents represent the shape variable $s \in S$ used to control the group of vehicles; i.e.:

$$s = (q_i^c, \ldots, q_i^c) \in R^{nN_c}, \quad i = 1, \ldots, N_c, \quad N_c < N \tag{6.7}$$

Following Definition 4., the rotational part $R \in SO(2)$ for $n = 2$ is given by:

$$\sum_{i=1}^{N_c} \mathrm{x}_i^c \mathrm{y}_i^c = 0, \quad N_c = 1,2 \tag{6.8}$$

where $q_i^c = (\mathrm{x}_i^c, \mathrm{y}_i^c) \in \mathbb{R}^2$. Similarly, the rotational part for $n = 3$, $R \in SO(3)$ is given by the following equation:

$$\sum_{i=1}^{N_c} \mathrm{x}_\mathrm{i}^\mathrm{c} \mathrm{y}_\mathrm{i}^\mathrm{c} = \sum_{i=1}^{N_c} \mathrm{x}_\mathrm{i}^\mathrm{c} \mathrm{z}_\mathrm{i}^\mathrm{c} = \sum_{i=1}^{N_c} \mathrm{y}_\mathrm{i}^\mathrm{c} \mathrm{z}_\mathrm{i}^\mathrm{c} = 0, \quad N_c = 1,2 \tag{6.9}$$

where $q_i^c = (\mathrm{x}_i^c, \mathrm{y}_i^c, \mathrm{z}_i^c) \in \mathbb{R}^3$.

The rotation R defined by Equation (6.8) or Equation (6.9) can be seen as the rotation diagonalising the inertia tensor of the system of virtual agents with respect to the centre and orientation in the frame $\{F\}$ [210]. The dimension of the abstract space $SE(n) \times \mathbb{R}^{nN_c}$, is therefore $2n + nN_c$ (assuming $N_c < N$) independent of the number of vehicles in the flock. Equation (6.4) and Equation (6.7) define the abstract state $\alpha = (g, s)$ of the group that can be controlled by the supervisory agent. It is assumed that this information is calculated offline and transmitted to the vehicles prior to deployment. Figure 6-1 shows the implementation architecture for navigating the group of vehicles using the abstract state α. In the proceeding section, calculation of the group abstract state α is presented for coverage control.

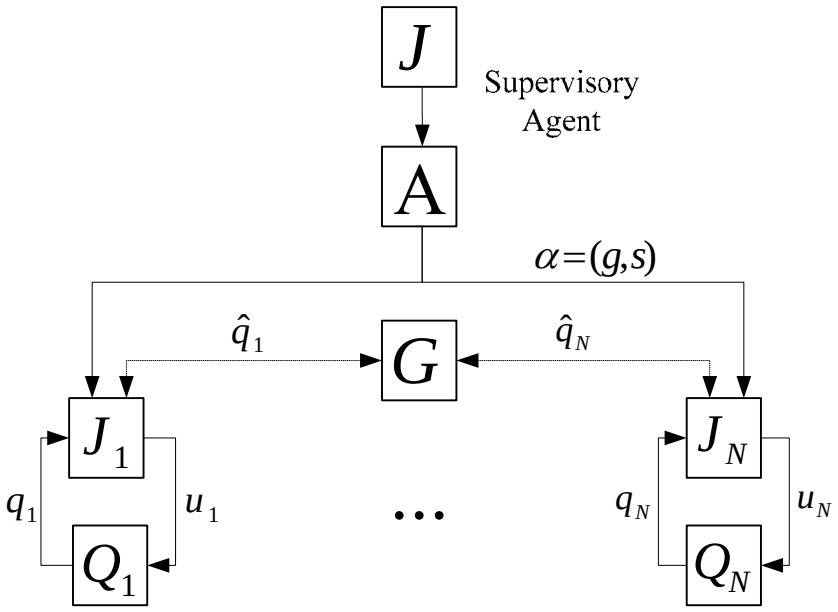

Figure 6-1. Implementation of the cooperative decentralised model predictive control scheme for a group of vehicles.

6.2. MOTION GENERATION AND SHAPE EVOLUTION

The problem of interest is to reduce the uncertainty of the environment by navigating a flock of vehicles through the environment. The trajectory used here is inspired by the parallel sweep trajectory presented in [345] (see Figure 6-2).

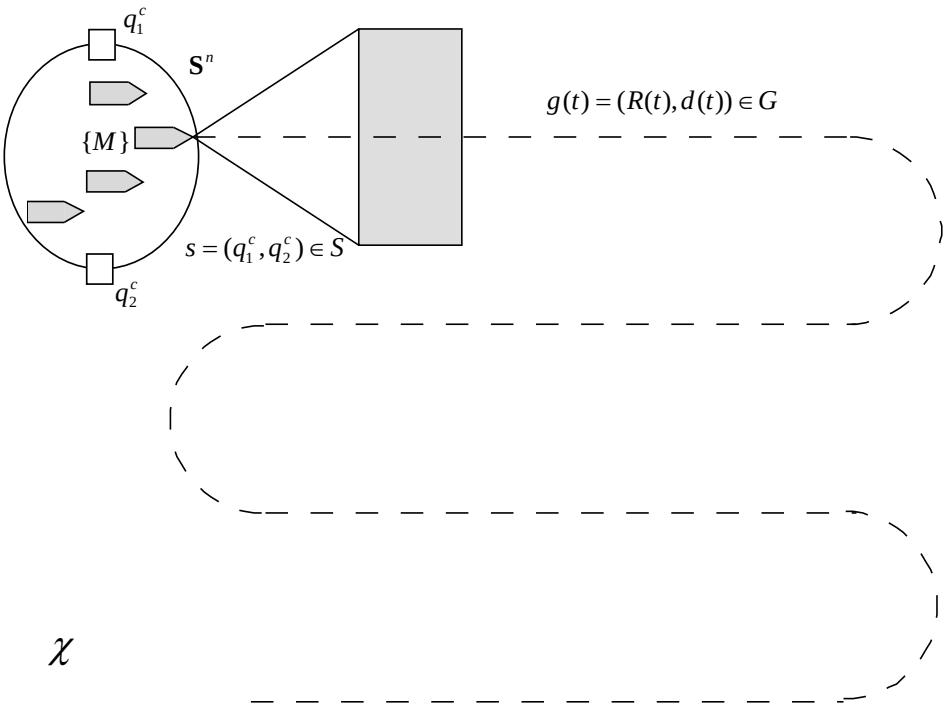

Figure 6-2. Sweep trajectory for coverage control.

From Figure 6-2, the sweep trajectory is piecewise continuous and consists of 7 trajectory primitives – 4 straight line and 3 semi-circular segments. Borrowing the notation of [346], a trajectory primitive is given by $\pi_i : [0, T_i] \mapsto (q_i(t), \dot{q}_i(t))$. Two trajectory primitives $\pi_1 : [0, T_1] \mapsto (q_1(t), \dot{q}_1(t))$, and $\pi_2 : [0, T_2] \mapsto (q_2(t), \dot{q}_2(t))$ are compatible $\pi_1 C \pi_2$ if there exists $g_{12} \in G$ such that $x_1(T_1) = \Psi(g_{12}, x_2(0))$, where C is a *compatibility relation* [346]. If $\pi_1 C \pi_2$, the concatenation π_1 and π_2 is defined as $\pi_1 \pi_2 : [0, T_1 + T_2] \to Q \times T_q Q$, with:

$$\pi_1 \pi_2 = \begin{cases} (q_1(t), \dot{q}_1(t)), & \text{if } t \le T_1 \\ (\Psi(g_{12}, q_2(t - T_2)), \dot{q}_2(t - T_1)), & \text{otherwise} \end{cases} \tag{6.10}$$

where $\Psi : G \times Q \to Q$ is left action of the group G on the state manifold Q. For convenience, only the first trajectory primitives shown in Figure 6-2 are considered for the motion generation problem (see Figure 6-3).

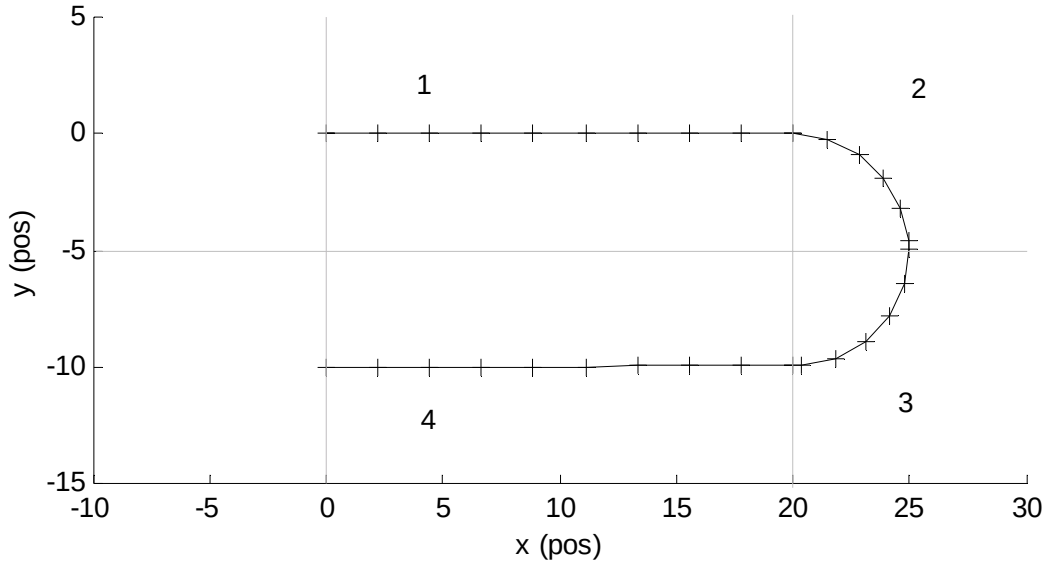

Figure 6-3. Trajectory segments of the parallel sweep trajectory.

Remark.

While the strategy described above reduces the uncertainty of the environment, constraining the motion of the vehicles to a flock configuration, inefficiently exploits the distributed nature of the mobile sensors. Vehicles are constrained to maintain a fixed inter-vehicle distance, and motion of each vehicle is dictated by the consensus of the flock. By allocating the vehicles to a region of the search space and relaxing the constraints induced by the flock lattice, the efficiency of the search can be drastically improved. The problem of optimally distributing mobile sensors in the environment, is known as the coverage control problem, and has been

investigated extensively in the literature [67, 90, 95, 98, 347-349]. Various search strategies have been proposed in the literature that have demonstrated exceptional performance with respect to a performance criterion, such as minimum energy, minimum completion, minimum uncertainty etc. In this chapter, the optimality of search strategy is of trivial concern. Rather, the purpose of this chapter is to demonstrate cooperative control strategies for a group of vehicles.

6.3. TASK DECOMPOSITION OF THE COOPERATIVE CONTROL PROBLEM

The cooperative objective for the group of vehicles is represented using the cost function in Equation (5.5):

$$l(x,u) = \sum_{i=1}^{N} l_i(x_i, u_i, \tilde{x}_i, \tilde{u}_i) \tag{6.11}$$

where $\tilde{x}_i = \{x_j \in \mathbb{R}^{n_j} \mid (j,i) \in E\}$, $\tilde{x}_i \in \mathbb{R}^{\tilde{n}_i}$, $\tilde{u}_i \in \mathbb{R}^{\tilde{m}_i}$ are the set of state and control inputs for neighbours v_j, $\forall j \in \mathcal{N}_i$, and $l_i : \mathbb{R}^{n_i} \times \mathbb{R}^{m_i} \times \mathbb{R}^{\tilde{n}_i} \times \mathbb{R}^{\tilde{m}_i} \to \mathbb{R}$ is a positive convex function describing the objectives of vehicle v_i, such that $l_i(x_i^e, u_i^e, \tilde{x}_i^e, \tilde{u}_i^e) = 0$ is an equilibrium.

The individual objective functions $l_i(x_i, u_i, \tilde{x}_i, \tilde{u}_i)$ are constructed using the decomposition of tasks. Each vehicle in the group is subject to a local vehicle objective, and a group cooperative objective. At the local vehicle level, the objective of each vehicle is to stabilise to a position in the local frame corresponding to the flock lattice. Stabilisation of the flock lattice in the local frame is achieved by minimising the structural energy and velocity mismatch in Section 3.2.4. Following the derivation in 3.2.4, the energy of a vehicle with neighbourhood $\mathcal{N}_i$ is given by:

$$\mathcal{E}_i(x_i, \tilde{x}_i) = \sum_{j \in \mathcal{N}_i} \phi_\rho(\Phi(q_j - q_i)) \cdot \mathbf{n}_{ij} + \sum_{j \in \mathcal{N}_i} (\dot{q}_j - \dot{q}_i) \tag{6.12}$$

where $\mathbf{n}_{ij}$ is the unit vector along the edge connecting vehicle v_i to vehicle v_j.

Equation (6.12) defines a cost function for local vehicle flocking:

$$l_i^f(x_i, \tilde{x}_i) := \mathcal{E}_i(x_i, \tilde{x}_i) = \sum_{j \in \mathcal{N}_i} \phi_\rho(\Phi(q_j - q_i)) \cdot \mathbf{n}_{ij} + \sum_{j \in \mathcal{N}_i} (\dot{q}_j - \dot{q}_i) \tag{6.13}$$

The convergence of a group of vehicles to the flock lattice describes a semi-rigid body model (see Section 4.11). The semi-rigid body model provides a means of coupling the vehicles and defining a group level behaviour using the abstract state $\alpha = (g, s)$ described in the previous section. The objective of the group, using the abstract state $\alpha = (g, s)$, is to navigate the flock

of vehicles through the environment from an arbitrary initial position and orientation $g(0) = (R(0), d(0))$ with shape $s(0)$, to a final desired position and orientation $g(1) = (R(1), d(1))$ with shape $s(1)$. This corresponds to the set of motion primitives in Section 6.2 describing the parallel sweep trajectory.

By choosing the motion of the centre of the virtual agents in Equation (6.5) as the reference trajectory for the flock of vehicles to navigate, the group task is reduced to tracking at the individual vehicle level. The tracking cost function for the ith vehicle is then defined as follows:

$$l_i^t(x_i, g) := \phi(q_i^c - d) \tag{6.14}$$

Equation (6.14) specifies the group cooperative objective, and the navigational feedback in Equation (3.51) that mitigates flock dissociation.

The last part of the cooperative objective is to stabilise the flock to the virtual structure defined by the virtual agents in Equation (4.122). Since the virtual structure constrains the position of vehicles in the flock to remain inside the n-sphere defined by (q_1^c, q_2^c), the group's compliance to the virtual structure is given by a constraint on the cooperative objective; i.e.:

$$\|q_i - \bar{q}\| \leq \|q_2^c - q_1^c\| \tag{6.15}$$

Since the positions of the virtual agents are time-varying, then the constraints in Equation (6.15) are also time-varying, and the shape of the flock is permitted to transform. In the next section, the optimal control problem for the group of vehicles is formulated for the centralised and decentralised implementation strategies.

6.4. THE COOPERATIVE CONTROL PROBLEM

Combining Equation (6.13) and Equation (6.14), the following objective function is defined for the ith vehicle:

$$l_i(x_i, u_i, \tilde{x}_i, \tilde{u}_i) := c_1 \cdot \sum_{j \in \mathcal{N}_i} \phi_\rho(\Phi(q_j - q_i)) \cdot \mathbf{n}_{ij} + c_2 \cdot \sum_{j \in \mathcal{N}_i} (\dot{q}_j - \dot{q}_i) + c_3 \cdot \phi(q_i^c - d) \tag{6.16}$$

where the terms $c_1, c_2, c_3 \geq 0$ have been introduced to weight the relative importance of each behaviour. The centralised cooperative objective for the collective group is then recovered by summing Equation (6.16) along $i = 1, \ldots, N$:

$$l(x, u) = \sum_{i=1}^{N} l_i(x_i, u_i, \tilde{x}_i, \tilde{u}_i) \tag{6.17}$$

Following the notation introduced in Chapter 5 for the cooperative decentralised model predictive control strategy, the cooperative control problem for the ith vehicle in the flock is given by:

$$J^*_{i,T}(x_i(t_k), \widehat{x}_i(t_k)) := \min_{\{\hat{u}_i(t_k)\}} \int_{t_k}^{t_{k+T}} l_i\big(\hat{x}_i(\tau^*_k \mid t_k), \hat{u}_i(\tau^*_k \mid t_k), \widehat{x}_i(\tau^*_k \mid t_k)\big) d\tau_k$$

Subject to:

$$\begin{gathered}
\dot{x}_i(\tau^*_k \mid t_k) = A_i x_i(\tau^*_k \mid t_k) + B_i u_i(\tau^*_k \mid t_k) \\
i = 1, \ldots, N, \quad \tau^*_k \in [t_k, t_{k-1+T}] \\
x_i(\tau^*_k \mid t_k) \in X_i, \quad u_i(\tau^*_k \mid t_k) \in U_i \\
(i, j) \in \mathcal{N}_i \\
\left\| \widehat{x}_{i_j}(\tau^*_k \mid t_{-1}) - \hat{x}_j(\tau^*_k \mid t_k) \right\| \le \kappa, \quad \forall j \in \mathcal{N}_i \\
\left\| \hat{x}_i(\tau^*_k \mid t_k) - d(\tau^*_k \mid t_k) \right\| \le \left\| q^c_2(\tau_k \mid t_k) - q^c_1(\tau_k \mid t_k) \right\| \\
x_i(t_k \mid t_k) = x_i(t_k) \\
x_i(t_{k+T} \mid t_k) \in X_f
\end{gathered} \tag{6.18}$$

At each sampling period t_k, vehicle v_i solves Problem (6.18) using the group information $\alpha(\tau^*_k \mid t_k) = (g(\tau^*_k \mid t_k), s(\tau^*_k \mid t_k))$ from the supervisory controller, the predicted states of its neighbours $\widehat{x}_i(t_k)$ over the proceeding horizon $\tau_k \in [t_k, t_{k+T}]$, its current state $x_i(t_k)$, and the set of predicted states transmitted to its neighbours at the previous sampling period (assumed states $\widehat{x}_{i\_j}(t_k)$). For the following, the neighbours v_j of a vehicle v_i are given by the ball bounded by the sensory and communication range r_i:

$$\mathcal{N}_i = \{v_j \subseteq N : \left\| q_j - q_i \right\| \le r_i\} \tag{6.19}$$

The neighbourhood in Equation (6.19) defines the information exchange topology for vehicle v_i with configuration graph $G_i(\mathcal{N}_i, E_i)$, and connectivity $E_i := \{e = (v_i, v_j) : v_j \in \mathcal{N}_i\}$. Given the cooperative control problem described above, the decentralised implementation scheme for the ith vehicle is given by Definition 4 in Chapter 5. In the following section, a simulation of the N-vehicle cooperative problem is presented.

6.5. NUMERICAL EXAMPLE

For the following simulation, a flock size of $N = 6$ is used for the cooperative coverage control problem. The dimension of the position vector for each vehicle is $n = 2$ and the group configuration is initialised along the line given by:

$$q_1(0)=\begin{bmatrix}3\\0\end{bmatrix},\quad q_2(0)=\begin{bmatrix}2\\0\end{bmatrix},\quad q_3(0)=\begin{bmatrix}1\\0\end{bmatrix},\quad q_4(0)=\begin{bmatrix}-1\\0\end{bmatrix},\quad q_5(0)=\begin{bmatrix}-2\\0\end{bmatrix},\quad q_6(0)=\begin{bmatrix}-3\\0\end{bmatrix} \tag{6.20}$$

Each vehicle is subject to the following control input constraints:

$$U_i=\{(u_1,u_2)\in\mathbb{R}^2 : -1\le u_j\le 1,\ j=1,2\} \tag{6.21}$$

and neighbourhood region:

$$\mathcal{N}_i=\{v_j\subseteq N : \|q_j-q_i\|\le 1.2 \tag{6.22}$$

The group objective is to track the parallel sweep trajectory shown in Figure 6-3 $(d,\dot{d})\in\mathbb{R}^4$. The parallel sweep trajectory is decomposed into 4 trajectory primitives as shown in Figure 6-3. The reference trajectory parameterised by time t for the centroid of the flock $(d,\dot{d})\in\mathbb{R}^4$ is given by

$$d(t)=\begin{cases}(t,\quad 0), & t\in[0,20]\\ (\frac{1}{2}t+20,\quad -\frac{1}{2}t+10) & t\in[20,30]\\ (-\frac{1}{2}t+40,\quad -\frac{1}{2}t+10), & t\in[30,40]\\ (-t+60,\quad -10), & t\in[40,\infty)\end{cases} \tag{6.23}$$

Note, the motion primitives described by Equation (6.23) correspond to the minimum-energy geodesics described in Section (4.71). Using the geodesics in Equation (6.23), the desired shape abstractions for the group are constructed.

Given the initial distribution of vehicles in Equation (6.20), the initial shape is bounded by the disk:

$$\mathbf{S}^2(0)=\{q\in\mathbb{R}^2 : \|q-\overline{q}\|\le\max\{\|\overline{q}-q_i\|\}\} \tag{6.24}$$

In this case, the radius of the initial disk $\mathbf{S}^2(0)$, is $R_0=1.5$. From Equation (3.48), the group of vehicles applying Protocol (3.34), converges to the region bounded by $R=\sqrt{2\mathcal{H}(q(0),\tilde{p}(0))}$. This provides the final shape of the flock lattice. The shape control problem for the group involves solving the two-point boundary value problem of two antipodal points on the initial disk to the final disk:

$$\mathbf{S}^2(1)=\{q\in\mathbb{R}^2 : \|q-\overline{q}\|\le\sqrt{2\mathcal{H}(q(0),\dot{q}(0))}\} \tag{6.25}$$

Let $q^c\in\mathbb{R}^4$, $\dot{q}^c\in\mathbb{R}^4$ denote the concatenated states of the virtual agents. The boundary conditions for the virtual agents for each trajectory segment are given by:

$$q^c(0)=\begin{bmatrix}0\\1.5\\0\\-1.5\end{bmatrix},\quad q^c(20)=\begin{bmatrix}20\\R\\20\\-R\end{bmatrix},\quad q^c(30)=\begin{bmatrix}25-R\\-5\\25+R\\-5\end{bmatrix},$$
$$q^c(40)=\begin{bmatrix}20\\-10+R\\20\\-10-R\end{bmatrix},\quad q^c(60)=\begin{bmatrix}0\\-10+R\\0\\-10-R\end{bmatrix} \tag{6.26}$$

where R is the shape spanned by the flock lattice described in Table 6-1 and solved using Equation (3.23), Equation (3.24), and Equation (6.25).

Table 6-1. Flock parameters for shape evolution.

d_{ij}	10
$r_i = r_j = r$	12
δ	$0.5r$

The interpolating motions for the virtual agents that yield the shape state $s(t) \in S$, is obtained by solving the set of geodesic equations in Equation (4.46). To solve the geodesic equations in Equation (4.46), the set of Christoffel symbols for each trajectory primitive must be calculated. Assume that the set of virtual agents are identical with masses $m_1 = m_2 = m$, and that the body-fixed frame of each agent is aligned with the principal axis. The following metric is considered for the minimum energy case:

$$M = \frac{1}{2}\begin{bmatrix}m_1 I_2 & 0\\0 & m_2 I_2\end{bmatrix} \tag{6.27}$$

The projection basis from Equation (4.114) and Equation (4.116) using the virtual agents' coordinates is given by:

$$C(q^c)=\begin{bmatrix}-\mathrm{y}_1^c & 1 & 0\\ \mathrm{x}_1^c & 0 & 1\\ -\mathrm{y}_2^c & 1 & 0\\ \mathrm{x}_2^c & 0 & 1\end{bmatrix},\quad D(q^c)=\begin{bmatrix}\frac{\left(\mathrm{x}_2^c-\mathrm{x}_1^c\right)}{\left(\mathrm{y}_1^c-\mathrm{y}_2^c\right)}\\ -1\\ \frac{\left(\mathrm{x}_1^c-\mathrm{x}_2^c\right)}{\left(\mathrm{y}_1^c-\mathrm{y}_2^c\right)}\\ 1\end{bmatrix} \tag{6.28}$$

Expanding Equation (6.27) along the rigid and semi-rigid projections yields:

$$\begin{aligned}M_{\sigma_r}(q^c) = \sigma_r \cdot M \cdot C(q^c)\cdot(C(q^c)^T \cdot M \cdot C(q^c))^T \cdot C(q^c)^T \cdot M + \ldots\\ \ldots + (1-\sigma_r)\cdot M \cdot D(q^c)(D(q^c)^T \cdot M \cdot D(q^c))^{-T} \cdot D(q^c)^T \cdot M\end{aligned} \tag{6.29}$$

To solve the boundary value problem for the shape state, define the following shape control variables for each segment of the trajectory as shown in Figure 6-4:

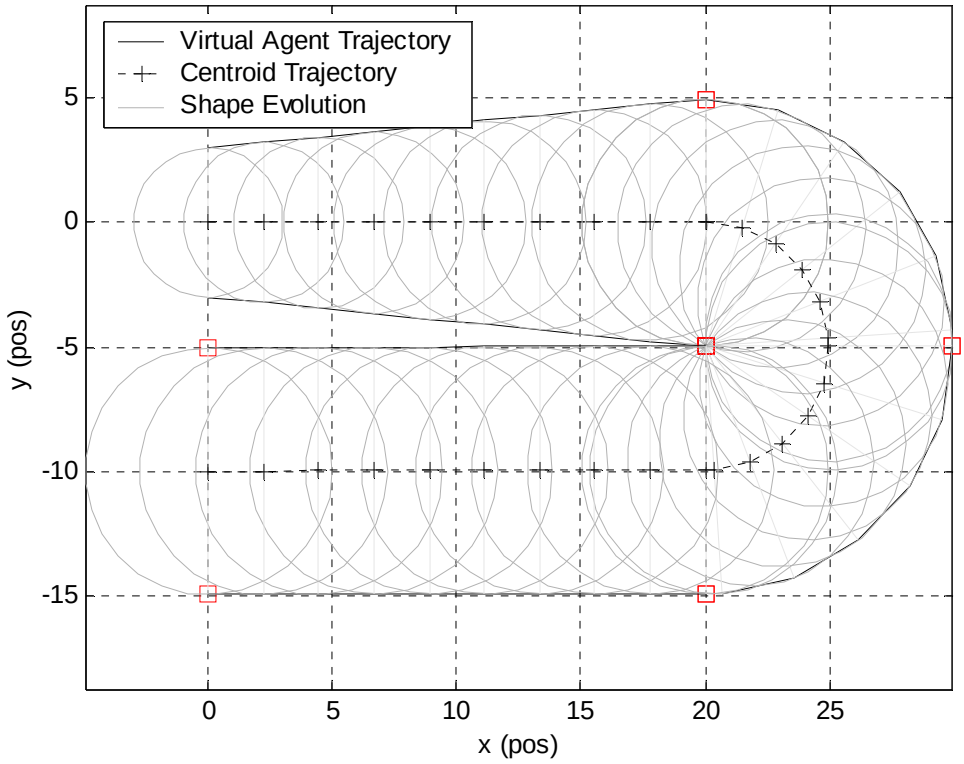

Figure 6-4. Desired shape evolution for the group of vehicles.

$$\sigma_r(t) = \begin{cases} 0.5 & t \in [0,20] \\ 0.99 & t \in [20,30] \\ 0.99 & t \in [30,40] \\ 0.99 & t \in [40,\infty) \end{cases} \tag{6.30}$$

From Equation (4.34), Equation (6.28), and Equation (6.29) the 64 Christoffel symbols for the motion of the two virtual agents are obtained (see Appendix B). Using Equation (4.46) and the Christoffel Symbols in Appendix A, the interpolating motions for the shape state for each motion primitive are calculated using a finite-difference method with 100 grid points [330] in MATLAB. Figure 6-4 shows the corresponding desired motions of the shape evolution for the collective flock. The paths traced out by the virtual agents provide the constraints on the cooperative decentralised model predictive problem in Equation (6.18).

For comparison, the centralised model predictive control scheme described in Section 5.1 is applied to the group of vehicles. In this scheme, a centralised feedback control architecture is used to solve the motion planning and shape evolution problem described in Equation (6.16). Following the implementation scheme in Section 5.1.2 and Section 5.1.3, the centralised finite horizon control problem for the group of vehicles with cost objective in Equation (6.16) is given by:

$$J_T^*(x(t_k)) := \min_{\{\hat{u}(t_k)\}} \int_{t_k}^{t_{k+T}} l\big(x(\tau_k \mid t_k), u(\tau_k \mid t_k)\big) d\tau_k + l^T\big(x(t_{k+T} \mid t_k)\big)$$

Subject to:

$$\begin{gathered}
\dot{x}_i(\tau_k \mid t_k) = f_i(x_i(\tau_k \mid t_k), u_i(\tau_k \mid t_k)) \\
i = 1, \ldots, N, \quad \tau_k \in [t_k, t_k + T] \\
x_i(\tau_k \mid t_k) \in X_i, \quad u_i(\tau_k \mid t_k) \in U_i \\
\tau_k \in [t_k, t_k + T] \\
g_{i,j}(x_i(\tau_k \mid t_k), x_j(\tau_k \mid t_k)) \le 0, \quad \forall j \in \mathcal{N}_i \\
x(t_k \mid t_k) = x(t_k) \\
x(t_{k+T} \mid t_k) \in X_f
\end{gathered} \tag{6.31}$$

where $l\big(x(\tau_k \mid t_k), u(\tau_k \mid t_k)\big)$ is the recovered cooperative objective in Equation (6.17) and $g_{i,j}(x_i(\tau_k \mid t_k), x_j(\tau_k \mid t_k)) \le 0$ are the nonlinear constraints associated with the shape spanned by the flock:

$$\left\| q_i - \bar{q} \right\| \le \left\| q_2^c - q_1^c \right\|, \quad \forall i = 1, \ldots, N \tag{6.32}$$

Given the abstract state $\alpha(t) = (g(t), s(t))$, the centralised and decentralised implementation schemes described in Chapter 5 are applied to the group of vehicles. For both cases, the following weighting parameters for each task in Problem (6.16) are arbitrarily selected $c_1 = c_2 = c_3 = 1$. Unless specified, a prediction horizon length of $T = 3.6$ seconds and an update period of 0.6 seconds are also used in both the centralised and decentralised strategies. To solve the optimal control problem, a global search strategy based on Particle Swarm Optimisation (PSO) [19, 27, 350, 351] is used.

Snapshots of the flock's evolution applying the centralised control scheme are shown in Figure 6-5. The desired centroidal motion $d \in g$ is also depicted in Figure 6-5 by the dashed centreline. The centroid of the group $\bar{q}$ at each sampling period is also shown by the circular marker in Figure 6-5. Tracking is achieved when the desired centroidal motion and the centroid of the flock are coincident. The corresponding tracking error, the evolution of the structural potential, and the applied control inputs of the flock are shown in Figure 6-6, Figure 6-7, and Figure 6-8 respectively. From Figure 6-6 and Figure 6-7, stabilisation of the flock configuration and minimisation of the tracking objective in Equation (6.16) is satisfied after $t = 13$ seconds. At $t \approx 17$ seconds, the tracking error increases and reaches a peak at $t \approx 20$ seconds. Comparison of Figure 6-6 with the boundary conditions in Equation (6.23) suggest a discontinuity between the concatenation of the first and the second trajectory segments shown in Figure 6-3. In addition, examination of the control inputs shown in Figure 6-8, reveal that each vehicle begins to apply a control input 3.6 seconds before intersection

with the second trajectory segment. This corresponds to the prediction horizon length and demonstrates the efficacy of model predictive control in plan generation for optimal performance. A similar phenomenon is also observed at $t \approx 40$ seconds. Between $t = 20$ and $t = 40$ seconds, the tracking performance of the group fails to stabilise to the minimum. During this period, the vehicles negotiate the twist induced by the geodesics connecting the second and third trajectory segments. The gradient of the curve, and the short period of the twist forces the vehicles to correct their heading and adjust their control inputs during the turn. This is shown in Figure 6-8 by the nonzero control inputs between $t = 20$ and $t = 40$ seconds. The group's failure to stabilise to the minimum during this period suggests that the response of the system is inadequate for the specified turn. Increasing the frequency of the sampling period will improve the transient response of the system at the cost of greater computational demand.

Remark.

From Figure 6-7, the group reaches a minimum structural energy at $t = 3.6$ *seconds before stabilising to a higher energy level at* $t > 13$ *seconds. This suggests that the final configuration does not conform to the ideal flock lattice with* $d_{ij} = 10$. *Rather, the stabilised flock configuration represents a compromise between the desired tracking objective and the desired flock configuration. A possible approach to resolve the arbitration between the possibly conflicting objectives is to separate the tasks in Equation (6.16). Using this approach, the optimisation problem becomes multi-objective. Multi-objective optimisation is not treated in this thesis. However, it is anticipated that the proposed framework is sufficiently general to accommodate the multi-objective formulation.*

For the decentralised implementation, the effect of the compatibility constraint κ is investigated. Figure 6-9 shows the trajectory of the flock using the centralised implementation scheme and the decentralised implementation scheme for varying κ. The corresponding tracking performance and structural energy are shown in Figure 6-11 and Figure 6-12 respectively. For illustrative purposes, the corresponding control input of the fourth vehicle $v = 4$ is shown in Figure 6-10. In general, the decentralised implementation scheme facilitates cooperation and achieves the desired objectives, with comparable (albeit suboptimal) performance to the centralised case.

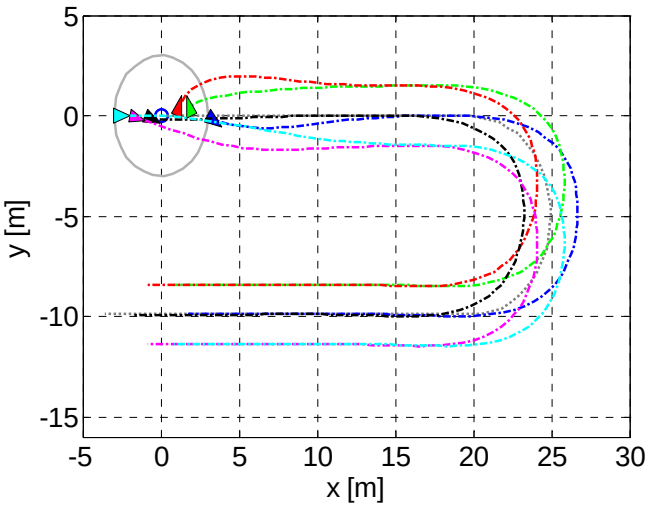

(a) t = 0.0s

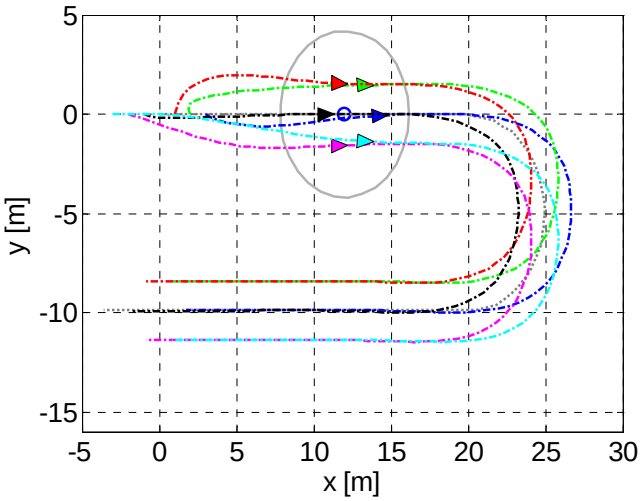

(b) t = 12.6s

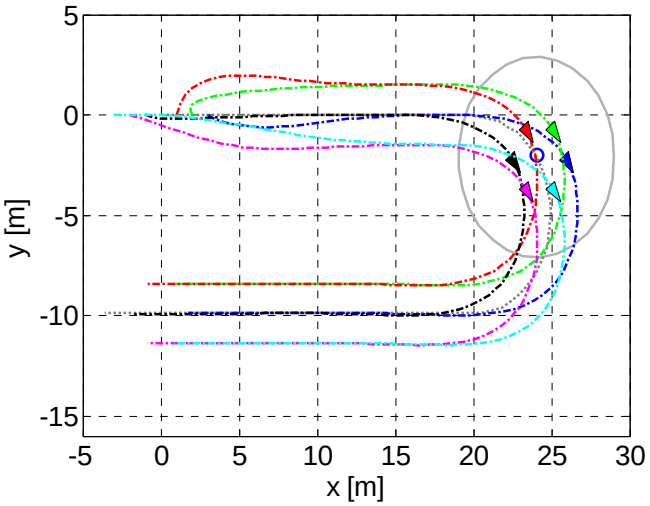

(c) t = 24.6s

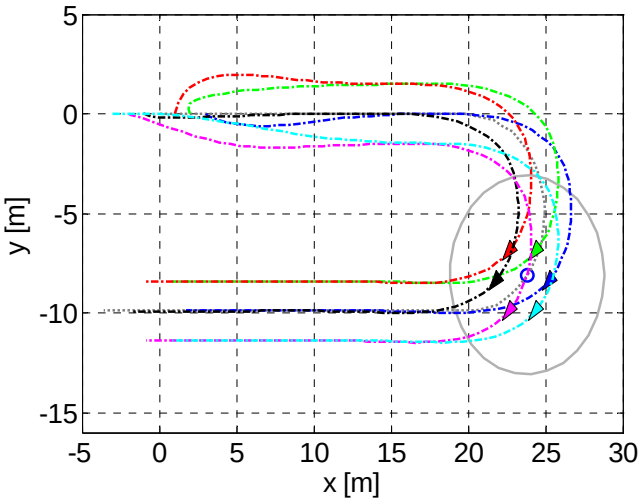

(d) t = 36.6s

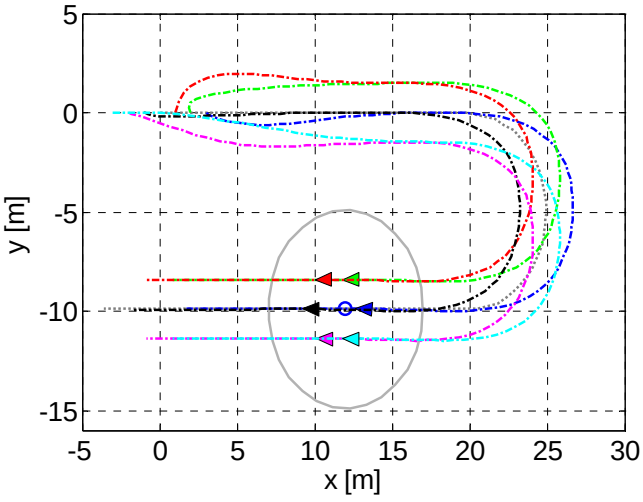

(e) t = 48.6s

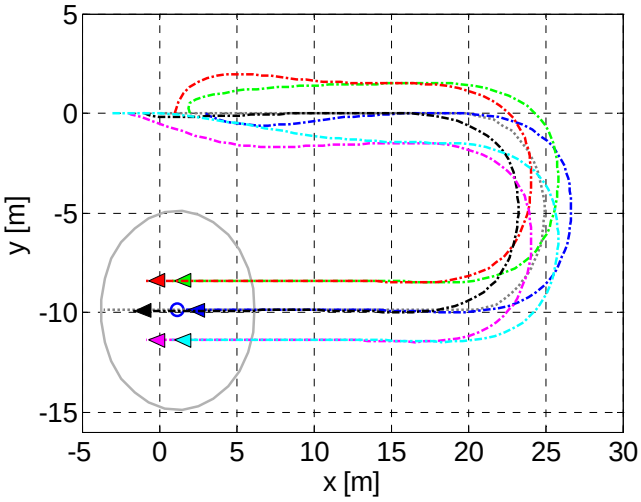

(f) t = 60.0s

Figure 6-5. Snapshots of the flock evolution using the centralised model predictive control scheme.

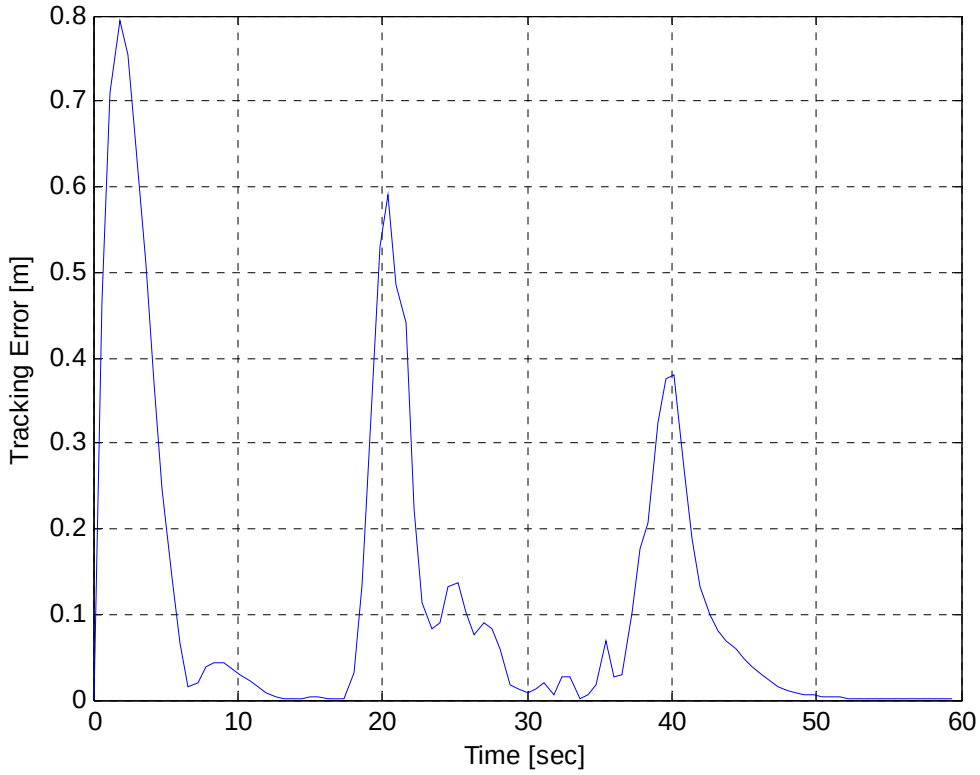

Figure 6-6. Tracking performance of the centralised implementation scheme.

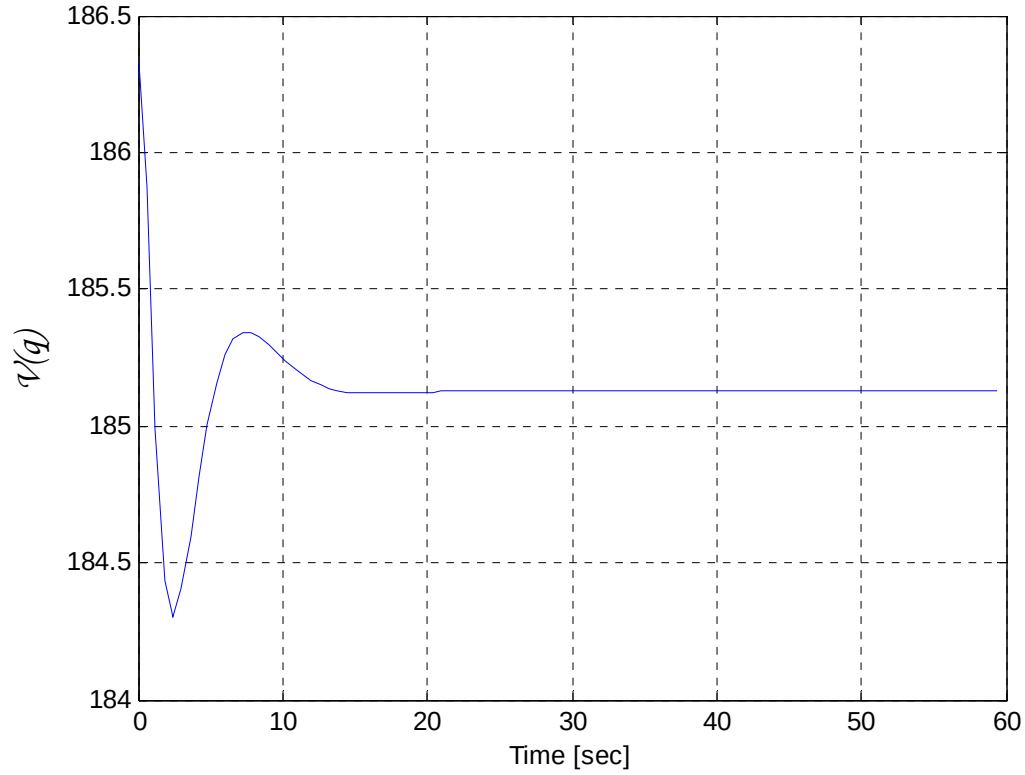

Figure 6-7. Convergence of the structural potential for the flock lattice.

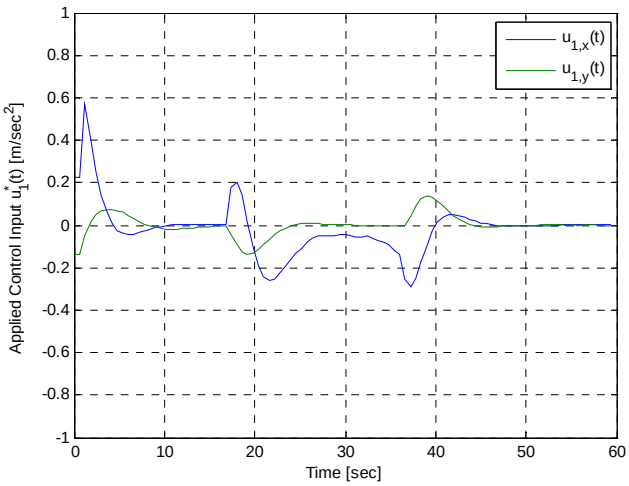

(a) v = 1

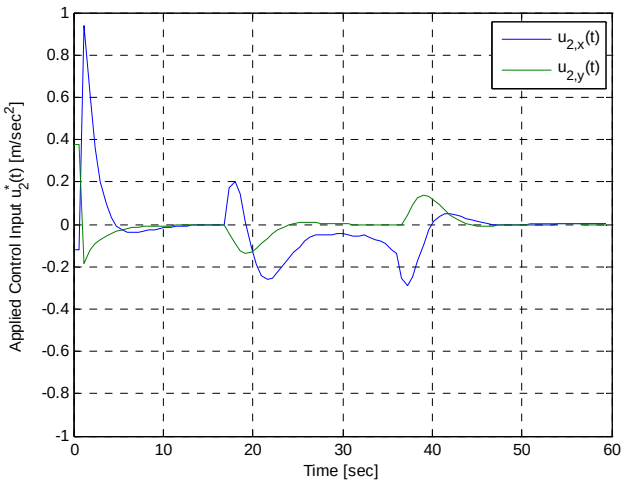

(b) v = 2

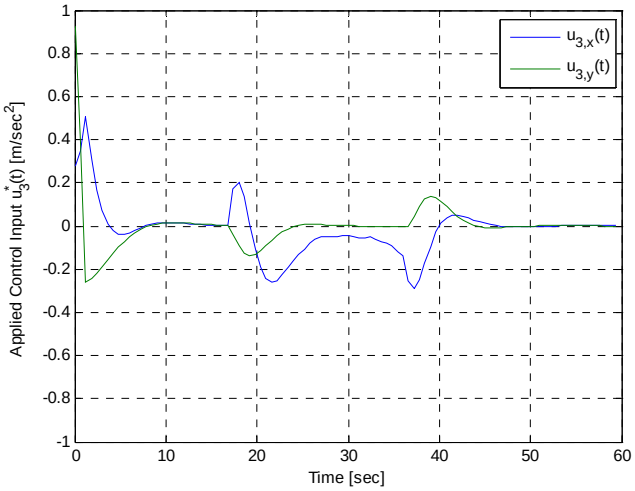

(c) v = 3

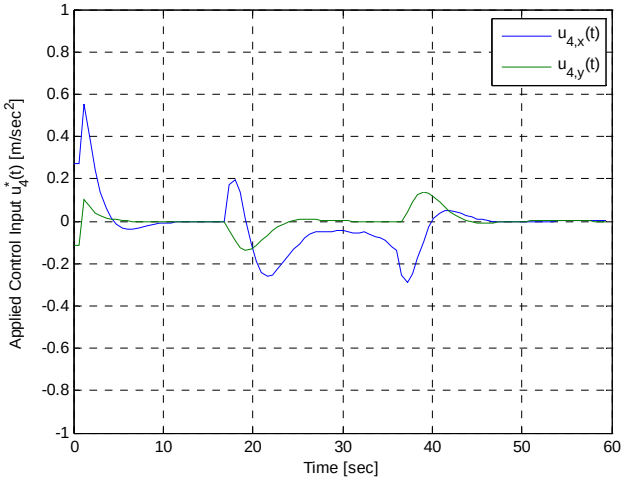

(d) v = 4

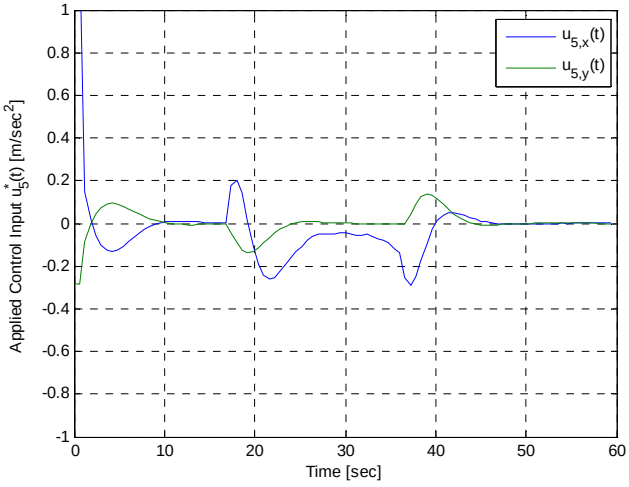

(e) v = 5

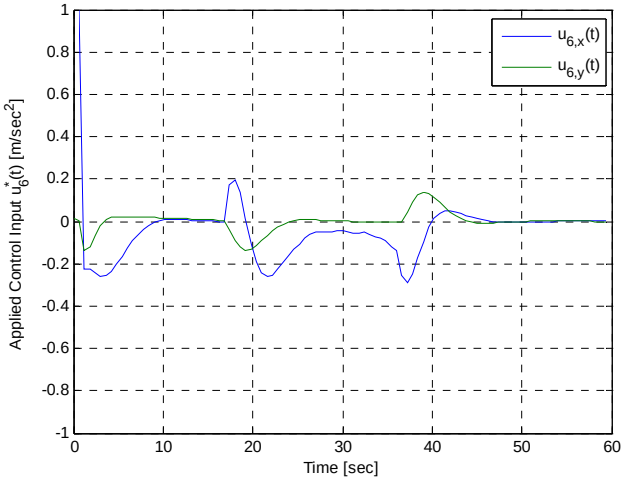

(f) v = 5

Figure 6-8. Demonstration of the applied control input for each vehicle using the centralised scheme.

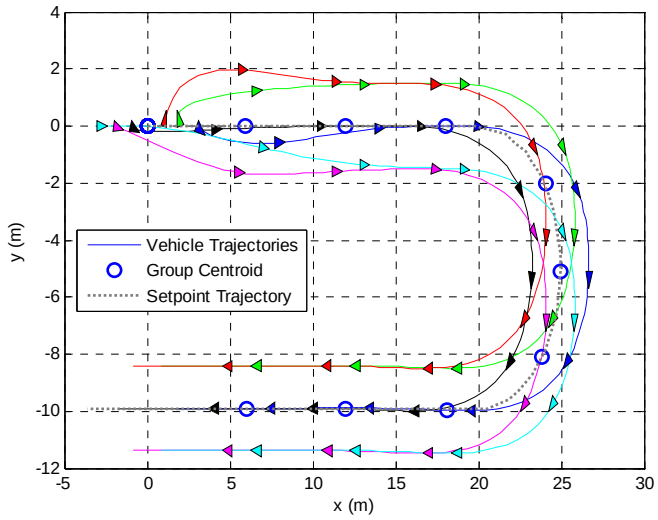

(a)

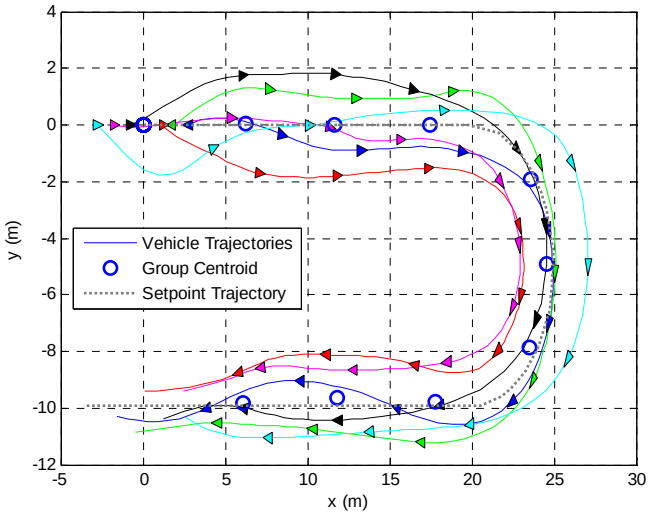

(b)

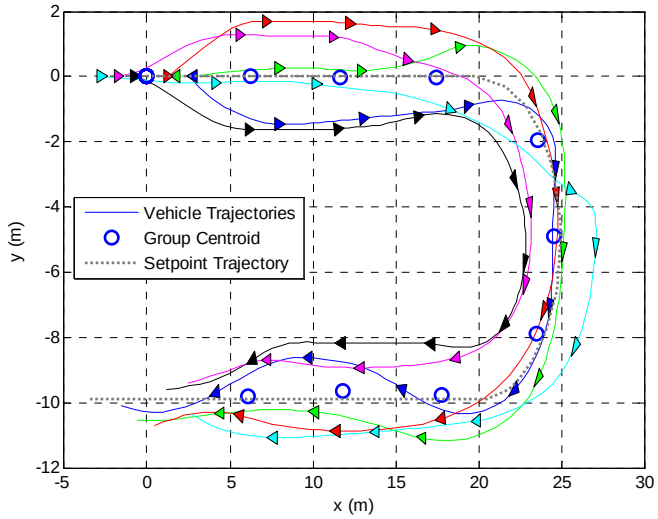

(c)

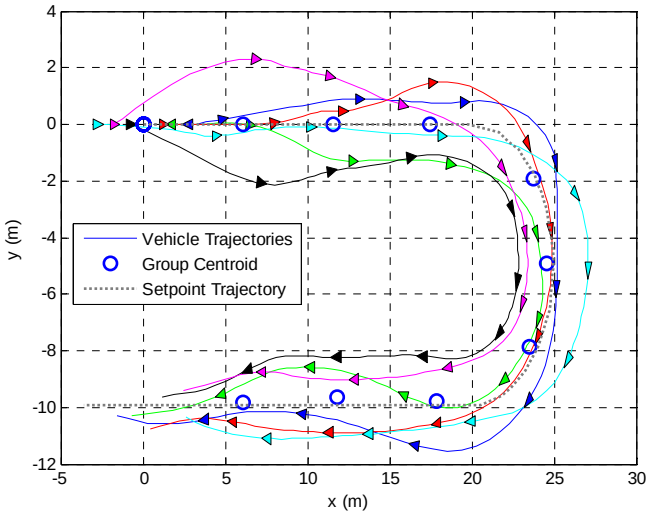

(d)

Figure 6-9. Flock evolution using the (a) centralised implementation scheme, and the decentralised implementation scheme with (b) $\kappa = \infty$, (c) $\kappa = 0.6$, and (d) $\kappa = 0.1$.

From Figure 6-11, relaxing the compatibility constraint ($\kappa \to +\infty$) induces a fast transient response with a sluggish settling time. This is in concert with the theoretical investigations posed in Section 5.5. The anticipated overshoot potentially induced by the mismatch between the assumed and applied states of neighbouring vehicles however; appear to be a conservative estimate on the convergence of the information consensus. In fact, the very same reason used to argue the propagation of information mismatch in neighbouring vehicles, i.e. the ability to generate new plans, is the same reason that allows the vehicles to gracefully reach a consensus with minimal chattering. This is due to the structure of the objective function. From Equation (6.18), the optimisation problem involves the plans of neighbours at each sampling period over the prediction horizon. Since vehicles must plan for future sampling periods using the previous plans of neighbouring vehicles (and only apply the first step of the predicted plans), the anticipated mismatch between the shared plans gradually tends to zero. This results in the appreciable convergence towards the equilibrium.

In contrast, constricting the compatibility constraint ($\kappa \to 0$), the settling time and the overshoot of the tracking error is further reduced. This is also illustrated by the stabilisation of the structural energy in Figure 6-12. However, strict compatibility constraints reduce the efficacy of the model predictive control scheme at developing successive plans significantly divergent from previous plans. This limits the vehicles' robustness to tolerate changes in the operating conditions. This is shown in Figure 6-11 by the large tracking errors at $t = 20$ and $t = 40$ seconds corresponding to the interface of adjoining trajectory segments.

One way to minimise these errors is to increase the prediction horizon and accommodate the sluggish response induced by the strict compatibility constraint. Increasing the prediction horizon however, incurs a larger computational penalty since the optimisation problem becomes large-scale. For illustrative purposes, the decentralised implementation scheme is demonstrated for $T = 3.6$ and $T = 6.0$ seconds using $\kappa = 0.06$. Figure 6-13 and Figure 6-14 shows the corresponding tracking error and evolution of the structural potential for the group of vehicles. For $T = 6.0$ seconds, the overshoot and settling time of the tracking error is significantly less than for $T = 3.6$ seconds. While this strategy can be employed to improve the transient behaviour of the vehicles, increasing the prediction horizon will inevitably lead to longer computational times and larger computational demands.

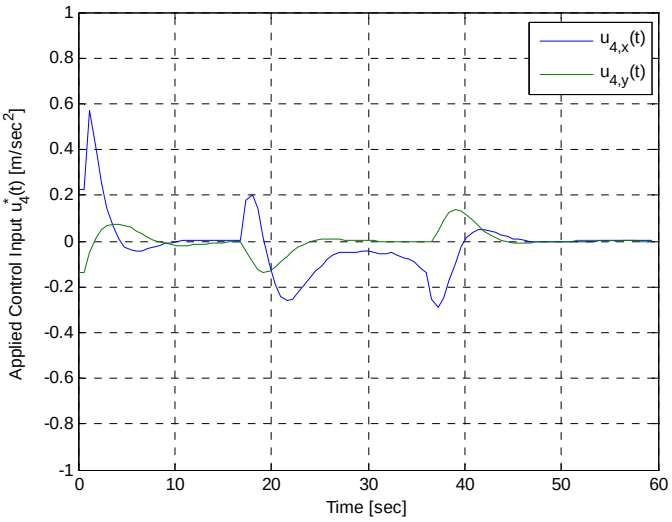

(a)

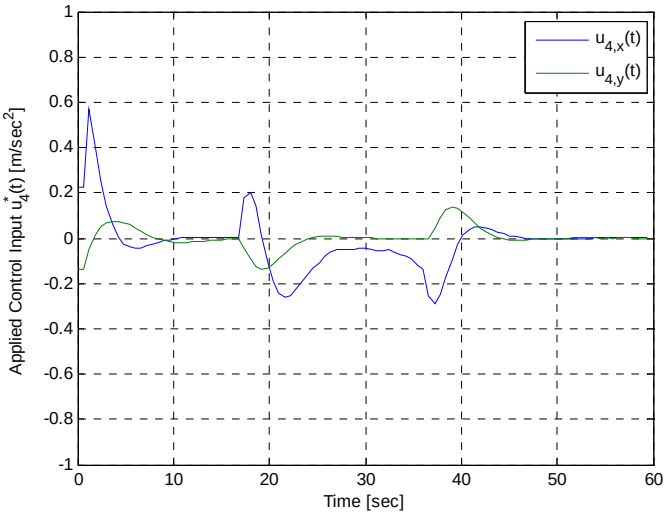

(b)

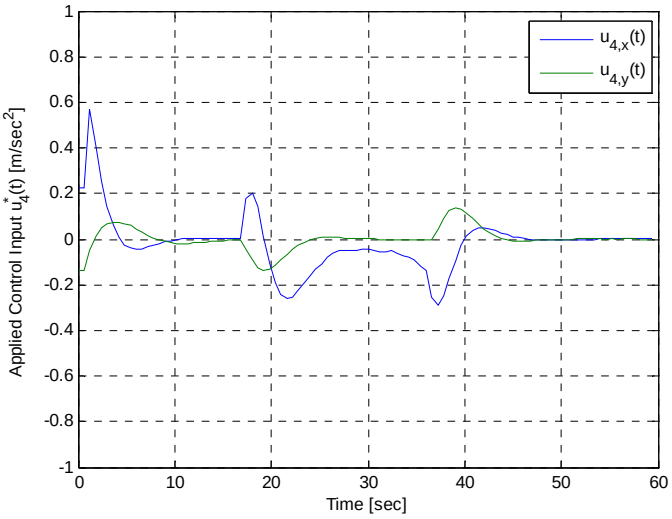

(c)

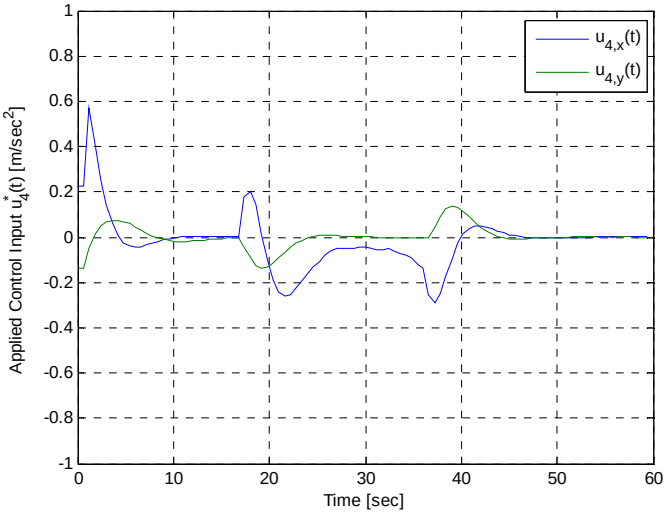

(d)

Figure 6-10. Comparison of the control input for vehicle v = 4 using the (a) centralised implementation scheme, and the decentralised implementation scheme with (b) $\kappa = \infty$, (c) $\kappa = 0.6$, and (d) $\kappa = 0.1$.

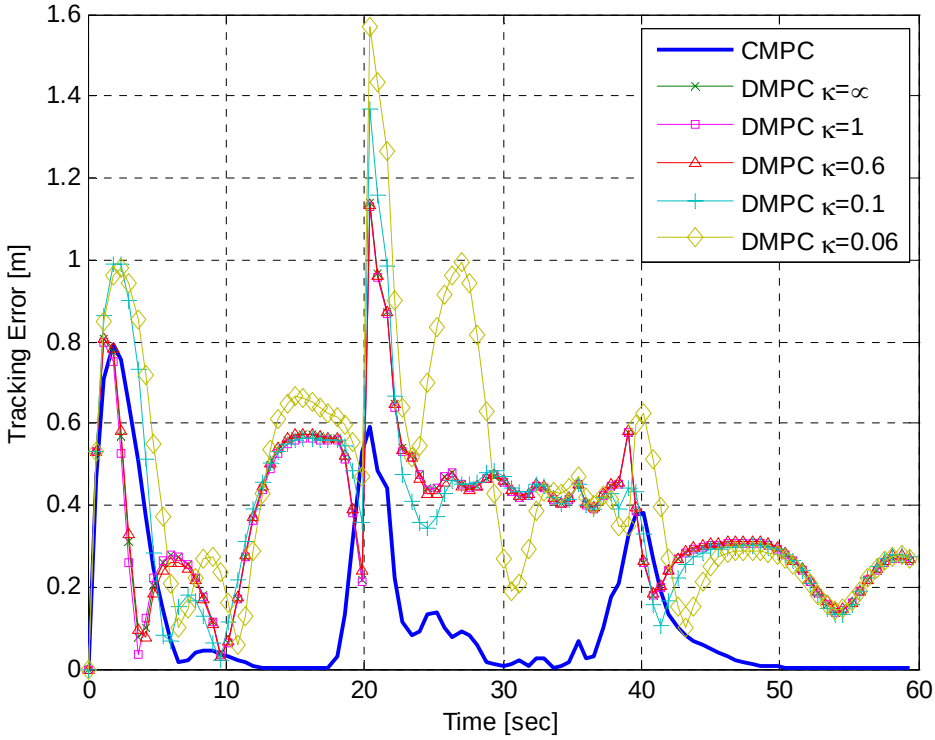

Figure 6-11. Comparison of the tracking performance for the centralised implementation scheme, and the decentralised implementation scheme for varying κ.

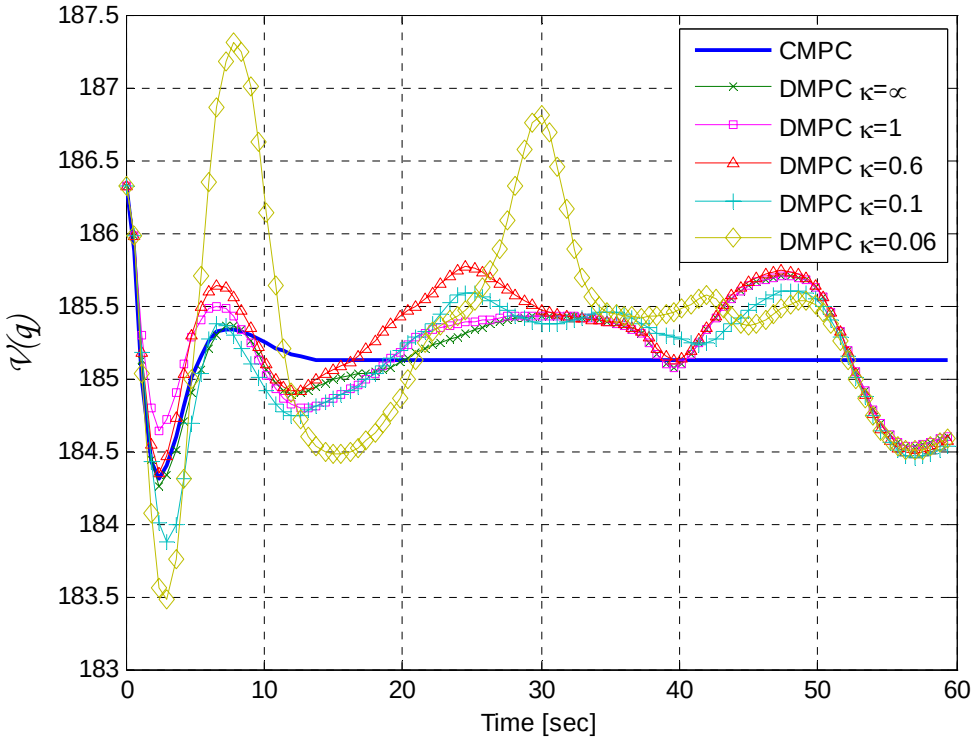

Figure 6-12. Comparison of the structural potential for the centralised implementation scheme, and the decentralised implementation scheme for varying κ.

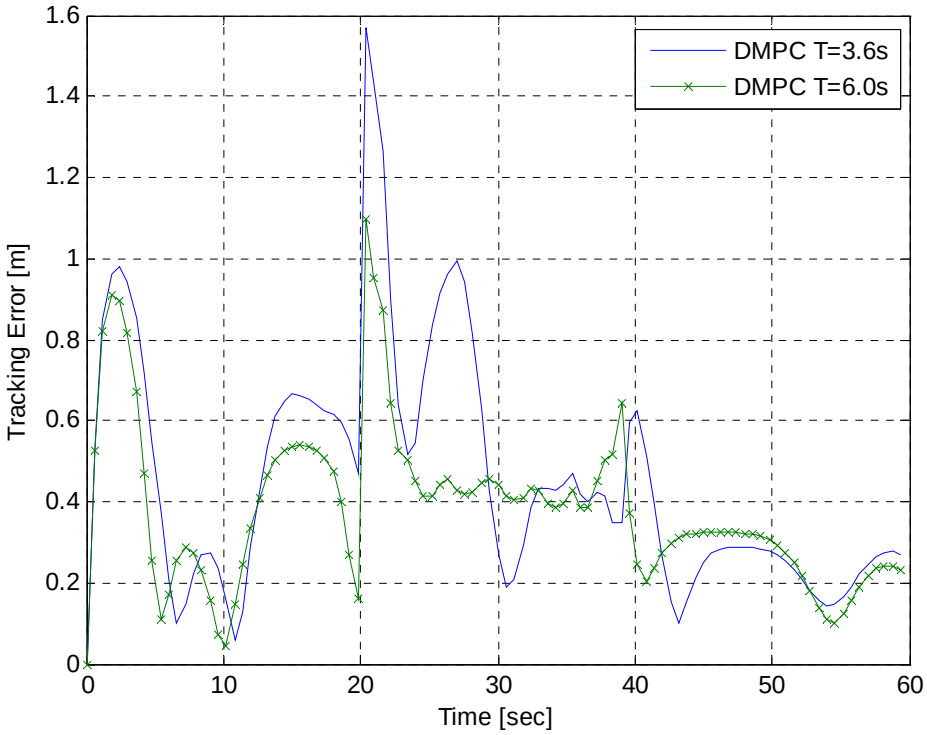

Figure 6-13. Effect of the prediction horizon length on the tracking performance using the decentralised implementation scheme.

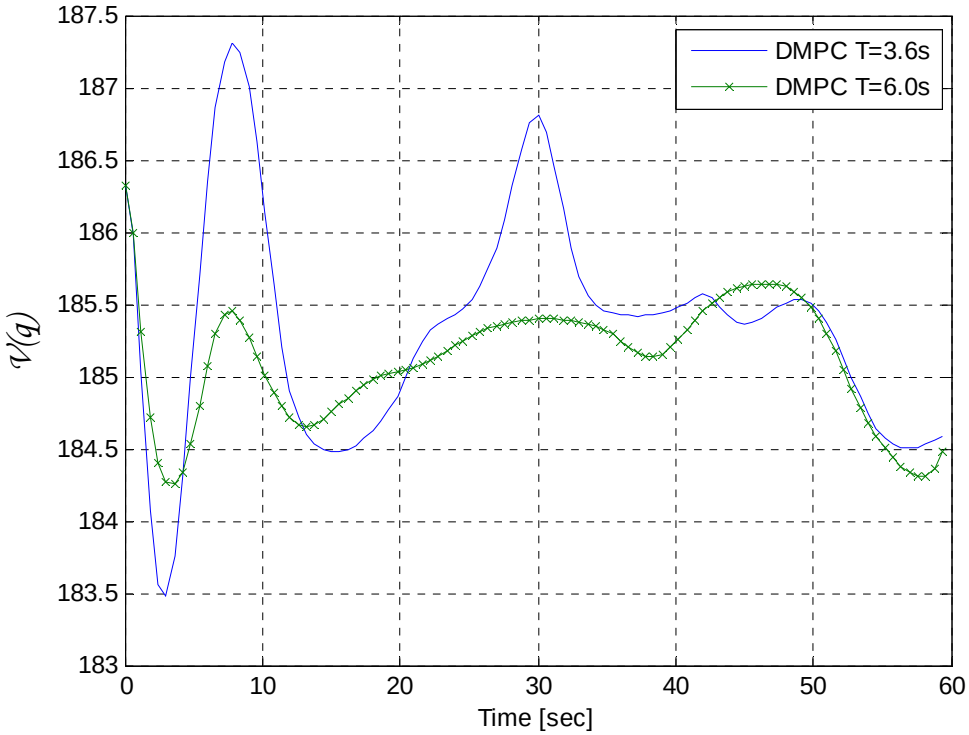

Figure 6-14. Effect of the prediction horizon length on the convergence of the flock configuration using the decentralised implementation scheme.

6.6. SUMMARY

In this chapter, the proposed cooperative control scheme developed in the previous chapters was implemented on a group of vehicles. The objective of the group was to maintain a flock lattice construction whilst adhering to the cooperative objectives specified by the supervisory controller. Cooperative objectives included the optimal motion of the group and evolution of the shape spanned by the flock configuration. Numerical experiments were presented to demonstrate the effectiveness of the proposed cooperative control framework. The decentralised cooperative control scheme was then compared to the traditional centralised model predictive control scheme presented in Section 5.1. In general, performance of the decentralised cooperative control strategy was comparable to the centralised implementation. Results also indicated that the compatibility constraint discussed in Section 5.3 was a conservative constraint on the distributed problem. In fact, strict application of the compatibility constraint reduced the efficacy of the model predictive control scheme to accommodate for changes in the environment. This was particularly evidenced by the large errors induced by the sudden change in direction between successive trajectory segments. Furthermore, implementation of the compatibility constraint was trivial during the trajectory segments. This was due to the inherent compatibility of the optimal predicted plans at successive update periods induced by the natural coupling of successive finite horizon problems. Without disturbances, such as changing objectives, or changing flock patterns, the vehicle's plans would naturally converge to a consensus due to the coupling in the cooperative objective. In fact, relaxing the compatibility constraint ($\kappa = \infty$) demonstrated good transient response (despite the investigations in Section 5.5) with comparable performance to the centralised implementation. It should be noted that this observation is only valid for applications where vehicle' plans are not subject to drastic changes or disturbances. While the strategy developed in the previous chapters has demonstrated potential in this chapter, the following chapter concludes with a discussion on the significance of the results and future areas of research.

Chapter 7. Conclusion and Recommendations

In this thesis the problem of controlling a large group of vehicles for cooperative tasks was investigated. A theoretical framework was presented that mapped the local vehicle behaviours to group behaviours. Methods to model the local vehicle behaviours using principles from natural flocks and swarms were presented, and group abstractions based on these interactions were derived. A decentralised cooperative control scheme was then developed to coordinate the actions of the individuals towards a group task represented at the group manifold. In the following section, a summary of the material presented in this thesis is provided. Major contributions of the work are highlighted before areas of future research are discussed.

7.1. CONTRIBUTIONS

For cooperative control of multiple agents, the exchange of information is necessary to coordinate the actions of individuals towards a common goal. Coordination involves consensus on the exchanged information. The distributed nature of the information flow, and the sufficient conditions for consensus on a time-invariant and time-varying communication network were investigated in Chapter 2. Using tools from algebraic graph theory, a theoretical framework for modelling and analysing the communication topology for a group of vehicles was presented. It was shown that the sum-of-squares (SOS) properties of the graph Laplacian naturally admit a distributed protocol for consensus on an information network. Application of the consensus protocol based on the SOS properties of the graph Laplacian was shown to asymptotically converge to the average value of the connected information network. Furthermore, the rate of convergence for a connected information graph using the distributed consensus protocol was bounded by the second smallest eigenvalue of the graph Laplacian. This provided a useful measure and guarantee to the network's performance.

The consensus protocol was then extended to the case of a switching network to model the spatiotemporal nature of the communication exchange topology for a group of vehicles.

Following the works of [46], it was shown that the switching network was piecewise continuous. The closed-form of the information flow was then derived by applying the consensus protocol. The resulting system provided a model for the evolution of information on a group of vehicles subject to spatially induced communication topologies. It was shown that the closed-form of the information flow was described by a hybrid differential autonomous system.

In Chapter 3, the SOS properties of the graph Laplacian that were used in Chapter 2 to derive a consensus protocol, were then extended to flocking behaviour for a group of vehicles. It was shown that the flocking behaviour is an example of consensus on a distributed system; where the information state represents the set of spatial constraints prescribed by Reynolds' flock model. Based on this premise, a mathematical model for flocking was presented using fixed inter-vehicle constraints. The configuration induced by this model was identified by a flock lattice. A simple distributed flock protocol was then constructed using Lennard-Jones type potentials. The Lennard-Jones type potentials provided a smooth energy functional to describe the conformity of the flock's configuration to the desired flock lattice. The minimum of the energy functional induced by the flock configuration was shown to correspond to the desired flock lattice. This provided an identifiable metric to control the convergence of the flock to the lattice construction. The flock protocol was then implemented as a simple PD controller to investigate the stability and performance of the flocking protocol for a group of point-like vehicles. It was shown that the group of vehicles converge to a configuration with fixed-inter vehicle distances; supporting the proposed model. The spatial constraints of the flock lattice, represented the first two behavioural traits of Reynolds' rules. A second term was introduced to produce flock alignment. This was known as the velocity alignment term. Together, the structural flock protocol and the velocity alignment term provided stable flocking. It was shown by simulation for higher-order systems that a group of vehicles applying the flock protocol, will only stabilise to the flock lattice given a specific set of initial conditions. A navigational feedback was introduced to help stabilise the system and provide a tangible representation of the cooperative group objective. These were further developed in Chapter 4.

Analysis of the interconnected group applying the flock protocol revealed that for a given initial configuration, the group of vehicles will converge to the largest subset of the Hamiltonian. This provided a shape abstraction that bounded the distribution spanned by the vehicles. Using this representation, the group could be treated as a unified virtual-structure

controllable at a supervisory level. The control problem at the supervisory level was then reduced to shape control and vehicle path planning for a single rigid body system. Trajectory generation and tracking for the individual vehicles were then treated at the local vehicle level by developing optimal cooperative control strategies in Chapter 5.

The problem of controlling the shape and motion of the group of vehicles as a rigid body was investigated in Chapter 4. The approach presented here exploited the symmetries induced by the converged flock lattice and the reduction of control to a lower-dimensional manifold. By using this approach, the notions of scalability and reductionism could be applied. Techniques from differential geometry were then used to establish the optimal conditions for navigating the group as a rigid body system. Conditions for optimality were given for the minimum energy, minimum acceleration, and minimum jerk cases. Analytical expressions for these were presented given a symmetric bi-invariant metric.

To control the shape, virtual agents were introduced along the surface of the n-sphere representing the distribution spanned by the N vehicles. Controlling the virtual agents (or antipodal points of the n-sphere) affected the expansion and contraction of the shape spanned by the group of vehicles and considered the group as a virtual structure. Using this approach, complex polygons representative of more elaborate flock configurations could be defined by specifying more virtual agents along the surface. However, increasing the number of points along the shape spanned by the vehicles increases the complexity of the path planning problem for the virtual structure, and alternative abstractions should be investigated.

In the case of a group of vehicles transitioning from a quasi-flock or disconnected configuration to the flock lattice, the vehicles were shown to violate the rigidity constraints of the rigid body model. The conditions that were presented for optimal motion generation were invalid since the group of vehicles was now identified by a semi-rigid body model. Projections along the rigidity preserving directions and rigidity violating directions were used to resolve the energy metric for the semi-rigid body model and define ‘suboptimal’ motions for the virtual agents to trace and map out a shape trajectory. Solving the trajectories for the virtual agents was approached by interpolating the motions and solving the boundary value problem associated to the geodesic flow equations. Boundary conditions were provided using the shape spanned by the initial configuration and the shape spanned by the Hamiltonian of the flock protocol. Solving the boundary value problem for the planar case of two virtual agents was demonstrated. It was shown that for this case, a total of 64 Christoffel Symbols need to be solved. While this strategy is sufficient for small groups of virtual agents, and can

even be applied to the motion generation of each vehicle, it is highly intractable to apply to motion generation of each vehicle or to increase the number of virtual agents.

To resolve the motion generation segment of the vehicles in the local frame, a cooperative control scheme was designed based on a decentralised model predictive control strategy in Chapter 5. The work exploited the predictive nature of the control scheme to permit negotiation and consensus between neighbouring vehicles at successive update periods. Here, the predicted states were used to represent the plans and intentions of vehicles at future sampling periods. The plans represented the state trajectories of the individuals that satisfied the cooperative objective and optimised the local vehicle behaviours. Formulating the cooperative objective and local objective in this way enabled the coherent resolution of the group task from the local behaviours. Sufficient conditions for consensus applying this strategy were also provided. It was shown that if vehicles transmitted information, and then deviated from their original plans in the proceeding update period, then the system would demonstrate poor convergence and ultimately poor cooperation. To resolve this issue, it was necessary to introduce a compatibility constraint that would penalise the behaviour of vehicles if they deviated too far from their previous plans. This ensured that the vehicles would be more cohesive. It was shown for small values of the compatibility constraint, consensus was sluggish. On the other hand, by relaxing the compatibility constraint, and permitting larger deviations between successive plans, the consensus on the coordination variable was difficult to achieve since vehicles would be permitted to deviate from their intentions at successive intervals. Nonetheless, the compatibility constraint was necessary to ensure cooperative behaviour, despite its limiting effect on the power of model predictive control. Finally, in Chapter 6, the theoretical framework for controlling the group as a collective, and the cooperative decentralised model predictive control scheme were implemented on a group of vehicles tasked with cooperative navigation. The objective of Chapter 6 was to demonstrate the application of the combined theoretical developments in the previous chapters to a cooperative control problem. Using the methods presented in Chapter 4, the shape and motion of the group was obtained for the group. These were used to represent the cooperative objective for the group of vehicles. Applying the cooperative control scheme in Chapter 5, it was demonstrated that the framework achieves cooperation in the local frame and satisfies the group objectives. For comparative purposes, a centralised implementation of the cooperative objective was also presented using traditional model predictive control. The decentralised cooperative control scheme achieved the desired

cooperative objective, and demonstrated similar performance to the centralised case when the compatibility constraint was relaxed. This suggested that the bounds on the compatibility constraint developed in Chapter 5 were conservative estimates for the case when the information is coupled in the cooperative objective. Furthermore, enforcing strict compatibility constraints prevented the vehicles from significantly deviating from previous plans and accommodating for changes in the operating conditions. In these scenarios, the performance of the decentralised cooperative control scheme was not optimal. It was shown that by increasing the sampling period and the frequency of information exchange, the behaviour of the decentralised cooperative control scheme with strict compatibility constraints could be recovered.

7.2. APPLICATION AND FUTURE WORK

The results presented in this thesis raise many questions and research possibilities. While the work has attempted to integrate as many of the relevant approaches and build on them to develop a unified model, there are still some avenues of research that need to be addressed for the practical implementation of this framework. In the following sections, several potential research directions are proposed.

7.2.1. INFORMATION FLOW AND CONSENSUS

In Chapter 2, a simplified model of the information exchange topology for a generalised distributed system was developed. Based on the SOS properties of the graph Laplacian, a simple consensus protocol was developed that would achieve consensus on the exchanged information state. It was assumed, for the purposes of generality, that the information was synchronised and perfect (lossless). In practice, the exchange of information through wireless media is subject to noise, uncertainty, interruption and delays; particularly for multi-vehicle applications. These can be caused by hardware limitations, interferences with the environment, the directivity of the transmitted information flow, or the ad-hoc nature of the communication network. The effect of these disturbances can invalidate the convergence properties of the proposed consensus protocols. Therefore, it is necessary to analyse asynchronous protocols with time delays to provide a more realistic model of multi-vehicle systems. Already, several authors [137, 209, 233, 308, 309] have begun investigating the effects of delays and asynchronicity on the consensus of information networks. These studies will help to further the understanding of multi-vehicle interactions in a realistic setting.

The situatedness of the information flow in a multi-vehicle system admits a switching communication network. It was shown for a group of vehicles with finite interaction range, that the switching network is piecewise continuous with dynamics governed by a hybrid differential autonomous equation. Analytical methods to solve these types of problems are currently an active area of research, with no explicit solutions known to exist. Understanding the behaviour of the switching network can provide insight into the switching instances of the network and the length of the dwell times. This can provide invaluable information in developing optimal coordination control strategies that exploit the dwell periods. For example, in the proposed cooperative decentralised model predictive control scheme, the prediction horizon and sampling period were determined based on an empirical investigation. By understanding the length of the dwell times and the switching instances, the cooperative decentralised model predictive control scheme can be optimised to exchange information only at the switching instances. This would reduce the frequency of information exchange and the power and bandwidth required to maintain continuous communication.

7.2.2. FLOCKING

In Chapter 3, a Lennard-Jones type artificial potential field was used to model the inter-agent behaviours of the vehicles in the flock. The Lennard-Jones type potential was constructed by fitting a smooth continuous function to the spatial constraints of Reynolds' rules. The resulting potential field was a continuously smooth approximation to the Euclidean norm. While this is sufficiently general, other Lennard-Jones type potentials could be used to model the intricate behaviours of natural flocks and swarms. Studies in the fields of particle physics, electrochemistry, molecular biology, and mathematical biology can provide an insight into the application of Lennard-Jones type potentials to modelling natural phenomena such as flocks and swarms.

By introducing secondary behaviours to the original flock model and accommodate for more realistic motions, the number of controllable parameters will be increased. These are represented by the weighting terms on each vector field corresponding to each additional behaviour. Until now, the weighting parameters were arbitrarily selected or deduced from empirical investigations. This was possible since the behaviour set was minimal and the influence of each parameter could be easily investigated through simulation. As the number of vehicles and/or number of behaviours is increased, the resolution of individual behaviours becomes more difficult using numerical simulation. A thorough investigation should be

performed to develop analytical expressions for the influence of the weighting parameters on the behaviours of the vehicles. This will provide a greater insight into the stability of the system, the influence of the vehicles on the cooperative objective, and ultimately, the development of an automatic tuning system for the individual vehicle controllers.

An issue pertinent to artificial potential field-based controllers is the emergence of local minima. In this thesis, the problem of local minima was briefly considered by introducing a navigational feedback term representative of the group cooperative objective. This provided a suitable means of coordinating the behaviours of the vehicles and directing the motion towards a global minimum. When the cooperative objective is not spatially dependent, or when the group is not coupled by a group cooperative objective, navigational feedback is unsuitable for avoiding local minima. In some cases, the navigational feedback can introduce unwanted local minima, such as navigation through an obstacle field. Methods to circumvent the existence of local minima should be investigated; and contingencies to overcome these minima should be developed. Possible contingencies could include reversion to a motion primitive such as loitering.

Other shape abstractions using the internal flock lattice model should also be investigated to broaden the applications of the flock. In this thesis, only the n-sphere bounding the flock distribution was considered. The n-sphere bound provides only one type of shape and limits the possible applications for a flock. Many applications require more complex shapes to be formed. Recently, authors have investigated the use of Fourier descriptors [352, 353] as a method of modelling the shape boundary for a group of vehicles. In these methods, two types of vehicles are distinguished; leaders and followers. The leaders assume positions along the perimeter of the desired shape, whilst followers ‘fill’ the internal volume. Using this approach, the artificial potential field can be modified to accommodate a secondary behaviour that forces the vehicles to conform to the shape and distribution specified by the Fourier descriptors. This approach has recently been applied by the authors to a group of vehicles for radar deception [215]. Using potential fields in this manner, involves a mapping on the navigational term.

A similar approach to using the shape conforming potential is the use of morphogenesis gradients. Morphogenesis gradients are inspired by the field of cellular biology. While highly speculative, it could be possible to define a global potential field that is coded into the vehicles. This global morphogenesis gradient determines the role or behaviour of the vehicle within the flock based on their relative distance from a placeholder (such as the desired

centroid of the flock). In this case, vehicles closer to the centre of the flock, might be required to have a stricter conformity to the flock lattice, whilst those further away, would assume the role of the leader agents, and switch to the required behaviour. The morphogenesis gradient essentially manifests itself in the weighting parameters of the flock behaviours. This approach is highly advantageous since it would be more amenable to scaling; i.e. virtual agents do not have to be defined explicitly at design time. Behaviours of the vehicles are determined based on their position in the gradient field and evolve with the flock.

7.2.3. GROUP MOTION PLANNING

The cooperative task in this thesis was demonstrated by considering the group navigation of the flock as a cooperative objective. The approach used was based on the assumption that the group adheres to a rigid body construction. By treating the flock as a rigid body system, optimal trajectories for the group could be derived using techniques from geometric control theory. These approaches provide a nice method for solving the motion generation problem on a left-invariant control system preserving the symmetric properties of the rigid flock. The transition from an initial configuration to a flock configuration, however, violates the rigidity constraints of the rigid body model, and the system is considered as a rigid body system. In this model, the motion of each vehicle in the flock features a rigidity preserving and rigidity violating component. In this thesis, the transition of the group from one configuration to the flock lattice was treated using a semi-rigid body system using a semi-rigid metric. The semi-rigid metric was constructed by introducing a shape control parameter to the rigid body metric and resolving the motions along the geodesic preserving and geodesic violating directions. One area of research involves the limits of this shape parameter. The relationship between the permissible boundary conditions, the stringency of the rigidity constraints, and the range of allowable shape parameters should be investigated. In this thesis, the boundary conditions were arbitrarily selected to violate the rigidity constraints; i.e. the initial shape and final shape were incompatible. By simulation, it was shown that only a small set of shape parameters exist for this type of navigation objective, and purely rigid body motions could not be achieved $\sigma_r = 1$. Understanding the relationship between the boundary conditions and the shape parameter provides an insight into the allowable motions of the group at the supervisory level and can further reinforce the notion of open-loop optimal commands.

Another area of extension (more aligned to practical implementation) is the effect of the shape boundary on object collisions. In natural flocks and swarms, the individuals can easily

bifurcate and converge around an obstacle to avoid collisions. Applying the shape boundary constraints prevents any excursions of the individuals from the desired shape. A potential conflict arises when the flock comes into contact with a physical object in the environment. Protocols must be developed to negotiate obstacles. This could be achieved by a finite-state automaton to switch between modes of behaviour. Possible modes could include flock loitering, flock bifurcation and convergence, and re-planning the desired centroidal path of the flock. Practical insights into safe switching modes for collision avoidance would be provided by a mission specialist and would be dependent on the desired objectives of the flock. Implementing a finite-state automaton naturally implies a relaxation of the shape boundary constraints to avoid collisions and prevent conflicts between the desired group's objectives and the allowable behaviours of the individuals. Therefore, the introduction of safe collision avoidance protocols would have to consider the significance of the shape boundary constraints.

Following the symmetric approach described in thesis, it is also possible to find the optimal motions of each vehicle rather than just the virtual agents. However, solving the geodesic flow equations is centralised since the geodesic flow equations are dependent on the coordinates in the local frame. While for small groups of vehicles (such as the subset of virtual agents), this is permissible, the approach is not readily scalable. As it was shown, solving for only two points on a planar manifold resulted in the simultaneous resolution of 8 differential equations with 64 Christoffel symbols relating to the semi-rigid metric. Ideally, the motions of each vehicle should exploit the nature of the geodesic flow. An avenue of research is to investigate the possibility of defining a geodesic bundle that represents the flow field of the flock that can be solved in a decentralised manner.

7.2.4. COOPERATIVE CONTROL VIA DECENTRALISED MODEL PREDICTIVE CONTROL

In this thesis, cooperation was achieved by the mutual exchange of plans and intentions between neighbouring vehicles to reach a consensus on some coordination variable, representative of the solution of the cooperative objective. A dependency of the cooperative decentralised model predictive control strategy is the compatibility constraint. The compatibility constraint restricts the power of traditional model predictive control to re-evaluate an optimisation problem under disturbance or changing environmental conditions. Research possibilities involve finding alternative approaches to reduce the limiting effect of

the compatibility constraint on finding new solutions. Possibilities include removing the compatibility constraint, and developing protocols to switch the controller and safeguard the vehicle.

Other areas that need to be investigated, is the effect of delays and asynchronicity. It was assumed that the computational time to resolve the optimisation problem at each prediction horizon was negligible. In practice, the vehicles require time to compute their solutions. Depending on the hardware processor capabilities, and the amount of information being received from neighbours, this can be a significant factor that could determine the feasibility of such an approach in real-world situations. In addition, the foundation of the decentralised model predictive control strategy was the information exchange. It was assumed that the information exchange is lossless, and synchronised, with no delays. Any disturbance to the flow of information will affect the stability and performance of the cooperative control scheme. Therefore, more realistic models of the information exchange topology need to be investigated and applied to the cooperative control scheme. Effects such as delays and packet losses should be investigated with context to the decentralised model predictive control strategy. To robustify the cooperative control strategy, contingencies should also be developed information is not received or corrupted due to communication dropouts and interference.

The effect of the sampling time on the convergence of the cooperative control scheme should also be investigated. It was shown in Chapter 6 how the transient behaviour with a strict compatibility constraint can be improved by increasing the frequency of the information flow. Bounds on the performance error and the compatibility constraint should be established to properly determine the frequency of the information exchange. This should ideally also consider the practical issues of the implementation. For example, in this thesis, it was assumed that the vehicles were able to freely send and receive information as needed. In practice, constraints on hardware and the vulnerability of information transmitted across a wireless medium limit the ability of vehicles to convey information over open channels of communication. An important area of investigation is the minimum amount of information required that achieves consensus, and the minimum frequency needed to demonstrate appreciable performance and fault tolerance.

The cooperative control problem in this thesis was formulated using a singular objective function combining the local behaviours of the vehicles with the desired group objectives of the flock. Weighting parameters were used to tune the relative importance of the individual

tasks in the distributed objective functions of each vehicle. While this approach was valid for tasks represented on the same solution space or in some way coupled, the same approach can not be effectively applied to applications where the tasks are conflicting and/or reside on different solution spaces. A more general approach (and one that treats the individual tasks and objectives independently) is multi-objective optimisation. Multi-objective optimisation can ensure that the solution is the best compromise between the vehicle's local objectives and the desired group's objectives. Recently, the authors have investigated the application of the proposed approach using multi-objective formulations with successful results [354].

7.2.5. IMPLEMENTATION

The main goal of this thesis was to present a unified framework in which a supervisory controller can control a large group of vehicles using a limited set of abstractions, and make the behaviour of the vehicles converge to the desired objectives. Due to limited simulation facilities and resources however, the cooperative control framework was only demonstrated for small-scale populations with simple integrator dynamics. Simplifying assumptions were made to construct an idealised setting that demonstrated the efficacy of the proposed approach. While these assumptions were used to promote the theory, application of the derived control laws into a realistic setting would provide practical insights into the limitations of the proposed framework. Possible extensions would include higher-order vehicle systems exhibiting nonlinear dynamics, large-scale populations with random attrition and extension, and high-fidelity models. Similarly, practical implementation issues on the information network should also be modelled to consider the validity of the approach on real-world multi-vehicle systems. These include the effect of asynchronicity, delays, uncertainty, and noise on the stability and performance of the cooperative control framework.

The cooperative framework proposed, has also only been demonstrated for applications that feature the spatial coordinates as a solution to the cooperative problem. The results suggest that the framework presented is amenable to many other multi-vehicle scenarios admitting a spatial representation. These include cooperative rendezvous, coverage control, intelligent traffic control, cooperative object manipulation, and self-assembly. Extensions to other non-spatial cooperative control problems, such as mathematical optimisation using distributed processors and distributed internet search agents, are also possible by formulating the objective as a cooperative control problem. Exploration of these ideas could validate the

generality of the approach and provide further insight into the practical capacities and limitations of the developed framework into multi-vehicle and multi-agent systems.

References

[1] Department of Defense, "Unmanned Aerial Vehicles Roadmap, 2002 - 2007," Office of Secretary of Defense 2002.

[2] H. V. D. Parunak and S. A. Brueckner, "Engineering Swarming Systems," in *Methodologies and Software Engineering for Agent Systems*: Kluwer, 2004, pp. 341 - 376.

[3] E. Bonabeau, G. Theraulaz, and M. Dorigo, *Swarm Intelligence: From Natural to Artificial Intelligence*. New York: Oxford University Press, 1999.

[4] H. Levine, E. Ben-Jacob, I. Cohen, and W.-J. Rappel, "Swarming Patterns in Microorganisms: Some New Modeling Results," presented at 45th IEEE Conference on Decision and Control, San Diego, CA, USA, 2006.

[5] A. Okubo, "Dynamical Aspects of Animal Grouping: Swarms, Schools, Flocks, and Herds," *Advances in Biophysics*, vol. 22, pp. 1 - 94, 1986.

[6] J. K. Parrish, S. V. Viscido, and D. Grünbaum, "Self-Organized Fish Schools: An Examination of Emergent Properties," *Biological Bulletin*, vol. 202, pp. 296 - 305, 2002.

[7] J. Terborgh, "Mixed Flocks and Polyspecific Associations: Costs and Benefits of Mixed Groups to Birds and Monkeys," *American Journal of Primatology*, vol. 21, pp. 87 - 100, 1990.

[8] P. B. S. Lissaman and C. A. Shollenberger, "Formation Flight of Birds," *Science*, vol. 168, pp. 1003 - 1005, 1970.

[9] J. P. Badgerow and F. R. Hainsworth, "Energy Savings Through Formation Flight? A Re-examination," *Journal of Theoretical Biology*, vol. 93, pp. 41 - 52, 1981.

[10] G. A. Dimock and M. S. Selig, "The Aerodynamic Benefits of Self-Organization in Bird Flocks," presented at 41st Aerospace Sciences Meeting and Exhibit, Reno, NV, USA, 2003.

[11] S. N. Singh and M. Pachter, "Adaptive Feedback Linearizing Nonlinear Close Formation Control of UAVs," presented at American Control Conference, Chicago, IL, USA, 2000.

[12] T. D. Seeley and P. K. Visscher, "Group Decision Making in Nest-Site Selection by Honey Bees," *Apidologie*, vol. 35, pp. 101-116, 2004.

[13] T. D. Seeley, P. K. Visscher, and K. Passino, "Group Decision-Making in Swarms of Honey Bees," *American Scientist*, vol. 94, pp. 220 - 229, 2006.

[14] C. Boesch, "Cooperative Hunting in Wild Chimpanzees," *Animal Behaviour*, vol. 48, pp. 653 - 667, 1994.

[15] C. Boesch, H. Boesch, and L. Vigilant, "Cooperative Hunting in Chimpanzees: Kinship or Mutualism," in *Cooperation in Primates and Humans*. Berlin: Springer Berlin Heidelberg, 2006, pp. 139 - 150.

[16] S. Creel and N. M. Creel, "Communal Hunting and Pack Size in African Wild Dogs, *Lycaon pictus*," *Animal Behaviour*, vol. 50, pp. 1325 - 1339, 1995.

[17] E. Bonabeau, G. Theraulaz, J.-L. Deneubourg, S. Aron, and S. Camazine, "Self-organization in Social Insects," *Trends in Ecology and Evolution*, vol. 12, pp. 188 - 193, 1997.

[18] M. Dorigo, V. Maniezzo, and A. Colorni, "The Ant System: Optimization by a Colony of Cooperating Agents," *IEEE Transactions on Systems, Man, Cybernetics - Part B: Cybernetics*, vol. 26, pp. 1 - 13, 1996.

[19] J. Kennedy and R. Eberhart, "Particle Swarm Optimization," presented at IEEE International Conference on Neural Networks, Perth, Australia, 1995.

[20] C. M. Breder, "Equations Descriptive of Fish Schools and Other Animal Aggregations," *Ecology*, vol. 35, pp. 361 - 370, 1954.

[21] K. Warburton and J. Lazarus, "Tendency-Distance Models of Social Cohesion in Animal Groups," *Journal of Theoretical Biology*, vol. 150, pp. 473 - 488, 1991.

[22] T. Chu, L. Wang, and S. Mu, "Collective Behavior Analysis of an Anisotropic Swarm Model," presented at 16th International Symposium on Mathematical Theory on Networks and Systems (MTNS 2004), Leuven, Belgium, 2004.

[23] H. Levine, W.-J. Rappel, and I. Cohen, "Self-organization in Systems of Self-propelled Particles," *Physical Review E*, vol. 63, pp. 017101-1 - 017101-4, 2000.

[24] A. Mogilner, L. Edelstein-Keshet, L. Bent, and A. Spiros, "Mutual Interactions, Potentials, and Individual Distance in a Social Aggregation," *Journal of Mathematical Biology*, vol. 47, pp. 353 - 389, 2003.

[25] C. Reynolds, "Flocks, Herds, and Schools: A Distributed Behavioral Model," presented at ACM SIGGRAPH '87, Anaheim, CA, USA, 1987.

[26] D. Grünbaum, "Schooling as a Strategy for Taxis in a Noisy Environment," *Evolutionary Ecology*, vol. 12, pp. 503 - 522, 1998.

[27] R. Eberhart and J. Kennedy, "A New Optimizer Using Particle Swarm Theory," presented at 6th IEEE International Symposium on Micro Machine and Human Science, Nagoya, Japan, 1995.

[28] S. Kirkpatrick, C. D. Gelatt, and P. Vecchi, "Optimization by Simulated Annealing," *Science*, vol. 220, pp. 671 - 680, 1983.

[29] G. Di Caro and M. Dorigo, "Antnet: Distributed Stigmergetic Control for Communications Networks," *Journal of Artificial Intelligence Research*, vol. 9, pp. 317 - 365, 1998.

[30] I. Aoki, "A Simulation Study on the Schooling Mechanism in Fish," *Bulletin of the Japanese Society of Scientific Fisheries*, vol. 48, pp. 1081 - 1088, 1982.

[31] A. Huth and C. Wissel, "The Simulation of Fish Schools in Comparison with Experimental Data," *Ecological Modelling*, vol. 75-76, pp. 135 - 145, 1994.

[32] R. Olfati-Saber, "A Unified Look at Reynolds Flocking Rules," California Institute of Technology, Pasadena, California CIT-CDS 03-014, September 2003.

[33] I. D. Couzin, J. Krause, R. James, G. D. Ruxton, and N. R. Franks, "Collective Memory and Spatial Sorting in Animal Groups," *Journal of Theoretical Biology*, vol. 218, pp. 1 - 11, 2002.

[34] M. Ballerini, N. Cabibbo, R. Candelier, A. Cavagna, E. Cisbani, I. Giardina, V. Lecomte, A. Orlandi, G. Parisi, A. Procaccini, M. Viale, and V. Zdravkovic, "Interaction Ruling Animal Collective Behavior Depends on Topological Rather Than Metric Distance: Evidence from a Field Study," *Proceedings of the National Academy of Sciences*, vol. 105, pp. 1232 - 1237, 2007.

[35] D. Grünbaum, S. V. Viscido, and J. K. Parrish, "Extracting Interactive Control Algorithms for Group Dynamics of Schooling Fish," in *Cooperative Control*, vol. 309/2004, *Lecture Notes in Control and Information Sciences*, V. Kumar, N. E.

Leonard, and A. S. Morse, Eds. Berling: Springer Berlin/Heidelberg, 2005, pp. 103 - 117.

[36] P. E. Ellis, "The Gregarious Behaviour of Marching *Locusta Migratoria Migratorioides* (R. & F.) Hoppers," *Journal of Experimental Biology*, vol. 30, pp. 214 - 233, 1953.

[37] L. Edelstein-Keshet, J. Watmough, and D. Grünbaum, "Do Traveling Band Solutions Describe Cohesive Swarms? An Investigation for Migratory Locusts," *Journal of Mathematical Biology*, vol. 36, pp. 515 - 549, 1998.

[38] J. D. Murray, *Mathematical Biology*. New York: Springer Verlag, 1989.

[39] L. Edelstein-Keshet, *Mathematical Models in Biology*. New York: Random House, 1988.

[40] J. G. Skellam, "Random Dispersal in Theoretical Populations," *Biometrica*, vol. 38, pp. 196 - 218, 1951.

[41] A. Mogilner and L. Edelstein-Keshet, "A Non-local Model for a Swarm," *Journal of Mathematical Biology*, vol. 38, pp. 534 - 570, 1999.

[42] C. M. Topaz and A. L. Bertozzi, "Swarming Patterns in a Two-Dimensional Kinematic Model for Biological Groups," *SIAM Journal of Applied Mathematics*, vol. 65, pp. 152 - 174, 2004.

[43] T. Vicsek, A. Czirok, E. Ben-Jacob, I. Cohen, and O. Shochet, "Novel Type of Phase Transition in a System of Self-Drive Particles," *Physical Review Letters*, vol. 75, pp. 1226 - 1229, 1995.

[44] J. Toner and Y. Tu, "Flocks, Herds, and Schools: A Quantitative Theory of Flocking," *Physical Review E*, vol. 58, pp. 4828 - 4858, 1998.

[45] R. Sepulchre, D. Paley, and N. Leonard, "Stabilization of Collective Motion of Self-Propelled Particles," presented at 16th Symposium of Mathematical Theory of Networks and Systems (MTNS2004), Leuven, Belgium, 2004.

[46] A. Jadbabaie, J. Lin, and A. S. Morse, "Coordination of Groups of Mobile Autonomous Agents Using Nearest Neighbor Rules," *IEEE Transactions on Automatic Control*, vol. 48, pp. 988 - 1001, 2003.

[47] V. Gazi and K. M. Passino, "Stability Analysis of Swarms," *IEEE Transactions on Automatic Control*, vol. 48, pp. 692 - 897, 2003.

[48] V. Gazi and K. M. Passino, "Stability Analysis of Social Foraging Swarms," *IEEE Transactions on Systems, Man, Cybernetics - Part B: Cybernetics*, vol. 34, pp. 539 - 557, 2004.

[49] V. Gazi and K. Passino, "Stability Analysis of Swarms," presented at American Control Conference, Anchorage, AK, USA, 2002.

[50] V. Gazi and K. Passino, "Stability Analysis in an Environment with an Attractant/Repellent Profile," presented at American Control Conference, Anchorage, AK, USA, 2002.

[51] V. Gazi and K. M. Passino, "A Class of Attraction/Repulsion Functions for Stable Swarm Aggregations," presented at IEEE Conference on Decision and Control, Las Vegas, NV, USA, 2002.

[52] T. Chu, L. Wang, and T. Chen, "Self-organized Motion in Anisotropic Swarms," *Journal of Control Theory and Applications*, vol. 1, pp. 77 - 81, 2003.

[53] L. Chen and L. Xu, "Collective Behavior of an Anisotropic Swarm Model Based on Unbounded Repulsion in Social Potential Fields," in *Computational Intelligence and Bioinformatics*, vol. 4115/2006. Berlin: Springer Berlin/Heidelberg, 2006, pp. 164 - 173.

[54] C. V. Goldman and J. S. Rosenschein, "Emergent Coordination through the use of Cooperative State-Changing Rules," presented at 12th National Conference on Artificial Intelligence, Seattle, WA, USA, 1994.

[55] J. P. Desai, J. Ostrowski, and V. Kumar, "Controlling Formations of Multiple Mobile Robots," presented at IEEE International Conference on Robotics and Automation, Leuven, Belgium, 1998.

[56] W. Kang, N. Xi, and A. Sparks, "Formation Control of Autonomous Agents in 3D Workspace," presented at IEEE International Conference on Robotics and Automation, San Francisco, CA, USA, 2000.

[57] R. W. Beard, J. Lawton, and F. Y. Hadaegh, "A Feedback Architecture for Formation Control," presented at American Control Conference, Chicago, IL, USA, 2000.

[58] C. J. Schumacher and R. Kumar, "Adaptive Control of UAVs in Close-Coupled Formation Flight," presented at American Control Conference, Chicago, IL, USA, 2000.

[59] F. Giulietti, M. Innocenti, M. Napolitano, and L. Pollini, "Dynamic and Control Issues of Formation Flight," *Aerospace Science and Technology*, vol. 9, pp. 65 - 71, 2005.

[60] D. P. Scharf, F. Y. Hadaegh, and S. R. Ploen, "A Survey of Spacecraft Formation Flying Guidance and Control (Part 1): Guidance," presented at American Control Conference, Denver, CO, USA, 2003.

[61] O. Junge, J. E. Marsden, and S. Ober-Blobaum, "Optimal Reconfiguration of Formation Flying Spacecraft - a Decentralized Approach," presented at 45th IEEE Conference on Decision and Control, San Diego, CA, 2006.

[62] S. Mandutianu, F. Hadaegh, and P. Elliot, "Multi-Agent System for Formation Flying Missions," presented at IEEE Aerospace Conference, Big Sky, MT, USA, 2001.

[63] D. Lee and P. Y. Li, "Formation and Maneuver Control of Multiple Spacecraft," presented at American Control Conference, Denver, CO, USA, 2003.

[64] W. Ren and R. W. Beard, "Decentralized Scheme for Spacecraft Formation Flying via the Virtual Structure Approach," *Journal of Guidance, Control, and Dynamics*, vol. 27, pp. 73 - 82, 2004.

[65] F. Zhang, M. Goldgeier, and P. S. Krishnaprasad, "Control of Small Formations Using Shape Coordinates," presented at International Conference on Robotics and Automation, Taipei, Taiwan, 2003.

[66] R. W. Beard, J. Lawton, and F. Y. Hadaegh, "A Coordination Architecture for Spacecraft Formation Control," *IEEE Transactions on Control Systems Technology*, vol. 9, pp. 777 - 790, 2001.

[67] I. I. Hussein and A. M. Bloch, "Dynamic Coverage Optimal Control for Interferometric Imaging Spacecraft Formations," presented at 43rd IEEE Conference on Decision and Control, Nassau, Bahamas, 2004.

[68] J. How, E. King, and Y. Kuwata, "Flight Demonstrations of Cooperative Control for UAV Teams," presented at AIAA 3rd Unmanned Unlimited Technical Conference, Workshop and Exhibit, Chicago, IL, USA, 2004.

[69] S. Venkataramanan and A. Dogan, "Nonlinear Control for Reconfiguration of UAV Formation," presented at AIAA Guidance, Navigation, and Control, Austin, TX, USA, 2003.

[70] I. I. Hussein, F. H. Zeitz, and A. M. Bloch, "Optimal Control and the Aircraft Radar Evasion Problem," presented at 2007 American Control Conference, New York City, NY, USA, 2007.

[71] L. C. Trost, "Unmanned Air Vehicles (UAVs) for Cooperative Monitoring," Sandia National Laboratories, Alburquerque, NM SAND2000-0185, January 2000.

[72] Y. Altshuler, V. Yanovsky, I. A. Wagner, and A. M. Bruckstein, "The Cooperative Hunters - Efficient Cooperative Search for Smart Targets Using UAV Swarms," presented at 2nd International Conference on Informatics in Control, Automation, and Robotics, Barcelona, Spain, 2005.

[73] R. Murphey and K. J. O'Neal, "A Cooperative Control Testbed Architecture for Smart Loitering Weapons," presented at 5th International Conference on Information Fusion, Annapolis, MD, USA, 2002.

[74] R. W. Beard, T. W. McLain, and M. Goodrich, "Coordinated Target Assignment and Intercept for Unmanned Air Vehicles," presented at 2002 IEEE International Conference on Robotics and Automation, Washington, DC, 2002.

[75] P. R. Chandler, "Cooperative Control of a Team of UAVs for Tactical Missions," presented at AIAA 1st Intelligent Systems Technical Conference, Chicago, IL, USA, 2004.

[76] E. W. Frew and D. A. Lawrence, "Cooperative Stand-off Tracking of Moving Targets," presented at AIAA Guidance, Navigation, and Control, San Francisco, CA, USA, 2005.

[77] B. J. Capozzi, "Evolution-Based Path Planning and Management for Autonomous Vehicles," Doctor of Philosophy, University of Washington, Washington, 2001.

[78] T. Maddula, A. A. Minai, and M. Polycarpou, "Multi-target Assignment and Path Planning for Groups of UAVs," presented at Conference on Cooperative Control and Optimization, Gainesville, FL, USA, 2002.

[79] M. Flint, E. Fernandez-Gaucherand, and M. M. Polycarpou, "Cooperative Control for UAV's Searching Risky Environments for Targets," presented at IEEE Conference on Decision and Control, Maui, HI, USA, 2003.

[80] D. Frelinger, J. Kvitky, and W. Stanley, *Proliferated Autonomous Weapons: An Example of Cooperative Behavior*. Santa Monica, CA: RAND, 1998.

[81] M. J. Mears, "Cooperative Electronic Attack Using Unmanned Air Vehicles," presented at American Control Conference, Portland, OR, USA, 2005.

[82] J. Kim and J. P. Hespanha, "Cooperative Radar Jamming for Groups of Unmanned Air Vehicles," presented at 43rd IEEE Conference on Decision and Control, Nassau, Bahamas, 2004.

[83] T. W. McLain, P. R. Chandler, S. Rasmussen, and M. Pachter, "Cooperative Control of UAV Rendezvous," presented at American Control Conference, Arlington, VA, 2001.

[84] K. Altenburg, J. Schlecht, and K. Nygard, "An Agent-Based Simulation for Modelling Intelligent Munitions," presented at 2nd International Conference on Simulation, Modelling and Optimization, Skiathos, Greece, 2002.

[85] D. J. Hauck, "Pandora's Box Opened Wide: UAVs Carrying Genetic Weapons," Center for Strategy and Technology Air War College, Air University, Alabama A264364, November 2005.

[86] L. Chin, K. Altenburg, and K. Nygard, "Synchronised Multi-Point Attack by Autonomous Reactive Vehicles with Simple Local Communication," presented at IEEE Swarm Intelligence Symposium SIS '03, Indianapolis, IN, USA, 2003.

[87] H. Yamaguchi, "A Cooperative Hunting Behavior by Mobile-Robot Troops," *International Journal of Robotics Research*, vol. 18, pp. 931 - 940, 1999.

[88] M. M. Polycarpou, Y. Yang, and K. M. Passino, "Cooperative Control of Distributed Multi-Agent Systems," in *IEEE Control Systems Magazine*, 2001.

[89] C. Turner, D. Kroetsch, K. Fregene, D. Hemingway, G. Lai, and D. Wang, "An Autonomous Multivehicle System for Reconnaissance," presented at Association for Unmanned Vehicle Systems: Millennial Event Competition, 2001.

[90] J. Cortés, S. Martínez, T. Karatas, and F. Bullo, "Coverage Control for Mobile Sensing Networks," *IEEE Transactions on Robotics and Automation*, vol. 20, pp. 243 - 255, 2004.

[91] D. H. Shim, H. Chung, H. J. Kim, and S. Sastry, "Autonomous Exploration in Unknown Urban Environments for Unmanned Aerial Vehicles," presented at AIAA Guidance, Navigation and Control Conference and Exhibit, San Francisco, CA, USA, 2005.

[92] K. Fregene, D. Kennedy, R. Madhavan, L. E. Parker, and D. Wang, "A Class of Intelligent Agents for Coordinated Control of Outdoor Terrain Mapping UGVs," *Engineering Applications of Artificial Intelligence*, vol. 18, pp. 513-531, 2005.

[93] R. W. Beard and T. W. McLain, "Multiple UAV Cooperative Search under Collision Avoidance and Limited Range Communication Constraints," presented at 42nd IEEE Conference on Decision and Control, Maui, HI, USA, 2003.

[94] S. Doctor, G. K. Venayagamoorthy, and V. G. Gudise, "Optimal PSO for Collective Robotic Search Applications," presented at Congress on Evolutionary Computation, Portland, OR, USA, 2004.

[95] I. I. Hussein and D. M. Stipanovic, "Effective Coverage Control for Mobile Sensor Networks," presented at 45th IEEE Conference on Decision and Control, San Diego, CA, USA, 2006.

[96] P. Vincent and I. Rubin, "A Framework and Analysis for Cooperative Search Using UAV Swarms," presented at ACM Symposium on Applied Computing, Nicosia, Cyprus, 2004.

[97] Y. Yang, A. A. Minai, and M. M. Polycarpou, "Decentralized Cooperative Search by Networked UAVs in an Uncertain Environment," presented at American Control Conference, Boston, MA, USA, 2004.

[98] E. U. Acar and H. Choset, "Sensor-based Coverage of Unknown Environments: Incremental Construction of Morse Decompositions," *International Journal of Robotics Research*, vol. 21, pp. 345 - 366, 2002.

[99] C. G. Cassandras and W. Li, "Sensor Networks and Cooperative Control," *European Journal of Control*, vol. 11, pp. 436 - 463, 2005.

[100] Z.-D. Wang, E. Nakano, and T. Matsukawa, "Cooperating Multiple Behavior-Based Robots for Object Manipulation," presented at IEEE/RSJ/GI International Conference on Intelligent Robots and Systems '94, 'Advanced Robotic Systems and the Real World' IROS '94, Munich, Germany, 1994.

[101] B. R. Donald, J. Jennings, and D. Rus, "Analyzing Teams of Cooperating Mobile Robots," presented at IEEE International Conference on Robotics and Automation, San Diego, CA, USA, 1994.

[102] D. J. Stilwell and J. S. Bay, "Toward the Development of a Material Transport System Using Swarms of Ant-Like Robots," presented at IEEE International Conference on Robotics and Automation, Atlanta, GA, USA, 1993.

[103] Y. Yamauchi, J. K. Tan, S. Ishikawa, and K. Kato, "On the Development of a Cooperative Work Strategy by Mulitple Robots," presented at 34th SICE Annual Conference, Hokkaido, Japan, 1995.

[104] G. Lionis and K. J. Kyriakopoulos, "Centralized Motion Planning for a Group of Micro Agents Manipulating a Rigid Object," presented at 13th Mediterranean Conference on Control and Automation, Limassol, Cyprus, 2005.

[105] H. V. D. Parunak, S. A. Brueckner, and J. J. Odell, "Swarming Coordination of Multiple UAVs for Collaborative Sensing," presented at 2nd AIAA Unmanned Unlimited Systems Technologies and Operations Aerospace Land and Sea Conference, San Diego, CA, USA, 2003.

[106] M. A. Kovacina, D. Palmer, G. Yang, and R. Vaidyanathan, "Multi-Agent Control Algorithms for Chemical Cloud Detection and Mapping Using Unmanned Air Vehicles," presented at IEEE International Conference on Intelligent Robots and Systems (ROS), Lausanne, Switzerland, 2002.

[107] K. P. Sycara, "Multiagent Systems," in *AI Magazine*, vol. 19, 1998, pp. 79-92.

[108] A. Ryan, M. Zennaro, A. Howell, R. Sengupta, and J. K. Hedrick, "An Overview of Emerging Results in Cooperative UAV Control," presented at 43rd IEEE Conference on Decision and Control, Atlantis, Paradise Island, Bahamas, 2004.

[109] D. M. Hart and P. A. Craig-Hart, "Reducing Swarming Theory to Practice for UAV Control," presented at IEEE Aerospace Conference, Big Sky, MT, USA, 2004.

[110] F. Y. Hadaegh, W.-M. Lu, and P. K. C. Wang, "Adaptive Control of Formation Flying Spacecraft for Interferometry," presented at IFAC, Madrid, Spain, 1998.

[111] J. P. Desai, J. P. Ostrowski, and V. Kumar, "Modeling and Control of Formations of Nonholonomic Mobile Robots," *IEEE Transactions on Robotics and Automation*, vol. 17, pp. 905-908, 2001.

[112] J. P. Desai, "A Graph Theoretic Approach for Modeling Mobile Robot Team Formations," *Journal of Robotic Systems*, vol. 19, pp. 511-525, 2002.

[113] C. Belta and V. Kumar, "Motion Generation for Formations of Robots: A Geometric Approach," presented at IEEE International Conference on Robots and Automata, Seoul, Korea, 2001.

[114] R. Bhatt, C. P. Tang, and V. Krovi, "Geometric Motion Planning and Formation Optimization for a Fleet of Nonholonomic Wheeled Mobile Robots," presented at IEEE International Conference on Robotics and Automation, New Orleans, LA, USA, 2004.

[115] M. Chaves, R. Day, L. Gomez-Ramos, P. Nag, A. Williams, and W. Zhang, "Vehicle Networks: Achieving Regular Formations," presented at American Control Conference, Denver, CO, USA, 2003.

[116] D. V. Dimarogonas and K. J. Kyriakopoulos, "Formation Control and Collision Avoidance for Multi-Agent Systems and a Connection Between Formation

Infeasibility and Flocking Behaviour," presented at 44th IEEE Conference on Decision and Control and 2005 European Control Conference (CDC-ECC '05), Seville, Spain, 2005.

[117] M. Egerstedt and X. Hu, "Formation Constrained Multi-agent Control," *IEEE Transactions on Robotics and Automation*, vol. 17, pp. 947 - 951, 2001.

[118] R. Fierro, P. Song, A. Das, and V. Kumar, "Cooperative Control of Robot Formations," in *Cooperative Control and Optimization*, vol. 66, *Applied Optimization*: Springer US, 2002, pp. 73 - 93.

[119] J. M. Fowler and R. D. Andrea, "Distributed Control of Close Formation Flight," presented at 41st IEEE Conference on Decision and Control, Las Vegas, Nevada, USA, 2002.

[120] Z. Jin and R. M. Murray, "Double-Graph Control Strategy of Multi-Vehicle Formations," presented at 43rd IEEE Conference on Decision and Control, Atlantis, Paradise Island, Bahamas, 2004.

[121] G. Lafferriere, A. Williams, J. Caughman, and J. J. P. Veerman, "Decentralized Control of Vehicle Formations," *Systems & Control Letters*, vol. 54, pp. 899 - 910, 2005.

[122] M. A. Lewis and K.-H. Tan, "High Precision Formation Control of Mobile Robots Using Virtual Structures," *Autonomous Robots*, vol. 4, pp. 387 - 403, 1997.

[123] P. Ögren, E. Fiorelli, and N. E. Leonard, "Formations with a mission: Stable Coordination of vehicle group maneuvers," presented at Symposium of Mathematical Theory Networks, Notre Dame, IN, 2002.

[124] R. Olfati-Saber and R. M. Murray, "Graph Rigidity and Distributed Formation Stabilization of Multi-Vehicle Systems," California Institute of Technology, Pasadena, California CDC02-INV2103, February 2001.

[125] Y.-L. Chuang, Y. R. Huang, M. R. D'Orsogna, and A. L. Bertozzi, "Multi-Vehicle Flocking: Scalability of Cooperative Control Algorithms Using Pairwise Potentials," presented at IEEE International Conference on Robotics and Automation, Roma, Italy, 2007.

[126] N. Moshtagh, A. Jadbabaie, and K. Daniilidis, "Distributed Geodesic Control Laws for Flocking of Nonholonomic Agents," presented at 44th IEEE Conference on Decision and Control, Seville Spain, 2005.

[127] H. G. Tanner, A. Jadbabaie, and G. J. Pappas, "Stable Flocking of Mobile Agents, Part I: Fixed Topology," presented at 42nd IEEE Conference on Decision and Control, Maui, HI, USA, 2003.

[128] H. G. Tanner, A. Jadbabaie, and G. J. Pappas, "Stable Flocking of Mobile Agents, Part II: Dynamic Topology," presented at 42nd IEEE Conference on Decision and Control, Maui, HI, USA, 2003.

[129] J. J. P. Veerman, G. Lafferriere, J. S. Caughman, and A. Williams, "Flocks and Formations," *Journal of Statistical Physics*, vol. 121, pp. 901 - 936, 2005.

[130] S. Murata, H. Kurokawa, and K. Shigeru, "Self-Assembling Machine," presented at IEEE International Conference on Robotics and Automation, San Diego, CA, USA, 1994.

[131] J. Bellingham, M. Tillerson, A. Richards, and J. P. How, "Multi-Task Allocation and Path Planning for Cooperating UAVs," presented at 2nd Annual Conference on Cooperative Control and Optimization, Gainesville, FL, USA, 2001.

[132] M. A. Darrah, W. M. Niland, and B. M. Stolarik, "Multiple UAV Dynamic Task Allocation Using Mixed Integer Linear Programming in a SEAD Mission," presented at Infotech@Aerospace, Arlington, VA, USA, 2005.

[133] M. Alighanbari and J. P. How, "Decentralized Task Assignment for Unmanned Aerial Vehicles," presented at 44th IEEE Conference on Decision and Control, and the European Control Conference, Seville, Spain, 2005.

[134] M. Scheutz, P. Schermerhorn, and P. Bauer, "The Utility of Heterogeneous Swarms of Simple UAVs with Limited Sensory Capacity in Detection and Tracking Tasks," presented at IEEE Swarm Intelligence Symposium, Pasadena, CA, USA, 2005.

[135] M. Kafil and I. Ahmad, "Optimal Task Assignment in Heterogeneous Distributed Systems," *IEEE Concurrency*, vol. 6, pp. 42 - 51, 1998.

[136] T. Schouwenaars, B. D. Moor, E. Feron, and J. How, "Mixed Integer Programming for Multi-Vehicle Path Planning," presented at European Control Conference, Porto, Portugal, 2001.

[137] P.-A. Bliman and G. Ferrari-Trecate, "Average Consensus Problems in Networks of Agents with Delayed Communications," presented at 44th IEEE Conference on Decision and Control, Seville, Spain, 2005.

[138] V. D. Blondel, J. M. Hendrickx, A. Olshevsky, and J. N. Tsitsiklis, "Convergence in multiagent, coordination, consensus, and flocking," presented at 44th IEEE Conference on Decision and Control, Seville, Spain, 2005.

[139] M. Mehyar, D. Spanos, J. Pongsjapan, S. H. Low, and R. M. Murray, "Distributed Averaging on Asynchronous Communication Networks," presented at 44th IEEE Conference on Decision and Control, 2005 and 2005 European Control Conference, Seville, Spain, 2005.

[140] L. Fang, P. J. Antsaklis, and A. Tzimas, "Asynchronous Consensus Protocols: Preliminary Results, Simulations and Open Questions," presented at 44th IEEE Conference on Decision and Control, 2005 and 2005 European Conference, Seville, Spain, 2005.

[141] J. N. Tsitsiklis, D. P. Bertsekas, and M. Athans, "Distributed Asynchronous Deterministic and Stochastic Gradient Optimization Algorithms," *IEEE Transactions on Automatic Control*, vol. AC-31, pp. 803 - 812, 1986.

[142] M. Dorigo, V. Trianni, E. Sahin, T. H. Labella, R. Gross, G. Baldassare, S. Nolfi, J.-L. Deneubourg, F. Mondada, D. Floreano, and L. M. Gambardella, "Evolving Self-Organizing Behaviors for a Swarm-bot," *Autonomous Robots*, vol. 17, pp. 223-245, 2003.

[143] D. S. Morgan and I. B. Schwartz, "Dynamic Coordinated Control Laws in Multiple Agent Models," *Physics Letters A*, vol. 340, pp. 121 - 131, 2005.

[144] J. A. Fax and R. M. Murray, "Graph Laplacians and Stabilization of Vehicle Formations," presented at IFAC World Congress, Barcelona, Spain, 2002.

[145] J. A. Fax and R. M. Murray, "Information Flow and Cooperative Control of Vehicle Formations," *IEEE Transactions on Automatic Control*, vol. 49, pp. 1465 - 1476, 2004.

[146] M. Mesbahi, "On State-Dependent Dynamic Graphs and their Controllability Properties," *IEEE Transactions on Automatic Control*, vol. 50, pp. 387 - 392, 2005.

[147] A. Muhammad, "Graphs, Simplicial Complexes and Beyond: Topological Tools for Multi-agent Coordination," Doctor of Philosophy, Georgia Institute of Technology, 2005.

[148] M. M. Zavlanos and G. J. Pappas, "Controlling Connectivity of Dynamic Graphs," presented at IEEE Conference on Decision and Control, and the European Control Conference, Seville, Spain, 2005.

[149] M. N. Huhns and L. M. Stephens, "Multiagent Systems and Societies of Agents," in *Multiagent Systems: A Modern Approach to Distributed Artificial Intelligence*, G. Weiss, Ed. London: The MIT Press, 1999, pp. 79 - 121.

[150] J. A. Fax, "Optimal and Cooperative Control of Vehicle Formations," California Institute of Technology, Pasadena, California, 2002.

[151] M. Tummala, C. C. Wai, and P. Vincent, "Distributed Beamforming in Wireless Sensor Networks," presented at Conference Record of the 39th Asilomar Conference on Signals, Systems, and Computers, Pacific Grove, CA, USA, 2005.

[152] E. Potter and J. Saillard, "Polarimetry Concept Applied to "High Resolution Electromagnetic Radar Imaging"," presented at Antennas and Propagation Society International Symposium, San Jose, CA, USA, 1989.

[153] Y. K. Lam, E. K. Wong, and C. K. Loo, "Explicit Communication in Designing Efficient Cooperative Mobile Robotic Systems," presented at IEEE International Conference on Robotics and Automation, Taipei, Taiwan, 2003.

[154] P. Dasgupta, S. O'Hara, and P. Petrov, "A Multi-agent UAV Swarm for Automatic Target Recognition," in *Defence Applications of Multi-Agent Systems*, vol. 3890/2006, *Lecture Notes in Computer Science*, J. G. Carbonell and J. Siekmann, Eds. Berlin: Springer Berlin/Heidelberg, 2006, pp. 80 - 91.

[155] T. X. Brown, S. Doshi, S. Jadhav, and J. Himmelstein, "Test Bed for a Wireless Network for Small UAVs," presented at AIAA 3rd Unmanned Unlimited Technical Conference, Chicago, IL, USA, 2004.

[156] W. Sheng, Q. Yang, and Y. Guo, "Cooperative Driving Based on Inter-vehicle Communications: Experimental Platform and Algorithm," presented at IEEE/RSJ International Conference on Intelligent Robots and Systems, Beijing, China, 2006.

[157] X. Yang, J. Liu, F. Zhao, and N. Vaidya, "A Vehicle-to-Vehicle Communication Protocol for Cooperative Collision Warning," presented at First Annual International Conference on Mobile and Ubiquitous Systems: Networking and Services, Urbana, IL, USA, 2004.

[158] Y. Kunyiyoshi, N. Kita, S. Rougeaux, S. Sakane, M. Ishii, and M. Kakikura, "Cooperation by Observation - the Framework and Basic Task Patterns," presented at IEEE International Conference on Robotics and Automation, San Diego, CA, USA, 1994.

[159] Y. Kunyiyoshi, J. Riekki, M. Ishii, S. Rougeaux, N. Kita, S. Sakane, and M. Kakikura, "Vision-based Behaviours for Multi-Robot Cooperation," presented at IEEE/RSJ International Conference Intelligent Robots and Systems, Munich, Germany, 1994.

[160] P. G. Otanez and M. E. Campbell, "Hybrid Cooperative Reconnaissance without Communication," presented at 44th IEEE Conference on Decision and Control, and the European Control Conference, Seville, Spain, 2005.

[161] R. Beckers, O. E. Holland, and J.-L. Deneubourg, "From Local Actions to Global Tasks: Stigmergy and Collective Robotics," in *Proceedings of Artificial-Life IV*: MIT Press, 1994.

[162] R. C. Arkin, "Cooperation without Communication: Multiagent Schema-based Robot Navigation," *Journal of Robotic Systems*, vol. 9, pp. 351 - 364, 1992.

[163] H. V. D. Parunak and S. A. Brueckner, "Ant-like missionaries and cannibals: Synthetic Pheromones for Distributed Motion Control," presented at 4th International Conference on Autonomous Agents, Barcelona, Spain, 2000.

[164] S. A. Brueckner and H. V. D. Parunak, "Multiple Pheromones for Improved Guidance," presented at 2nd DARPA-JFACC Symposium on Advances in Enterprise Control, Minneapolis, MN, USA, 2000.

[165] H. V. D. Parunak, M. Purcell, and R. O'Connell, "Digital Pheromones for Autonomous Coordination of Swarming UAV's," presented at First AIAA Unmanned Aerospace Vehicles, Systems, Technologies, and Operations Conference, Portsmouth, VA, USA, 2002.

[166] Y. U. Cao, A. S. Fukunaga, and A. B. Kahng, "Cooperative Mobile Robotics: Antecdents and Directions," *Autonomous Robots*, vol. 4, pp. 1 - 23, 1997.

[167] C. Belta and V. Kumar, "Abstraction and Control for Groups of Robots," *IEEE Transactions on Robotics*, vol. 20, pp. 865 - 875, 2004.

[168] L. Chaimowicz and V. Kumar, "A Framework for the Scalable Control of Swarms of Unmanned Ground Vehicles with Unmanned Aerial Vehicles," presented at 10th International Conference on Robotics and Remote Systems for Hazardous Environments, Gainesville, FL, USA, 2004.

[169] G. S. Sukhatme, J. F. Montgomery, and R. T. Vaughan, "Experiments with Cooperative Aerial-Ground Robots," in *Robot Teams: From Diversity to Polymorphism*, T. Balch and L. E. Parker, Eds.: A. K. Peters, Ltd., 2001.

[170] B. J. Capozzi and J. Vagners, "Evolution as a Guide for Autonomous Vehicle Path Planning and Coordination," presented at IEEE Aerospace Conference, Big Sky, MT, USA, 2002.

[171] A. Pongpunwattana and R. Rysdyk, "Real-Time Planning for Multiple Autonomous Vehicles in Dynamic Uncertain Environments," *Journal of Aerospace Computing, Information, and Communication*, vol. 1, pp. 580 - 604, 2005.

[172] J. Bellingham, M. Tillerson, M. Alighanbari, and J. P. How, "Cooperative Path Planning for Multiple UAVs in Dynamic and Uncertain Environments," presented at 41st IEEE Conference on Decision and Control, Las Vegas, NV, USA, 2002.

[173] S. Zelinski, T. J. Koo, and S. Sastry, "Optimization-based formation reconfiguration planning for autonomous vehicles," presented at IEEE International Conference on Robotics and Automation, Taipei, Taiwan, 2003.

[174] R. Fierro and K. Wesselowski, "Optimization-Based Control of Multi-Vehicle Systems," in *Cooperative Control*, vol. 309/2004, *Lecture Notes in Control and Information Sciences*, V. Kumar, N. E. Leonard, and A. S. Morse, Eds. Berlin: Springer Berling/Heidelberg, 2005, pp. 63 - 78.

[175] D. Fogel and L. Fogel, "Optimal Routing of Multiple Autonomous Underwater Vehicles through Evoluionary Programming," presented at Symposium on Autonomous Underwater Vehicle Technology, Washington DC, USA, 1990.

[176] C. Belta and V. Kumar, "Trajectory Design for Formations of Robots by Kinetic Energy Shaping," presented at IEEE International Conference on Robotics and Automation, Washington DC, USA, 2002.

[177] M. Adams, W. Hall, M. Hanson, G. Zacharias, W. McEneaney, and B. Fitzpatrick, "Mixed Initiative Planning and Control Under Uncertainty," presented at 1st AIAA Unmanned Aerospace Vehicles, Systems, Technologies, and Operations Conference and Workship, Portsmouth, VA, USA, 2002.

[178] L. Chaimowicz, N. Michael, and V. Kumar, "Controlling Swarms of Robots using Interpolated Implicit Functions," presented at IEEE International Conference on Robotics and Automation, Barcelona, Spain, 2005.

[179] T. Fukuda and S. Nakagawa, "Dynamically Reconfigurable Robotic System," presented at IEEE International Conference on Robotics and Automation, Philadelphia, PA, USA, 1988.

[180] T. Fukuda, S. Nakagawa, Y. Kawauchi, and M. Buss, "Structure Decision method for Self Organising Robots based on Cellstructures-CEBOT," presented at IEEE International Conference on Robotics and Automation, Scottsdale, AZ, USA, 1989.

[181] G. Beni, "The Conept of Cellular Robotic System," presented at Third IEEE International Symposium on Intelligent Control, Arlington, VA, USA, 1988.

[182] S. Hackwood and G. Beni, "Self-organization of Sensors for Swarm Intelligence," presented at IEEE International Conference on Robotics and Automation, Nice, France, 1992.

[183] H. Asama, A. Matsumoto, and Y. Ishida, "Design of an Automonous And Distributed Robot System: Actress," presented at IEEE/RSJ International Workshop on Intelligent Robots and Systems, Tsukuba, Japan, 1989.

[184] L. E. Parker, "On the Design of Behaviour-based Multi-robot Teams," *Journal of Advanced Robotics*, vol. 10, pp. 521 - 568, 1996.

[185] L. E. Parker, "ALLIANCE: An Architecture for Fault-Tolerant Multi-Robot Cooperation," *IEEE Transactions on Robotics and Automation*, vol. 14, pp. 220 - 240, 1998.

[186] H. Asama, M. K. Habib, I. Endo, K. Ozaki, A. Matsumoto, and Y. Ishida, "Functional Distribution Among Multiple Mobile Robots in an Autonomous and Decentralized Robot System," presented at IEEE International Conference on Robotics and Automation, Sacramento, CA, USA, 1991.

[187] L. E. Parker, "Designing Control Laws for Cooperative Agent Teams," presented at IEEE International Conference on Robotics and Automation, Atlanta, GA, USA, 1993.

[188] N. E. Leonard and E. Fiorelli, "Virtual Leaders, Artificial Potentials and Coordinated Control of Groups," presented at 40th IEEE Conference on Decision and Control, Orlando, FL, USA, 2001.

[189] M. Egerstedt, X. Hu, and A. Stotsky, "Control of Mobile Platforms Using a Virtual Vehicle Approach," *IEEE Transaction on Automatic Control*, vol. 46, pp. 1777 - 1782, 2001.

[190] D. M. Stipanovic, G. Inalhan, R. Teo, and C. J. Tomlin, "Decentralized Overlapping Control of a Formation of Unmanned Aerial Vehicles," *Automatica*, vol. 40, pp. 1285-1296, 2004.

[191] E. W. Justh and P. S. Krishnaprasad, "A Simple Control Law for UAV Formation Flying," Institute for Systems Research TR 2002-38, 2002.

[192] G. H. Elkaim and M. Siegel, "A Lightweight Control Methodology for Formation Control of Vehicle Swarms," presented at IFAC, Prague, Czech Republic, 2005.

[193] G. H. Elkaim and R. J. Kelbley, "Extension of a Lightweight Formation Control Methodology to Groups of Autonomous Vehicles," presented at 8th International Symposium on Artificial Intelligence, Robotics and Automation in Space, Munich, Germany, 2005.

[194] L. Fang and P. J. Antsaklis, "Decentralized Formation Tracking of Multi-vehicle Systems with Nonlinear Dynamics," presented at 14th Mediterranean Conference on Control and Automation, Ancona, Italy, 2006.

[195] T. Balch and R. C. Arkin, "Behavior-based Formation Control for Multirobot Teams," *IEEE Transactions on Robotics and Automation*, vol. 14, pp. 926 - 939, 1998.

[196] T. Balch and M. Hybinette, "Social Potentials for Scalable Multi-Robot Formations," presented at IEEE International Conference on Robotics and Automation, San Francisco, CA, USA, 2000.

[197] J. P. Desai, "Modelling Multiple Teams of Mobile Robots: A Graph Theoretic Approach," presented at IEEE/RSJ International Conference on Intelligent Robots and Systems, Maui, HI, USA, 2001.

[198] J. A. Marshall and M. E. Broucke, "On Invariance of Cyclic Group Symmetries in Multiagent Formations," presented at 44th IEEE Conference on Decision and Control, 2005 and 2005 European Control Conference, Seville, Spain, 2005.

[199] A. Muhammad and M. Egerstedt, "Connectivity Graphs as Models of Local Interactions," presented at 43rd IEEE Conference on Decision and Control, Atlantis, Paradise Island, Bahamas, 2004.

[200] R. Olfati-Saber and R. M. Murray, "Agreement Problems in Networks with Directed Graphs and Switching Topology," presented at 42nd IEEE Conference on Decision and Control, Maui, HI, USA, 2003.

[201] M. Mesbahi, "On a Dynamic Extension of the Theory of Graphs," presented at 2002 American Control Conference, Anchorage, AK, 2002.

[202] M. Mesbahi, "State-Dependent Graphs," presented at 42nd IEEE Conference on Decision and Control, Maui, HI, USA, 2003.

[203] Y. Kim and M. Mesbahi, "On Maximizing the Second Smallest Eigenvalue of a State-dependent Graph Laplacian," presented at 2005 American Control Conference, Portland, OR, USA, 2005.

[204] H. Tanner, "On the Controllability of Nearest Neighbour Interconnections," presented at IEEE Conference on Decision and Control, Atlantis, Paradise Island, Bahamas, 2004.

[205] G. Lafferriere, J. Caughman, and A. Williams, "Graph Theoretic Methods in the Stability of Vehicle Formations," presented at American Control Conference, Boston, MA, USA, 2004.

[206] C. Gonazalez and K. A. Morgansen, "Stabilization of Dynamic Vehicle Formation Configurations Using Graph Laplacians," presented at IFAC World Congress, Prague, Czech Republic, 2005.

[207] J. A. Marshall, M. E. Broucke, and B. A. Francis, "Formations of Vehicles in Cyclic Pursuit," *IEEE Transactions on Automatic Control*, vol. 49, pp. 1963 - 1974, 2004.

[208] W. Ren and R. W. Beard, "Consensus Seeking in Multiagent Systems Under Dynamically Changing Interaction Topologies," *IEEE Transactions on Automatic Control*, vol. 50, pp. 655 - 661, 2005.

[209] L. Fang and P. J. Antsaklis, "Information Consensus of Asynchronous Discrete-time Multi-agent," presented at American Control Conference, Portland, OR, USA, 2005.

[210] N. Michael, C. Belta, and V. Kumar, "Controlling Three Dimensional Swarms of Robots," presented at IEEE International Conference on Robotics and Automation, Orlando, FL, USA, 2006.

[211] W. Ren, R. W. Beard, and T. W. McLain, "Coordination Variables and Consensus Building in Multiple Vehicle Systems," in *Series Lecture Notes in Control and Information Sciences*, vol. 309, V. Kumar, N. E. Leonard, and A. S. Morse, Eds. Block Island: Springer-Verlag, 2003, pp. 171 - 188.

[212] P. R. Chandler, M. Pachter, and S. Rasmussen, "UAV Cooperative Control," presented at American Control Conference, Arlington, VA, USA, 2001.

[213] J. Lin, A. S. Morse, and B. D. O. Anderson, "The Multi-Agent Rendezvous Problem," presented at 42nd IEEE Conference on Decision and Control, Maui, HI, USA, 2003.

[214] D. Bauso, L. Giarre, and R. Pesenti, "Attitude Alignment of a Team of UAVs under Decentralized Information Structure," presented at IEEE International Conference on Control Applications, Istanbul, Turkey, 2003.

[215] O. Ilaya and C. Bil, "Distributed and Cooperative Decision Making for Multi-UAV Systems with Applications to Electronic Warfare," presented at 7th AIAA Aviation Technology, Integration and Operations Conference, Belfast, Northern Ireland, 2007.

[216] G. Inalhan, D. M. Stipanovic, and C. J. Tomlin, "Decentralized Optimization, with Application to Multiple Aircraft Coordination," presented at 41st IEEE Conference on Decision and Control, Las Vegas, NV, USA, 2002.

[217] B. Johansson, C. M. Carretti, and M. Johansson, "On Distributed Optimisation using Peer-to-Peer Communications in Wireless Sensor Networks," presented at 5th Annual IEEE Communications Society Conference on Sensor, Mesh, Ad Hoc Communications and Networks, San Francisco, CA, USA, 2008.

[218] B. Johansson, A. Speranzon, M. Johansson, and K. H. Johansson, "Distributed Model Predictive Consensus," presented at 17th International Symposium on Mathematical Theory of Networks and Systems, Kyoto, Japan, 2006.

[219] R. W. Beard, T. W. McLain, D. Nelson, D. Kingston, and D. Johanson, "Decentralized Cooperative Aerial Surveillance using Fixed-Wing Miniature UAVs," *Proceedings of the IEEE*, vol. 94, pp. 1306 - 1324, 2006.

[220] D. V. Dimarogonas and K. J. Kyriakopoulos, "On the Rendezvous Problem for Multiple Nonholonomic Agents," *IEEE Transactions on Automatic Control*, vol. 52, pp. 916 - 922, 2007.

[221] S. Martínez, J. Cortes, and F. Bullo, "On Robust Rendezvous for Mobile Autonomous Agents," presented at IFAC World Congress, Prague, Czech Republic, 2005.

[222] S. L. Smith, "Strategies for Rendezvous and Formation Stabilization of Multi-agent Systems," Master of Applied Science, University of Toronto, Toronto, 2005.

[223] S. L. Smith, M. E. Broucke, and B. A. Francis, "Curve Shortening and its Application to Multi-agent Systems," presented at 44th IEEE Conference on Decision and Control, 2005 and 2005 European Control Conference, 2005, Seville, Spain, 2005.

[224] J. Cortés, S. Martínez, and F. Bullo, "Robust Rendezvous for Mobile Autonomous Agents via Proximity Graphs in Arbitrary Dimensions," *IEEE Transactions on Automatic Control*, vol. 51, pp. 1289 - 1298, 2004.

[225] J. R. Lawton, B. J. Young, and R. W. Beard, "A Decentralized Approach to Elementary Formation Maneuvers," presented at IEEE International Conference on Robotics and Automation, San Francisco, CA, USA, 2000.

[226] W. Ren, "Consensus Strategies for Cooperative Control of Vehicles Formations," *IET Control Theory and Applications*, vol. 1, pp. 505 - 512, 2007.

[227] W. Ren, "Consensus Based Formation Control Strategies for Multi-Vehicle Systems," presented at American Control Conference, Minneapolis, MN, USA, 2006.

[228] D. V. Dimarogonas and K. J. Kyriakopoulos, "A Connection Between Formation Control and Flocking Behavior in Nonholonomic Multiagent Systems," presented at IEEE Conference on Robotics and Automation, Orlando, FL, USA, 2006.

[229] R. Olfati-Saber, "Flocking for Multi-Agent Dynamic Systems: Algorithms and Theory," *IEEE Transaction on Automatic Control*, vol. 51, pp. 401 - 420, 2006.

[230] H. G. Tanner, A. Jadbabaie, and G. J. Pappas, "Flocking in Fixed and Switching Networks," *Submitted to IEEE Transactions on Automatic Control*, 2005.

[231] P. Ögren, E. Fiorelli, and N. E. Leonard, "Cooperative Control of Mobile Sensor Networks: Adaptive Gradient Climbing in a Distributed Environment," *IEEE Transactions on Automatic Control*, vol. 49, pp. 1292 - 1302, 2004.

[232] D. P. Spanos, R. Olfati-Saber, and R. M. Murray, "Dynamic Consensus on Mobile Networks," presented at 16th IFAC World Congress, Prague, Czech Republic, 2005.

[233] R. Olfati-Saber and R. M. Murray, "Consensus Problems in Networks of Agents with Switching Topology and Time-Delays," *IEEE Transactions on Automatic Control*, vol. 49, pp. 1520 - 1533, 2004.

[234] J. Cortés, "Finite-time Convergent Gradient Flows with Applications to Network Consensus," *Automatica*, vol. 42, pp. 1993 - 2000, 2006.

[235] W. Ren, R. W. Beard, and E. M. Atkins, "Information Consensus in Multivehicle Cooperative Control," in *IEEE Control Systems Magazine*, 2007, pp. 71 - 82.

[236] R. Olfati-Saber and R. M. Murray, "Consensus Protocols for Networks of Dynamic Agents," presented at American Control Conference, Denver, CO, USA, 2003.

[237] L. Moreau, "Stability of Continuous-Time Distributed Consensus Algorithms," presented at 43rd IEEE Conference on Decision and Control, Atlantis, Paradise Island, Bahamas, 2004.

[238] W. Ren, "Consensus Seeking, Formation Keeping, and Trajectory Tracking in Multiple Vehicle Cooperative Control," Doctor of Philosophy, Brigham Young University, 2004.

[239] L. Moreau, "Stability of Multiagent Systems with Time-Dependent Communication Links," *IEEE Transactions on Automatic Control*, vol. 50, pp. 169 - 182, 2005.

[240] W. Ren, "Second-order Consensus Algorithm with Extensions to Switching Topologies and Reference Models," presented at American Control Conference, New York City, NY, USA, 2007.

[241] W. Yang, A. L. Bertozzi, and W. Xiaofan, "Stability of a Second Order Consensus Algorithm with Time Delay," presented at 47th IEEE Conference on Decision and Control, Cancun, Mexico, 2008.

[242] M. Fiedler, "Algebraic Connectivity of Graphs," *Czechoslovak Mathetmatical Journal*, vol. 23, pp. 298 - 305, 1973.

[243] Z. Cao, M. Tan, S. Wang, Y. Fan, and B. Zhang, "The Optimization Resarch of Formation Control for Multiple Mobile Robots," presented at 4th World Congress on Intelligent Control and Automation, Shanghai, P. R. China, 2002.

[244] H. G. Tanner, A. Jadbabaie, and G. J. Pappas, "Coordination of Multiple Autonomous Agents," presented at 11th Mediterranean Conference on Control and Automation, Rhodes, Greece, 2003.

[245] W. Ren and E. M. Atkins, "Distributed Multi-vehicle Coordination Control via Local Information Exchange," *International Journal of Robust and Nonlinear Control*, vol. 17, pp. 1002 - 1033, 2007.

[246] R. M. Murray, "Recent Research in Cooperative Control of Multivehicle Systems," *Journal of Dynamic Systems, Measurement, and Control*, vol. 129, pp. 771 - 583, 2007.

[247] R. L. Raffard, C. J. Tomlin, and S. P. Boyd, "Distributed Optimization for Cooperative Agents: Application to Formation Flight," presented at 2004 IEEE Conference on Decision and Control, Nassau, Bahamas, 2004.

[248] A. Chaudhry, K. Misovec, and R. D'Andrea, "Low Observability Path Planning for an Unmanned Aerial Vehicle Using Mixed Integer Linear Programming," presented at 43rd IEEE Conference on Decision and Control, Atlantis, Paradise Island, Bahamas, 2004.

[249] A. Richards and J. P. How, "Aircraft Trajectory Planning with Collision Avoidance Using Mixed Integer Linear Programming," presented at American Control Conference, Anchorage, AK, 2002.

[250] J. Peng and S. Akella, "Coordinating Multiple Robots with Kinodynamic Constraints along Specified Paths," in *Algorithmic Foundations of Robotics V*, vol. 7. Berlin: Springer Berlin/Heidelberg, 2002, pp. 221 - 238.

[251] T. Shibata and T. Fukuda, "Coordinative Behavior in Evolutionary Multi-Agent System by Genetic Algorithm," presented at IEEE International Conference on Neural Networks, San Francisco, CA, USA, 1993.

[252] A. Pongpunwattana, R. Wise, R. Rysdyk, and A. J. Kang, "Multi-vehicle Cooperative Control Flight Test," presented at 25th Digital Avionics Systems Conference, Orlando, FL, USA, 2006.

[253] D. Soloway and P. J. Haley, "Aircraft Reconfiguration Using Neural Generalized Predictive Control," presented at American Control Conference, Arlington, VA, USA, 2001.

[254] C. Belta and V. Kumar, "Optimal Motion Generation for Groups of Robots: A Geometric Approach," *ASME Journal of Mechanical Design*, vol. 126, pp. 63 - 70, 2004.

[255] F. Bullo, "Trajectory Design for Mechanical Control Systems: from Geometry to Algorithms," *European Journal of Control*, vol. 10, pp. 397 - 410, 2004.

[256] Y. Kuwata, A. Richards, T. Schouwenaars, and J. P. How, "Decentralized Robust Receding Horizon Control for Multi-vehicle Guidance," presented at American Control Conference, Minneapolis, MN, USA, 2006.

[257] A. Richards and J. How, "A Decentralized Algorithm for Robust Constrained Model Predictive Control," presented at American Control Conference, Boston, MA, USA, 2004.

[258] T. Schouwenaars, J. How, and E. Feron, "Decentralized Cooperative Trajectory Planning of Multiple Aircraft with Hard Safety Guarantees," presented at AIAA Guidance, Navigation and Control Conference, Providence, RI, USA, 2004.

[259] T. Schouwenaars, M. Valenti, E. Feron, and J. How, "Implementation and Flight Test Results of MILP-based UAV Guidance," presented at IEEE Aerospace Conference, Big Sky, MT, USA, 2005.

[260] D. Jia and B. H. Krogh, "Distributed Model Predictive Control," presented at American Control Conference, Arlington, VA, 2001.

[261] N. Motee and A. Jadbabaie, "Distributed Receding Horizon Control of Spatially Invariant Systems," presented at American Control Conference, Minneapolis, MN, USA, 2006.

[262] N. Motee and B. Sayyar-Rodsari, "Optimal Partitioning in Distributed Model Predictive Control," presented at American Control Conference, Denver, CO, USA, 2003.

[263] T. Keviczky, F. Borelli, and G. J. Balas, "A Study on Decentralized Receding Horizon Control for Decoupled Systems," presented at American Control Conference, Boston, MA, USA, 2004.

[264] T. Keviczky and G. J. Balas, "Flight Test of a Receding Horizon Controller for Autonomous UAV Guidance," presented at 2005 American Control Conference, Portland, OR, USA, 2005.

[265] T. Keviczky, "Decentralized Receding Horizon Control for Large Scale Dynamically Decoupled Systems," Doctor of Philosophy, University of Minnesota, 2005.

[266] F. Borelli, T. Keviczky, K. Fregene, and G. J. Balas, "Decentralized Receding Horizon Control of Cooperative Vehicle Formations," presented at 44th IEEE Conference on Decision and Control, and the European Control Conference, Seville, Spain, 2005.

[267] W. B. Dunbar, "Distributed Receding Horizon Control of Multiagent Systems," California Institute of Technology, Pasadena, California, 2004.

[268] W. B. Dunbar, "Distributed Receding Horizon Control of Coupled Nonlinear Oscillators: Theory and Application," presented at IEEE Conference on Decision and Control, San Diego, CA, USA, 2006.

[269] W. B. Dunbar and R. M. Murray, "Model Predictive Control of Coordinated Multi-vehicle Formations," presented at IEEE Conference on Decision and Control, Las Vegas, NV, USA, 2002.

[270] W. B. Dunbar and R. M. Murray, "Distributed Receding Horizon Control for Multi-Vehicle Formation Stabilization," *Automatica,* vol. 42, pp. 549-558, 2006.

[271] Y. Kuwata and J. P. How, "Stable Trajectory Design for Highly Constrained Environment using Receding Horizon Control," presented at 2004 American Control Conference, Boston, MA, USA, 2004.

[272] E. Camponogara, D. Jia, B. H. Krogh, and S. Talukdar, "Distributed Model Predictive Control," *IEEE Control Systems Magazine,* vol. 22, pp. 44 - 52, 2002.

[273] T. Keviczky, F. Borelli, and G. J. Balas, "Stability Analysis of Decentralized RHC for Decoupled Systems," presented at 44th IEEE Conference on Decision and Control, 2005 European Control Conference, Seville, Spain, 2005.

[274] Y. Chen and Z. Wang, "Formation Control: A review and A New Consideration," presented at IEEE/RSJ International Conference on Intelligent Robots and Systems, Edmonton, Canada, 2005.

[275] D. H. Kim, H. O. Wang, G. Ye, and S. Shin, "Decentralized Control of Autonomous Swarm Systems Using Artificial Potential Functions: Analytical Design Guidelines," presented at 43rd IEEE Conference on Decision and Control, Atlantis, Paradise Island, Bahamas, 2004.

[276] R. A. Brooks, "A Robust Layered Control System for a Mobile Robot," *IEEE Journal of Robotics and Automation*, vol. RA-2, pp. 14 - 23, 1986.

[277] R. C. Arkin, "Motor Schema Based Navigation For A Mobile Robot: An Approach to Programming by Behavior," presented at IEEE International Conference on Robotics and Automation, Rayleigh, NC, USA, 1987.

[278] O. Khatib, "Real-Time Obstacle Avoidance for Manipulators and Mobile Robots," *International Journal of Robotics and Research*, vol. 5, pp. 90 - 98, 1986.

[279] S. S. Ge and Y. J. Cui, "New Potential Functions for Mobile Robot Path Planning," *IEEE Transactions on Robotics and Automation*, vol. 16, pp. 615 - 620, 2000.

[280] E. Rimon and D. E. Koditschek, "Exact Robot Navigation Using Artificial Potential Functions," *IEEE Transactions on Robotics and Automation*, vol. 8, pp. 501-518, 1992.

[281] K. Sigurd and J. How, "UAV Trajectory Design Using Total Field Collision Avoidance," presented at AIAA Guidance, Navigation, and Control Conference, Austin, TX, USA, 2003.

[282] S. Waydo, "Vehicle Motion Planning Using Stream Functions," California Institute of Technology, Pasadena, California CDS Technical Report 2003-001, May 2003.

[283] R. Olfati-Saber, "Flocking with Obstacle Avoidance," California Institute of Technology, Pasadena, California CIT-CDS 03-006, February 2003.

[284] R. Olfati-Saber, "Flocking for Multi-Agent Dynamic Systems: Algorithms and Theory," California Institute of Technology, Pasadena, California CIT-CDS 2004-005, June 2004.

[285] H. J. Kim, D. H. Shim, and S. Sastry, "Flying Robots: Sensing, Control and Decision Making," presented at IEEE International Conference on Robotics and Automation, Washington, DC, USA, 2002.

[286] G. H. Elkaim and R. J. Kelbley, "A Lightweight Formation Control Methodology for a Swarm of Non-holonomic Vehicles," presented at IEEE Aerospace Conference, Big Sky, MT, USA, 2006.

[287] H. G. Tanner and A. Kumar, "Towards Decentralization of Multi-robot Navigation Functions," presented at IEEE International Conference on Robotics and Automation, Barcelona, Spain, 2005.

[288] S. S. Ge, C.-H. Fua, and K. W. Lim, "Multi-robot Formations: Queues and Artificial Potential Trenches," presented at IEEE International Conference on Robotics and Automation, New Orleans, LA, USA, 2004.

[289] A. Howard, M. J. Mataric, and G. S. Sukhatme, "Mobile Sensor Network Deployment using Potential Fields: A Distributed, Scalable Solution to the Area Coverage Problem," presented at 6th International Symposium on Distributed Autonomous Robotics Systems, Fukuoka, Japan, 2002.

[290] C. Belta and V. Kumar, "Motion Generation for Groups of Robots: A Centralized, Geometric Approach," presented at ASME Design Engineering Technical Conference, Montreal, Canada, 2002.

[291] M. Zefran, V. Kumar, and C. B. Croke, "On the Generation of Smooth Three-Dimensional Rigid Body Motions," *IEEE Transactions on Robotics and Automation*, vol. 14, pp. 576 - 589, 1998.

[292] K.-H. Tan and M. A. Lewis, "Virtual Structures for High-Precision Cooperative Mobile Robotic Control," *IEEE/RSJ International Conference Intelligent Robots and Systems*, vol. 1, pp. 132 - 139, 1996.

[293] Y.-C. Lai, S. Chenney, and S. Fan, "Group Motion Graphs," presented at Eurographics/ACM SIGGRAPH Symposium on Computer Animation, Los Angeles, CA, USA, 2005.

[294] R. Olfati-Saber and R. M. Murray, "Distributed Cooperative Control of Multiple Vehicle Formations Using Structural Potential Functions," presented at 15th IFAC World Congress, Barcelona, Spain, 2002.

[295] H. G. Tanner, G. J. Pappas, and V. Kumar, "Leader-to-Formation Stability," *IEEE Transactions on Robotics and Automation*, vol. 20, pp. 443 - 455, 2004.

[296] B. Nabet and N. E. Leonard, "Shape Control of a Multi-agent System Using Tensegrity Structures," presented at 3rd IFAC Workshop on Lagrangian and Hamiltonian Methods for Nonlinear Control, Nagoya, Japan, 2006.

[297] R. E. Skelton, J. W. Helton, R. Adhikari, J.-P. Pinaud, and W. Chan, "An Introduction to the Mechanics of Tensegrity Structures," in *The Mechanical Systems Design Handbook*: CRC Press, 2001.

[298] F. Park, "Distance Metrics on the Rigid Body Motions with Applications to Mechanism Design," *ASME Journal of Mechanical Design*, vol. 117, pp. 48 - 54, 1995.

[299] C. Belta and V. Kumar, "Trajectory Design for Formations of Robots by Kinetic Energy Shaping," 2002.

[300] R. C. Smith and P. Cheeseman, "On the Representation and Estimation of Spatial Uncertainty," *The International Journal of Robotics Research*, vol. 5, pp. 56 - 68, 1986.

[301] J. J. Leonard and H. Durrant-Whyte, "Simultaneous Map Building and Localization for an Autonomous Mobilebot," presented at IEEE/RSJ International Workshop on Intelligent Robotics and Systems, IROS 91, Osaka, Japan, 1991.

[302] H. Durrant-Whyte and T. Bailey, "Simultaneous Localisation and Mapping (SLAM): Part 1 The Essential Algorithms," in *Robotics and Automation Magazine*, vol. 13, 2006, pp. 99 - 110.

[303] B. Grocholsky, H. Durrant-Whyte, and P. Gibbens, "An Information-Theoretic Approach to Decentralised Control of Multiple Autonomous Flight Vehicles," presented at Sensor Fusion and Decentralised Control in Robotic Systems III, Boston, MA, USA, 2000.

[304] C. Godsil and G. Royle, *Algebraic Graph Theory*. New York: Springer-Verlag, 2001.

[305] R. Diestel, *Graph Theory*, 3 ed. Heidelberg: Springer, 2005.

[306] N. Biggs, *Algebraic Graph Theory*, 2 ed. Cambridge: Cambridge University Press, 1993.

[307] R. Brualdi and H. Ryser, *Combinatorial Matrix Theory*. New York: Cambridge University Press, 1991.

[308] D. B. Kingston and R. W. Beard, "Discrete-Time Average-Consensus under Switching Network Topologies," presented at 2006 American Control Conference, Minneapolis, MN, USA, 2006.

[309] Y. G. Sun, L. Wang, and G. Xie, "Average Consensus in Directed Networks of Dynamic Agents with Time-Varying Communication Delays," presented at 45th IEEE Conference on Decision and Control, San Diego, CA, USA, 2006.

[310] C. W. Wu, "Algebraic Connectivity of Directed Graphs," *Linear and Multilinear Algebra*, vol. 53, pp. 203 - 223, 2005.

[311] W. Ren, R. W. Beard, and E. M. Atkins, "A Survey of Consensus Problems in Multi-agent Coordination," presented at American Control Conference, Portland, OR, USA, 2005.

[312] A. Tiwari, J. Fong, J. M. Carson III, R. Bhattacharya, and R. M. Murray, "A Framework for Lyapunov Certificates for Multi-Vehicle Rendezvous Problems," presented at American Control Conference, Boston, MA, USA, 2004.

[313] P. K. C. Wang and F. Y. Hadaegh, "Formation Flying of Multiple Spacecraft with Autonomous Rendezvous and Docking Capability," *IET Control Theory and Applications*, vol. 1, pp. 494 - 504, 2007.

[314] P. Hamann and V. Mehrmann, "Numerical Solution of Hybrid Systems of Differential-Algebraic Equations," *Computer Methods in Applied Mechanics and Engineering*, vol. 197, pp. 693 - 705, 2007.

[315] L. Xie, H. Ogai, and Y. Inoe, "Numerical Solving of Hybrid Dynamic Switching System and its Application," *International Journal of Innovative Computing, Information and Control*, vol. 2, pp. 849 - 862, 2006.

[316] R. Olfati-Saber, W. B. Dunbar, and R. M. Murray, "Cooperative Control of Multi-Vehicle Systems Using Cost Graphs and Optimization," presented at American Control Conference, Denver, CO, USA, 2003.

[317] S. Nair, "Stabilization and Synchronization of Networked Mechanical Systems," Doctor of Philosophy, Princeton University, 2006.

[318] R. L. Bishop and S. I. Goldberg, *Tensor Analysis on Manifolds*. New York: Dover Publishing, 1980.

[319] R. M. Murray, Z. Li, and S. S. Sastry, *A Mathematical Introduction to Robotic Manipulation*: CRC Press Inc, 1994.

[320] A. D. Lewis, "Simple Mechanical Control Systems with Constraints," *IEEE Transactions on Automatic Control*, vol. 45, pp. 1420 - 1436, 2000.

[321] F. Bullo, "Nonlinear Control of Mechanical Systems: A Riemannian Geometry Approach," Doctor of Philosophy, California Institute of Technology, Pasadena, California, 1999.

[322] B. C. Hall, *Lie Groups, Lie Algebras, and Representations: An Elementary Introduction*. New York: Springer-Verlag, 2003.

[323] C. Belta, "Geometric Methods for Multi-Robot Planning and Control," University of Pensylvania, 2003.

[324] M. Zefran, "Continuous Methods for Motion Planning," Doctor of Philosophy, University of Pennsylvania, Philadelphia, 1996.

[325] M. P. do Carmo, *Riemannian Geometry*. Boston: Birkhauser, 1992.

[326] A. D. Lewis, "Aspects of Geometric Mechanics and Control of Mechanical Systems," California Institute of Technology, Pasadena, California 1995.

[327] C. Belta and V. Kumar, "On the Computation of Rigid Body Motion," *Electronic Journal of Computational Kinematics*, vol. 1, 2002.

[328] C. Belta and V. Kumar, "An SVD-Based Projection Method for Interpolation on SE(3)," *IEEE Transactions on Robotics and Automation*, vol. 18, pp. 334 - 345, 2002.

[329] G. Liu and Z. Li, "A Unified Geometric Approach to Modeling and Control of Constrained Mechanical Systems," *IEEE Transactions on Robotics and Automation*, vol. 18, pp. 574 - 587, 2002.

[330] L. F. Shampine and J. Kierzenka, "Solving Boundary Value Problems for Ordinary Differential Equations in MATLAB with bvp4c," vol. 2008. Natick, MA: The MathWorks, Inc, 2000.

[331] I. I. Hussein and A. M. Bloch, "Optimal Control of Under-Actuated Systems with Application to Lie Groups," presented at American Control Conference, Portland, OR, USA, 2005.

[332] A. M. Bloch, N. E. Leonard, and J. E. Marsden, "Controlled Lagrangians and the Stabilization of Mechanical Systems I: First Matching Theorem," *IEEE Transactions on Automatic Control*, vol. 45, pp. 2253 - 2269, 2000.

[333] A. M. Bloch, D. E. Chang, N. E. Leonard, and J. E. Marsden, "Controlled Lagrangians and the Stabilization of Mechanical Systems II: Potential Shaping," *IEEE Transactions on AUtomatic Control*, vol. 46, pp. 1556 - 1571, 2001.

[334] J. M. Maciejowski, *Predictive Control with Constraints*. Great Britain: Pearson Education Limited, 2002.

[335] Y. Xia, "A New Neural Network for Solving Linear Programming Problems and its Applications," *IEEE Transactions on Neural Networks*, vol. 7, pp. 525-529, 1996.

[336] Y. Xia and G. Feng, "A Modified Neural Network for Quadratic Programming with Real-Time Applications," *Neural Information Processing - Letters and Reviews*, vol. 3, pp. 69-76, 2004.

[337] Y. Xia and J. Wang, "Neural Network for Solving Linear Programming Problems with Bounded Variables," *IEEE Transactions on Neural Networks*, vol. 6, pp. 515-519, 1995.

[338] Y. Xia and J. Wang, "A Dual Neural Network for Kinematic Control of Redundant Robot Manipulators," *IEEE Transactions on Systems, Man, Cybernetics - Part B: Cybernetics*, vol. 31, pp. 147 - 154, 2001.

[339] Y. Xia and J. Wang, "A Recurrent Neural Network for Solving Nonlinear Convex Programs Subject to Linear Constraints," *IEEE Transactions on Neural Networks*, vol. 16, pp. 379 - 386, 2005.

[340] Y. Zhang, J. Wang, and Y. Xia, "A Dual Neural Network for Redundancy Resolution of Kinematically Redundant Manipulators Subject to Joint Limits and Joint Velocity Limits," *IEEE Transactions on Neural Networks*, vol. 14, pp. 658 - 667, 2003.

[341] H. Chen and F. Allgower, "A Quasi-Infinite Horizon Nonlinear Model Predictive Control Scheme with Guaranteed Stability," *Automatica*, vol. 34, pp. 1205 - 1217, 1998.

[342] H. Michalska and D. Q. Mayne, "Robust Receding Horizon Control of Constrained Nonlinear Systems," *IEEE Transactions on Automatic Control*, vol. 38, pp. 1623 - 1633, 1993.

[343] D. Q. Mayne, J. B. Rawlings, C. V. Rao, and P. O. M. Scokaert, "Constrained Model Predictive Control: Stability and Optimality," *Automatica*, vol. 35, pp. 789 - 814, 2000.

[344] S. S. Keerthi and E. G. Gilbert, "Optimal Infinite-Horizon Feedback Laws for a General Class of Constrained Discrete-Time Systems: Stability and Moving-Horizon Approximations," *Journal of Optimization Theory and Applications*, vol. 57, pp. 265 - 293, 1988.

[345] D. Kurabayashi, J. Ota, T. Arai, and E. Yoshida, "Cooperative Sweeping by Multiple Mobile Robots," presented at IEEE International Conference on Robotics and Automation, Minneapolis, MN, USA, 1996.

[346] E. Frazzoli, M. A. Dahleh, and E. Feron, "Maneuver-based Motion Planning for Nonlinear Systems with Symmetries," *IEEE Transactions on Robotics and Automation*, vol. 21, pp. 1077 - 1091, 2005.

[347] J. Cortés, S. Martínez, and F. Bullo, "Spatially-distributed Coverage Optimization and Control with Limited-Range Interactions," *ESIAM: Control Optimisation and Calculus of Variations*, vol. 11, pp. 691 - 719, 2005.

[348] E. M. Arkin and H. Refael, "Approximation Algorithms for the Geometric Covering Salesman Problem," *Discrete Applied Mathematics*, vol. 55, pp. 197 - 218, 1994.

[349] H. Choset, E. U. Acar, A. A. Rizzi, and J. Luntz, "Exact Cellular Decompositions in terms of Critical Points of Morse Functions," presented at IEEE International Conference on Robotics and Automation, San Francisco, CA, USA, 2000.

[350] K. Lei, Y. Qiu, and Y. He, "A Novel Path Planning for Mobile Robots Using Modified Particle Swarm Optimizer," presented at 1st International Symposium on Systems and Control in Aerospace and Astronautics, Harbin, China, 2006.

[351] K. E. Parsopoulos and M. N. Vrahatis, "Recent Approaches to Global Optimisation Problems Through Particle Swarm Optimisation," *Natural Computing*, vol. 1, pp. 235 - 306, 2002.

[352] S. Kalantar and U. Zimmer, "Distributed Shape Control of Homogeneous Swarms of Autonomous Underwater Vehicles," *Autonomous Robots*, 2006.

[353] S. Kalantar and U. Zimmer, "Contour-Shape Formation Control for Autonomous Underwater Vehicles Using Canonical Shape Descriptors and Deformable Models," presented at IEEE International Conference on Marine Technology and Ocean Science, Kobe, Japan, 2004.

[354] O. Ilaya, "Multi-objective Decentralized Model Predictive Control for Cooperative Multi-UAV Systems," presented at AIAA Guidance, Navigation, and Control Conference, Hilton Head, USA, 2007.

Appendix A. LaSalle's Invariance Principle

Let $V:\mathbb{R}^n \to \mathbb{R}$ *be a locally positive definite function such that on the compact set* $\Omega_c = \{x \in \mathbb{R}^n : V(x) \le c\}$, $\dot{V}(x) \le 0$. *Define:*

$$S = \{x \in \Omega_c : \dot{V}(x) = 0\} \tag{A.1}$$

As $t \to \infty$, *the trajectory tends to the largest invariant set inside* S. *Moreover, if* S *contains no invariant sets other than* $x = 0$, *then* 0 *is asymptotically stable.*

Appendix B. Christoffel Symbols for 2 Rigid Bodies in a Plane

The 64 Christoffel symbols for two vehicles in a plane derived using MATLAB are listed below:

$$\Gamma^1_{1,1} := \frac{m_2(4\sigma_r - 2)(x_1 - x_2)(y_1 - y_2)^2}{\sigma_r(m_1 + m_2)\left((x_1 - x_2)^2 - (y_1 - y_2)^2\right)^2}$$

$$\Gamma^1_{1,2} := -\frac{m_2(4\sigma_r - 2)(x_1 - x_2)^2(y_1 - y_2)^2}{\sigma_r(m_1 + m_2)\left((x_1 - x_2)^2 - (y_1 - y_2)\right)^2}$$

$$\Gamma^1_{1,3} := -\frac{m_2(4\sigma_r - 2)(x_1 - x_2)(y_1 - y_2)^2}{\sigma_r(m_1 + m_2)\left((x_1 - x_2)^2 - (y_1 - y_2)^2\right)^2}$$

$$\Gamma^1_{1,4} := -\frac{m_2(4\sigma_r - 2)(x_1 - x_2)^2(y_1 - y_2)}{\sigma_r(m_1 + m_2)\left((x_1 - x_2)^2 - (y_1 - y_2)^2\right)^2}$$

$$\Gamma^1_{2,1} := -\frac{m_2(4\sigma_r - 2)(x_1 - x_2)^2(y_1 - y_2)}{\sigma_r(m_1 + m_2)\left((x_1 - x_2)^2 - (y_1 - y_2)^2\right)^2}$$

$$\Gamma^1_{2,2} := \frac{m_2(4\sigma_r - 2)(x_1 - x_2)^3}{\sigma_r(m_1 + m_2)\left((x_1 - x_2)^2 - (y_1 - y_2)^2\right)^2}$$

$$\Gamma^1_{2,3} := \frac{m_2(4\sigma_r - 2)(x_1 - x_2)^2(y_1 - y_2)}{\sigma_r(m_1 + m_2)\left((x_1 - x_2)^2 - (y_1 - y_2)^2\right)^2}$$

$$\Gamma^1_{2,4} := \frac{m_2(4\sigma_r - 2)(x_1 - x_2)^3}{\sigma_r(m_1 + m_2)\left((x_1 - x_2)^2 - (y_1 - y_2)^2\right)^2}$$

$$\Gamma^1_{3,1} := -\frac{m_2(4\sigma_r - 2)(x_1 - x_2)(y_1 - y_2)^2}{\sigma_r(m_1 + m_2)\left((x_1 - x_2)^2 - (y_1 - y_2)^2\right)^2}$$

$$\Gamma^1_{3,2} := -\frac{m_2(4\sigma_r - 2)(x_1 - x_2)^2(y_1 - y_2)}{\sigma_r(m_1 + m_2)\left((x_1 - x_2)^2 - (y_1 - y_2)^2\right)^2}$$

$$\Gamma^1_{3,3} := \frac{m_2(4\sigma_r - 2)(x_1 - x_2)(y_1 - y_2)^2}{\sigma_r(m_1 + m_2)\left((x_1 - x_2)^2 - (y_1 - y_2)^2\right)^2}$$

$$\Gamma^1_{3,4} := -\frac{m_2(4\sigma_r - 2)(x_1 - x_2)^2(y_1 - y_2)}{\sigma_r(m_1 + m_2)\left((x_1 - x_2)^2 - (y_1 - y_2)^2\right)^2}$$

$$\Gamma^1_{4,1} := \frac{m_2(4\sigma_r - 2)(x_1 - x_2)^2(y_1 - y_2)}{\sigma_r(m_1 + m_2)\left((x_1 - x_2)^2 - (y_1 - y_2)^2\right)^2}$$

$$\Gamma^1_{4,2} := -\frac{m_2(4\sigma_r - 2)(x_1 - x_2)^3}{\sigma_r(m_1 + m_2)\left((x_1 - x_2)^2 - (y_1 - y_2)^2\right)^2}$$

$$\Gamma^1_{4,3} := -\frac{m_2(4\sigma_r - 2)(x_1 - x_2)^2(y_1 - y_2)}{\sigma_r(m_1 + m_2)\left((x_1 - x_2)^2 - (y_1 - y_2)^2\right)^2}$$

$$\Gamma^1_{4,4} := \frac{m_2(4\sigma_r - 2)(x_1 - x_2)^3}{\sigma_r(m_1 + m_2)\left((x_1 - x_2)^2 - (y_1 - y_2)^2\right)^2}$$

$$\Gamma^2_{1,1} := \frac{m_2(4\sigma_r - 2)(y_1 - y_2)^3}{\sigma_r(m_1 + m_2)\left((x_1 - x_2)^2 - (y_1 - y_2)^2\right)^2}$$

$$\Gamma^2_{1,2} := -\frac{m_2(4\sigma_r - 2)(x_1 - x_2)(y_1 - y_2)^2}{\sigma_r(m_1 + m_2)\left((x_1 - x_2)^2 - (y_1 - y_2)^2\right)^2}$$

$$\Gamma^2_{1,3} := -\frac{m_2(4\sigma_r - 2)(y_1 - y_2)^3}{\sigma_r(m_1 + m_2)\left((x_1 - x_2)^2 - (y_1 - y_2)^2\right)^2}$$

$$\Gamma^2_{1,4} := -\frac{m_2(4\sigma_r - 2)(x_1 - x_2)(y_1 - y_2)^2}{\sigma_r(m_1 + m_2)\left((x_1 - x_2)^2 - (y_1 - y_2)^2\right)^2}$$

$$\Gamma^2_{2,1} := -\frac{m_2(4\sigma_r - 2)(x_1 - x_2)(y_1 - y_2)^2}{\sigma_r(m_1 + m_2)\left((x_1 - x_2)^2 - (y_1 - y_2)^2\right)^2}$$

$$\Gamma^2_{2,2} := \frac{m_2(4\sigma_r - 2)(x_1 - x_2)^2(y_1 - y_2)}{\sigma_r(m_1 + m_2)\left((x_1 - x_2)^2 - (y_1 - y_2)^2\right)^2}$$

$$\Gamma^{2}_{2,3} := \frac{m_2(4\sigma_r - 2)(x_1 - x_2)(y_1 - y_2)^2}{\sigma_r(m_1 + m_2)\left((x_1 - x_2)^2 - (y_1 - y_2)^2\right)^2}$$

$$\Gamma^{2}_{2,4} := -\frac{m_2(4\sigma_r - 2)(x_1 - x_2)^2(y_1 - y_2)}{\sigma_r(m_1 + m_2)\left((x_1 - x_2)^2 - (y_1 - y_2)^2\right)^2}$$

$$\Gamma^{2}_{3,1} := -\frac{m_2(4\sigma_r - 2)(y_1 - y_2)^3}{\sigma_r(m_1 + m_2)\left((x_1 - x_2)^2 - (y_1 - y_2)^2\right)^2}$$

$$\Gamma^{2}_{3,2} := -\frac{m_2(4\sigma_r - 2)(x_1 - x_2)(y_1 - y_2)^2}{\sigma_r(m_1 + m_2)\left((x_1 - x_2)^2 - (y_1 - y_2)^2\right)^2}$$

$$\Gamma^{2}_{3,3} := \frac{m_2(4\sigma_r - 2)(y_1 - y_2)^3}{\sigma_r(m_1 + m_2)\left((x_1 - x_2)^2 - (y_1 - y_2)^2\right)^2}$$

$$\Gamma^{2}_{3,4} := -\frac{m_2(4\sigma_r - 2)(x_1 - x_2)(y_1 - y_2)^2}{\sigma_r(m_1 + m_2)\left((x_1 - x_2)^2 - (y_1 - y_2)^2\right)^2}$$

$$\Gamma^{2}_{4,1} := \frac{m_2(4\sigma_r - 2)(x_1 - x_2)(y_1 - y_2)^2}{\sigma_r(m_1 + m_2)\left((x_1 - x_2)^2 - (y_1 - y_2)^2\right)^2}$$

$$\Gamma^{2}_{4,2} := -\frac{m_2(4\sigma_r - 2)(x_1 - x_2)^2(y_1 - y_2)}{\sigma_r(m_1 + m_2)\left((x_1 - x_2)^2 - (y_1 - y_2)^2\right)^2}$$

$$\Gamma^{2}_{4,3} := -\frac{m_2(4\sigma_r - 2)(x_1 - x_2)(y_1 - y_2)^2}{\sigma_r(m_1 + m_2)\left((x_1 - x_2)^2 - (y_1 - y_2)^2\right)^2}$$

$$\Gamma^{2}_{4,4} := \frac{m_2(4\sigma_r - 2)(x_1 - x_2)^2(y_1 - y_2)}{\sigma_r(m_1 + m_2)\left((x_1 - x_2)^2 - (y_1 - y_2)^2\right)^2}$$

$$\Gamma^{3}_{1,1} := -\frac{m_2(4\sigma_r - 2)(x_1 - x_2)(y_1 - y_2)^2}{\sigma_r(m_1 + m_2)\left((x_1 - x_2)^2 - (y_1 - y_2)^2\right)^2}$$

$$\Gamma^{3}_{1,2} := \frac{m_2(4\sigma_r - 2)(x_1 - x_2)^2(y_1 - y_2)}{\sigma_r(m_1 + m_2)\left((x_1 - x_2)^2 - (y_1 - y_2)^2\right)^2}$$

$$\Gamma^{3}_{1,3} := \frac{m_2(4\sigma_r - 2)(x_1 - x_2)(y_1 - y_2)^2}{\sigma_r(m_1 + m_2)\left((x_1 - x_2)^2 - (y_1 - y_2)^2\right)^2}$$

$$\Gamma^{3}_{1,4} := \frac{m_2(4\sigma_r - 2)(x_1 - x_2)^2(y_1 - y_2)}{\sigma_r(m_1 + m_2)\left((x_1 - x_2)^2 - (y_1 - y_2)^2\right)^2}$$

$$\Gamma^{3}_{2,1} := \frac{m_2(4\sigma_r - 2)(x_1 - x_2)^2(y_1 - y_2)}{\sigma_r(m_1 + m_2)\left((x_1 - x_2)^2 - (y_1 - y_2)^2\right)^2}$$

$$\Gamma^{3}_{2,2} := -\frac{m_2(4\sigma_r - 2)(x_1 - x_2)^3}{\sigma_r(m_1 + m_2)\left((x_1 - x_2)^2 - (y_1 - y_2)^2\right)^2}$$

$$\Gamma^{3}_{2,3} := -\frac{m_2(4\sigma_r - 2)(x_1 - x_2)^2(y_1 - y_2)}{\sigma_r(m_1 + m_2)\left((x_1 - x_2)^2 - (y_1 - y_2)^2\right)^2}$$

$$\Gamma^{3}_{2,4} := \frac{m_2(4\sigma_r - 2)(x_1 - x_2)^3}{\sigma_r(m_1 + m_2)\left((x_1 - x_2)^2 - (y_1 - y_2)^2\right)^2}$$

$$\Gamma^{3}_{3,1} := \frac{m_2(4\sigma_r - 2)(x_1 - x_2)(y_1 - y_2)^2}{\sigma_r(m_1 + m_2)\left((x_1 - x_2)^2 - (y_1 - y_2)^2\right)^2}$$

$$\Gamma^{3}_{3,2} := \frac{m_2(4\sigma_r - 2)(x_1 - x_2)^2(y_1 - y_2)}{\sigma_r(m_1 + m_2)\left((x_1 - x_2)^2 - (y_1 - y_2)^2\right)^2}$$

$$\Gamma^{3}_{3,3} := -\frac{m_2(4\sigma_r - 2)(x_1 - x_2)(y_1 - y_2)^2}{\sigma_r(m_1 + m_2)\left((x_1 - x_2)^2 - (y_1 - y_2)^2\right)^2}$$

$$\Gamma^{3}_{3,4} := \frac{m_2(4\sigma_r - 2)(x_1 - x_2)^2(y_1 - y_2)}{\sigma_r(m_1 + m_2)\left((x_1 - x_2)^2 - (y_1 - y_2)^2\right)^2}$$

$$\Gamma^{3}_{4,1} := -\frac{m_2(4\sigma_r - 2)(x_1 - x_2)^2(y_1 - y_2)}{\sigma_r(m_1 + m_2)\left((x_1 - x_2)^2 - (y_1 - y_2)^2\right)^2}$$

$$\Gamma^{3}_{4,2} := \frac{m_2(4\sigma_r - 2)(x_1 - x_2)^3}{\sigma_r(m_1 + m_2)\left((x_1 - x_2)^2 - (y_1 - y_2)^2\right)^2}$$

$$\Gamma^{3}_{4,3} := \frac{m_2(4\sigma_r - 2)(x_1 - x_2)^2(y_1 - y_2)}{\sigma_r(m_1 + m_2)\left((x_1 - x_2)^2 - (y_1 - y_2)^2\right)^2}$$

$$\Gamma^{3}_{4,4} := -\frac{m_2(4\sigma_r - 2)(x_1 - x_2)^3}{\sigma_r(m_1 + m_2)\left((x_1 - x_2)^2 - (y_1 - y_2)^2\right)^2}$$

$$\Gamma^{4}_{1,1} := -\frac{m_2(4\sigma_r - 2)(y_1 - y_2)^3}{\sigma_r(m_1 + m_2)\left((x_1 - x_2)^2 - (y_1 - y_2)^2\right)^2}$$

$$\Gamma^{4}_{1,2} := \frac{m_2(4\sigma_r - 2)(x_1 - x_2)(y_1 - y_2)^2}{\sigma_r(m_1 + m_2)\left((x_1 - x_2)^2 - (y_1 - y_2)^2\right)^2}$$

$$\Gamma^{4}_{1,3} := \frac{m_2(4\sigma_r - 2)(y_1 - y_2)^3}{\sigma_r(m_1 + m_2)\left((x_1 - x_2)^2 - (y_1 - y_2)^2\right)^2}$$

$$\Gamma^{4}_{1,4} := \frac{m_2(4\sigma_r - 2)(x_1 - x_2)(y_1 - y_2)^2}{\sigma_r(m_1 + m_2)\left((x_1 - x_2)^2 - (y_1 - y_2)^2\right)^2}$$

$$\Gamma^{4}_{2,1} := \frac{m_2(4\sigma_r - 2)(x_1 - x_2)(y_1 - y_2)^2}{\sigma_r(m_1 + m_2)\left((x_1 - x_2)^2 - (y_1 - y_2)^2\right)^2}$$

$$\Gamma^{4}_{2,2} := -\frac{m_2(4\sigma_r - 2)(x_1 - x_2)^2(y_1 - y_2)}{\sigma_r(m_1 + m_2)\left((x_1 - x_2)^2 - (y_1 - y_2)^2\right)^2}$$

$$\Gamma^{4}_{2,3} := -\frac{m_2(4\sigma_r - 2)(x_1 - x_2)(y_1 - y_2)^2}{\sigma_r(m_1 + m_2)\left((x_1 - x_2)^2 - (y_1 - y_2)^2\right)^2}$$

$$\Gamma^{4}_{2,4} := \frac{m_2(4\sigma_r - 2)(x_1 - x_2)^2(y_1 - y_2)}{\sigma_r(m_1 + m_2)\left((x_1 - x_2)^2 - (y_1 - y_2)^2\right)^2}$$

$$\Gamma^4_{3,1} := \frac{m_2\left(4\sigma_r - 2\right)\left(y_1 - y_2\right)^3}{\sigma_r\left(m_1 + m_2\right)\left(\left(x_1 - x_2\right)^2 - \left(y_1 - y_2\right)^2\right)^2}$$

$$\Gamma^4_{3,2} := \frac{m_2\left(4\sigma_r - 2\right)\left(x_1 - x_2\right)\left(y_1 - y_2\right)^2}{\sigma_r\left(m_1 + m_2\right)\left(\left(x_1 - x_2\right)^2 - \left(y_1 - y_2\right)^2\right)^2}$$

$$\Gamma^4_{3,3} := \frac{m_2\left(4\sigma_r - 2\right)\left(y_1 - y_2\right)^3}{\sigma_r\left(m_1 + m_2\right)\left(\left(x_1 - x_2\right)^2 - \left(y_1 - y_2\right)^2\right)^2}$$

$$\Gamma^4_{3,4} := \frac{m_2\left(4\sigma_r - 2\right)\left(x_1 - x_2\right)\left(y_1 - y_2\right)^2}{\sigma_r\left(m_1 + m_2\right)\left(\left(x_1 - x_2\right)^2 - \left(y_1 - y_2\right)^2\right)^2}$$

$$\Gamma^4_{4,1} := -\frac{m_2\left(4\sigma_r - 2\right)\left(x_1 - x_2\right)\left(y_1 - y_2\right)^2}{\sigma_r\left(m_1 + m_2\right)\left(\left(x_1 - x_2\right)^2 - \left(y_1 - y_2\right)^2\right)^2}$$

$$\Gamma^4_{4,2} := \frac{m_2\left(4\sigma_r - 2\right)\left(x_1 - x_2\right)^2\left(y_1 - y_2\right)}{\sigma_r\left(m_1 + m_2\right)\left(\left(x_1 - x_2\right)^2 - \left(y_1 - y_2\right)^2\right)^2}$$

$$\Gamma^4_{4,3} := \frac{m_2\left(4\sigma_r - 2\right)\left(x_1 - x_2\right)\left(y_1 - y_2\right)^2}{\sigma_r\left(m_1 + m_2\right)\left(\left(x_1 - x_2\right)^2 - \left(y_1 - y_2\right)^2\right)^2}$$

$$\Gamma^4_{4,4} := -\frac{m_2\left(4\sigma_r - 2\right)\left(x_1 - x_2\right)^2\left(y_1 - y_2\right)}{\sigma_r\left(m_1 + m_2\right)\left(\left(x_1 - x_2\right)^2 - \left(y_1 - y_2\right)^2\right)^2}$$